Department Chemie
Fachgebiet Theoretische Chemie
Technische Universität München

Relativistic Density Functional Studies on Ligated Transition Metal Clusters

Alexander Genest

Vollständiger Abdruck der von der Fakultät für Chemie der Technischen Universität München zur Erlangung des akademischen Grades eines

Doktors der Naturwissenschaften (Dr. rer. nat.)

genehmigten Dissertation.

Vorsitzender: Univ.-Prof. Dr. U. K. Heiz

Prüfer der Dissertation:

1. Univ.-Prof. Dr. N. Rösch
2. Univ.-Prof. Dr. K. Köhler

Die Dissertation wurde am 22.05.2007 bei der Technischen Universität München eingereicht und durch die Fakultät für Chemie am 25.06.2007 angenommen.

Danksagung

Mein besonderer Dank gilt Herrn Prof. Dr. Notker Rösch für die Vergabe des interessanten Themas, die Bereitstellung hervorragender Rahmenbedingungen, sein großes persönliches Engagement bei der Betreuung dieser Arbeit und vor allem dafür, dass er mein Interesse für die theoretische Chemie geweckt hat.

Herrn Dr. Sven Krüger danke ich für die ausgezeichnete fachliche Betreuung, die unermüdliche Bereitschaft zu wissenschaftlichen Diskussionen und die vielen wertvollen Anregungen, die entscheidend zum Gelingen dieser Arbeit beigetragen haben.

Herrn Prof. W. Domcke und den Mitgliedern seines Arbeitskreises möchte ich ebenso wie Frau R. Mösch für das angenehme Klima am Lehrstuhl danken.

Meinen Studienkollegen Herrn Dr. Florian Schlosser und Herrn Dr. Georg Eickerling sowie meinem langjährigen Kollegen Herrn Dr. André Woiterski sei hier besonders für die freundschaftliche und kollegiale Zusammenarbeit und die zahlreichen gemeinsamen Aktivitäten gedankt. Außerdem bin ich den Herrn Dr. A. Matveev und Dr. A. Shor für die kompetente Hilfestellung bei technischen Fragen und Problemen jeglicher Art dankbar. Mein Dank gilt selbstverständlich auch allen derzeitigen und früheren Mitgliedern des Arbeitskreises für die angenehme Atmosphäre sowie interessante Diskussionen und Vorträge. An dieser Stelle seien A. B. Mohammad, S. Bosko, Dr. M. García-Hernández, Dr. C. Inntam, A. Kremleva, Dr. K. H. Lim, Dr. L. Moskaleva, Dr. V. Nasluzov, Dr. K. Neyman, R. S. Ray, Dr. G. Shamov, Dr. K. Siriwong, E. Vladimirov, Dr. A. Voityuk, M. Winkler und Dr. I. Yudanov genannt.

Speziell möchte ich Frau Dr. Parawan Chuichay für Ihre zahlreichen motivierenden Worte und Ermunterungen danken, welche diese Arbeit entscheidend erleichtert haben. Nicht zuletzt gilt mein ganz besonderer Dank meiner Familie, insbesondere meiner Schwester und meinen Eltern, die mir meine Ausbildung ermöglicht haben und mich während dieser Zeit großzügig und liebevoll unterstützt haben.

Meinen Eltern

Contents

1 Introduction 1

2 Chemical Background 5

2.1 Definition and basic concepts of metal clusters 5
2.2 Experimental issues 8
2.3 Transition metal clusters in theoretical chemistry 11

3 Computational Method 15

3.1 Relativistic Density Functional Method: The DKH Approach 16
3.1.1 Relativistic effects 16
3.1.2 Relativistic density functional theory 17
3.2 Computational Details 19
3.3 Evaluation of methods 21
3.3.1 Basis set contractions 21
3.3.2 Evaluation of exchange correlation functionals 22
3.3.3 Comparison of the scalar relativistic approach to ECPs 24
3.4 The QM/MM approach 25

4 Results and Discussion 29

4.1 The impurities H, C, and O at Pd_4 clusters 29
4.1.1 Background 29
4.1.2 Methodological details 30
4.1.3 Bare clusters 31
4.1.4 Clusters with impurity atoms 35
4.1.4.1 High symmetry models 35
4.1.4.2 Low symmetric models 42
4.1.5 Conclusions 50

4.2 Two Hydrogen atoms on tetrairidium clusters 52
4.2.1 Background 52
4.2.2 Computational Details 53
4.2.3 Results and Discussions 54
4.2.3.1 General trends 56
4.2.3.2 Comparison of similar structures 64
4.2.4 Summary and conclusions 67
4.3 The cluster $Au_{13}(SR)_n$ with R = H, CH_3 and n = 4, 6, 8 69
4.3.1 Background 69
4.3.2 Models 71
4.3.3 Results and Discussion 74
4.3.3 Summary and conclusions 87
4.4 $Cu_{13}(SCH_2CH_3)_8$: Comparison of DF and IMOMM calculations 90
4.4.1 Background 90
4.4.2 The IMOMM implementation of ParaGauss 91
4.4.3 Computational details 91
4.4.4 The model cluster $Cu_{13}(SCH_2CH_3)_8$ 92
4.4.5 QM calculations on the cluster $Cu_{13}(SCH_2CH_3)_8$ 95
4.4.6 IMOMM calculations on the cluster $Cu_{13}(SCH_2CH_3)_8$ 101
4.5.3 Conclusions 109
4.5 The cluster compound $Au_{55}[P(C_6H_5)_3]_{12}Cl_6$ 111
4.5.1 Experimental results 111
4.5.2 Density functional calculations 117
4.5.3 Methodological details 117
4.5.3.1 Bare Au_{55} 118
4.5.3.2 Phosphine ligand models 120
4.5.3.3 Model phosphine ligands PH_3 on Au_{55} 121
4.5.3.4 Chlorine coordination on Au_{55} 122
4.5.3.5 $Au_{55}[PH_3]_{12}Cl_6$ 124
4.5.4 Conclusions 136

5 Summary 138

Appendix A – Basis Sets 142

Bibliography 151

List of Abbreviations

au	atomic units
BP	Becke-Perdew (functional)
Calc.	calculated
DF	density functional
DFT	density functional theory
DK	Douglas-Kroll (procedure)
DKH	Douglas-Kroll-Hess (procedure)
DKS	Dirac-Kohn-Sham (method, Hamiltonian)
ECP	effective core potential
EXAFS	extended x-ray absorption fine structure spectroscopy
Exp.	experimental
FC	frozen core
FF	fitting function(s)
GGA	generalized gradient approximation (of xc functional)
HF	Hartree-Fock (method)
IP	ionization potential
KS	Kohn-Sham (method, Hamiltonian)
LCGTO	linear combination of Gaussian-type orbitals
LDA	local density approximation (of xc functional)
MO	molecular orbital
QM	quantum mechanics
RECP	relativistic effective core potential
RI	resolution of the identity (approach)
SCF	self-consistent field (procedure)

SO	spin-orbit (interaction, method)
SNSO	screened nuclear (potential) spin-orbit (method)
SR	scalar relativistic
TEM	transmission electron microscopy
vdW	van der Waals
VWN	Vosko-Wilk-Nusair (functional)
xc	exchange-correlation (functional, potential, energy)

1 Introduction

Materials can be designed to have properties which are useful to serve in every day life.[1] Also the area of molecular chemistry is well understood and molecular properties are designable.[2] For both types of matter the properties depend on the elements contained and on the atomic connectivity. Clusters, metal clusters in particular, constitute a separate class of materials in between bulk on the one hand and the molecular state on the other.[3,4] In bulk materials molecules or atoms are surrounded by their neighbors in a specific coordination determining a particular crystal structure. The surface of a piece of material contains lower coordinated atoms and will therefore have slightly different properties compared to the bulk itself.[5] In general boundary effects of low coordinated atoms constitute a perturbation of the order inside the material.[6] As long as the sample is big enough and the surface a negligible fraction of the material, that perturbation will have little influence on the ordering inside.[6] On going from massive junks of material to very small particles, the perturbation due to surface effects becomes stronger and influences the properties to a larger degree,[6] up to a level, where properties can no longer be derived from those of the bulk material.[7] The transition between the scaleable and the non-scalable regimes may be specific for the property and the material under study, as will be detailed later. As an example an icosahedral cluster of 309 atoms is mentioned where the number of atoms at the surface (162) is approximately equal to the number of atoms “inside” (147).[8] For palladium this particle is at approximately 2 nm in diameter. The existence of scaleable and a non-scaleable regimes, for which one can or cannot predict properties by extrapolation from the bulk, constitutes a new dimension in the design of materials. It is the size dependency of properties which makes clusters a separate class of materials.[9,10]

From this point of view it is obvious that small metal clusters, which are in the focus of this thesis, are not simply an intermediate between bulk material and molecules. They offer a whole new set of unique properties which are not predictable in a simple way. For example Au_{55} turned out to be far more stable against oxidation than bulk gold or Au atoms.[11] It is a very interesting feature that not only the atoms control the properties of the material but also the size of the conglomerate.[7,10] This opens an interesting field of

research on materials, which are tunable by controlling their size. Unfortunately the size control also turned out to be one of the key difficulties in producing clusters with defined properties, because clusters normally tend to agglomerate and coagulate, and form larger entities or are so reactive that they quickly form new compounds.[12] Therefore most clusters have to be stabilized, supported or passivated, and comparison to free clusters can shed light on the behavior of the actual species. To prevent clusters from coagulation several strategies of either saturating open valences at the cluster surface or immobilization within some framework can be used to stabilize them.[12] One common route to prevent coagulation of clusters is to attach ligands at the surface, which saturate the open valences and work as a kind of chaperone to keep clusters apart from each other.[12-15] As ligands are often bound covalently to the metal particle the effect of such stabilization on the clusters has to be investigated to gain more insight in the resulting properties of the desired compound.[16] Unfortunately not only ligands preventing coagulation, but also impurities binding at cluster surfaces can influence properties of the clusters. Understanding these effects is mandatory for the goal of nanoscience to design materials with specific properties. To generate knowledge for such predictions, one first needs to analyze structural motives and obtain insight from the cluster materials that are already known.

Understanding the mechanisms that determine properties of small metal particles and to predict the changes of such properties with respect to the bulk or the molecular limit is one of the key issues of nanosciences.[17,18] Different models and theories have been developed to rationalize certain macroscopic properties like optical features or conductivity.[3] Despite of intense research activities, there are still open questions especially about structures, connectivity, ligand coordination and site as well as regarding the influence of the various ligands on cluster properties. By means of quantum chemistry calculations this thesis would like to contribute to the understanding of these quite fundamental issues of cluster-ligand interactions and their effects on properties; this research field recently has been growing rapidly.[3] The present work focuses on investigating structures and interactions of transition metal clusters with small non-metallic heteroatoms or ligand molecules. From these calculations rationalizations and predictions can be gleaned that in the end will facilitate tailoring of materials with new and interesting properties.

Here, a short overview over the structure of this work is presented. Chapter 2 provides some chemical background to metal clusters and their interactions with ligands and indicates where this is important for science and applications. Chapter 3 illustrates the density functional method used throughout this thesis and gives insight into different computational models applied. Chapter 4 presents computational results, including

comparison to other results where available. First the effect of main group atom impurities H, C, O on Pd_4 clusters will be explored (Section 4.1). Next the effect of two hydrogen atoms on Ir_4 is investigated extending a previous study which reported the effects of a single H on Ir_4. Then Au_{13} with 4, 6 or 8 thiolate ligands in a comparable coordination mode is discussed as well as the effect of different ligand coverages. In the following section a hybrid QM/MM method is studied and its potential for treating species with large ligands at the molecular mechanics level is evaluated, while the metal core of the ligated cluster is investigated by a density functional approach. In the last section of Chapter 4 calculations on the cluster $Au_{55}(P(C_6H_5)_3)_{12}Cl_6$ are presented, which has been claimed to be one of the biggest gold clusters of well defined nuclearity.[3,19] Finally, in Chapter 5, a summary of the results and an outlook on topics of future studies is given.

2 Chemical Background

2.1 Definition and basic concepts of metal clusters

Very large clusters which are normally addressed as colloids can easily be formed and have been used by mankind since approximately 2000 years, because gold colloids form nice purple colors and were used for decoration purposes.[3] An early definition by F.A. Cotton identifies a metal cluster as a "*finite group of metal atoms participating in direct metal-metal bonds*",[20] where this finite group of metal atoms can comprise from several to thousands of atoms. In the literature exist several subcategories like nanocrystals, nanoparticles, colloids which categorize clusters according to their size.[21] As already mentioned in the Introduction, for clusters there are in general two distinct size regions which are defined due to their size dependent change of properties.[7] For the so called scaleable regime various properties change proportional to the cluster radius,[10] while for cluster sizes smaller than that, in the so-called non-scaleable regime, changes of properties are not predictable from information about larger clusters.[7] In this non-scaleable size region or molecule-like regime even the removal of one single atom from the metal cluster can change the properties significantly so that for example a desired oxidation stability vanishes or a catalytic activity is diminished.[7,11,22] In general this regime is characterized by irregularities in how properties depend on cluster size.

Generally one notes a higher stability for metal clusters with specific nuclearity. Normally this stability occurs at certain "magic" numbers (6, 13, 19, 38, 40, 44, 55, 85, 147, etc)[15,23,24] of atoms which can be deducted from the standard fcc lattice, a propensity to form perfectly spherical structures or the presence of particular electronic shell closing. From a geometrical point of view these "magic" numbers describe arrangements in which closed geometric shells of either icosahedral (13, 55, 147), octahedral (6, 19, 44, 85, 146) or cuboctahedral (13, 55, 147) symmetries are achieved. Important numbers of metal atoms

to reach a closed electronic shell are 2, 8, and 20. To rationalize why dispersed colloidal gold particles change their color (from metallic gold to purple) and other particular properties one has to keep in mind that these clusters no longer exhibit properties related to bulk material, but develop new properties depending on their size. So-called quantum size effects come into play when the de Broglie wavelength of the valence electrons is of the same order as the size of the cluster itself.[3] Then the particles start to act as a zero-dimensional quantum box (dot) according to quantum mechanical rules. The mobile electrons, confined to the cluster, show characteristic collective oscillations of the electron gas in the nanoparticle, the so-called plasmon resonance band.[3] Gold clusters in the 5–20 nm range feature their plasmon resonance band at 530 nm, which gives rise to the purple color used since ancient times.[3] Unlike the bulk metals, metal clusters feature a gap between the highest occupied and lowest unoccupied molecular orbitals, which also depends on the size of the cluster.[10] Thus one can understand why specific cluster effects are only measurable when clusters are produced with as a size dispersion as small as possible.

Clusters exhibiting special properties have to be stable enough to endure standard conditions for their practical usage. There are two processes which jeopardize ensembles of clusters of a definite nuclearity. The free energy of a system of clusters is reduced if they interact either with each other or their environment. For one, clusters tend to agglomerate and coagulate which means they form larger entities by "melting", at least partly, together; in this way the formerly uniform size distribution broadens with time, which, in turn, will wash out size specific properties.[3] Secondly, metal clusters have open valences on their surface which leaves them chemically unsaturated and reactive.[3,15] A solvent or air environment can easily lead to chemical reactions and thus to ligand coverage or modification due to impurities.[15] Different strategies were designed to protect metal clusters against these two key sources of impurification and decomposition.[3,15] To avoid coagulation, cluster have to be stabilized in the desired size and they have to be prevented from coming into touch with each other. A suitable strategy is, for example, to immobilize small clusters inside zeolite cages where they have no possibility to come close to each other.[3] Another approach relies on embedding metal clusters in an organic matrix, e.g., a polymer, which inhibits the mobility and separates the clusters from each other.[3] An alternative for overcoming the reactivity of the cluster surface is chemical passivation of the metal atoms on the cluster surface.[15] This is possible in a classical fashion by attaching ligands to the surface, but also by adding a layer of more inert metal atoms, i.e. by constructing so-called core-shell particles which exist in several varieties.[3] Despite of the higher stability of such complex clusters, often additional ligands have to be used to

saturate the surface shell and to protect it from environmental influences.[3] For instance, coinage metals Cu, Ag, Au are mixed with Pd or Pt to produce core shell particles.[3,25] No clear stoichiometry was found; rather alloys of varying composition were formed from both metals.[3] When saturating open valences at the surface of a cluster, [15] often bulky ligands are used to protect binding sites from reactions with impurities coming from the environment.[15] As a secondary effect, bulky ligands form a buffer which prevents the metal clusters from coming close to each other.[15] Unfortunately the chemical bond of the ligand will have an effect on the cluster itself and modify its properties as well. Till now, it is unclear to some extent how strong the influence of the ligand is on the cluster and how this effect can be used to tune properties.[16] A further problem is that in many cases a reference for the pure cluster is missing because only ligated species are known.

Ligands also offer possibilities for modifications which may make it easier to adjust the properties of the system as a whole.[15] One can for example tune the separation between clusters by the length and bulkiness of ligands and by their steric requirements.[15] Especially organic ligands introduce vast possibilities of synthesis routes; several of them are accessible even when the ligands are already bound to a cluster.[15] For example, ω-bromoalkanethiol as ligand of a transition metal cluster can undergo a standard S_{N2} reaction with an alkylamine to exchange the bromine.[26] A place exchange reaction of ligands on a cluster offers another way of introducing new functionalities.[27] This exchange route allows to synthesize clusters with a certain nuclearity in cases, where it is difficult to reach that goal directly with the type of ligand whose functionality is desired in the end. For example, one generates 1.5 nm gold nano particles with phosphine ligands and then replaces these ligands by thiolates.[28] The possibilities opened up by ligands can be used to prepare tail groups with a specially designed functionality to modify the interaction of the clusters with their environment.[15] This can considerably facilitate the immobilization of clusters because chemical bonds to a substrate can be formed to fix clusters at desired positions.[3] Another option introduced by the flexibility of the tail group is to connect clusters via a ligand, which is functionalized with cluster binding capabilities at both ends.[29] This strategy helps to control the spacing between clusters and has even been used to transport charge between two clusters which gives first prospects of nano electronics.[30] This type of immobilization controls not only the minimal distance but also the next-nearest neighbor is kept within a certain range.[29] Depending on the linkage capabilities of the ligands, superstructures can be formed with ligated metal clusters as building blocks.[29] Linear (one-dimensional), layer-type (two-dimensional) and crystal-type (three-dimensional) structures have been grown.[3,18,31-33] A big hope for nanosciences in this area is to find ligand cluster arrangements which undergo a pre-determined self-assembly,

controlled only by reactants and reaction conditions. Several experiments successfully showed that such kind of ordering can be achieved, but often only a fraction of the cluster layers exhibited a definite ordered structure.[18,34] Thus, near-field ordering is able to control the closer surrounding of a cluster, but there is essentially no control of long-range order because of the dynamics of the aggregation.[34] Sometimes a patterning of metal clusters is induced by a template which is removed later.[3] Films of clusters can be also generated by a Langmuir-Blodgett technique where one allows clusters to arrange themselves on a fluid medium; subsequently, they are transferred to a different substrate. With this approach well-ordered layers have been generated and characterized.[35] Having described possibilities for designing experimentally materials from clusters, we will next discuss the basic synthesis of clusters as such.

2.2 Experimental issues

Often a top-down strategy is used, where a bulk material is broken down into smaller pieces which then will be size selected, in contrast to a bottom-up strategy where clusters are assembled from smaller building blocks.[25] Various procedures have been pursued to synthesize clusters of definite sizes.[3,15,17,21] A common way to produce size selected clusters is to generate them in ultra high vacuum and select them by means of mass spectroscopy from a molecular beam.[22,36] The mass selection provides clusters of a well defined size and helps to investigate their properties. Unfortunately for practical purposes one needs to synthesize larger quantities which should be stable under standard conditions. This actually is the key issue for designing new materials. As discussed before attaching ligands to the surface is one possibility to produce chemically stable clusters besides immobilization by zeolites or polymers and other substances.[3,36] In the wet chemical approach which relies often on the reduction of transition metal precursors, the ligands have to be introduced as early as possible.[13-15] The wet chemical bottom-up cluster synthesis itself normally already involves coagulation and the arrangement of transition metal atoms has to come to halt at a certain step of the reaction.[14,15] Although most chemical synthesis routes mentioned here are developed to generate gold clusters, one can adapt them also to other transition metals.

Because gold is more stable under standard conditions, we will discuss gold clusters first here. First synthesis recipes for gold nano particles were introduced by Turkevich in 1951, where citrate was used to reduce $HAuCl_4$ in water, generating gold clusters with a diameter of about 20 nm with a rather loose shell of ligands.[37] The cluster synthesis of

$Au_{55}(PPh_3)_{12}Cl_6$ first reported by Schmid et al. in 1981 remained for a long time special because it was able to produce ligand covered clusters, which were claimed to be monodisperse and 1.4 nm in diameter.[3,19] The key aspect was to reduce with diborane the precursor molecule (Ph_3PAuCl) which already contains a bulky ligand, ready to shield the cluster.

A different kind of ligand was first introduced by Mulvaney and Giersig, who used thiols of varying chain lengths.[38] Using these thiol ligands Brust and Schiffrin designed a two phase synthesis generating gold clusters which are thermally stable and do not decompose in air.[13] The stability of these clusters is clearly an advantage because the ligated clusters can be repeatedly isolated and dissolved in organic solvents; also, thiols offer a route to functionalization. This two-phase synthesis uses a phase transfer catalyst, which transports the Au(III) species from the aqueous phase into the organic layer, where it is reduced by a boronhydride in the presence of the thiol.

$$m\mathrm{AuCl_4^-} + n\mathrm{RSH} + 3m\ \mathrm{e^-} \rightarrow 4m\mathrm{Cl^-} + \mathrm{Au_m(RSH)_n}$$

Here special advantage is taken of the strong Au-S bonds, which give the clusters their extraordinary stability.[13] Clusters produced by this synthesis route have a size range of 1–3 nm and the most abundant cluster sizes are in the range of 2.0–2.5 nm. It was found that cuboctahedral and icosahedral structures dominate. The size distribution is tunable by varying the thiol/gold ratio. For larger values of this ratio, clusters have a smaller average core size, similar as a fast addition of the reductant and cooled solution produces smaller clusters with a lower dispersity.[3] Thiol ligands have the further advantage that they can undergo place exchange reactions with other functionalized thiols.[26]

For small clusters, which are used for catalytic purposes, a fixation on a support is preferable for catalytic purposes as well as for stabilization. Often immobilized clusters are generated by distributing a highly mobile precursor species over the support, subsequently generating clusters from these precursor molecules. For instance, carbonylated Ir precursor molecules ($Ir_4(CO)_{12}$) were brought onto a TiO_2 support; then the CO molecules were removed by heating the sample to generate small supported Ir clusters.[39]

The characterization of clusters is somewhat tedious because most often one is not faced with a uniform material with just one compound, but rather with an ensemble of different sizes. Additional problems are that the compounds are not volatile and not very stable, and they do not exhibit a long-range crystalline order. Therefore, it is hard to produce monodisperse probes of a unique species. If metal clusters are stabilized on a support, one has only a low density of the interesting species. Therefore, the most common characterization technique is high resolution transmission electron microscopy (HRTEM);

with that technique, one is able to depict cluster cores and to determine rough the size distribution and the shape of the clusters.[3,13,40] For example, with HRTEM it was found that the truncated octahedral shape is dominant for alkanethiol protected gold clusters.[3] After the mean diameter of the cluster cores is determined the average number of atoms can be estimated as well. Other valuable information can be obtained by scanning tunneling microscopy (STM) and atomic force microscopy (AFM). Both techniques are essential for depicting the surface of the cluster in good resolution and to gain information about topologies of the clusters. Related to STM are tunneling current experiments on the conductivity of clusters to explore whether clusters have continuous bulk-like behavior or whether the quantum mechanical regime is already dominating for a given cluster size.[11] The oxidation states of the atoms comprising the cluster can be determined by measuring the core levels of the metals which are indicative of the charge, state, and the chemical environment (XANES).[41] Another important option for investigating smaller clusters in the non-scalable regime is EXAFS spectroscopy, which determines the environment of certain nuclei and provides average bond lengths, coordination numbers and hints regarding how many atomic shells are in the environment of the investigated atom. EXAFS determines all these quantities from an analysis of the fine structure pattern of absorbed x-rays at the absorption edge of certain elements. Such fine structure patterns originate from photoelectrons that are scattered back by surrounding atoms; these surrounding centers affect the absorption probabilities at certain photon energies.[42] As there are seldom monodisperse clusters one will only be able to determine averages over all different clusters in a given sample. Yet another approach to gain information about (small) clusters is to adsorb small molecules like CO or N_2 on the clusters and to investigate the changes in the vibrations of these molecules.[43-45] Also mass spectroscopy may be invoked to determine the nuclearity distributions and the compositions of clusters.[3] Mass spectroscopy is also a common tool for verifying the success of a synthesis and for determining the cluster size distribution generated by this specific synthesis.[15,46]

There exist several problems with the characterization of clusters or materials built from clusters. The size distributions and the non-uniformity cause problems for accurately determining geometries. Accurate methods like x-ray diffraction would need single crystals of a minimum size which are impossible to get, as the materials commonly are not uniform enough. For smaller clusters with a well defined nuclearity there exist such geometrical data. An example are large CO covered Ni-Pt clusters which crystallize well because they are a charged species with counter ions.[47] For even larger metal clusters, such as Au_{55}, no crystals suitable for x-ray diffraction could be obtained.[19] Other obstacles preventing the investigation of structures are non-uniformly distributed impurities. The

binding properties of ligands are also often unclear as is the chemical state of the ligand head group.[16] These are aspects where combining experimental and theoretical work seems most promising for generating new insight.

2.3 Transition metal clusters in theoretical chemistry

Accurate calculations of the electronic structure are essential for describing transition metal clusters as they need a good correlation treatment because of their mostly open d-shells, close lying states, and many valence electrons. For heavier atoms relativistic effects have to be taken into account as well. Electronic structure calculations become more complicated, the more electrons and nuclei are in a system. The computational costs increase therefore also with the number of atoms. From this, one can already see why calculations on transition metal clusters will be very demanding tasks for any *ab initio* based computational method. Luckily as discussed before clusters often have highly symmetric shapes which maybe used to cut down the computational effort. Therefore when accurate methods are employed highly symmetric models are often used, while when there is no symmetry assumed for the model mostly simplified methods are used on big clusters to save computational time. For smaller clusters, which have only some transition metal atoms, a description with highly accurate methods without symmetry constraints is possible but the computational effort increases rapidly with the atom count. The cluster sizes treatable by accurate methods vary of course with the chosen method, highly accurate multi-reference methods can treat about 5 atoms while modern density functional methods can describe clusters with up to 309 atoms.[48,49] Only force field approaches are capable of modeling very big clusters with thousands of atoms or disordered structures.

This shows already the first difficulty for a computational description of large transition metal clusters: finding a suitable model which is computationally feasible but still realistic enough to generate insights and understanding in clusters and their properties, e.g., a correct description of the electronic structure or magnetic moments. As for metal atoms, especially of heavy elements, methods are needed which include an accurate treatment of correlation, often density functional methods are used.[50] For those heavier atoms additionally a relativistic treatment of the electronic structure is essential for accuracy and is in many investigations introduced by means of a special description, which replaces core electrons by effective potentials.[50] These effective core potentials (ECPs) provide a standard route to include relativistic effects in calculations and are therefore widespread. In contrast, in the calculations of this thesis, a scalar relativistic all-electron

treatment has been employed, which gives more accurate results, but increases the computational effort; because of its complexity, this computational strategy is used less often than effective core potentials.

In addition, the complexity of the calculations increases when clusters with ligands are to be described. Ligands attached to the clusters usually have a lower symmetry than their adsorption site on the cluster. Pertinent questions address the number of ligands attached to the cluster, the charge of the ligands, steric effects among the ligands, and the potential role of weak interactions. Real ligands can often be replaced by a smaller model ligand.[16] A further problem to be addressed by computational models is, that clusters are often synthesized in a wet-chemical process which influences their properties while calculations are easiest to do on cluster "in vacuum". Another issue, that makes calculations more complicated, is that real clusters can have interactions with their neighbors, for example when synthesized in an array.

Actually there are solutions for all these computational problems but each single one complicates the calculation so that normally a selection for the desired model is made. One of these models are pure metal clusters in gas phase, which do not include any of the problems mentioned above. Accurate calculations of these clusters provide insights into the regimes of quantum size effects and where a scalable regime starts and how well this scaling compares to the bulk. Various studies investigating the size dependency of properties for different clusters exist for metals such as Pd or Au.[10,49,51] Here the scalable regime can be used to extrapolate the computed quantities and compare them to bulk values which gives hint to the quality of the results.

Typical ligands used experimentally for transition metal clusters are thiolates, phosphines, or CO. There are fewer theoretical investigations on ligated clusters and in these studies ligands are often simplified, as longer ligands increase computational costs and destroy symmetry of the cluster. An example for such a simplified representation of ligands is the replacement of a hydrocarbon chain by hydrogen atom or a methyl group for thiolate ligands in a study on $Au_{38}SH_{24}$.[16,52] An alternative strategy is to model the regions of the ligand which are farther away from the cluster by a force field approach, which is capable of handling organic systems in sufficient quality. This so-called QM/MM approach has also been tested on thiolate chains[53] and is addressed in a later chapter in this thesis. Another environment effect which can be cumbersome for computational modeling is the support for immobilization of clusters which often also has an effect on the electron structure and has to be included in the model as well. Such aspects are especially difficult to model, as most supports are a bulk material. There have been several attempts to include these effects into calculations. Clusters on support can be modeled by embedding them in

an environment of point charges or/and in a cluster model of a surface.[54] Also periodic models of clusters can be computed and help to improve insight.[55]

In this series of investigations to be reported, the focus shall be on cluster-ligand interactions in an accurate fashion, to expand the scarce knowledge in that area.

3 Computational Method

All calculations in this thesis were carried out with the parallel code PARAGAUSS[56,57] that is based on the LCGTO-FF-DF method (linear combination of Gauss-type orbitals fitting function density functional).[58] Distinguishing features of PARAGAUSS are the consequent parallel implementation of all demanding tasks, an efficient scalar relativistic treatment of heavy atoms, and various approaches for describing interactions of a system with its surrounding. These approaches include a quantum mechanics/molecular mechanics method (QM/MM),[59] a polarizable continuum model (PCM) to simulate solvent effects,[60] cluster embedding in an elastic polarizable environment (EPE),[54] and its extension covEPE to covalent substrates.[61] Another very important feature is the full utilization of symmetry in almost all procedures, which allows a speed-up of the calculations for symmetric species or models.[62]

In the following sections, the density functional method as well as a discussion of parameters used are presented. As mentioned before, treatment of heavy atoms such as palladium, iridium, and gold requires relativistic effects to be taken into account. Thus, inclusion of these effects in the density functional method applied will be briefly discussed (Section 3.1). Then some details of the used implementation of the density functional method will be discussed (Section 3.2). In Section 3.3, the evaluation of standard basis sets as well as basis sets in combination with relativistic effective core potentials will be described. In the last part of this chapter the concept of QM/MM methods will be presented (Section 3.4), as it has been used for ligated metal clusters.

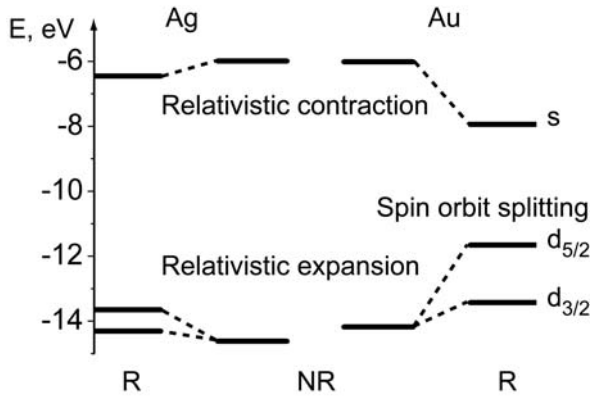

Figure 3.1. Valence levels of silver and gold atoms calculated nonrelativistically (NR) and relativistically (R). Adapted from Ref. 63; values from Dirac-Fock calculations (Ref. 64).

3.1 Relativistic Density Functional Method: The DKH Approach

3.1.1 Relativistic effects

Relativistic effects can formally be understood as all effects in the electronic structure and derived properties of atoms or molecules, which result from reducing the speed of light from an infinite to its finite value.[63] In quantum chemistry this implies a replacement of the non-relativistic Schrödinger equation by the relativistic Dirac equation.

Relativistic effects become substantial for elements starting even from a nuclear charge of about Z = 30.[63] Nevertheless, relativistic effects on the valence electrons are in general expected to be chemically important only for higher values of the nuclear charge; they become relevant for second-row transition metals ($Z \geq 39$) and are essential for a correct treatment of third-row transition metals and heavier elements. ($Z \geq 71$).

In chemistry three main effects are usually considered:[63] (i) the direct effects: *s* and *p* atomic orbitals are contracted and stabilized in energy, (ii) the indirect effects: *d* and *f* atomic orbitals expand and are destabilized, and (iii) spin-orbit interaction splits atomic levels with angular momentum $l > 0$ into two sub-shells with total angular momenta $j = l \pm ½$.[63] In Fig. 3.1, these effects are schematically illustrated for atomic gold and silver valence orbitals. From this figure it becomes clear that for gold only relativistic effects make it different from silver.[64] The spin-orbit splitting of valence orbitals can be comparable to chemical bond energies and in the case of the gold atom it is 1.7 eV for the 5d shell (compare Fig 3.1). Consideration of relativistic effects shows that many well-known properties of materials can only be explained within relativistic quantum

mechanics.[63] For instance the spectacular color of gold (Z = 79) is connected to relativistic effects.[63]

3.1.2 Relativistic density functional theory

In recent years, density functional (DF) methods have become quite popular and for many applications now form the standard approach, being more frequently used than the traditional wave-function based methods such as Hartree-Fock (HF), second-order Møller-Plesset perturbation theory (MP2), and configuration interaction (CI). For various chemical problems, DF methods furnish a sufficiently accurate, yet computationally efficient description of molecular structures and energetics.[65]

Within the DF approach the energy of a system is minimized with respect to variations of the electron density which forms the central quantity.[66] Hohenberg and Kohn proved that the electron density of the ground state of a system *uniquely* determines the ground state wave function and hence all properties of the ground state, in the presence of a static external potential.[67] The corresponding variational procedure is usually carried out by solving the Kohn-Sham (KS) equations, Eq. (3.1). These represent an one-electron problem governed by an effective potential ν_{eff} that comprises the (external) nuclear potential ν_{nuc}, the classical Coulomb or Hartree potential due to the electron-electron interaction ν_{coul}, and the exchange-correlation (xc) potential ν_{xc}, Eq. (3.3).[66,68]

$$\hat{h}_{KS}\psi_i = \varepsilon_i\psi_i \tag{3.1}$$

$$\hat{h}_{KS} = -\tfrac{1}{2}\nabla^2 + \nu_{eff} \tag{3.2}$$

$$\nu_{eff} = \nu_{nuc} + \nu_{ee} = \nu_{nuc} + \nu_{coul} + \nu_{xc} \tag{3.3}$$

In principle, the Kohn-Sham formalism allows one to solve the electronic structure problem exactly. However, the exact form of the exchange-correlation potential ν_{xc} is unknown. It includes quantum many particle effects of the electron-electron interaction beyond the classical Coulomb interaction of a charge density, and a part of the kinetic energy. Formally, ν_{xc} is given as the functional derivative of the corresponding exchange-correlation energy E_{xc} with respect to the density ρ, Eq. (3.4).

$$\nu_{xc}[\rho](\vec{r}) = \frac{\delta}{\delta\rho(\vec{r})} E_{xc}[\rho] \tag{3.4}$$

Different approximations are used to describe ν_{xc}.[65] The local density approximation (LDA) is derived from the homogenous electron gas and assumes that ν_{xc} is a simple

function of the density ρ.[65] The generalized gradient approximation (GGA) improves this approximation by taking into account the gradient of the electron density.[65] Hybrid functionals mix explicitly density-dependent parts of the GGA form and the exact non-local exchange energy of the KS determinant, using a fixed ratio.[65] In Section 3.3.2, the performance of LDA and GGA functionals will be discussed for representative cluster systems.

The relativistic analogue of the KS Hamiltonian, Eq. (3.2), is the Dirac-Kohn-Sham (DKS) Hamiltonian. However, solving the resulting DKS equation, Eq. (3.5), requires a notably larger computational effort due to the four-component nature of the solutions that are inherently complex-valued and describe positron as well as electron degrees of freedom.[69]

$$\hat{h}^{(4)}_{DKS}\psi^{(4)}_i = \varepsilon_i \psi^{(4)}_i \tag{3.5}$$

The Douglas-Kroll approach,[70] as worked out by Hess and collaborators for molecular systems (DKH)[71] and wave function based methods, affords a two-component variational DF formalism. The DKH transformation of the Hamiltonian in the DKS equation, Eq. (3.7), is used to decouple electron and positron degrees of freedom to second order in the effective one-electron potential of the KS theory.[69,72-74] This unitary transformation leads to the DK Hamiltonian, Eq. (3.8), decoupled to second order in v_{eff}/E_p, where E_p is the relativistic energy of a free particle of momentum p:

$$\hat{h}^{(4)}_{DKS} = c\vec{\alpha}\cdot\vec{p} + \beta c^2 + v_{eff} \tag{3.6}$$

$$\hat{h}^{(2)}_{DK2} = U\hat{h}^{(4)}_{DKS}U^{\dagger} \tag{3.7}$$

$$\hat{h}^{(2)}_{DK2} = E_p + v^{rel}_{nuc} + v^{rel}_{coul} + v^{rel}_{xc} \qquad E_p = c\sqrt{p^2 + c^2} \tag{3.8}$$

In the DFT context, the transformation as well as its application is restricted in most practical cases to the nuclear potential v_{nuc}, i.e. one approximates $U[v_{eff}] \approx U[v_{nuc}]$, Eq. (3.9).[75,76] The electron-electron (ee) interaction, comprising the Hartree potential v_{coul} and the exchange-correlation potential v_{xc}, are added afterwards in their nonrelativistic forms.

$$\hat{h}^{(2)}_{DK2} = E_p + v^{rel}_{nuc} + v_{coul} + v_{xc} \tag{3.9}$$

This Douglas-Kroll variant will be denoted as DKnuc method. The DKH formalism yields a scalar relativistic (SR) variant if one neglects spin-orbit (SO) interaction; otherwise, one arrives at a SO variant of the method.[77] Although the one-component SR method provides molecular structures and energetics that are often sufficiently accurate, an adequate treatment of SO interaction can be indispensable for open-shell problems involving heavy atoms. Especially effects on atomization energies can be significant

because the ground state configuration of many heavy element atoms is strongly affected by SO interaction.[78,79]

A more accurate method is achieved when the DKH transformation of the DKS equation is extended to include a self-consistent treatment of the electron-electron interaction (referred to as DKee).[76] This approach has been implemented for the Hartree potential based on $U[\nu_{eff}] \approx U[\nu_{nuc}, \nu_{coul}]$, leading to the Hamiltonian Eq. (3.10).[80]

$$\hat{h}_{DK2}^{(2)} = E_p + \nu_{nuc}^{rel} + \nu_{coul}^{rel} + \nu_{xc} \tag{3.10}$$

Screening of ν_{nuc} by ν_{coul} significantly improves the SO splitting of heavy atoms as well as g-tensor shifts in molecular systems.[76,81]

3.2 Computational Details

All calculations were carried out with the LCGTO-FF-DF (linear combination of Gaussian-type orbitals fitting function density functional) method[58] as implemented in the parallel code PARAGAUSS.[56,57] The relativistic density functional method applied is based on the second-order Douglas-Kroll-Hess (DKH) approach to the Dirac-Kohn-Sham problem (see Section 3.1.2)[72,74] Spin-polarized calculations were performed for all investigated systems either because the electron count was uneven (Cu_{13}, Au_{13}, Au_{55}) or the possibility of magnetic moments had to be considered (Ir_4, Pd_4).

The Kohn-Sham orbitals (see Section 3.1.2) were represented by flexible Gaussian-type basis sets, contracted in a generalized fashion using atomic eigenvectors from spin-averaged atomic LDA calculations in I_h symmetry. I_h symmetry is used in this context to have a separate irreducible representation for each angular momentum. The size of the primitive basis sets and the corresponding contracted basis is given in the notation (n_0s, n_1p, n_2d, n_3f) and [N_0s, N_1p, N_2d, N_3f], respectively. n_l and N_l denote the number of orbital exponents or contracted radial functions, respectively, which are associated with an angular momentum of *l*. The following basis sets were used: for Au (19s, 15p, 10d, 6f)[82] contracted to [9s, 8p, 5d, 2f], for Ir (21s, 17p, 12d, 7f)[83] contracted to [8s, 7p, 5d, 3f], for Pd (18s, 13p, 9d)[84] contracted to [7s, 6p, 4d], and for Cu (15s, 11p, 6d),[85,86] contracted to [6s, 4p, 3d]. The light atoms were described by standard basis sets:[87] (12s, 9p, 1d) → [6s, 5p, 1d] for Cl and P,[87a,b,d], (12s, 9p, 2d) → [6s, 5p, 2d] for S,[87c] (9s, 5p, 1d) → [5s, 4p, 1d] for C and O, [87b,d] and (6s, 1p) → [4s, 1p] for H. [87b,e] For the reasons of consistency with a previous study of H on Ir_4,[83] a second type of H basis (6s, 2p) → [3s, 2p][88] for this type of calculations was employed. The exponents and contractions of all basis sets are given in Appendix A.

In the LCGTO-FF-DF method, the classical Coulomb contribution to the electron-electron interaction is evaluated via an approximate representation of the electron density, using an auxiliary Gaussian-type basis set.[58] In this way computationally demanding four-center integrals can be efficiently avoided at the expense of three-center integrals only. The size of the auxiliary basis sets is specified by the notation (n_0s, n_1r^2, m_1p, m_2d, m_3f). The exponents of the corresponding s- and r^2-type "fitting functions" were constructed from the s- and p-functions of the orbital basis by scaling by a factor of 2.[58] For Au and Cu only every second p-exponent was used due to reasons of numerical stability. In addition, five p-, d-, and f-type "polarization exponents" were added on each center, each as geometric series with a progression factor of 2.5, starting with 0.1, 0.2, and 0.3 au, respectively (see Appendix A). Thus, the auxiliary charge density basis sets were (19s, $7r^2$, 5p, 5d, 5f) for Au, (20s, $17r^2$, 5p, 5d, 5f) for Ir, (18s, $13r^2$, 5p, 5d) for Pd, (15s, $5r^2$, 5p, 5d) for Cu, (12s, $9r^2$, 5p, 5d) for Cl, (12s, $9r^2$, 5p, 5d) for S, (12s, $9r^2$, 5p, 5d) for P, (9s, $5r^2$, 5p, 5d) for C and O, and (6s, $1r^2$, 5p) for all calculations involving H.

Throughout this work, a LDA functional as parameterized by Vosko, Wilk, and Nusair (VWN),[89] and a GGA functional as suggested by Becke and Perdew (BP) were used.[90,91] LDA often yields more accurate results for geometries and frequencies but overestimates binding energies,[92–94] whereas gradient-corrected functionals yield improved binding energies (Section 3.1.3).[95,96] Structures were optimized at the LDA level, invoking a quasi-Newton algorithm and analytical forces.[97] In view of the well-known overestimation of LDA binding energies, the GGA-BP functional was applied self-consistently to calculate binding energies at the LDA-optimized geometry. In the geometry optimizations, the total energy and elements of the density matrix were required to converge to 10^{-8} au; for the largest component of the displacement gradient vector and the update step length, the convergence criteria were set to 10^{-6} au. Ionization potentials and electron affinities were calculated by the ΔSCF approach calculating the species with one electron less and one more, respectively.

The grid for the numeric integration of the exchange-correlation functional was chosen as a superposition of atom-centered spherical grids.[98] This grid construction implies a Lebedev angular integration grid of order 19 (locally accurate up to angular momentum L = 19);[99-101] PARAGAUSS specific radial and angular grid parameters NRAD = 70 and NANG = 171 were used for all atoms, except for Ir_4H_2 species were throughout NANG = 231 was employed.[57] For typical complexes these grids comprise 20000 points for Ir, about 16000 points for the other metals (Au, Pd, Cu), 12000 for Cl, S, P, and 7000 for O, C, and H centers, respectively. For geometry optimizations the derivatives of weights of the grid points have to be taken into account to calculate the forces variationally. To make this

Table 3.1 Comparison of all-electron results for the Au_{13} cluster in O_h symmetry with different basis sets[b] and contractions to a relativistic small core pseudo potential.[a] Structures were optimized using the VWN functional, BP energies were evaluated in a single-point fashion. Binding energies per Au atom (BE) are given in kJ/mol, the average Au-Au distance is given in Å.

		Basis set			
	Pseudo potential[a]	[9.8.5.2][b]	[11.10.7.3][b]	(19s,15p,10d,6f)	(21s,17p,10d,7f)
BE VWN	261	284	286	286	275
BE BP	174	194	196	196	185
Au-Au	2.775	2.730	2.728	2.728	2.735

[a] Ref. 106 [b] Standard contractions from basis set (19s,15p,10d,6f)

derivative of the weights less complicated the grids keep their orientation in PARAGAUSS during the optimization. This can introduce small errors when molecules change their orientation during optimization or two molecules with different orientations are compared. An evaluation of the uncertainties introduced by the missing rotational invariance of the grid showed, that standard parameters for the angular part can lead to variations in binding energies of about 5 kJ/mol and of up to 0.04 Å in bond lengths in cases where soft degrees of freedom are present and the molecule is free to rotate. Therefore the number of grid points was increased for Ir_4 (Section 4.2) and some Pd_4 (Section 4.1) clusters to reduce these uncertainties where necessary.

3.3 Evaluation of methods

After briefly sketching fundamental aspects of how to model chemical systems by means of density functional methods, the accuracy of this approach will be discussed in this section, using typical examples. First basis sets will be explored, later the accuracy of evaluating the BP energy at VWN geometries will be tested and at last a comparison between relativistic effective core potentials and the scalar relativistic all-electron DKH method will be made.

3.3.1 Basis set contractions

An evaluation of the quality of the contraction of the basis set is necessary to estimate the accuracy of the results versus computational effort. For Pd, Cu and Au such comparisons have been done using the VWN functional for optimizations and a single point BP calculation at that geometry to evaluate energetics. For iridium a previously used

contraction has been employed that had been tested before.[83] Several tests have been done for the contractions, [9s, 8p, 5d, 2f] and [11s, 10p, 7d, 3f], compared to the uncontracted basis set on Au_{13} clusters to estimate the accuracy. Results are listed in Table 3.1.

For bare Au_{13} in O_h symmetry the deviation in binding energy per gold atom was 2 kJ/mol (or 1 %) and deviations in geometry were smaller than 0.005 Å when both contractions are compared. Nevertheless in this example using the smaller contraction lead to 30 % faster calculations. For the same cluster the variation from the larger contraction to the corresponding uncontracted basis set has been determined to be less than 1 kJ/mol in binding energy and at most 0.002 Å in one Au-Au bond length (cf. Table 3.1). When the uncontracted basis set used (19s, 15p, 10d, 6f) is compared to a larger uncontracted gold basis set of (21s, 17p, 10d, 7f) the interatomic distance for Au_{13} is accurate up to 0.005 Å and the gold binding energy per atom is overestimated by 4 %. When the cluster is covered with 8 SH ligands in bridged axial configuration in D_{4h} symmetry (cf. Figure 4.8 c) the deviation in binding energy per SH ligand between both contractions is 2 kJ/mol (or 1 %) as well and the maximum geometrical difference in bond lengths is below 0.005 Å.[102] For Cu_{13} clusters in O_h symmetry similar tests were made and the maximal deviation between the [6s, 4p, 3d] contraction used and the uncontracted basis set[85,86] was 2 kJ/mol (or 1%) in binding energy per Cu atom and 0.005 Å in the metal bonds. For Pd the cluster Pd_4 was probed with un- as well as the contracted basis set [7s, 6p, 4d].[84] A difference of 2 kJ/mol per atom (or 1 %) was found for the binding energy as well as a variation in the bond length of less than 0.001 Å. In general contractions used provide a considerable gain in computational efficiency with errors of about 5 kJ/mol per atom and less than 0.01 Å in bond lengths compared to calculations with the corresponding uncontracted basis sets.

3.3.2 Evaluation of exchange correlation functionals

Two different exchange-correlation functionals were tested to determine the most adequate description of metal cluster systems: an LDA functional as parameterized by Vosko, Wilk, and Nusair (VWN),[89] and a GGA functional as suggested by Becke and Perdew (BP).[90,91] As mentioned before, energetics were evaluated employing a GGA functional at geometries evaluated at the LDA level. However, as the LDA structure usually is slightly different from the GGA minimum, the “single-point’ GGA evaluation is somewhat inconsistent. Thus, for a more consistent treatment one can apply GGA functionals also for the optimizations, but one has to be aware that in general bond distances will be slightly overestimated.

Differences between these two strategies are usually small and may depend on the systems investigated. For instance, binding energies in gold coated nickel clusters differ by at most 5 kJ/mol per atom compared to full GGA calculations, i.e. about 2% of the absolute binding energy.[103] Similarly 32 Pd_4 clusters with an adsorbed heteroatom (C, O, or H) atom have been compared in this work. Table 3.2 shows the detailed results for binding energies evaluated by both approaches. As expected, VWN-BP binding energies are slightly underestimating the full BP results. Evidently the single-point strategy is more

Table 3.2 Differences in binding energies per atom between single point VWN – BP approach and pure BP optimization for various Pd_4X, X = H, C, O species. Designations are explained later in Section 4.1. Energies in kJ/mol.

		High symmetry				Low symmetry		
Impurity	Structure[a]	VWN/BP	BP	Δ	Isomer[a]	VWN/BP	BP	Δ
H	T	173	166	-7	T(T-B)	227	236	9
	B	296	296	0	T(T-H)	244	253	9
	H	273	273	0	T(H-T)	282	291	9
	C	232	230	-2	B(H-B)	283	292	8
	F	212	210	-1	B	295	303	8
					F	213	219	6
					F(F-C)	279	287	8
C	T	402	403	1	T	401	411	9
	B	559	560	1	H	632	643	11
	H	628	629	1	B	562	571	10
	C	609	608	-1	F	623	631	8
	F	625	625	0	F(F-C)	643	653	9
					CP	655	663	8
O	T	315	317	2	T	315	325	10
	B	365	367	3	H	358	361	2
	H	353	356	3	B	365	376	11
	C	165	167	2	F	197	209	12
	F	202	204	3				
AAD[b]				2				9

[a] T = Top, B = bridge, H = threefold (hollow), F = fourfold and C = central, CP = Complex

[b] Average of absolute deviations

reliable for highly symmetric species with an absolute average deviation of 2 kJ/mol. For lower symmetries as C_s and C_1 the deviation increases to 9 kJ/mol, which is still rather accurate. In lower symmetries there exist more degrees of freedom which allow stronger relaxation when one uses the BP86 functional self-consistently. The exception in the high symmetric case (-7 kJ/mol) of hydrogen bound in an on-top position derives from close lying electronic states, where different states are obtained depending on the functional used for optimization. The overall absolute average deviation in binding energy is 6 kJ/mol per adsorbed atom.

An example for better geometries is also easily found with Au_2 were the VWN geometry optimization finds 2.463 Å in good agreement with the experimental value of 2.472 Å,[104] while BP yields 2.522 Å which is 2 % off. The experimental binding energy per Au atom is 111 kJ/mol. The BP single point yields for this binding energy 109 kJ/mol while a optimization with BP gives 110. This is also a 1% deviation but such small energy differences as 1 kJ/mol are in general below the accuracy of the method, while geometries in general can be as accurate as 0.01 Å.[96] Thus, the approximate LDA-GGA approach can be applied with reasonable confidence.

3.3.3 Comparison of the scalar relativistic approach to ECPs

Most theoretical studies on gold clusters rely on effective core potentials to include relativistic effects.[16,50,51,53,105] A comparison has been done to evaluate the relative quality of results from both approaches. For that reason the Stuttgart relativistic small core pseudo potential with an (8s, 6p, 5d) uncontracted orbital basis set has been applied as it describes a relatively small core of 60 electrons by a pseudo potential; a tested fit basis set is available for the LCGTO-FF-DF method.[106] The Au atom, the dimer Au_2 and the cluster Au_{13} were selected for this comparison. A test with Au_{55} was unsuccessful as the relatively large orbital basis of the pseudo potential caused convergence problems which could only be resolved by making the basis smaller. As that would have caused an inconsistency among the Au basis sets, tests on Au_{55} have not been pursued any further.

First tests on the pseudo potential were done on ionization potential and electron affinity of the gold atom. In the IP ECPs deviate by 0.39 eV, and scalar relativistic results by 0.42 eV from the experimental value of 9.225 eV while for the EA pseudo potentials yield a 0.11 eV and the scalar relativistic method gives a 0.06 eV deviation from the experimental value of 2.308 eV. For Au_2 ECPs give a bond distance of 2.486 Å, the scalar relativistic result is 2.463 Å, while the experimental distance for the gold dimer is 2.472 Å.

Thus, both approaches are comparable in accuracy. Binding energies per atom for Au_2 are 99 kJ/mol evaluated with ECPs, 109 kJ/mol are found with the scalar relativistic approach, while the experimental value amounts to 111 kJ/mol.

Table 3.1 illustrates the results on Au_{13} of this comparison. The energetics show that the pseudo potential gives lower binding energies per Au atom for Au_{13} than any contraction of the orbital basis employed. Essentially 20 kJ/mol are missing from the binding energy per gold atom compared to contracted basis sets as well as the full orbital (19s, 15p, 10d, 6f) basis. These deviations for an Au cluster were considered too large to justify a strategy based on pseudo potentials. The nearest-neighbor distance Au-Au, 2.730 Å, obtained in a scalar relativistic treatment of Au_{13} with the [9s, 8p, 5d, 2f] contraction, deviated 0.045 Å from result obtained with the pseudo potential basis basis set, 2.775 Å. With the large uncontracted (21s, 17p, 10d, 7f) basis an average gold-gold distance of 2.735 Å is found, very close to other scalar relativistic results with a smaller basis set. Therefore, the scalar relativistic all-electron method was chosen for its better accuracy even though the required computer time was twice as long with the [9s, 8p, 5d, 2f] contraction. Overall the scalar relativistic all-electron treatment yields more accurate geometrical results and gives the possibility to improve the results by invoking more flexible basis sets. Another advantage is that, as mentioned before, one can avoid numerical instabilities that occur when one applies the uncontracted orbital basis of the pseudo potential in calculations on larger metal clusters.

3.4 The QM/MM approach

Accurate quantum chemistry methods are restricted to calculations on small to mid-size systems. Large molecular species, like complexes with bulky ligands occurring in homogeneous catalysis or biomolecules, still have to be treated either by a less accurate approach or a combination of quantum mechanical and molecular mechanics methods (QM/MM).[107–109] Combined approaches like the integrated molecular orbitals / molecular mechanics (IMOMM) method,[110] a QM/MM variant, have found widespread use for treating systems where only a small part has to be described with high accuracy and the remaining part of the system can be considered as an “environment”, exerting steric constraints or acting as a support. Typical examples of such systems are homogenous catalysts with bulky ligands,[111,112] metal centers of heterogeneous catalysts at oxide surfaces or in zeolites cavities,[113] self-assembled monolayers at gold surfaces,[53] solvated complexes,[114–116] and large molecules of biological interest.[117–119] The IMOMM method is

also well suitable for clusters with bulky ligands, which are very complex when described with quantum mechanical methods. Several interaction types of ligated transition metal clusters have to be treated on an accurate quantum chemical level, as there are metal–metal, and metal–ligand interactions, because these comprise a complicated electronic structure underneath. Simpler interactions such as nonbonding ligand–ligand (e.g., van-der-Waals interaction) and the ligands themselves can be easily treated with a force field method. The first applications of such a partitioning scheme to ligated metal clusters appeared only recently on $Cu_4(SCH_2CH_3)_2$[59] as well as on $Cu_{13}(SCH_2CH_3)_8$ clusters.[120]

In a QM/MM approach, one starts with partitioning a complex system *XY* into a "central" part *X*, treated by an accurate QM method, and its "environment" *Y*, described in an approximate way at a MM level. Correspondingly, one separates the total energy as

$$E(XY) = E_{\mathrm{QM}}(X) + E_{\mathrm{MM}}(Y) + E_{\mathrm{INT}}(X,Y) \tag{3.11}$$

In the IMOMM method,[110] one approximates the interaction energy $E_{\mathrm{INT}}(X,Y)$ between the two subsystems by its value at the lower level of accuracy (MM),

$$E_{\mathrm{INT}}(X,Y) \approx E_{\mathrm{INT}}^{appr}(X,Y) = E_{\mathrm{MM}}(XY) - E_{\mathrm{MM}}(X) - E_{\mathrm{MM}}(Y). \tag{3.12}$$

This results in an “extrapolation” or “difference” scheme:[109,110]

$$E(XY) \approx E_{appr}(XY) = E_{\mathrm{QM}}(X) + E_{\mathrm{MM}}(XY) - E_{\mathrm{MM}}(X) \tag{3.13}$$

For ligand-stabilized metal clusters one conveniently separates the system XY in the central part X, comprising the metal cluster and the ligand head groups, and the surrounding Y containing the rest of the ligand shell. Thus the boundary between QM and MM partitions of the system *XY* intersects covalent bonds (frontier bonds) of the ligands. It

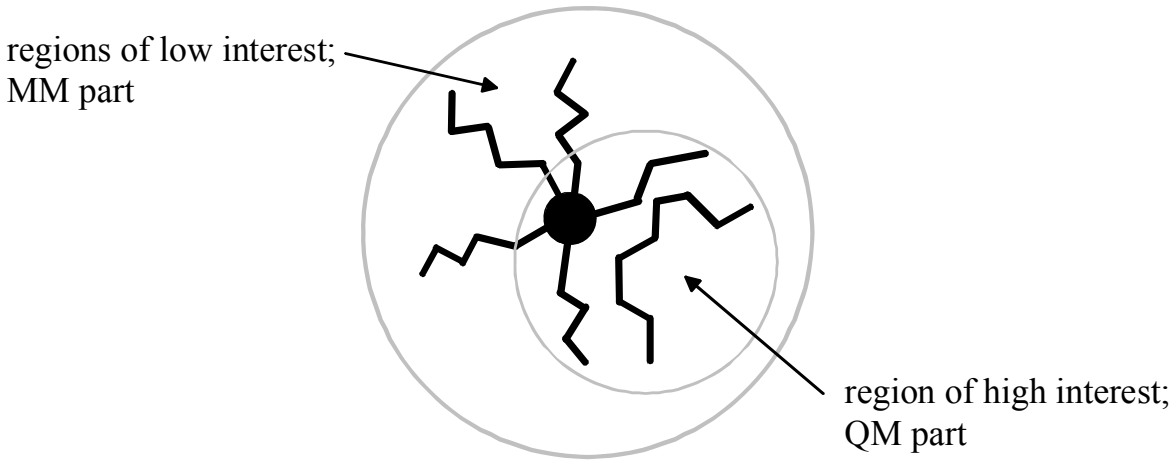

Figure 3.2 Partitioning a system into QM and MM part according to regions of interest

is customary to cap the resulting "dangling" bonds of the QM region by "link atoms",[121] which are conventionally chosen as hydrogen atoms. Different from the original approach,[110] the IMOMM implementation of PARAGAUSS[59] employed in this work constrains the location $\vec{R}_2$ of link atoms to lie in the direction of the corresponding frontier bond from an atom at $\vec{R}_1$ (QM side) to an atom at $\vec{R}_3$ (MM side), by applying a fixed scaling factor g:[122]

$$\vec{R}_2 = \vec{R}_1 + g\left(\vec{R}_3 - \vec{R}_1\right) \tag{3.14}$$

Alternatively, one may keep these link bonds at a fixed length. Both procedures yield very similar results if the various parameters are suitably chosen.[59] The approach described above has been applied in this work to various structural isomers of $Cu_{13}(SCH_2CH_3)_8$ (Section 4.4).

4 Results and Discussion

4.1 The impurities H, C, and O at Pd_4 clusters

4.1.1 Background

Palladium is widely used in industrial processes to activate hydrogen, thus there is considerable interest in understanding the catalytic activity of this element.[123,124] Palladium clusters are widely used in catalytic hydrogenation, oxidation, and reduction of hydrocarbons.[125,126] In a variety of experimental and theoretical studies, properties of Pd surfaces, supported Pd clusters, and Pd clusters in the gas phase have been reported.[126-132] On the other hand, definite information on the modification of Pd clusters by ligands or impurities is scarce.

The structure, electronic and magnetic properties of small metal clusters, either in the gas phase or on support, can be strongly affected by impurities. As mentioned in section 2, metal clusters can easily be contaminated by reactions of supported clusters with surface active sites (e.g. OH groups),[133,134] the decomposition of molecular ligands (e.g. CO) adsorbed on the metal moiety[135-137] or direct adsorption of small molecules from the gas phase.[138] From several computational studies it was concluded that supported metal clusters produced from carbonylated precursors are not free of heteroatoms.[133,134,136] Although impurity atoms can have a strong influence on the properties of metal clusters, experimental knowledge about the presence of heteroatoms and their influence on the clusters is very limited because controlled synthesis of such samples as well as spectroscopic studies present quite a challenge.[139] Scarcity of experimental information motivated theoretical model studies of small transition metal clusters interacting with impurities. Heteroatoms H, C, and O were modeled as impurities of M_4 clusters (M= Ni, Pt, Fe)[140-143] and of Ni_5;[144] furthermore, coordination of one and two hydrogen ligands was studied in detail for Ir_4.[83,145] These impurity atoms were selected not only for their

importance in gas-phase chemistry of size selected clusters, but also with regard to heterogeneous catalytic systems where supported transition metal clusters often are utilized as components of active multifunctional catalysts.[146,147] Various bonding situations have been determined for impurity atoms. In Ni_4H and Ni_4O the impurity atom adopts a two-fold coordinated position at an edge of the tetrahedral Ni_4 cluster.[140] Three structures were located for Ni_4C with carbon preferentially exhibiting four-fold coordination.[140] Hydrogen atom was determined to coordinate preferably in terminal fashion on Ir_4[83,145] and Pt_4.[141] On Fe_4 carbon is bound at a hollow site, while for oxygen it is advantageous to bind in bridge coordination.[142,143]

The present work focuses on how single impurity atoms affect the structure and other properties of the cluster Pd_4. As in similar studies,[140-143] hydrogen, carbon, and oxygen have been selected as heteroatoms as these main group elements are abundant in a variety of catalytic reactions, e.g., hydrogenation, oxidation or reduction.[148-150]. To contribute to the understanding of the effect of impurity atoms on small metal particles, preferred binding sites, bond distances, energetics, electronic structure of Pd_4 and also vibrational frequencies of normal modes have been determined. In particular, the latter information may help to identify the structure of such systems in comparison with experiment.

4.1.2 Methodological details

In all calculations, the elements of the density matrix were converged to at least 10^{-8} au in the SCF procedure. Geometries were considered to be converged when the maximum component of the energy gradient and the length of the optimization step had dropped below 10^{-5} au. The spin contamination S^2 was small for all investigated structures and deviation from the theoretical result was in all cases smaller than 0.04.

Ligand binding energies were calculated according to

$$E_b = E_{tot}[Pd_4] + E_{tot}[X] - E_{tot}[Pd_4X] \qquad (4.1)$$

The total energy of the most stable Pd_4 isomer was taken as a reference. Charges on atoms were evaluated with help of a Mulliken population analysis as well as by fitting the electrostatic potential (potential derived charges – PDCs).[151] Apparent variances introduced by the orientational independence of the grid were accepted as long as they translated to deviations in bond lengths lower than 0.005 Å, otherwise the angular grid parameter NANG was increased to 291.

The computational procedure was checked for Pd_2 by comparing calculated results with experimental data. The calculated binding energy, 131 kJ/mol, reproduces the

experimental value, 99±15,[152] with typical accuracy of GGA calculations.[96,153] The present computational result is close to that of other studies employing pure GGA functionals, 123–134 kJ/mol.[51,154-157] Hybrid DFT methods yield smaller values, 88 kJ/mol [158] and 93 kJ/mol, which agree better with experiment.[154] With the present computational approach, a bond length of 2.44 Å is obtained; this value is about 0.06 Å shorter than the results of other GGA optimization procedures, 2.48–2.56 Å.[51,154-157] In agreement with the lower value for the binding energy, longer Pd-Pd distances, 2.50 Å[158] and 2.53 Å,[154] resulted from hybrid DFT calculations. The Pd-Pd stretching frequency, 236 cm^{-1}, calculated in the present work slightly overestimates the experimental value, 210±10 cm^{-1}.[159] This is not unexpected as the calculated value for the binding energy is somewhat too high compared with experiment and the calculated bond distance seems somewhat too short.

For bare Pd_4 and impurity decorated clusters Pd_4X, calculations were started with highly symmetric structures; subsequently, these symmetry constraints were released as found necessary. To check for local minima of the potential energy hypersurface which would not be reachable when starting from high symmetry structures, the impurity atom was moved by ~0.05 Å from the "ideal" position of each complex towards each nearby binding site and optimization was re-started with the symmetry constraints reduced as appropriate. All local minima were confirmed by a normal mode analysis.

In th next section density functional results for Pd_4 and its interaction with impurity atoms H, C, and O will be presented. After examining the bare Pd_4 cluster as reference, the influence of the impurity atoms will be discussed.

4.1.3 Bare clusters

The bare Pd_4 cluster was found to be most stable in tetrahedral shape (Table 4.1).[48,51,123,126,148,149,154-158,160] As interaction with an impurity may induce a change of structure, also other arrangements were explored, besides tetrahedral (T_d) also square planar (D_{4h}), and rhombic (C_{2v}) structures, with subsequent reduction of these high symmetry constraints. To obtain the latter structure, an edge of the tetrahedron can be elongated, generating butterfly-like configurations, to reach finally a planar structure. With four atoms in one plane, the symmetry guided structure optimization described above is able to reach rhombic, rectangular, and quadratic isomers. Further opening of bonds ultimately leads to a linear arrangement.

Bare Pd_4 has often been studied computationally[48,51,123,126,148,149,154-158,160] and the discussion is started by commenting on these earlier results which are collected in

literature Table 4.1, sorted by the computational method used. All previous studies found a triplet ground state for the bare cluster Pd_4. Three studies obtained a regular,[48,155,156] all others slightly distorted tetrahedral structures in the ground state. Among all these investigations, individual bond distances vary from 2.51 Å to 2.78 Å. In general, bond lengths from GGA calculations were mostly shorter than those predicted by hybrid functionals. Ref. 155, which includes relativistic effects by a perturbation treatment, gave a Pd-Pd distance of 2.75 Å, a value at the experimental distance of bulk Pd, 2.748 Å.[51] As nearest-neighbor distances in metal clusters scale with cluster size,[161] this result does not seem reliable. A MRSDCI calculation also resulted in a long Pd-Pd bond distance, 2.69 Å.[48] In the present study, bond lengths from LDA calculations were shorter than those from GGA calculations, as one might have expected. Values of the binding energy range from 474 to 658 kJ/mol (Table 4.1). Concomitant with the shorter bond lengths of GGA results, BP values are larger than those obtained with other methods. (Only the present

Table 4.1 Comparison of computational results for the most stable isomers of Pd_4. Binding energies BE_t per cluster in kJ/mol, average <Pd-Pd> distance in Å .

Symmetry	Method[a]	Relativistic[b]	State[c]	BE_t	<Pd-Pd>	Ref
C_{2v}	HB-B3LYP	PP	$^3B_2$	481	2.66	154
C_s	HB-B3LYP	PP	$^3A''$	460[d]	2.66	148
C_s	HB-B3LYP	PP	$^3A''$	–	2.66	124
C_1	HB-B3LYP	PP	^3X	474	2.66	126
C_2	HB-B3PW91	PP	^3X	495	2.64	158
T_d	MRSDCI+Q	PP	$^3T_1$	543	2.69	48
C_s	PlW[e]-GGA-PW	PP	—	637	2.59	160
T_d	PlW[e]-GGA-PW	PP	^3X	646	2.61	156
T_d	GGA-BP	PT	^3X	658	2.75	155
D_{2d}	GGA-BP	PP	$^3A_2$	628	2.62	51
C_{2v}	GGA-BP	DK	^3X[f]	643	2.61	157
C_{2v}	GGA-BP	DK	$^3A_2$	639	2.61	This work
C_{2v}	LDA-VWN[g]	DK	$^3A_2$	631	2.55	This work

[a] HB= Hybrid SP=SinglePoint with BP; see Chapter 3, Computational Details
[b] PP = Pseudo potential, DK= Douglas-Kroll scalar relativistic
PT = relativistic effects included by first-order perturbation theory
[c] If the state was not reported, the multiplicity is given followed by X.
[d] ZPE corrected, ZPE amounts in this work to 20 kJ/mol
[e] PlW = Plane Wave
[f] No well separated ground state found
[g] Energetics from a single point BP calculation on VWN geometry

LDA results do not conform to this correlation.) As observed for Pd_2, hybrid methods yield a notably lower binding energy, compared to other methods. In three studies, two of which employ the B3LYP[124,148] method and a third one the PW functional,[160] the tetrahedrally shaped cluster in C_{2v} symmetry is described to undergo a distortion and stabilize in C_s symmetry. [124,148,160] Bond distances differ from a C_{2v} structure by 0.01 Å[160] and 0.11 Å[124,148], but are in two cases less than 0.01 Å[124,148] if a structure with C_{3v} symmetry is used as reference. Planar or linear geometries were never found as most favorable structure.

From the above comparison for Pd_4, the present computational approach is expected to yield shorter bond lengths and higher binding energies compared results from hybrid DFT studies. This investigation was started with tetrahedral shaped Pd_4 clusters. Reduction of symmetry from T_d down to C_{2v} symmetry is necessary because in T_d symmetry the highest-occupied spinorbital is three-fold degenerate, but occupied by only one electron; a Jahn-Teller distortion will result in a configuration of lower energy. Also a D_{2d} distorted tetrahedral structure was tested to compare with results in the literature.[51] Distorted tetrahedral shapes were found to be most favorable with binding energies BE_t (per cluster) of about 630 kJ/mol. The corresponding BE_t values of the square planar and rhombic structures were calculated smaller: ~70 and ~90 kJ/mol, respectively (Table 4.2). In agreement with other studies[51,124,126,148,154,157,158,160] a distorted tetrahedral structure was determined as ground state. Note, however, that the energy differences between the various distorted tetrahedral isomers are very small, at the accuracy limit of the computational method. After all, the tetrahedral shapes in D_{2d} and C_{2v} symmetry differ by ~0.01 Å in bond lengths and by less than 1 kJ/mol in the total (!) binding energy. A normal mode analysis confirmed the structures in D_{2d} and C_{2v} symmetry to represent local minima. In this case, these small deviations likely are related to different symmetry constraints and the implied orientation of the grid, rather than different isomers. All structures of quasi-tetrahedral shape exhibit a triplet state. Note that in Table 4.1 the C_{2v} results have been included for comparison with results of other studies.

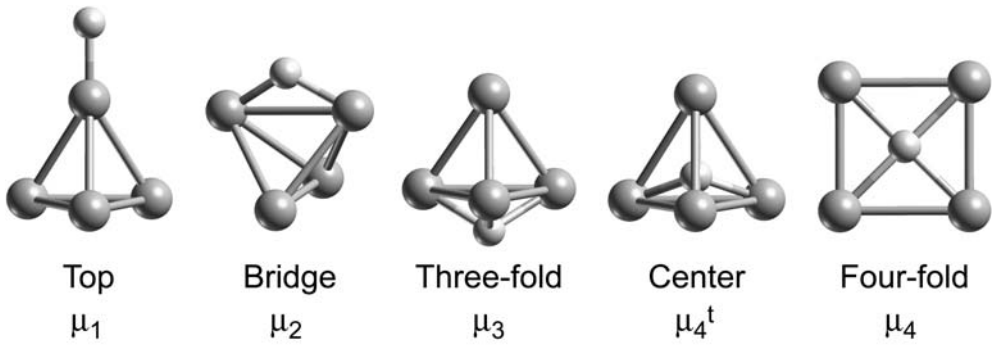

Figure 4.1 Investigated high-symmetry sites of impurity atoms H, C, and O on Pd_4: top (μ_1), bridge (μ_2), three-fold (μ_3) hollow, center (μ_4^t), four-fold (μ_4).

For the square planar and rhombic shapes, singlet states were found; the triplet states of these structures were 16 and 14 kJ/mol, respectively, higher in energy. A normal mode analysis revealed the rhombic structure with D_{2h} symmetry to be a transition state. The single imaginary frequency represented an out-of-plane motion of the tips of the rhombus. A search for a local minimum of butterfly type between the flat and tetrahedral stationary points the lead back to the C_{2v} distorted tetrahedral structure. Therefore, all three-dimensional structures of Pd_4, characterized in this work, are related to a tetrahedron. Note that with the BP functional one finds in all cases analogous structures, but with longer Pd-Pd distances, by about 0.07 Å.

The planar structures feature shorter average Pd-Pd distances, 2.42 and 2.50 Å, respectively, than the tetrahedral isomers, 2.55 Å (Table 4.2). This reflects the lower (average) coordination numbers of the atoms in the planar structures.[9,10]

Table 4.2 Calculated structures of Pd_4 and their properties: total binding energy BE_t per cluster (kJ/mol), average distance <Pd-Pd> (Å), average coordination number CN, not completely occupied orbitals OS,[a] multiplicity M, ionization potential IP, electron affinity EA, highest occupied (HOMO), and lowest unoccupied (LUMO) spin orbital (the latter data in eV).

Structure	Symmetry	BE_t	<Pd-Pd>	CN	OS[a]	M	IP	EA	HOMO	LUMO
tetrahedral	T_d	627	2.546	3	t_1^4	3	6.68	1.25	-4.14	-3.01
tetrahedral	C_{3v}[b]	628	2.551	3	e^2	3	6.76	1.23	-4.13	-3.08
tetrahedral	D_{2d}	630	2.547	3	e^2	3	6.73	1.22	-4.17	-4.13
tetrahedral	C_{2v}	631	2.546	3	$b_2^1b_1^1$	3	6.72	1.31	-4.16	-4.14
square planar	D_{4h}	562	2.424	2	−	1	7.33	1.64	-4.67	-4.36
rhombic	D_{2h}	543	2.498	2.5	−	1	7.42	1.86	-4.86	-4.50

[a] Kohn-Sham orbitals in order of increasing energies.

[b] Configuration fixed

Reducing the symmetry from T_d to C_{3v}, D_{2d}, or C_{2v} changes Pd-Pd distances by about 0.05 Å. This produces only very small splittings of the three-fold degenerate, highest occupied spin orbital that appears with T_d symmetry constraints: 0.04 eV (D_{2d}) and 0.02 eV (C_{2v}). Concomitantly, the values of the ionization potential (IP) and the electron affinity (EA) hardly vary (Table 4.2). For the most stable structure of Pd_4 the IP was calculated at 6.72 eV and EA at 1.31 eV. Planar structures show increased IP values, 7.33 and 7.42 eV, and EA values, 1.64 and 1.86 eV, for square and rhombic species, respectively. These larger values are in line with a stabilization of HOMO and LUMO levels.

4.1.4 Clusters with impurity atoms

4.1.4.1 High symmetry models

The discussion starts with the results for Pd_4 clusters with single H, C or O heteroatoms. In line with an analogous study of Ni_4,[140] these impurity atoms were first placed at high symmetry positions (see above), exploring one- to four-fold coordination (Fig. 4.1). One- to three-fold coordination was investigated for tetrahedral structures while four-fold coordination was examined for a square planar conformation. Structures have been labeled by the type of impurity coordination as μ_1 – top, μ_2 – bridge, μ_3 – hollow, μ_4 – four-fold and μ_4^t – central. First the effects of hydrogen at high-symmetry sites will be discussed, to be continued with carbon and oxygen. For each impurity atom the discussion of the properties starts with the outside coordination sites top, bridge, three-fold (hollow), and then turns to results for positions inside the cluster center and four-fold coordination.

Fig. 4.1 shows the optimized results for the coordination of ***hydrogen***. The quasi-tetrahedral shape of the metal moiety is conserved, when a hydrogen atom is coordinated outside the cluster. The structure with a singly coordinated hydrogen species is the least stable, with a binding energy of only 173 kJ/mol, whereas a binding energy of 286 kJ/mol was calculated for coordination at a bridge position (Table 4.3). Hydrogen with three-fold coordination is bound by 273 kJ/mol. Inspection of HOMO character and occupation shows that for top and three-fold coordination a Jahn-Teller distortion will occur whereas H at a bridge site should be stable with respect to symmetry reduction. Therefore, the most stable coordination at bridge site may represent an energy minimum.

The IP values decrease from top (7.33 eV) to three-fold (6.73 eV) coordination. The electron affinity is largest for top (1.99 eV), lowest (1.25 eV) for two-fold and for three-fold (1.37 eV) coordination slightly higher than at the bridge site. Most structures of Pd_4H

have a doublet electronic state. Only for H at the top site a quartet state was determined which is 145 kJ/mol more stable than the doublet and 135 kJ/mol more stable than the sextet. The size of the HOMO-LUMO gap does not show any obvious relationship with the coordination number of the heteroatom. It is 0.1 eV for one- and two-fold, but 1.1 eV for three-fold position. The charge of the hydrogen center from a Mulliken analysis varies from -0.1 e at the bridge site to 0 e at the top site to 0.2 e for three-fold coordination. To check this seemingly unsystematic behavior, potential-derived charges were calculated: -0.4 e for top coordination, -0.3 e for bridge and three-fold coordination. All potential-derived charges of H are negative. The corresponding errors of the fitted electrostatic potential can be quite large, up to 70 %, but the resulting values $q_{PDC}(H)$ appear to be reasonable.

Structures with hydrogen at the center of square or tetrahedral Pd_4, with binding energies of 212 and 232 kJ/mol, respectively, are less favorable than those with hydrogen coordinated outside. For coordination inside the metal moiety, Pd-H bonds are calculated rather short, 1.66 Å, when H is at the center of a tetrahedron, but rather long, 1.81 Å, when H is at the center of a square (Table 4.2). The short Pd-H bonds of H inside the tetrahedron can be considered to result of balancing the space requirements of the heteroatom and extending simultaneously six strong Pd-Pd bonds. Indeed, when hydrogen is placed inside the tetrahedron, the average Pd-Pd distance is the longest among all structures studied for Pd_4H, 2.71 Å. These differences in Pd-H distances of H inside square-planar and tetrahedral Pd_4 are connected to the available space inside these two geometrical bodies. The distance from the center to a corner of a tetrahedron is 61% of the length of an edge while for a square that fraction is 71%. Thus, the radius of a sphere at the center of a tetrahedron of four spheres is 11% of the edge length, whereas in the case of a square that fraction is 21%. Using the appropriate Pd-Pd distances from Table 4.2, one calculates a radius of 0.28 Å for a sphere at the center of tetrahedral Pd_4 and of 0.51 Å at the center of the square-planar Pd_4. This rationalizes nicely why Pd-Pd distances increase more when an impurity is placed inside a tetrahedron than in square-planar Pd_4. The same situation holds for all three kinds of impurity atoms (Table 4.3); especially for the larger impurity atoms C and O this model explains nicely the strong distortions of the Pd_4 framework. For hydrogen this increase in Pd-Pd distances is weakest, in line with the fact that is has the smallest atomic radius, 0.53 Å.[162] In fact, for four-fold coordination inside square-planar Pd_4, the average Pd-Pd distance is the same as for top coordination, 2.56 Å, only 0.01 Å longer than in the ground state of bare Pd_4 (Table 4.2). This nicely confirms the above consideration where one arrives at a sphere radius inside a square that essentially equals the atomic radius of hydrogen. The configuration indicates that for tetrahedral central coordination a

Jahn-Teller distortion will occur whereas H at a four-fold site of square-planar Pd_4 should be stable with respect to symmetry reduction.

For central and four-fold coordination IPs of 6.92 and 7.11 eV were determined; these values are similar to those calculated for H at a bridge position. Electron affinities are 1.60 eV for central coordination and 1.48 eV for H at a four-fold position in the center of square-planar Pd_4. The HOMO-LUMO gap is 0.3 eV for four-fold and 1.5 eV for central coordination. The Mulliken charge of H is -0.6 e for coordination inside the tetrahedral and 0.5 e for coordination inside the square planar Pd_4. The corresponding potential-derived charges are -0.4 and -0.3 e for central coordination inside a tetrahedron and a square, respectively. For central coordination inside a tetrahedron, both types of atomic charges assume the most negative values of all structures studied; in contrast, the H charge is the smallest (or even positive) for four-fold inside square-planar Pd_4.

From their electronic characteristics inside and outside coordinated complexes are not easily distinguishable by experiment. To decide whether a Pd_4 cluster has an impurity hydrogen adsorbed, the spin state may be the best indicator. IP and EA values of Pd_4 and Pd_4H are quite similar, except for the most likely bridge position where an increase in IP of 0.3 eV is predicted. A similar difference in IP is found for the inside coordinations, but these are not very stable.

Table 4.3 High symmetry models of hydrogen, carbon or oxygen as impurity atoms X on Pd_4. The binding energy BE are referenced to the most stable structure of bare Pd_4. Also shown are the symmetry, the multiplicity M, and the not completely occupied orbitals OS[a] as well as the ionization potential IP, the electron affinity EA, the direct HOMO-LUMO gap Δ, the Mulliken charge $q_M(X)$, the potential derived charge $q_{PDC}(X)$, the Pd-X distance, and the average distance <Pd-Pd>. Binding energies in kJ/mol, spectroscopic parameters in eV, bond lengths in Å.

	Site[b]	Sym.	BE	M	OS[a]	IP	EA	Δ	$q_M(X)$	$q_{PDC}(X)$	Pd-X	<Pd-Pd>
Pd_4H	μ_1	C_{3v}	173	4	$a_2^1a_1^1e^3$	7.33	1.99	0.11	0.00	-0.42	1.59	2.56
	μ_2[c]	C_{2v}	286	2	b_1^1	6.76	1.25	0.10	-0.07	-0.31	1.64	2.60
	μ_3	C_{3v}	273	2	e^3	6.73	1.37	1.06	0.23	-0.27	1.73	2.62
	μ_4^t	T_d	232	2	t_1^5	6.92	1.60	1.46	-0.56	-0.39	1.66	2.71
	μ_4	D_{4h}	212	2	a_{2g}^1	7.11	1.48	0.26	0.54	-0.27	1.81	2.56
Pd_4C	μ_1	C_{3v}	402	1	–	7.09	1.59	0.40	-0.24	-0.42	1.66	2.56
	μ_2	C_{2v}	559	1	–	7.05	1.64	0.51	-0.25	-0.81	1.78	2.66
	μ_3	C_{3v}	628	1	–	7.12	1.50	0.84	-0.43	-0.79	1.87	2.65
	μ_4^t	T_d	609	3	t_2^2	6.21	1.84	1.17	-1.04	-0.79	1.82	2.97
	μ_4	D_{4h}	625	3	e_u^2	6.76	1.83	1.22	-0.33	-0.94	1.89	2.67
Pd_4O	μ_1	C_{3v}	315	5	$a_2^1a_1^1e^2$	8.03	1.82	1.81	-0.29	-0.59	1.78	2.54
	μ_2	C_{2v}	365	3	$b_1^1b_2^1$	7.37	1.73	0.31	-0.39	-0.93	1.88	2.60
	μ_3	C_{3v}	353	3	e^2	7.23	1.49	0.67	-0.42	-0.61	1.97	2.66
	μ_4^t	T_d	165	3	t_2^4	6.33	1.70	0.37	-0.81	-0.63	1.91	3.11
	μ_4	D_{4h}	202	3	e_u^2	6.93	1.71	0.12	-0.68	-0.62	1.96	2.77
Pd_4		D_{4h}	563	1	–	7.33	1.64	0.31				2.42
		C_{2v}	631	3	$b_2^1b_1^1$	6.72	1.31	0.02				2.55

[a] Orbitals ordered from left to right according to increasing energy of spinorbitals.

[b] μ_1 = Top, μ_2 = bridge, μ_3 = three-fold (hollow), μ_4 = four-fold and μ_4^t = central.

[c] Angular integration grid accurate up to angular momentum l = 29, grid parameter NANG = 291; see Ref. 163.

Among the configurations studied, on-top is also the weakest bound position of a ***carbon*** atom. Overall, the interaction of C with Pd_4 is strongest. This can be seen that even C at a top site, with a binding energy of 402 kJ/mol, is more strongly bound than H or O atoms in their most favorable positions (Tab. 4.3). Unlike hydrogen the bridge position is the second weakest coordination site of carbon, bound by 559 kJ/mol. For three-fold coordination, the binding energy of carbon is calculated at 628 kJ/mol. Apparently, higher

coordination is quite favorable for a C atom as is to be expected from general bonding trends of carbon. Compared to the inter-metal bond strength of Pd_4, 105 kJ/mol per bond, the high binding energies indicate that there should be a strong influence on the Pd_4 cluster for any of the inspected impurities, but strongest for carbon.

Low and outside coordinated carbon atoms induce an ionization potential of about 7.1 eV. Compared to the IP of Pd_4 (C_{2v}) of 6.72 eV one- to three-fold coordination increases the ionization potential by ~0.4 eV. With ~1.6 eV the electron affinity of one- to three-fold coordinated carbon atoms is increased by 0.3 eV compared to the bare cluster. As for a hydrogen impurity, the HOMO-LUMO gap is quite large for three-fold coordination (0.84 eV). One- and two-fold coordination sites for carbon result in a gap of 0.4 eV to 0.5 eV. As small gaps go inline with higher reactivity the low coordinated species should be most active. The charge on carbon according to Mulliken is -0.25 e for one- and two-fold coordination and decreases to -0.4 e for three-fold. With potential-derived charges a top bound carbon is predicted to acquire -0.6 e, while two- and three-fold coordination results in a charge of -0.8 e. The Pd-C distance increases with the coordination number for outside coordination like in the case for hydrogen as impurity. For Pd-C top coordination yields 1.66 Å, bridge 1.78 Å, and three-fold 1.87 Å. Top has 2.56 Å, bridge 2.66 Å, three-fold 2.65 Å as average Pd-Pd bond length. While a top coordination of carbon has negligible influence on the average Pd-Pd bond length compared to the bare Pd_4 other outside coordination sites increase it by 0.1 Å.

A binding energy of 609 kJ/mol was calculated for coordination of carbon at a central position inside tetrahedral Pd_4; the binding energy at a four-fold central site, 625 kJ/mol, is similar to the value obtained for three-fold coordination. The electronic states indicate that carbon in a central position on tetrahedral Pd_4 is not stable with respect to a Jahn-Teller distortion: the adsorption complex of carbon inside the Pd_4 cluster features a triplet state which is an increase in multiplicity compared to outside coordinated carbon. This is unique among all other impurities investigated here. Pd_4 clusters with C in central positions have low ionization potentials of 6.21 eV and 6.76 eV for tetrahedral and square Pd_4, respectively. The IP of a complex with carbon at the center of a square planar Pd_4 is 0.5 eV smalleer than for bare the cluster Pd_4. The electron affinity is highest for carbon coordinated inside Pd_4 with ~1.8 eV. The HOMO-LUMO gap is large for these central coordinations of carbon (1.17 and 1.22 eV). The Mulliken charges of carbon inside tetrahedral Pd_4 are -1 e and -0.3 e for coordination inside square-planar Pd_4; the corresponding potential-derived charges are -0.8 and -0.9 e, respectively. The Pd-C distances of these complexes are 1.82 Å (tetrahedron) and 1.89 Å (square). The Pd-Pd bond length of square-planar Pd_4C is calculated at 2.67 Å. That distance increases to 2.97

Å in the tetrahedral structure; this value is very large, 0.4 Å longer than in tetrahedral Pd_4, even considerably larger than the experimental value of bulk Pd, 2.75 Å. A calculation of the metal framework alone shows that this structure is destabilized by 118 kJ/mol compared to the ground state in C_{2v}. This structure is mostly stabilized as four Pd atoms bind strongly to carbon. These strong Pd-C bonds hint to very stable structures if the Pd atoms can be arranged more favorably. This stability of high coordinated carbon came to no surprise since for carbon on Ni_4 a three- or four-fold coordinated place is also preferred in high symmetry.[140]

On top placement of ***oxygen*** produces a strong Pd-O binding energy of 315 kJ/mol. With 353 kJ/mol three-fold coordinated oxygen is nearly as strongly bound as in bridge position, where a binding energy of 365 kJ/mol was calculated. This is higher than the binding energy for hydrogen but nearly 200 kJ/mol less than for carbon. As for hydrogen the number of unpaired spins is increased in the case of on top coordination to 4 compared to 2 in other positions of the O impurity. The ionization potentials vary from 7.23 to 8.03 eV for outside impurity binding sites; it is largest for coordination on top. The EA values decrease from 1.82 to 1.49 eV with increasing coordination number of the impurity. The HOMO-LUMO gap is largest for top coordination, 1.81 eV, but only 0.3 and 0.7 eV for two- and three-fold coordination. The Mulliken charge of oxygen, -0.3 e, is the smallest (in absolute terms) for top coordination, more negative values result for higher coordination, up to -0.42 e for three-fold coordination.With -0.6 e, potential-derived charges are smallest (in absolute terms) for top and three-fold coordination; a more negative value results for bridge coordination, -0.9 e. The Pd-O distance increases linearly with coordination from 1.78 Å (topo) to 1.97 Å (three-fold). Correspondingly, for one- to three-fold coordination the average metal-metal distance increases from 2.54 Å to 2.66 Å.

Oxygen as impurity binds weakest in the central position, by only 165 kJ/mol, which is even weaker than hydrogen in on top position. In the four-fold position the O impurity is also weakly bound (202 kJ/mol). Partially filled degenerated orbitals will lead to a Jahn-Teller distortion in case of a central positioned oxygen impurity. For inside coordination the four-fold site has a higher IP (6.93 eV) and slightly increased EA (1.71 eV) compared to the central coordination with 6.33 and 1.70 eV, respectively. The HOMO-LUMO gap amounts to 0.37 eV for central and 0.12 eV for four-fold coordination inside Pd_4. For inside coordination more negative charges are calculated by Mulliken charges compared to outside coordination, while PDCs yield charges for inside coordinations comparable to oxygen at the three-fold site. With 1.91 and 1.96 Å, respectively, oxygen heteroatoms at tetrahedral and four-fold coordination in square planar Pd_4 have Pd-O distances between those calculated for two- and three-fold positions. The Pd-O bond for central coordination

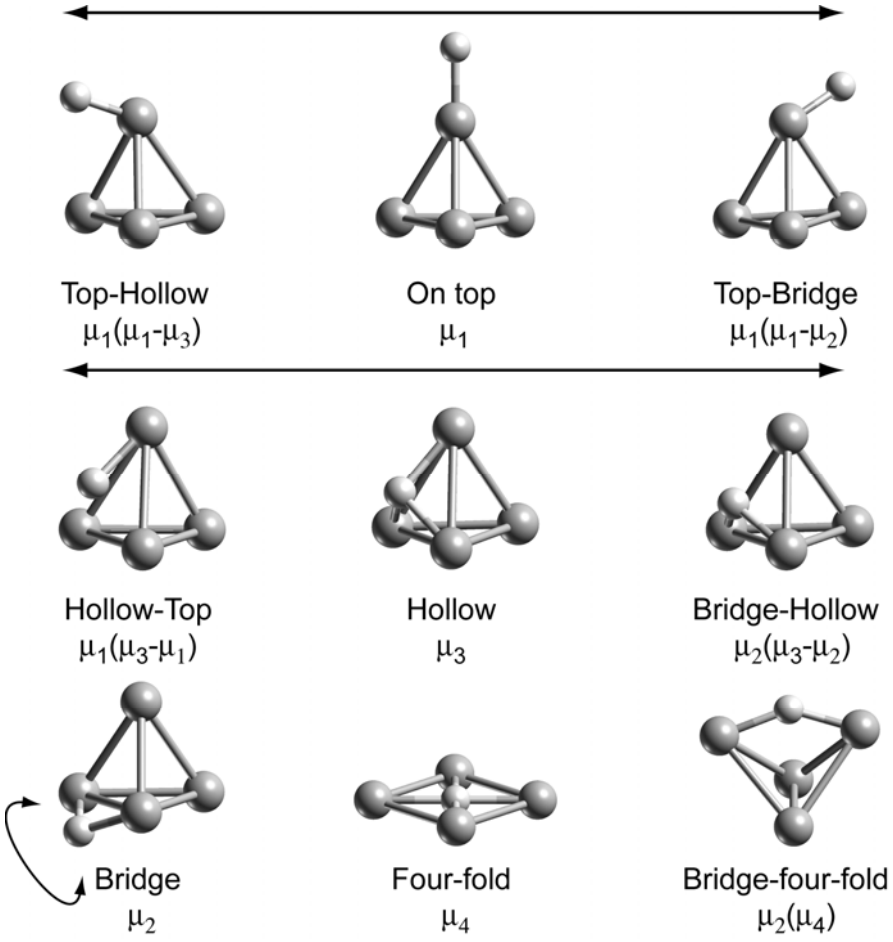

Figure 4.2. Distortions from high symmetry structures calculated for Pd_4H in C_s symmetry. The arrows depict the movement of the impurity toward the nearest highly symmetric coordination site.

is quite short when compared to three- or four-fold coordination; see the above discussion for hydrogen as heteroatom. The average Pd-Pd distances clearly reflect the bonding competition. The value of 3.11 Å for tetrahedral coordination is far from any realistic Pd-Pd bond distances: the tetrahedral hole is simply too small for oxygen.

Altogether the expected order of binding energies from C > O > H has been found. Compared to corresponding diatomics H_2, O_2, CO, it is found that molecular oxygen and hydrogen, with binding energies of 567 and 465 kJ/mol, respectively, can be cleaved by interaction with Pd_4 clusters. The cleavage of CO with a binding energy of 1092 kJ/mol (1083 kJ/mol from experiment) by Pd_4 clusters is unfavorable by 100 kJ/mol. The carbon-hydrogen bond as exemplified in the CH_4 molecule (473 kJ/mol) could also be broken by Pd_4. Thus, impurity binding energies on Pd_4 are strong enough to dissociate or at least activate various small molecules.

4.1.5 Low symmetric models

As a number of symmetric structures of Pd_4X revealed partially occupied degenerate HOMO orbitals (Table 4.3), the symmetry constraints have been released to allow distortions and to find lower lying minima. Most apparently this is interesting for hydrogen because three of the investigated complexes (with H at μ_1, μ_3, and μ_4^t sites) will undergo a Jahn-Teller distortion. For carbon distortions are expected for four-fold coordination, while Pd_4O in top, hollow and four-fold coordination features an e^2 open shell configuration which could lead to a Jahn-Teller distortion.

All complexes with an impurity at central coordination and a partially filled degenerate HOMO transformed changed into other coordination modes and will not be discussed further. Again hydrogen will be the first impurity discussed, followed by carbon and oxygen. Lowering of symmetry to C_s was used to facilitate locating stationary points.

For all stationary points a frequency calculation was performed and only structures which represent local energy minima are shown. Structures have been labeled by the type of impurity coordination as μ_1 – top, μ_2 – bridge, μ_3 – hollow, μ_4 – four-fold, and CP – complex-like. To distinguish structures of same coordination type resulting from different initial high symmetry structures also the starting coordination and the direction of distortion are indicated in parentheses, where necessary. Thus, $\mu_1(\mu_3–\mu_1)$ means a hollow starting site distorted in direction to the ideal top site, resulting in terminally coordinated geometry.

For ***hydrogen*** in ideal on top position the comparably low binding energy and the not completely filled degenerate HOMO of e type leads to a distortion that stabilizes this isomer. Interestingly the optimization in C_s symmetry resulted in configurations that can best be classified as intermediate between top and the next high symmetry sites, the bridge and the three-fold-hollow site. The change of the Pd-Pd-H angle from the ideal high symmetry site to the new intermediate site was in both cases more than 50° (Figure 4.2). None of these structures is more stable than the ideal bridge or hollow site. For $\mu_1(\mu_1\text{-}\mu_2)$ the binding energy of hydrogen increased by 54 kJ/mol to 227 kJ/mol, which is still 58 kJ/mol lower than the binding energy at bridge coordination.

Table 4.4 Low symmetry structures of Pd_4X. Binding energies BE are referenced to the most stable configuration of bare Pd_4, Additionally zero point energy corrected binding energy BE_0, multiplicity M, the not completely occupied orbitals OS[a], the direct HOMO-LUMO gap Δ, the Mulliken charge q(X), the Pd-X distance, and the average <Pd-Pd> distance are depicted. Binding energies are given in kJ/mol, the gap in eV, and lengths in Å.

Impurity	Isomer[b]	BE	BE_0[c]	M	OS[a]	Δ	q(X)	Pd-X	<Pd-Pd>
H	$\mu_1(\mu_1\text{-}\mu_2)$	227	200	2	$37a''^1$	0.26	-0.01	1.50	2.57
	$\mu_1(\mu_1\text{-}\mu_3)$	244	216	2	$37a''^1$	0.21	0.07	1.50	2.57
	$\mu_1(\mu_3\text{-}\mu_1)$	282	253	2	$37a''^1$	0.06	0.21	1.63/1.82	2.62
	$\mu_2(\mu_3\text{-}\mu_2)$	283	251	2	$56a'^1$	0.10	0.20	1.65/2.02	2.61
	μ_2[d]	286	252	2	$56a'^1$	0.10	0.01	1.64	2.60
	$\mu_2(\mu_4)$	279	249	2	$56a'^1$	0.10	0.18	1.61	2.58
	μ_4	213	188	2	$37a''^1$	0.26	0.54	1.81	2.55
C	μ_1	401	392	1	–	0.40	-0.24	1.66	2.56
	μ_2	562	551	1	–	0.49	-0.28	1.79	2.64
	μ_3	632	621	1	–	0.82	-0.42	1.87/1.87	2.65
	μ_4	623	612	3	$38a''^1\,58a'^1$	1.22	-0.34	1.89	2.67
	$\mu_4(\mu_4)$	643	631	1	–	0.42	-0.99	1.85/1.87	2.75
	CP	655	642	1	–	0.69	-0.68	1.87	2.56
O	μ_1	315	308	5	$37a''^1\,59a'^1\,38a''^1\,60a'^1$	1.79	-0.29	1.78	2.54
	μ_2	365	357	3	$38a''^1 59a'^1$	0.31	-0.39	1.88	2.60
	μ_3	358	350	3	$38a''^1\,59a'^1$	0.64	-0.44	1.94/1.96	2.68
	μ_4	197	190	3	$38a''^1\,59a'^1$	0.11	-0.68	1.96	2.77

[a] Orbitals ordered from left to right according to increasing energy of spinorbitals.

[b] μ_1 = Top, μ_2 = bridge, μ_3 = three-fold (hollow), μ_4 = four-fold and CP = Complex

[c] BE corrected by zero point energy

[d] Angular integration grid accurate up to angular momentum l = 29, grid parameter NANG = 291; see Ref. 163.

A frequency calculation yielded 2516, 970 (parallel to the bridge) and 926 cm^{-1} (perpendicular to the bridge) for mainly hydrogen (>98%) containing modes. This corresponds to a strong stretching mode and two nearly degenerated bending modes. In general, modes containing the motion of hydrogen were well separated from metal vibrations in all cases. The distortion towards the hollow coordination, structure $\mu_1(\mu_1\text{-}\mu_3)$

is stabilized even 17 kJ/mol more, to 244 kJ/mol. The gap increases for $\mu_1(\mu_1\text{-}\mu_3)$ by 0.10 eV and for $\mu_1(\mu_1\text{-}\mu_2)$ by 0.15 eV. In line with the stabilization, the Pd-H distance is shortened from 1.59 Å for ideal T to 1.50 Å for $\mu_1(\mu_1\text{-}\mu_2)$ and $\mu_1(\mu_1\text{-}\mu_3)$. The average metal bond lengths hardly change, by only 0.01 Å compared to the high symmetry configuration μ_1. For $\mu_1(\mu_1\text{-}\mu_3)$ there are three frequencies (2579, 1100, 1002 cm^{-1}; cf. Table 4.5) with strong contributions of hydrogen. When hydrogen is distorted from the ideal hollow position similarly as before two stationary points were found: one in the direction to the top site, $\mu_1(\mu_3\text{-}\mu_1)$, and one in the direction to the bridge site, $\mu_2(\mu_3\text{-}\mu_2)$. In both cases the binding energy is increased by about 10 kJ/mol to 282 kJ/mol for $\mu_1(\mu_3\text{-}\mu_1)$ and to 283 kJ/mol for $\mu_2(\mu_3\text{-}\mu_2)$ compared to the high symmetry three-fold site. The HOMO-LUMO gap is lowered to 0.06 and 0.10 eV for $\mu_1(\mu_3\text{-}\mu_1)$ and $\mu_2(\mu_3\text{-}\mu_2)$, respectively. With regard to energy and character, the corresponding HOMO and LUMO fit the corresponding e-set of the high symmetry structures. The three equivalent Pd-H bonds of the symmetric H site, 1.73 Å, are transformed to 1.63 Å and 1.82 Å (2x) for $\mu_1(\mu_3\text{-}\mu_1)$ and 2.02 and 1.65 Å (2x) for $\mu_2(\mu_3\text{-}\mu_2)$. From Figure 4.2 it is clearly visible that for $\mu_2(\mu_3\text{-}\mu_2)$ only the turning of H around the Pd-Pd bridge bond is missing to reach the C_{2v} symmetric bridge (μ_2) position. Nevertheless this rotation corresponds to an elongation of the distance of hydrogen to a third (apical) Pd atom from 2.02 Å for $\mu_2(\mu_3\text{-}\mu_2)$ to 2.99 Å for ideal bridge coordination. To confirm that these two structures are really different isomers, restricted geometry optimizations with different fixed angles around the bridged Pd-Pd bond have been performed to scan the energy profile for this rotation. Indeed a small barrier of ~10 kJ/mol (LDA) has been detected, when the hydrogen is 2.20 Å away from the apical Pd center. An indication of the different state of these two-fold coordinated structures gives the difference in the charge of H, which differs by 0.2 e. Additionally a changed energetical order of orbitals is found between the two isomers. Further evidence for different configurations is also provided by a detailed population analysis. When hydrogen moves from $\mu_2(\mu_3\text{-}\mu_2)$ to μ_2 coordination, the H contributions to several MOs change. For example the three orbitals below the HOMO with minority spin direction have smaller d populations (by 0.1) for the bridged Pd atoms and a corresponding increase in the other two Pd atoms when H is moved to the ideal bridge position. This indicates also a change of character of these orbitals which is in C_s symmetry not necessarily manifested in a change of the orbital label.

The average metal bond length is nearly invariant to this distortion; only for the isomer $\mu_2(\mu_3\text{-}\mu_2)$ there is a very small shortening of 0.01 Å. Vibrational frequencies with 99% of the kinetic energy on hydrogen are 2066, 2026 and 1153 cm^{-1} for $\mu_2(\mu_3\text{-}\mu_2)$ and

2041, 1632 and 1158 cm^{-1} for $\mu_1(\mu_3\text{-}\mu_1)$. Thus, the distorted bridge configuration has two nearly degenerate modes, while the ideal bridge has one higher frequency of 2200 cm^{-1}. The bridge site is the stationary point in the searched configuration space with the lowest energy among; it is a stable local minimum. On going to the low symmetry isomer, changes in all parameters from the high symmetry bridge configuration are small. The binding energy of hydrogen at the bridge site, 286 kJ/mol, is the same as the previously discussed bridge coordination of H in C_{2v}.[163] The Pd-H distance and the average metal distances remain unchanged. The three vibrational frequencies, at 2200, 2097, and 1188 cm^{-1}, represent modes which involve motion of hydrogen to more than 99%. The two modes with frequencies above 2000 cm^{-1} are a bending vibration parallel to and a stretching mode perpendicular to the bridge. This means that the C_{2v} symmetric structure represents the minimum.

Hydrogen in a square-planar Pd_4 cluster was also optimized in C_s symmetry, but there was essentially no change compared to that high-symmetry structure. Binding energy, gap and Pd-H distance remained the same; the average metal-metal distance was shortened by 0.01 Å. The relevant vibrational frequencies of hydrogen were calculated at 1690, 1689 and 766 cm^{-1} (Table 4.5), where the lowest value corresponds to an out-of-plane vibration. Lifting hydrogen out of the plane resulted in a nearly bridge-like conformation where the heteroatom is inserted into a Pd-Pd bond of a tetrahedron (cf. Figure 4.2, $\mu_2(\mu_4)$). This $\mu_2(\mu_4)$ coordination had a larger binding energy, by 66 kJ/mol; the HOMO-LUMO gap decreased to 0.1 eV and the charge of H was reduced to 0.18 e. The Pd-H bond lengths shortened considerably, to 1.61 Å, while the average Pd-Pd distance increased by 0.03 Å. Computed vibrational frequencies at 2302, 1480 and 1165 cm^{-1} had a hydrogen contribution of more than 98%. These values are far away from the frequencies which were calculated for bridge conformation μ_2 (Table 4.5). From the computed frequencies the zero point energy corrections could be evaluated. In general binding energies are lowered by 25 to 34 kJ/mol by zero point energy corrections. The zero point energy corrected binding energies BE_0 narrow the range for the energetically nearly degenerated structures of bridge or terminal hydrogen coordination type to 249 – 253 kJ/mol. When zero point corrections are applied the $\mu_1(\mu_3\text{-}\mu_1)$ structure turns out to be by 1 kJ/mol more stable than the ideal μ_2 site.

In summary, from the high-symmetry structures only bridge and four-fold coordination are confirmed to be local minima. All other structures were more or less affected by Jahn-Teller type distortions. Nevertheless, as for the symmetric models bridge coordination is confirmed by unrestricted calculations to be the most stable structure for

Pd_4H, but there are several almost degenerate isomers of this type (Table 4.4). For Ni_4H a bridge coordination has also been found to be the most stable one with a similar binding energy of 285 kJ/mol.[140]

From an orbital analysis of the high symmetry cases of Pd_4 with ***carbon*** as heteroatom one predicts that only the four-fold coordinated structures undergo a Jahn-Teller distortion. For Pd_4C isomers the very same series of low symmetry model calculations as with Pd_4H was carried out, beginning with the top coordinated structure. As expected, tilting of carbon is not favorable; the C_{3v} symmetric structure represents a local minimum, as confirmed by a normal mode analysis. The vibrational mode with the largest most contribution of carbond (~ 90%) is a stretching mode of 1027 cm^{-1}. Other modes (146, 144 cm^{-1}), which represent mainly carbon bending, have mixed contributions from Pd atoms and carbon (~60%). Also the effect of symmetry reduction on bridge coordinated carbon is small; the binding energy increases by 3 kJ/mol. Most parameters like HOMO energy and the average Pd-Pd bonds did not change at all. There are three vibrational modes with significant (> 76%) contribution of carbon, namely at 826, 715 and 209 cm^{-1}, which represent (asymmetric) in-bridge stretching, (symmetric) stretching, and bending perpendicular to bridge, respectively. The three-fold coordination showed a similar behavior. Distortions away from the ideal hollow site are small; a shift of 0.002 Å towards top position of carbon was calculated, which is below the numerical noise introduced by the grid as stated in the computational details (cf. above). The binding energy increased slightly, to 632 kJ/mol, while the charge of carbon and the average Pd-Pd distance remain at the same values as for the high-symmetry coordination site. The HOMO-LUMO gap was lowered by 0.02 eV. Thus, also in C_s symmetry three-fold coordinated carbon binds strongly. There are three normal modes with carbon contributions of ~90%; the corresponding frequencies are at 591, 601 and 696 cm^{-1}.

Carbon in the center of square-planar Pd_4 was found to be a stable minimum although it has an e^2 HOMO configuration in the high symmetry structure that could lead to a Jahn-Teller distortion. This can be rationalized if one assumes that the spin splitting is larger than the energy gain due to orbital stabilization upon symmetry reduction and spin pairing. Thus, symmetry reduction yields a degenerated set of spin orbitals a’ and a”, which originally formed the e set of orbitals. The binding energy remains essentially unchanged, and the structure keeps D_{4h} symmetry. The three vibrational modes with carbon contributions of at least 94% have frequencies of 762, 762 and 358 cm^{-1}. The degenerated set corresponds to motions within the plane of the metal framework while the remaining mode represents an out-of-plane motion.

Table 4.5 Vibrational frequencies of low symmetry structures of Pd_4X (in cm^{-1}). The nomral modes as classified as Pd-X if the impurity atom is mainly involved (> 50%), otherwise as Pd-Pd.

System	Isomer[a]	Pd-X	Pd-Pd
Pd_4			272, 153, 153, 149, 117, 110
Pd_4H	$\mu_1(\mu_1\text{-}\mu_2)$	2516, 970, 926	262, 196, 169, 158, 108, 98
	$\mu_1(\mu_1\text{-}\mu_3)$	2579, 1100, 1002	264, 197, 185, 153, 131, 98
	$\mu_1(\mu_3\text{-}\mu_1)$	2040, 1632, 1158	255, 191, 173, 132, 118, 102
	$\mu_2(\mu_3\text{-}\mu_2)$	2066, 2026, 1153	265, 203, 169, 156, 137, 131
	μ_2	2200, 2097, 1188	268, 211, 171, 170, 143, 130
	$\mu_2(\mu_4)$	2302, 1480, 1165	254, 176, 166, 164, 140, 103
	μ_4	1690, 1689, 766	238, 190, 190, 186, 110, 43
Pd_4C	μ_1	1027, 146, 144	272, 206, 204, 170, 109, 102
	μ_2	696, 601, 591	240, 169, 165, 141, 102, 93
	μ_3	826, 715, 209	251, 185, 165, 154, 117, 99
	μ_4	762, 762, 358	265, 169, 164, 164, 161, 14
	$\mu_4(\mu_4)$	872, 687, 665	257, 157, 133, 103, 75, 38
	CP	936, 672, 672	277, 194, 121, 75, 74, 49
Pd_4O	μ_1	761, 270, 99	187, 184, 176, 141, 140, 92
	μ_2	545, 442, 388	231, 166, 157, 136, 92, 89
	μ_3	630, 508, 212	253, 176, 147, 132, 121, 100
	μ_4	607, 607, 147	227, 154, 121, 121, 117, 57

[a] μ_1 = Top, μ_2 = bridge, μ_3 = three-fold (hollow), μ_4 = four-fold and CP = Complex

When the central carbon was moved outside the plane, another stable structure, $\mu_4(\mu_4)$, was found (Fig. 4.3a). It may be described as carbon inside a Pd_4 butterfly structure, but it is also topologically reminiscent of the $\mu_2(\mu_4)$ structure of Pd_4H. This structure $\mu_4(\mu_4)$ essentially obeys four bonding interactions to carbon, where one Pd-C bond is 1.85 Å long and the other three are 1.87 Å. These bonds to the impurity are slightly shortened, by 0.02 and 0.04 Å, when this $\mu_4(\mu_4)$ structure is compared to the simple μ_4 structure. The $\mu_4(\mu_4)$ structure can also be viewed as a complex of three-fold coordinated carbon, with a fourth Pd atom introduced coordinating at one plane of a three-fold pyramidal structure. Accordingly the average Pd-Pd distance is increased to 2.75 Å, with single Pd-Pd bond lengths being 2.72, 2.73 and 2.81 Å. Compared to the four-fold

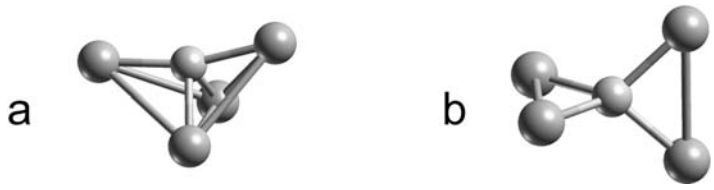

Figure 4.3. a) A bathtub conformation, found when lowering the symmetry for a carbon in a four-fold position on Pd_4C, Structure $\mu_4(\mu_4)$. b) The complex like isomer with two Pd_2 units attached to a central carbon, Structure CP.

coordination inside flat Pd_4 the binding energy is increased by 20 to 643 kJ/mol. The HOMO-LUMO gap is reduced to 0.42 eV and the heteroatom bears an electronic charge of -1 e, hence clearly represents a carbidic complex. The electronic structure is a singlet.

A more "complex-like" structure is also found for Pd_4C (Fig. 4.3b). This isomer has the largest binding energy, 655 kJ/mol, and it shows an larger gap, 0.69 eV, than the $\mu_4(\mu_4)$ isomer. The charge on the carbon atom is -0.68 e. The Pd-C distances are 1.87 Å; this value is comparable to distances in the $\mu_4(\mu_4)$ isomer. The average Pd-Pd distance is rather short, 2.56 Å, and comparable to terminal coordination. This can be rationalized by inspection of the structure (Fig. 4.3b) which exhibits a D_{2d} symmetry with two Pd dimers having a bond length of 2.56 Å, which is by 0.12 Å elongated compared to a Pd_2. The two Pd_2 units are coordinated side-on with perpendicular orientation relative to each other. This rather stable structure exhibits a singlet state. Vibrational modes with a carbon contribution of more than 92% are 936, 672 and 672 cm^{-1}, where modes with a frequency of 672 cm^{-1} are degenerate, moving the carbon atom parallel to a Pd dimer and perpendicular to the other one and vice versa. This structure represents the ground state for the Pd_4C molecule. Zero point energy corrections to the binding energy are essentially uniform for Pd_4C so that basically a shift of 9-13 kJ/mol results. For Ni_4C the a structure analogous to $\mu_4(\mu_4)$ has been found to be the ground state with a binding energy of 640 kJ/mol.[140]

As for the other two impurities the symmetry was also reduced for ***oxygen*** containing clusters and the stability was probed for the previously found stationary points determined with symmetry constraints. The high symmetry structures μ_1, μ_3 and μ_4 exhibit a half filled e orbital, while structure μ_4^t features an incompletely filled t set (Table 4.3). Thus, Jahn-Teller distortions can be expected. Top coordinated oxygen yields the same binding energy in C_s symmetry than before. Other properties are also quite comparable; see Tab 4.4. As with C_{3v} constraints, the configuration has 4 unpaired electrons forming a quintet. Interestingly the higher spin compared to other coordinations originates solely from the oxygen and the Pd atoms to which it is attached. Each of them carries one unpaired electron, based on a Mulliken analysis, while the remaining two Pd atoms carry about half

a spin each. As for carbon there is one impurity vibration with a high frequency 762 cm^{-1} (86% oxygen contribution). Other modes are considerable softer, with 99 and 92 cm^{-1} and O contributions of 64% and 48%, respectively. As for the high-symmetry model, oxygen bridging two Pd atoms remained the most favorable binding position with a binding energy of 365 kJ/mol, representing the ground state for Pd_4O. Also the other parameters did not change upon symmetry reduction. In the configuration now the HOMO (37 a''^2) is fully occupied, while two spin orbitals below stay without their filled counterparts, which are higher in energy than the HOMO level, and produce a triplet (Table 4.3, Table 4.4). Two vibrational modes at 630 and 508 cm^{-1} contain more than 86% contribution of oxygen, while a third mode of 212 cm^{-1} has a contribution of 57 % oxygen. The hollow coordination also turned out to be a stable stationary point when the symmetry was reduced. Compared to the corresponding high-symmetry structure μ_3 the binding energy increased by 5 kJ/mol to 358 kJ/mol. In C_s symmetry, the HOMO (e^2) of the high-symmetry model splits into two orbitals, separated by 0.01 eV, which indicates an admixture of another orbital. Some geometry distortion occurred; especially the oxygen is no longer coordinated in an ideal three-fold place. Oxygen is now closer to the Pd atoms and it is by 0.01 Å slightly shifted towards the top site. Accordingly the average metal-metal distance is increased by 0.02 Å. The vibrational modes with 545, 442 and 388 cm^{-1} exhibit major oxygen contributions (about 89%). The configuration is a triplet state as already seen for the higher symmetry C_{3v}.

The four-fold coordination inside square-planar Pd_4 is for oxygen similarly unfavorable as for hydrogen (Table 4.4). Properties, except the binding energy and the gap, remain unchanged upon symmetry reduction. The binding energy was slightly lowered, by 5 kJ/mol, and the gap decreased by 0.01 eV. The geometrical rearrangement was less than 0.004 Å, which is the increase in the Pd-Pd bonds. Such small changes mean that the structure should be regarded as D_{4h} symmetric structure. Two sets of degenerated spin orbitals are found in C_s symmetry which represent a mixture of the e- with the a_{2u}-orbital of the high-symmetry structure. The electronic structure represents a triplet state. The three normal modes with strong oxygen contributions (> 92 %) comprise a degenerate set at 607 cm^{-1} and a mode at 147 cm^{-1}. A distorted four-fold coordination was not found for Pd_4O. When applying a distortion from a four-fold place in the direction of a butterfly shape, the optimization went straight to the bridged structure. Thus, indeed in all cases where a Jahn-Teller type distortion can occur, the spin splitting remained the determining interaction and left the two corresponding spin orbitals nearly degenerated for all pertinent cases, which are top, hollow and four-fold coordination of oxygen. For oxygen the shifts by zero point energy corrections amount to 7-8 kJ/mol, so that no changes in the order of stability of

isomers occur. For Ni_4O a by 90 kJ/mol higher binding energy of 455 kJ/mol has been found for oxygen at a bridge site.[140]

Finally the results obtained in this work shall be compared to previous studies. Two other publications investigated a single carbon or hydrogen atom on Pd_4.[126,149] Bertani et al. found with the hybrid B3LYP functional and effective core potentials a bridge-coordinated hydrogen on Pd_4 as most favorable with a binding energy of 259 kJ/mol,[126] which is lower than the present finding (Table 4.4). Also the bond length of two times 1.66 Å compares well to the results of this work with a bond length of 1.63 Å and a binding energy of 294 kJ/mol (Table 4.4). These authors also presented results for Pd_4C where a complex like structure consisting of two Pd dimers connected by a central carbon has been obtained.[126] For this complex Pd-C bond lengths of 1.95 Å and a binding energy of 528 kJ/mol was found. The present scalar relativistic all-electron calculation for this isomer resulted also in a high binding energy of 655 kJ/mol and, concomitantly, a shorter bond length of 1.87 Å. Nevertheless, the real cluster-like structure of isomer $\mu_4(\mu_4)$ is only 11 kJ/mol higher in energy (Table 4.4).

The binding energies calculated in this work are higher than those reported with the hybrid B3LYP functional, where additionally thermal corrections were applied. Another study (with ECPs)[149] of Bertin et al. also employing a B3LYP functional found three-fold hollow coordination as the preferred site for hydrogen on Pd_4 with a binding energy per H of 272 kJ/mol compared to 262 kJ/mol found for the bridge site. This isomer had Pd-H distances of 2x 1.84 Å and 1.68 Å. This is close to the $\mu_1(\mu_3\text{-}\mu_1)$ isomer from this work which has very similar bond lengths and is also among the most stable isomers.

4.1.6 Conclusions

The properties of Pd_4 clusters were investigated with hydrogen, carbon and oxygen as typical impurity atoms which may occur under experimental conditions in catalytic reactions. A scalar relativistic all-electron approach was used to account for relativistic effects which are important in the second row of transition metals.[157] As a general strategy the configuration space was searched by first identifying stationary points of highly symmetric structures; subsequently, the symmetry was reduced and the structure of the systems was distorted to probe for lower lying minima in the neighborhood of the previously found stable geometries. Especially for hydrogen on Pd_4 this strategy produced a large variety of stationary points between the high symmetry sites. The most stable structure of Pd_4H is determined as a bridged configuration with C_{2v} symmetry with a

binding energy of 294 kJ/mol which is about two times the binding energy per Pd atom in Pd_4. For Pd_4C, several symmetric structures were classified as local minima. For the four-fold position a distorted butterfly was found with incorporated carbon as most stable cluster isomer with a binding energy of 643 kJ/mol, while also a complex-like structure as reported in the literature[126] was confirmed to be by 11 kJ/mol more stable. This structure consists of a carbon atom bridging two Pd dimers. For oxygen also several symmetric isomers were determined. Bridge coordination was calculated to be the most stable one with a binding energy of 365 kJ/mol and shows C_{2v} symmetry.

4.2 Two Hydrogen atoms on tetrairidium clusters

4.2.1 Background

The interaction of hydrogen with transition metals is of fundamental importance for heterogeneous catalysis.[164-166] The active species of dispersed transition metal catalysts are often small clusters. Their catalytic activity is related to properties, which differ from those of corresponding bulk metal or of low index metal surfaces, often studied in surface science. Like other metals of group 10, supported iridium clusters show great potential for various catalytic applications.[39,167–169]. Iridium clusters on different supports, like zeolites or metal oxides, act as heterogeneous catalysts in the transformations of hydrocarbons similarly as Pd clusters do.[39,167-169] On the one hand, hydrogen assumes a role as reactant, but could also be important as an impurity modifying the active metal species. Metal-metal bond distances of supported Ir clusters from EXAFS studies[39,167,168,170–172] were reported to be always longer than any calculated results for clusters in the gas phase or even on support.[133,173–174] One rationalization of this discrepancy implied, that light atoms such as H, C, or O are attached to the supported transition metal species active as catalysts, but are not easily detectable by experiments.[133,174,175] These impurities may occur during the preparation or usage of the catalyst.[176] Based on model systems, it has been demonstrated computationally that impurity atoms indeed elongate Ir-Ir bonds.[173] Another example for the effect of heteroatoms on supported metal clusters is a computational study on zeolite-supported Rh_6, where hydrogen atoms originating via reverse spillover due to interaction of the metal cluster with the hydroxyl groups of the support have been suggested as impurities.[133] Studying effects of impurity atoms on geometry, electronic structure, and chemical properties of small isolated metal particles thus is important for understanding at the atomic level heterogeneous catalysts that are based on finely dispersed supported metal species.[134,177,178] While comparable work on the interaction of two hydrogen atoms with metal clusters has been already done for several other metals, e.g. Al,[179] Fe,[180] Co,[180] Ni,[181,182] Cu,[149] Pd,[149,150] Rh,[183] and Pt,[184,185] investigations on Ir clusters and their compounds are scarce. Therefore in this chapter, the interaction of two hydrogen atoms with an isolated Ir_4 cluster will be examined continuing an earlier study of single hydrogen atoms coordinated to Ir_4.[83]

Recently, the cluster Ir_4 as well as its interaction with a single H atom was studied.[83] There, the most stable isomer of Ir_4 was found to exhibit a square-planar structure and a ground state with eight unpaired electrons, in agreement with an earlier computational result.[186] Experiments suggest tetrahedral Ir_4 to be preferred on supports;[39,172] in the gas

phase, that structure was calculated 49 kJ/mol less stable.[83] Other structures like distorted rhombus, butterfly or tetrahedral geometries were 45–90 kJ/mol less stable than the square planar alignment.[83] Optimization of H attached to various structures of Ir_4 leads to several stable minima with H coordinated in terminal or bridging fashion. Terminal H coordination leads to a strong binding energy of about 315 kJ/mol, which is comparable to the binding energy per Ir atom in the cluster Ir_4, 310–320 kJ/mol. Binding energies of bridge coordinated hydrogen atoms amount to 195–258 kJ/mol depending on the cluster structure underneath.[83] No species with higher coordination of the H ligand have been identified.[83] While a terminal coordination of hydrogen did not lead to any distortion for square planar species, some structures like a tetrahedral one were strongly deformed.[83] For most of the investigated structures the metal–ligand interaction energy is strong enough to allow a dissociative attachment of a hydrogen molecule to two such clusters. Most preferred structures were of type with H coordinated as in Figure 4.4. Bond lengths of H-Ir vary from 1.59 to 1.64 Å for top and 1.74 to 1.93 Å for bridge coordination of hydrogen. On the butterfly structure highly asymmetric bridges were found which might be better classified as pseudo top coordination because the smaller distances fall in the region of 1.67–1.68 Å, while a distance of 1.84–1.91 Å t a second Ir is found.[83] On square planar clusters, hydrogen coordination reduces the nonet multiplicity of Ir_4 to a quartet.[83] For tetrahedral or butterfly shaped clusters quartets and doublets are found as multiplicities.[83]

In the present study this earlier work on Ir_4H is extended to Ir_4H_2. This species is especially interesting because it allows a direct examination of the energetics of H_2 activation on a single Ir_4 cluster, an important reaction for Ir_4 as catalyst. After a brief discussion of computational details, a variety of isomers determined for Ir_4H_2 shall be described; the focus will be on the relative stability of the isomers and the modes of ligand coordination. First, different groups of Ir_4H_2 shall be classified and discussed according to geometric properties; then similar isomers will be compared in more detail.

4.2.2 Computational Details

The gradient-corrected exchange-correlation functional suggested by Becke and Perdew (BP)[90,91] was employed in a self-consistent fashion. Geometry optimizations have been converged until forces on atoms as well as the step size of the optimization procedure dropped below 10^{-6} au. Charges were assigned to the atomic centers by analyzing the electrostatic potential.[97,151]

Almost all structures inspected show a spin contamination of less than 1%. A single

exception is a structure where two hydrogen atoms are terminally coordinated to the same Ir center (Fig. 4.6b); there, the spin contamination of the singlet state is estimated at 10% on the basis of the Kohn-Sham determinant. The spin multiplicity of states has been checked by comparing to the energies of neighboring multiplicities, carrying out single-point calculations with fixed number of unpaired electrons at the ground state geometry. In cases where the total energy of these neighboring (spin) states differed by less than 15 kJ/mol, the geometry was relaxed in addition, to allow a more accurate comparison.

All structures have been confirmed as local minima of the potential energy surface by means of a normal mode analysis. For ease of calculation, the structures were pre-optimized with C_s symmetry constraints. If the bond distances of the relaxed structure differed by less than 0.001 Å from the corresponding values obtained with symmetry constraints, then the corresponding geometry was considered exhibiting a higher symmetry.

The (average) binding energy E_B of the hydrogen atoms to the cluster is defined as

$$E_B(H) = -[E(Ir_4H_2) - E(Ir_4) - 2\times E(H)]/2$$

and the energy, ΔE, of dissociative interaction of H_2 on Ir_4 as

$$\Delta E(H_2) = -[E(Ir_4H_2) - E(Ir_4) - E(H_2)]$$

The latter interaction energy has been corrected for zero point energies (ZPE). Positive values of E_B and ΔE indicate that coordination of H to Ir_4 or dissociative adsorption of H_2 on Ir_4 are exothermic processes, respectively. When comparing either type of energies, the most stable isomer of Ir_4 was used, the square-planar structure with a nonet ground state,[83] as reference.

4.2.3 Results and Discussions

Coordination of two hydrogen atoms to Ir_4 results in a large number of possible structures for the complexes Ir_4H_2. A bare Ir_4 cluster yields stable tetrahedral, rhombic and square topologies.[83] If one counts topologically different arrangements of two H atoms at topologically different structural motifs of the Ir_4 framework, one finds 15 structures for a tetrahedron, 24 for a rhombus, and 11 for a square-planar structure. In this listing, one- to four-fold coordination were considered, as well as coordination of one H atom inside a tetrahedral cluster. The rhombus structure, topologically equivalent to the butterfly, entails a rather large number of topologically different complexes because that metal framework

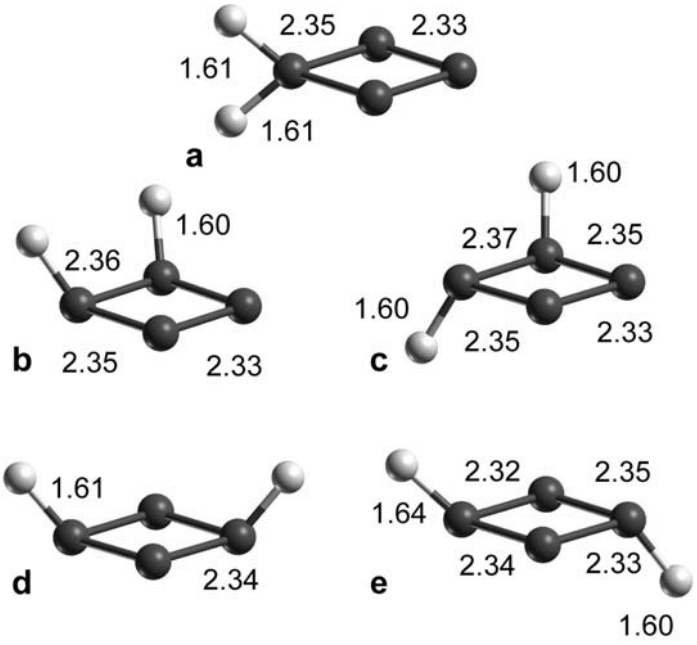

Figure 4.4 Structures and geometry parameters of square-planar isomers of Ir_4H_2: a) tts, b) ttn 1, c) ttn 2, d) tto 1, e) tto 2. For the labeling, see text.

exhibits Ir atoms with different coordination numbers, CN = 2 or 3. For many of these 50 different structures, also a number of orientational isomers are possible; hence, a complete survey of all structures obviously turns into a rather demanding task. Therefore, the focus was on low-coordinated sites of square-planar and butterfly-shaped Ir_4 (Figs. 4.4 and 4.6) because, with the results for Ir_4H in mind,[83] one expects to find the more stable isomers among these structures. In addition, H coordination to tetrahedral Ir_4 (Fig. 4.5) was inspected as these structures may provide reference species for supported Ir_4.[39,167-169]

To facilitate the discussion, a three-character short-hand notation will be used for the structural characterization of isomers of Ir_4H_2. The first two symbols denote the coordination mode of the two H atoms: t – top, b – bridge, h – hollow (three-fold coordinated). The third character indicates the relative arrangement of the two H coordination sites: s – both H atoms coordinate to the same Ir center, n – H atoms coordinate at neighboring Ir atoms, and o – other. In the latter case, the two H atoms coordinate to Ir atoms that are separated by a metal center which is not directly involved in H binding. In cases where for a given isomer of Ir_4 more than one structure with the same sites occupied by H ligands was found, consecutive numbering extended this labeling.

For H attachment to butterfly-shaped Ir_4, coordination of H to "outer" (CN = 2) or "inner" Ir atoms ("hinge", CN = 3) of the central bridge calls for further distinction. These two structural variants were labeled as o (outer site) and i (inner site), according to the adsorption sites in use. As an example for the full notation, the structure "tbn oi" (Fig. 3n)

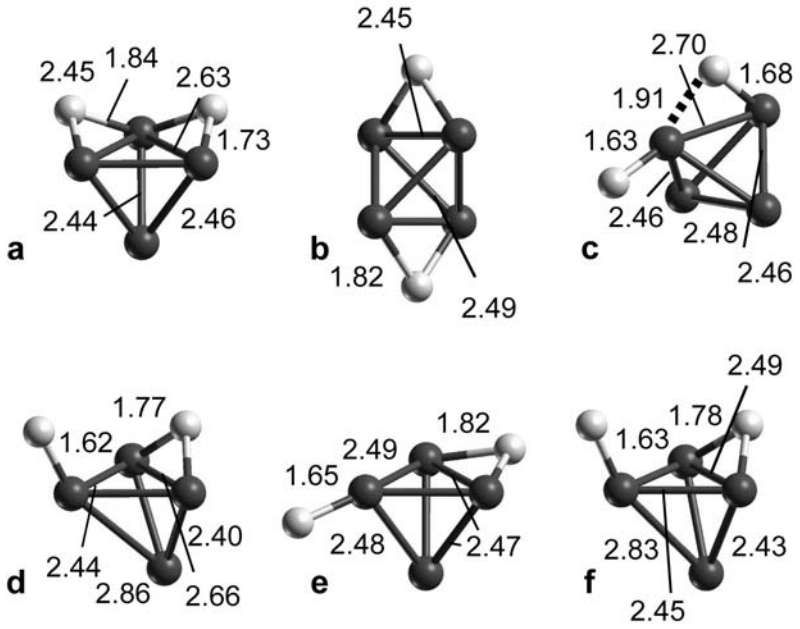

Figure 4.5 Structures and geometry parameters of tetrahedral isomers of Ir_4H_2: a) bbn, b) bbo, c) tbs, d) tbn 1, e) tbn 2, f) tbn 3. For the labeling, see text.

is mentioned. This label identifies a cluster where one H atom is singly coordinated and the other one is at a bridge position; the former H atom connects to an "outer" Ir (CN = 2) atom of the butterfly, while the latter one bridges the two "inner" Ir atoms (CN = 3).

The discussion is started with an overview of general trends and shall then be turned to a more detailed comparison between similar structures.

4.2.3.1 General trends

First, various coordination modes of two H atoms at the square-planar isomer of Ir_4 (Fig. 4.4) were examined as this type of cluster had been determined to be the most stable structure of Ir_4H, with the H atom coordinated in top position.[83] While several local minima with tt coordination of the two H atoms were obtained, no stable minimum was found for tb and bb structures. When optimizations were started from the structures tbn, bbn, and bbs, tt type minima resulted. This is in line with the findings for Ir_4H, where bridge coordination of H has been demonstrated to be a saddle point.[83]

For the butterfly isomer of Ir_4, this survey was restricted essentially to tt type structures (Fig. 4.6). For Ir_4H in butterfly structure, top coordination is more stable than bridging structures;[83] therefore, also for two H ligands, a tt coordination can be expected. To check this, also selected tbn structures were inspected (Fig. 4.6). For the tetrahedral structure of Ir_4 all possible coordination modes of H atoms on the cluster surface were

explored, but the position at the center of the tetrahedron was excluded because this latter case had been demonstrated to be unstable for Ir_4H.[83] Thus, six types of structures were distinguished for a tetrahedron, with tt, tb, th, bb, bh, and hh coordination of the two H atoms. All structures with three-fold coordinated H atoms (th, bh, and hh) evolved during optimization to structures with lower coordinated H atoms. The starting geometries th and bh resulted in tb structures. The structure hhn, the only meaningful one of hh type, deformed to a bb geometry. When the geometry optimization was started with a tt structure, the tetrahedron opened and yielded a butterfly (open tetrahedral) structure for the metal framework. In short, the tetrahedral structure of Ir_4 was found to be stable only for tb and bb coordination modes (Fig. 4.5).

Already a rough overview of Table 4.6 reveals that two hydrogen ligands prefer top coordination on the square-planar structures, with binding energies E_B per H of 312–318 kJ/mol, independent of structural details. Interestingly, this binding energy is essentially the same as that for the most stable isomer of Ir_4H,[83] where the H ligand is bound by 315 kJ/mol to square-shaped Ir_4 in top coordination. Thus, the binding capacity of Ir_4 is not affected by coordination of a single H atom and a second atom binds with about the same bond strength as the first one. For terminal coordination of H atoms (tt) on butterfly shaped Ir_4, slightly lower binding energies were calculated, ranging from 270 to 300 kJ/mol. This decrease of binding energy per H atom is partially due to a variation of the structure of Ir_4; the butterfly structure is ~75 kJ/mol less stable than the square-planar structure.[83] As the total energies of square-planar and butterfly shaped Ir_4H_2 tt species differ at most 96 kJ/mol, the conclusion is that the Ir-H bonds are of similar strength in both groups of structures. H binding energies per atom amount to 290–320 kJ/mol when a bare Ir_4 is taken as reference, which confirms the comparability.

tb isomers of butterfly shape on average are less stable. Their E_B values range from 249 to 271 kJ/mol per H atom (Table 4.6). For the 13 butterfly tt structures examined, an average binding energy per H atom of 288 kJ/mol was calculated. For butterfly tb isomers, the average E_B value for 7 isomers is 261 kJ/mol. A similar preference of terminal over bridging coordination was found for structures with a tetrahedral Ir_4 moiety. Tetrahedral tb isomers exhibit H binding energies of 268–302 kJ/mol, thus are of comparable stability as tt isomers of butterfly shape, whereas the corresponding bb isomers exhibit low E_B values of 273 and 264 kJ/mol.

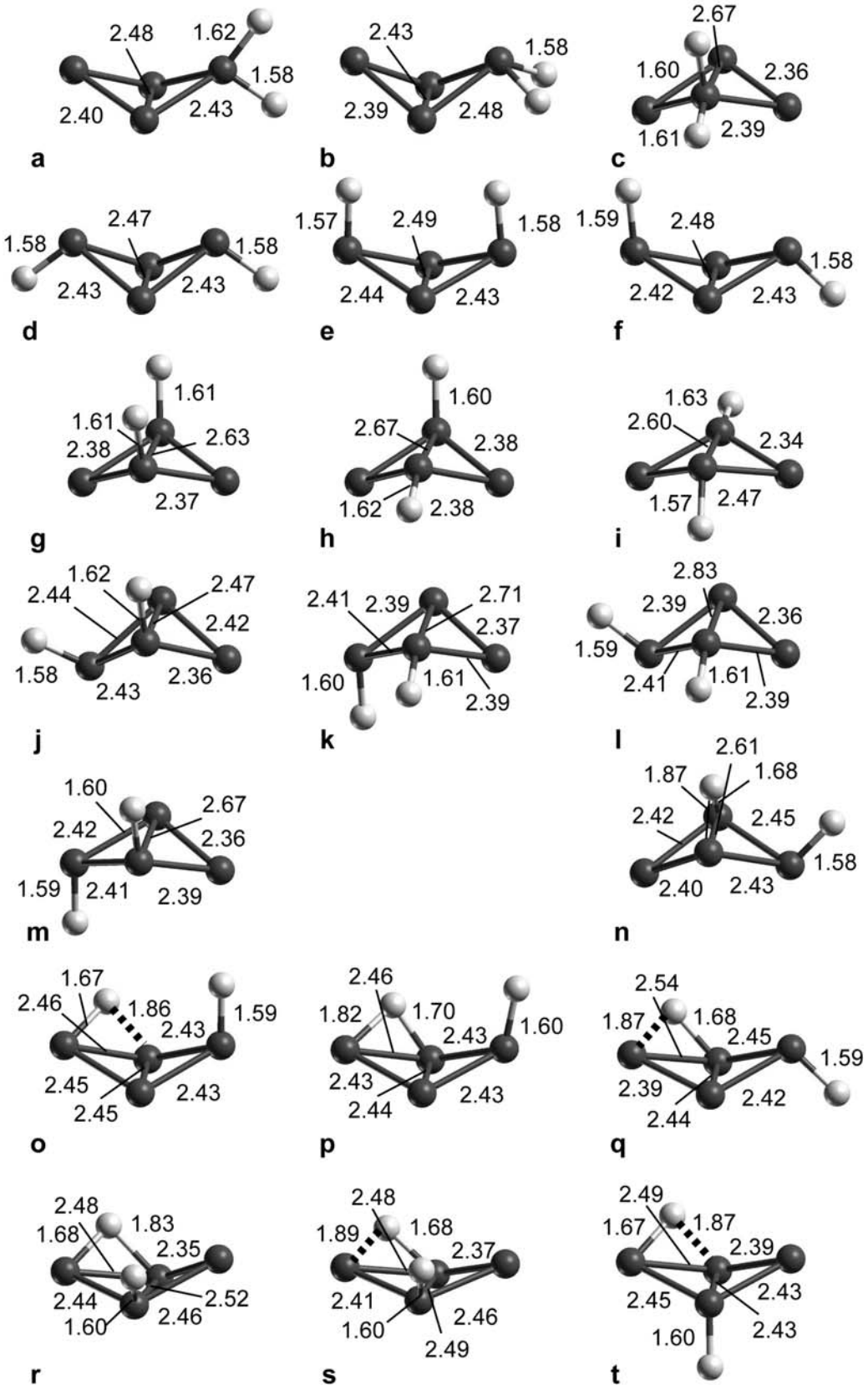

Figure 4.6 Structures and geometry parameters of butterfly-shaped isomers of Ir_4H_2: a) tts oo 1, b) tts oo 2, c) tts ii, d) tto oo 1 e) tto oo 2, f) tto oo 3, g) ttn ii 1, h) ttn ii 2, i) ttn ii 3, j) ttn io 1, k) ttn io 2, l) ttn io 3, m) ttn io 4, n) tbn oi, o) tbn oo 1, p) tbn oo 2, q) tbn oo 3, r) tbn io 1, s) tbn io 2 t) tbn io 3. For the labeling, see text.

Table 4.6 Calculated properties of isomers of Ir_4H_2: bond length H-Ir and average bond length Ir-Ir (Å), average binding energy[a] E_B per H atom, interaction energy[b] ΔE of dissociative H_2 adsorption (kJ/mol), direct HOMO-LUMO gap ε_{HL} (eV), electronic configuration[c] and term symbol. For the labels characterizing structures, see text.

Structure	Sym	H-Ir	Ir-Ir	E_B	ΔE	ε_{HL}	Configuration	State
square-planar								
tts	C_s	1.61, 1.61	2.34	316	166	0.40	$92a'^1\,93a'^1$	$^3A'$
ttn1	C_s	1.60, 1.60	2.35	312	157	0.29	$75a''^1 76a''^1 80a'^1 77a''^1$	$^5A''$
ttn2	C_1	1.60, 1.60	2.35	317	169	0.32	$154a^1 155a^1 156a^1 157a^1$	^5A
tto1	C_{2v}	1.61, 1.61	2.34	318	170	0.60	$40b_1^1\,93a_1^1$	$^3A'$
tto2	C_i	1.60, 1.60	2.34	316	165	0.25	$155a^1\,156a^1$	^3A
tetrahedral								
bbn	C_1	1.75, 1.80, 1.75, 1.80	2.52	273	85	0.47	$155a^1\,156a^1$	^3A
bbo	C_{2v}	1.82, 1.82, 1.82, 1.82	2.48	264	57	0.59	$54a_1^2$	$^1A_1$
tbs	C_s	1.63, 1.91, 1.68	2.51	302	136	0.77	$63a''^2$	$^1A'$
tbn1	C_1	1.62, 1.77, 1.77	2.53	275	86	0.32	$155a^1\,156a^1$	^3A
tbn2	C_1	1.65, 1.82, 1.82	2.48	282	98	0.69	$155a^2$	^1A
tbn3	C_s	1.63, 1.78, 1.78	2.51	268	74	0.20	$63a''^2$	$^1A'$
butterfly								
tts oo1	C_s	1.62, 1.58	2.43	285	106	0.51	$63a''^2$	$^1A'$
tts oo2	C_s	1.58, 1.58	2.44	270	73	0.57	$92a'^2$	$^1A'$
tts ii	C_s	1.61, 1.60	2.44	288	109	0.67	$92a'^1 64a''^1$	$^3A''$
tto oo1	C_s	1.58, 1.58	2.44	303	140	0.57	$63a''^2$	$^1A'$
tto oo2	C_s	1.57, 1.58	2.45	292	114	0.66	$63a''^2$	$^1A'$
tto oo3	C_1	1.58, 1.59	2.43	301	133	0.60	$155a^2$	^1A
ttn ii1	C_1	1.62, 1.62	2.41	283	100	0.44	$155a^2$	^1A
ttn ii2	C_s	1.61, 1.62	2.44	288	108	0.67	$92a'^1\,64a''^1$	$^3A''$
ttn ii3	C_s	1.63, 1.57	2.44	273	80	0.38	$92a'^1\,64a''^1$	$^3A''$
ttn io1	C_1	1.58, 1.62	2.43	289	111	0.54	$155a^2$	^1A
ttn io2	C_1	1.61, 1.60	2.45	292	116	0.48	$155a^1\,156a^1$	^3A
ttn io3	C_1	1.61, 1.59	2.47	297	126	0.27	$155a^1\,156a^1$	^3A
ttn io4	C_1	1.59, 1.60	2.45	284	99	0.41	$155a^1\,156a^1$	^3A
tbn oi	C_1	1.58, 1.68, 1.87	2.46	267	64	0.40	$155a^1\,156a^1$	^3A
tbn oo1	C_1	1.59, 1.67, 1.86	2.44	266	63	0.53	$155a^2$	^1A
tbn oo2	C_1	1.60, 1.70, 1.82	2.44	265	59	0.50	$155a^2$	^1A
tbn oo3	C_1	1.59, 1.68, 1.87	2.44	271	70	0.61	$155a^1\,156a^1$	^3A
tbn io1	C_1	1.62, 1.66, 1.86	2.47	250	29	0.40	$154a^1 155a^1 156a^1 157a^1$	^5A
tbn io2	C_1	1.60, 1.68, 189	2.44	249	25	0.45	$155a^1\,156a^1$	^3A
tbn io3	C_1	1.60, 1.67, 187	2.44	262	52	0.50	$155a^1\,156a^1$	^3A

[a] Relative to the square-planar (most stable) structure of Ir_4

[b] $\Delta E = E(Ir_4) + E(H_2) - E(HIr_4)$ is the reaction energy of $H_2Ir_4 \rightarrow Ir_4 + H_2$, corrected for the zero-point energy.

[c] The HOMO and partially occupied orbitals are shown.

The reactivity of Ir_4 with respect to molecular hydrogen is characterized by the energy ΔE of dissociative adsorption of H_2 (Table 4.6). First of all, this uptake reaction was found to be exothermic for all isomers inspected. For twofold terminal H coordination at the square-shaped cluster, the value of ΔE reaches 170 kJ/mol, whereas tt coordination at butterfly and tb coordination at tetrahedral structures are characterized by lower ΔE values of about 70–140 kJ/mol. The lowest ΔE values, 25–85 kJ/mol, were calculated for tetrahedral bb and butterfly tb isomers. This trend of ΔE values is trivially in line with the trend of H atom binding energies discussed above. Comparison with the most stable isomer of Ir_4H reveals[83] that the reactivity of Ir_4H is not lower than that of Ir_4. Dissociative coordination of H_2 is exothermic in either case, with interaction energies ΔE of ~85 kJ/mol per adsorbed H atom. Note that with Ir_4H as product two metal clusters are involved in dissociative adsorption of H_2.

Inspection of Ir-H bonds reveals that top coordination results in shorter bonds than determined for bridging ligands. For terminal H ligands, Ir-H bonds lengths are 1.57–1.63 Å. The shortest values, below 1.60 Å, were obtained for various butterfly structures and not for the most stable square-planar tt isomers (Table 4.6). This hints at a strong bond, which again confirms that the bond strengths of top-bound hydrogen atoms on butterfly and square-type structures are comparable. For bridging ligands on Ir_4, a wider range of longer interatomic distances, 1.66–1.91 Å, was determined. For tetrahedral isomers, symmetric (Fig. 4.5 b, d–f) as well as asymmetric (Fig. 2 a, c) two-fold coordination of H atoms was found. Asymmetric two-fold H coordination is related to the cases where one of the H atoms is bridging and the second H atom is bound to one of the Ir atoms involved in the bridge. In contrast, for butterfly type isomers, only asymmetric bridging H coordination was calculated (Fig. 4.6 n–t), where the shorter bonds are almost 1.70 Å and the longer ones ~1.85 Å. In this case, isomers where both H atoms are coordinated to the same Ir atom were not examined. An asymmetric bridging configuration was even obtained when the bridging H atom is coordinated to equivalent Ir atoms (Fig. 4.6 n).

Comparison to the structures of Ir_4H again corroborates the conclusion made above on the basis of interaction energies: the second H ligand exerts only a minor effect on Ir-H bond lengths. Also for Ir_4H, top-coordinated ligands feature bond lengths of 1.57–1.64 Å and asymmetric bridging geometries were obtained with very similar parameters (Ir-H on tetrahedron 1.74 and 1.83 Å, on butterfly about 1.67 and 1.84–1.91 Å) as for Ir_4H_2.[83] As already observed for bare Ir_4,[83] the average Ir-Ir bond length scales with the metal-metal coordination of the cluster, from ~2.35 Å for square planar isomers (CN = 2) to ~2.44 Å for butterfly structures (CN = 2.5) and ~2.48–2.53 Å for tetrahedral species (CN = 3).

Taking bare Ir_4 as reference, one does not notice strong effects of bonding competition as a consequence of the joint coordination of two H ligands. The average Ir-Ir bond of square-planar Ir_4 (2.36 Å) is even by 0.01 Å longer than that of corresponding Ir_4H_2 species. For the other two types of isomers, only a weak tendency to longer Ir-Ir distances was calculated (Table 4.6). Tetrahedral Ir_4 exhibits a metal-metal distance of 2.48 Å,[83] which increases to 2.48–2.53 Å in Ir_4H_2. For butterfly shaped isomers, the average Ir-Ir bond of Ir_4 is 2.41–2.43 Å[83] while 2.42–2.48 Å are obtained for Ir_4H_2. Thus, also on the basis of these geometric parameters, coordination of two H atoms to Ir_4 can be qualified as essentially independent of each other, accompanied by only small effects on the geometry of the Ir_4 cluster. This shows that essential features of Ir_4 survive when only two H atoms are coordinated.

Calculated vibrational frequencies of Ir_4H_2 complexes (Table 4.7) also follow the principal pattern, which was observed in the previous study of Ir_4H systems.[83] In almost all cases, vibrational modes are easily separated into H-Ir and Ir-Ir modes because for most isomers metal-metal vibrations are softer than modes involving H (Table 4.7) and do not mix with H-Ir modes. Also stretching and bending modes of the H ligands are easily separable (Table 4.7). However, it is not possible in some cases to assign the modes to one of the two ligands. Frequencies of H-Ir stretching vibrations of terminally coordinated H ligands were calculated between 2072 (square planar tts) and 2440 cm^{-1} (butterfly tbn io2). Independent of the cluster structure, most of these frequencies were found between 2200 and 2300 cm^{-1}. A larger spread of values is observed for the stretching modes of bridge coordinated H ligands. For tetrahedral bb and tb isomers, these frequencies were calculated between 1300 and 2100 cm^{-1}. Higher stretching frequencies were obtained for the bridging H ligands of butterfly tb isomers (2000–2250 cm^{-1}, Table 4.7). Stretching frequencies of more than 2000 cm^{-1} are typically found for asymmetric binding of two-fold coordinated H atoms. As these values are already close to the frequencies characteristic for terminally bound H atoms, asymmetric bridge coordination can also be classified as “quasi-terminal” coordination (Figs. 4.6 n–t). The H bending modes of tt isomers show typical frequencies in the range 300–800 cm^{-1}, while tb and bb isomers feature a bending mode of higher frequency, of 800–1300 cm^{-1}; structure tbn 3 is an exception (Table 4.7). These normal modes show a strong component parallel to the Ir-Ir bond that is being bridged by the adsorbate. Very soft modes, between 40 and 280 cm^{-1}, were calculated for the Ir_4 moiety of all species (Table 4.7).

In general, the number of unpaired spins of Ir_4H_2 is in line with the results for Ir_4H. In other words, addition of an H ligand may increase or decrease the number of unpaired electrons by one, compared to Ir_4H. Tetrahedral isomers feature singlet and triplet ground

states (Table 4.6), as follows from the doublet state determined for tetrahedral isomers of Ir_4H with a bridge coordinated ligand.[83] By the same token, quartet states of square-planar Ir_4H evolved to triplet or quintet states for Ir_4H_2. Isomers of Ir_4H_2 with butterfly structures were calculated to feature singlet and triplet ground states; only in a single case (tbn io1) a quintet state is adopted (Table 4.6).

Inspecting the spin states of different butterfly structures of Ir_4H_2 (Fig. 4.6), one notes that for tt isomers triplet states preferentially correspond to structures with long distances between the two central Ir atoms of the butterfly (CN = 3); Ir-Ir values typically are above 2.60 Å. In contrast, singlet states go along with shorter central Ir-Ir bonds of 2.43–2.49 Å. On the other hand, for isomers of tb type, no correlation between the length of the central Ir-Ir bond and spin multiplicity of the ground state could be detected. Different from the other structures, for butterfly type isomers, the number of unpaired electrons preferentially decreases compared to Ir_4H, which features doublet and quartet states for its various butterfly isomers.[83] An exception is the structures tbn io1, for which a quintet state was determined.

The various isomers of Ir_4H_2 exhibit direct HOMO-LUMO gaps, i.e. gaps between spin orbitals of same spin orientation, of 0.2–0.8 eV. Inspection of Table 4.6 does not seem to provide any correlation between the stability of the different isomers and the size of the HOMO-LUMO gap.

Potential-derived charges indicate that the transfer of electron density from the metal moiety to a hydrogen ligand is relatively local. Charges of H ligands vary between -0.3 and -0.6 e, independent of the ligand coordination. Ir atoms directly involved in Ir-H bonds carry positive charges of 0.2–0.6 e. Larger values were obtained when two H atoms were connect to a single Ir atom. Extreme values of Ir charges were determined for the tetrahedral isomer tbs and the butterfly tts, 0.8 and 0.9 e, respectively. Most Ir atoms not involved in ligand bonding show charges smaller than ±0.1 e; there are only a few cases where charges of ±0.2 e have been obtained. These results are again qualitatively similar to those previously obtained for Ir_4H.[83]

Overall, Ir_4 clusters with the same framework topology, but carrying one or two H ligands, do not differ in essential fashion regarding geometric and electronic characteristics. The second H atom of Ir_4H_2 is bound in much the same way as the (first) H atom of Ir_4H, with relatively little mutual influence.

Table 4.7 Vibrational frequencies of normal modes of various isomers of Ir_4H_2 (cm^{-1}). For the labels characterizing structures, see text.

Structure	H-Ir		Ir-Ir
	stretching	bending[a]	
square-planar			
tts	2072, 2113	314, 467, 486, 751	122–254
ttn1	2257, 2272	*295*, 574, 593, 648	99–246
ttn2	2247, 2265	*171*, 431, 544, 661	103–248
tto1	2184, 2261	401, 446, 487, 500	94–252
tto2	2244, 2257	377, 449, 575, 616	121–248
tetrahedral			
bbn	1305, 1330	451, 557, 752, 934	138–259
bbo	2090, 2119	701, 708, 769, 771	125–279
tbs	1692, 2247	484, 550, 617, 987	126–268
tbn1	1474, 2302	310, 480, 644, 837	77–255
tbn2	1677, 2267	401, 438, 630, 1101	64–278
tbn3	1797, 2215	293, 412, 513, 627	68–270
butterfly			
tts oo1	2148, 2262	285, 360, 518, 616	64–262
tts oo2	2228, 2228	262, 527, 588, 752	57–269
tts ii1	2182, 2220	387, 438, 537, 667	67–259
tto oo1	2253, 2291	*102*, *217*, 643, 804	73–258
tto oo2	2297, 2326	480, 512, 626, 677	54–251
tto oo3	2224, 2278	*241*, 606, 628, 784	68–255
ttn ii1	2241, 2268	*308*, 447, 514, 716	72–250
ttn ii2	2253, 2258	469, 526, 563, 619	61–254
ttn ii3	2260, 2306	389, 459, 535, 628	72–251
ttn io1	2255, 2283	419, 453, 561, 639	41–269
ttn io2	2202, 2263	390, 531, 564, 683	69–254
ttn io3	2255, 2281	494, 501, 633, 733	40–263
ttn io4	2254, 2268	438, 488, 695, 829	68–252
tbn oi	2036, 2200	393, 624, 815, 986	46–244
tbn oo1	2144, 2213	403, 526, 644, 914	62–254
tbn oo2	2168, 2199	369, 624, 651, 1293	67–257
tbn oo3	2156, 2212	372, 540, 674, 1330	71–254
tbn io1	2207, 2252	441, 532, 593, 1265	48–247
tbn io2	2247, 2440	428, 503, 662, 1162	65–249
tbn io3	2221, 2251	470, 561, 634, 1109	65–268

[a] Values in italics indicate admixtures of Ir modes with 20% or more.

4.2.3.2 Comparison of similar structures

The discussion of general trends will be followed by a more detailed inspection of each group of isomers with the same structure of the Ir_4 moiety and the same or similar modes of H coordination.

As discussed above, the most stable Ir_4H_2 isomers were found for the square-planar structure of Ir_4 with tt ligand coordination. However, it is somehow unexpected that all these isomers are essentially degenerate, with E_B values per H atom ranging from 312 to 318 kJ/mol, independently of the relative positions and orientations of the two H ligands (Fig. 4.4). Even when two H ligands share the same Ir center (isomer tts), no essential variation of stability or structure was found in comparison to species where the two H atoms are separated (isomers ttn or tto). This observation also holds when one compares isomers, which deviate only in ligand orientation, e.g. the pairs ttn1 and ttn2 or tto1 and tto2. Ir-Ir bond lengths, too, deviate only slightly from those calculated for the ideal square-planar Ir_4 frame, 2.36 Å,[83] and scatter at most 0.02 Å around the average values (Fig. 4.4). In line with a weak bonding competition, the longest Ir-Ir bonds of 2.36 and 2.37 Å are calculated for ttn1 and ttn2, respectively, for the Ir-Ir bond between H decorated Ir atoms. Also Ir-Ir-Ir angles remain rather unchanged, at 90±1°, with the strongest deviation of 1.5° obtained for the tts isomer. Thus, it is not surprising that the vibrational frequencies of the various square-planar isomers are similar as well (Table 4.7). However, the stretching frequencies of the square-planar isomer tts are by ~100 cm^{-1} lower compared to the corresponding frequencies of other square-planar tt isomers. This softening of the H-Ir stretching modes can be taken as a weak sign of bonding competition when two H atoms share the same Ir center. With regard to all other features, the binding of the two H ligands is independent.

For butterfly shaped isomers, as discussed above, binding energies E_B were lower than for the square-planar structures. Again, there seems to be essentially no bonding competition between the two H ligands. For tt isomers, similar H-Ir and average Ir-Ir bond lengths were calculated if the two H ligands are attached to the same (tts), neighboring (ttn) or distant (tto) centers of the metal moiety. Nevertheless, a rather weak trend to larger binding energies with increasing distance of H sites is found by averaging binding energies E_B of H atoms. For the three tto isomers, E_B values of 299 kJ/mol were calculated. Slightly lower values, 287 kJ/mol and 281 kJ/mol, are obtained when one averages over the seven ttn-type and the three tts-type butterfly structures, respectively. Interestingly, singlet ground states in most cases go along with short bond lengths for the inner Ir atoms of the butterfly framework (CN = 3), whereas these atoms are more separated in structures with a

triplet ground state (see above). Structure ttn ii1 does not conform with this trend (Figure 4.6 g). The length of the central "hinge" bond of butterfly tt isomers correlates also with the H coordination. If both H atoms coordinate to inner Ir atoms (isomers tt ii), this bond elongates, thus reducing the effective Ir-Ir coordination which then is favorable for the stabilization of a high-spin state. In line with this rationalization, singlet states are obtained for tt oo type structures whereas singlets and triplets are obtained for tt io isomers (Table 4.6). As obtained for isomers with a square-planar metal framework, the H-Ir stretching frequencies of butterfly structures exhibit a propensity to somewhat lower values when the two H ligands are coordinated to the same Ir atom (tts structures, Table 4.7).

The largest H binding energy E_B in the group of butterfly tbn isomers, 271 kJ/mol, was obtained for an oo-type structure (tb oo3, Table 4.6). Somewhat lower E_B values have been calculated for isomers where the terminal H ligand is attached to a "hinge" atom (tbn io). Singlet states were obtained for oo-type structures, with the exception of the most stable tbn-type structure tbn oo3, while io- and oi-type isomers show triplet and quintet states. Similar to Ir_4H with H in bridge coordination,[83] the bridging ligand binds in a notably asymmetric fashion (Table 4.6). Interestingly, two such structures could be identified, where short and long Ir-H bridge bonds are interchanged between two separate minima (tbn oo1 and oo2, Figs. 4.6 o and 4.6 p; tbn io1 and io2, Figs. 4.6 r and 4.6 s). Thus, variation of the orientation of H ligands will lead to even more stable or meta-stable minima than examined in the present work. In all other aspects, the isomers of butterfly tb type are remarkably similar. Also, H bridging of the two three-fold coordinated inner Ir atoms or of an inner and outer Ir atom, does not induce any characteristic differences in geometry, energy, or electronic structure. Only the stretching frequencies are somewhat lower for coordination at inner bridge atoms; cf. tbn oi to other tbn structures (Table 4.7).

Finally, the tetrahedral isomers are discussed, where only tb and bb type structures have been found to be stable. Concomitant with the preference for terminally coordinated H ligands, tb structures are on average more stable than bb structures with E_B values of 282 kJ/mol and 269 kJ/mol, respectively. It is somewhat unexpected that the tbs structure (Fig. 4.5 c) with E_B = 302 kJ/mol is more stable than the three other complexes with tbn coordination, although in that case both H atoms are coordinated effectively at a single Ir center. On the other hand, the bridging H ligand forms the most asymmetric bridge found for all isomers, with the long Ir-H contact at 1.91 Å (Table 4.6). This strongly asymmetric bridging geometry leads to an effective terminal coordination of both H ligands, which rationalizes the relatively high stability of this isomer. Most of the other bridging H arrangements on the tetrahedral cluster are symmetrical. Isomers tbn 1 and tbn 3 form an interesting pair of structures which even show a similar orientation of H ligands, but differ

in the length of the Ir-Ir bond bridged by the H atom and in the multiplicity of the ground state. Independent optimizations of singlet and triplet states for these two structures confirmed that they represent distinct local minima on the ground state potential energy surface, and not ground and excited states of the same structure. The structure bbo (Fig. 4.5 b) is noteworthy as it features a rather high symmetry, C_{2v}; this result was confirmed by optimization without symmetry constraints.

Vibrational stretching modes of tb isomers show the typical pattern of a higher frequency assigned to the terminal H ligand and a lower one to the bridging ligand. This result is surprising for the tbs structure with a strongly asymmetric H bridge. Inspection of the displacements of the atoms involved in the soft stretching frequency of the tbs isomer with 1692 cm^{-1} confirmed that the bridging atom moves perpendicular to the bridge; an Ir-H stretching motion involving the second H atom mixes to a small amount. Thus, although the short bond distance of the bridging atom (1.68 Å) is close to the typical value for terminal coordination, the normal modes strongly resemble the typical behavior of other tetrahedral tb isomers. No obvious trends could be identified for other properties of tetrahedral clusters Ir_4H_2 with bb and tb coordination. Also, there does not seem to be a structure-based argument to rationalize the preferred spin multiplicities. Most of these structures exhibit a singlet configuration, in accordance with the singlet state of the Ir_4 tetrahedron,[83] whereas the isomers tbn1 and bbn were determined to be more stable as triplets (Table 4.6).

It is interesting to compare these findings with those reported for other transition metal cluster species M_4H_2 with bridge coordination of H (bb structures).[149,150,180-183] In most cases (M = Fe, Co, Pd, Rh), tetrahedral structures of the M_4 clusters are preferred or have been considered. For Fe_4 a tetrahedral structure is found for the ground state, and two hydrogen atoms are adsorbed separated in neighboring bridge positions.[180] For Co_4 a butterfly geometry is found to be the ground state and two hydrogen atoms are most favorably separately coordinated on neighboring edges of this butterfly.[180] For a tetrahedral Pd_4, which is shown to be the ground state in Section 4.1, the opposed edges are found to be the most favorable binding place for two separated hydrogen atoms.[149,150] On tetrahedral Pt_4 two hydrogens are predicted to coordinate terminally on one Pt atom.[185] On Rh_4 clusters a H_2 molecule has been calculated to adsorb most preferred with both hydrogen atoms coordinated to neighboring edges.[183] Also for Rh_6, bridge coordination was found to be most stable for 1, 3 and 4 hydrogen atoms.[174] For Pd_4 and Rh_4 singlet multiplicities are found to be stable while for Fe_4 and Co_4 higher magnetic moments with up to 14 unpaired electrons are predicted.[180] For tetrahedral Ir_4, only structures exhibiting bridging hydrogen ligands could be found. Nevertheless, for Ir_4H_2, tetrahedral bb structures are less stable

than tb structures, and even less stable than species with a square planar Ir_4 moiety.

4.2.4 Summary and conclusions

This study extended previous work on Ir_4 and Ir_4H with all-electron scalar-relativistic density functional calculations to the cluster Ir_4 ligated by two H atoms. Structures with square-planar, butterfly-shaped, and tetrahedral Ir_4 unit have been examined. Although not intended to be exhaustive, the present investigation was able to identify a relatively large number of stable isomers, mainly of butterfly-type. The binding energy of the second H atom was calculated to be about the same as that of the first H ligand. The most stable group of isomers features an approximately square-planar Ir_4 cluster, with the H ligands coordinated in terminal fashion. Different conformers of this type feature average binding energies per H atom between 312 and 318 kJ/mol. In general, terminal coordination of both H atoms is energetically preferred; structures with one or two ligands in bridge position are less stable. In contrast, hydrogen is known to prefer bridging positions for tetrahedral Fe, Co, Ni,Pd, Pt and Rh clusters.[149,150,174,180,181,183–185] The preference of terminal coordination of H on Ir_4 may well be connected to the high-spin ground state of Ir_4, because a higher coordination of H atoms induces a stronger perturbation of the electronic structure of the metal cluster, hence spin quenching. Most of the bridging H ligands, especially those at butterfly shaped isomers, where found to bind in strongly asymmetric fashion and thus may be better classified as “quasi-terminally” coordinated. This interpretation was corroborated by an analysis of the corresponding Ir-H normal modes; the corresponding frequencies are very close to those of truly terminally coordinated H ligands.

Structures with ligands at higher coordinated sites, e.g. at threefold hollow sites on tetrahedral Ir_4, are not stable; during optimization, they transformed into isomer structures with lower coordination of H ligands. Overall, the various isomers exhibit very similar binding energies of H ligands. For two terminally coordinated H atoms, average binding energies per ligand were calculated from 270 to 318 kJ/mol whereas lower values, 249–302 kJ/mol, were obtained for species with one or both of the H ligands at bridge positions. For all structures examined, the metal-ligand interaction energy is strong enough to allow dissociative hydrogen attachments to the cluster Ir_4. Interestingly, even attachment of two H ligands does not induce a complete pairing of the 8 unpaired spins of a square-planar Ir_4 cluster. For structures of this type, triplet and quintet ground states have been obtained, whereas tetrahedral and butterfly-type species yield singlet and triplet states, with one

exception (a quintet state).

The results of the present computational study have to be taken with due caution when one aims at interpreting properties of supported Ir_4 particles because the metal-support interaction may well be strong enough to change the energetic preference. After all, many structurally rather different isomers lie rather close in energy. In zeolites a tetrahedral structure has been found as most stable and the support makes hydrogen adsorption on supported Ir_4 by 20 kJ/mol per atom less favorable.[187]

In principle a dynamic treatment of the complex Ir_4H_2 is required as this system exhibits a large number of structures as a consequence of varying ligand orientation, which nevertheless are almost degenerate, especially when topologically equivalent. Yet, such a study would be quite demanding because a very accurate treatment of the electronic structure is necessary. In particular, the varying number of unpaired electrons, which are associated with the different spatial configurations, seems to put such a treatment well beyond present computational capabilities.

4.3 The cluster $Au_{13}(SR)_n$ with R = H, CH_3 and n = 4, 6, 8

4.3.1 Background

Since their first synthesis,[13] gold clusters stabilized by alkylsulfanyl ligands SR attracted increasing interest as building blocks for nanostructures. Their versatile chemistry allows easy functionalization and modification with potential applications in various areas of technological importance.[3,15] With their tunable properties, such clusters are useful to contact biomolecules in a well defined way.[3,188,189] Assembled in ordered arrays, gold-thiolate clusters are expected to form interesting quantum dot materials for nanoelectronics. [33,36] However, despite considerable experimental effort, there are still many questions open with respect to the fundamental properties of thiolate-stabilized gold clusters.[15] Even seemingly simple geometric aspects like the coordination type of the sulfur head group at the gold cluster are still controversially discussed.[16,190 - 197]

There have been several theoretical efforts to contribute to the understanding of structure, bonding, and electronic characteristics of this class of cluster compounds. Some density functional (DF) calculations, using models of one[190] or two[191] thiolate ligands interacting with gold, aimed at determining the binding site and examined the electronic structure with respect to thiolates as electronic linkers. For methylsulfanyl SMe on Au_{13}, a threefold hollow position has been calculated,[190] whereas for 2 SMe ligands a bridge coordination was determined for self assembled monolayers on an Au(111) surface.[191] The interaction of an alkylsulfanyl with small gold species of a few atoms was also studied with DF approaches.[193,194,198 - 203] Thiolate covered gold clusters with more than hundred Au atoms and thiolates with long alkane substituents have been treated with simplified methods,[192] where different coordination sites have been found to be occupied on a single cluster. For the cluster $Au_{38}(SMe)_{24}$, assuming a truncated cuboctahedral structure with ligands attached to bridge sites, in a detailed study using an pseudopotential plane-wave density functional approach,[16] a bridge coordination was determined for the ligands. There is computational evidence based on DF calculations that disordered isomers are preferred for bare gold clusters;[204-206] also for thiolate covered species, disordered structures of the metal core have been proposed to be more stable than symmetric clusters.[207] The computational studies of gold-thiolate clusters thus far focused on selected structures only, and quantitative (absolute) results on bond lengths and especially ligand binding energies are rare.

The coordination site of alkylsulfanyl ligands on Au clusters and surfaces is also the subject of intense debate. While early experiments suggested threefold coordination,[208]

photoelectron diffraction[209] as well as normal incidence X-ray standing wave results[210] propose on-top adsorption, for SMe as well as for sulfanyls with longer alkyl chains, on the Au(111) surface. A high resolution electron energy loss study, on the other hand, has been interpreted to show multiple adsorption sites to be occupied, which change in dependence of the alkyl chain length.[211] In addition, DF calculations lead to different conclusions about the binding site of short chain alkyl thiolates.[212] Only some representative examples shall be mentioned. A Car-Parinello molecular dynamics study found threefold coordination of SMe on Au(111),[213] whereas in an optimization of a slab model with periodic boundary conditions[214,215] the bridge site has been found to be favorable for the same system, as well as for thiolates with longer substituents.[215]

A remark regarding nomenclature is appropriate. While one may refer to $Au_m(SR)_n$ clusters as gold-thiols, the designation gold-thiolate clusters seems preferable although a complete charge separation where ligands carry a full negative charge, SR^-, shall not be implied. Furthermore, the term alkylsulfanyl will be used when the radical character of SR ligands is emphasized; it will be clear from the context, when "sulfanyl" refers in a generic fashion both to SH and SR moieties.

The goal of the present work is to contribute to the understanding of thiolate-covered gold clusters by means of a model study applying an accurate all-electron relativistic density functional approach. The small cluster model Au_{13} has been chosen as it allowed to inspect a larger number of structures of the ligand shell. Sulfanyl SH as a model ligand as well as methylsulfanyl SMe = SCH_3 as the smallest alkylthiol-derived radicals have been considered. To gain insight in the effect of ligand coverage, 4, 6, and 8 ligands have been attached to the model cluster at various coordination sites. In this way, a systematic computational study on how properties of gold thiolate clusters vary with structure, ligand type, and coverage is presented.

This work extends a previous study on $Au_{13}(SR)_n$, n = 4, 6, and 8.[102] While in this earlier investigation open structures for $Au_{13}(SR)_6$ with low Au–Au coordination have been obtained, in the course of this study also structures with compact Au_{13} cluster cores have been determined. Due to these new data a consistent database for the clusters $Au_{13}(SR)_n$, n = 4, 6, 8 is available, which allows a systematic inspection of properties in dependence of increasing ligand coverage for the ligands SH and SMe. In the following, first the model compounds chosen are introduced. Then the results calculated for structural, energetic, and electronic properties are presented and discussed.

4.3.2 Models

The cuboctahedral model system Au_{13} is the smallest cluster with a bulk like 12-fold coordinated central atom. This model was selected due to its small size, high symmetry, and the large number of symmetry subgroups; taken together, this allows an efficient treatment of different ligand coordinations and orientations for a varying number of ligands. As reference for structures and energies, Au_{13} clusters in O_h symmetry as well as with applied symmetry constraints according to the subgroups D_{4h}, D_{3d}, and D_{2h} are presented in Table 4.8.[102] These structures of lower symmetry have to be regarded as models because there is evidence that the ground state structure of Au_{13} may be not ordered.[204-206,216] On the other hand, ordered high symmetry structures have been found experimentally for the metal cores of larger Au cluster species.[17,217,218]

Figure 4.7 shows the cluster Au_{13} in cuboctahedral symmetry, featuring pertinent symmetry elements as well as labels of facets and atoms. In the following the central atom will be referred to by the label C. Au atoms in the surface of cluster are distinguished by axial (A) and equatorial (E) coordination with respect to a chosen main symmetry axis of the structure under consideration. In D_{4h} and D_{2h} symmetry, the cluster is terminated at top and bottom by one of its six (100) facets, each composed of four axial gold atoms. Four equatorial atoms form a square in the horizontal symmetry plane. In D_{3d} symmetry, (111) facets terminate the cluster at top and bottom, each formed by three axial atoms. The middle layer of the cluster now consists of the central atom, surrounded by a hexagon of six equatorial atoms (see Figure 4.7).

Various ligand coordination sites were examined on the cluster model Au_{13} by attaching 4, 6, and 8 SR ligands according to D_{2h}, D_{3d}, and D_{4h} symmetry, respectively (Fig. 4.8). When the structures are optimized with respect to all degrees of freedom

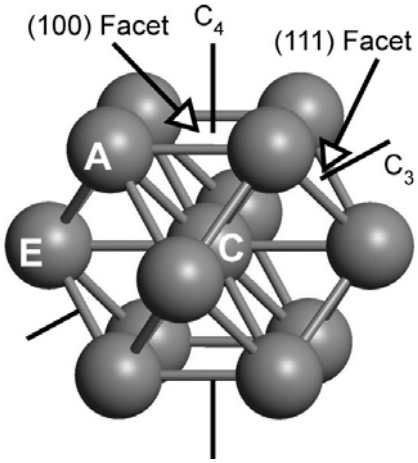

Figure 4.7. Cuboctahedral cluster Au_{13}: symmetry axes C_4 and C_3, facets and labels of atoms (C = central, E = equatorial, and A = axial).

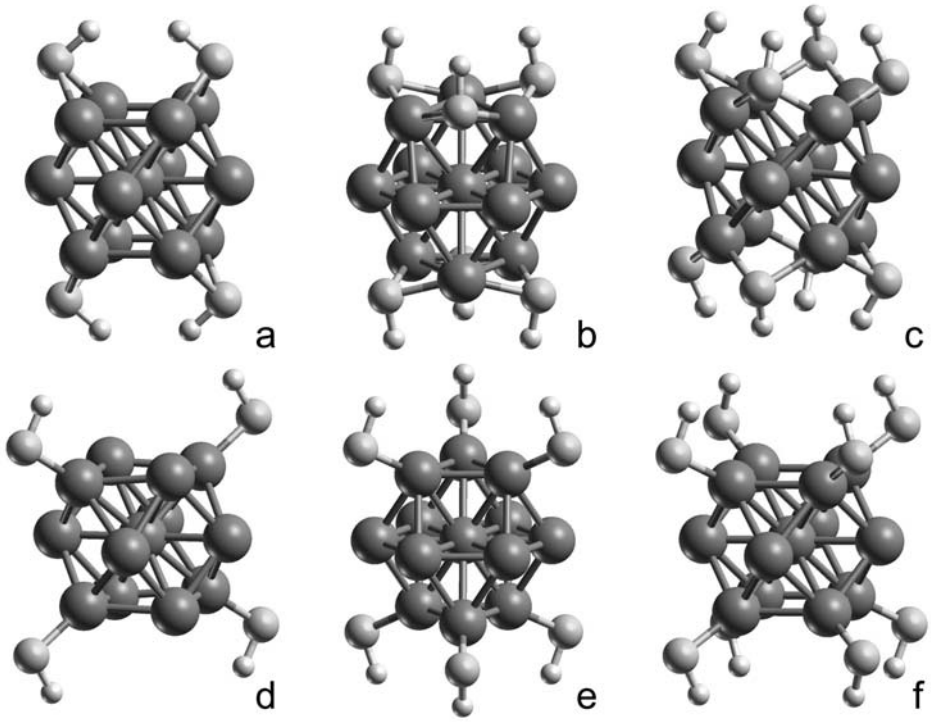

Figure 4.8. Four, six, and eight SH ligands on Au_{13} for axial ligand orientation, with D_{2h}, D_{3d}, and D_{4h} symmetry constraints, respectively. a), b), and c): bridge coordination (b ax); d), e), and f): top coordination (t ax).

compatible with these symmetry constraints, ligands can move to a certain extent between different high-symmetry sites (Fig. 4.9); this allows one to scan various sites without having to resort to a computationally demanding lower symmetry. If eight ligands are treated in D_{4h} symmetry, ligands are attached singly coordinated (top) to Au atoms of the top and bottom (100) facets or between these atoms in bridge coordination. Bridge coordination allows the ligands to move closer to the horizontal symmetry plane of the cluster and thus to the center of the triangular (111) facet on the cluster surface representing a threefold coordination for the S head atom (Fig. 4.9a). On the other hand, top coordination permits only a slight movement of the ligand in the vicinity of that site (Fig. 4.9b). In the case of D_{2h} symmetry, the various surface sites are accessible in the same way, except that now only two instead of four ligands are placed near the top and bottom facets of the cluster, respectively.

As indicated by the arrows in Figures 4.9c and 4.9d, D_{3d} symmetry provides more freedom for positioning the six ligands treated in that case because the horizontal symmetry plane is missing. During geometry optimization, a set of ligands can, in principle, move from the top face of the cluster to the bottom face and vice versa. In the symmetries D_{4h} and D_{2h}, this is not possible as symmetry equivalent ligands would meet each other. As illustrated by Figure 4.9c, ligands at bridge positions of top and bottom facets of Au_{13}, arranged in a starting configuration of D_{3d} symmetry, may also reach fourfold coordinated sites. In that symmetry, adjacent threefold sites as well as bridge positions different from those of the top or bottom facets are accessible when starting from on-top coordination at the top/bottom (111) facets (Fig 4.9d). By moving even further, the ligands may reach again fourfold sites which are equivalent to those close to the starting bridge configuration (Fig. 4.9d). To scan various ligand coordination modes in D_{3d} symmetry, several starting positions were chosen, as indicated by the grey circles in Figures 4.9c and d. Overall, this series of models covers top, bridge, threefold, and, where applicable, also fourfold coordination of SR ligands at coverage values S:Au between 0.3 and 0.6, which corresponds to the range determined experimentally for larger clusters.[14,15,219]

Besides inspection of various coordination sites, also different ligand orientations have been considered. In the starting geometries, the S-R bond of the ligands was oriented either in the direction of the main axis (axial orientation) or about perpendicular to it (equatorial orientation). Examples of optimized structures for axial and equatorial orientations are given in Figure 4.10.

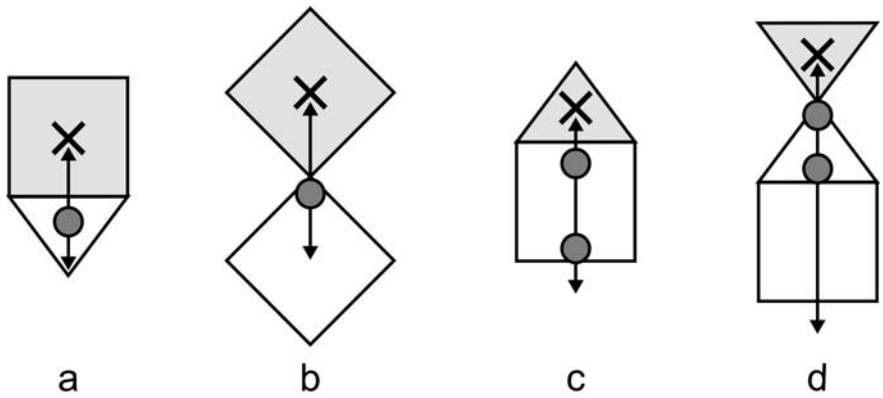

Figure 4.9. Determination of the sulfur sites in symmetry-restricted geometry optimizations of thiolate-ligated Au_{13} clusters. The freedom of movement from a starting site (marked as grey circle) is indicated by arrows; crosses mark the main symmetry axes on the "top" facets (shaded in grey). a) D_{nh}, bridge–hollow site; b) D_{nh}, top site; c) D_{3d}, bridge–fourfold site; d) D_{3d}, top–threefold site.

Table 4.8 Structural and electronic properties of the Au_{13} cluster model for various symmetry constraints. Average nearest-neighbor distance <d> as well as Au-Au bond lengths C-A and C-E in Å, binding energy BE per atom in kJ/mol, ionization potential IP and electron affinity EA in eV. The configuration is characterized by the four highest-lying orbitals, which are listed in the order of spin averaged orbital energies. For the atom labels C, A, and E, see Fig. 4.7.

Cluster	Distances			A-C-A	BE	IP	EA	Configuration
	<d>	C-A	C-E					
O_h	2.730	2.730	2.730	60.0	193.6	7.17	3.77	$a_{1u}^2 t_{2g}^5$
D_{4h}	2.731	2.764	2.664	59.1	194.1	7.21	3.66	$a_{1u}^2 e_g^4 b_{2g}^1$
D_{3d}	2.733	2.740	2.725	60.7	194.4	7.19	3.74	$a_{1u}^2 e_g^4 a_{1g}^1$
D_{2h}	2.731	2.764	2.664	59.1	194.1	7.12	3.66	$a_{1u}^2 b_{3g}^2 b_{2g}^2 b_{1g}^1$

4.3.3 Results and Discussion

In the following the computational results will be discussed starting with the bare Au_{13} cluster. Then the results for ligated cluster models are presented. Depending on the starting configuration, a variety of different structures has been obtained, even though the flexibility of the models was constrained by symmetry. The discussion will be started with "regular structures" where ligand coordination does not affect the Au-Au coordination in a significant way, implying only a moderate distortion of the internal structure of the cluster core. Most of these structures were obtained when ligands were attached to top and bottom facets of the Au_{13} cluster. Subsequently, structures will be briefly mentioned where metal bonds are considerably elongated, leading to strongly deformed cluster cores, which will be referred to as "irregular structures" (see an earlier presentation).[102] Structures of this type are preferentially found in D_{3d} symmetry when ligands where arranged around the central layer of the metal cluster. As will be discussed below, the flexibility of the Au_{13} core allows quite a variety of ligand arrangements on the cluster surface. Therefore, the set of structures obtained in this study cannot be regarded as exhaustive.

For $Au_{13}(O_h)$ a bond length of 2.73 Å and a binding energy per atom of 194 kJ/mol were calculated (Table 4.8). Because the highest occupied molecular orbital (HOMO) in O_h symmetry is not completely filled (t_{2g}^5), a Jahn-Teller distortion results when the symmetry is reduced. However, symmetry lowering entailed only small changes in shape and binding energy per metal atom (Table 4.8). The average Au-Au distance increased at most 0.003 Å, hence remained essentially constant. The binding energy per atom increased by up to 0.8 kJ/mol (D_{3d}, Table 4.8), which leads to an overall stabilization of the cluster by 10 kJ/mol only. In D_{4h} symmetry, the bond length C-A between central and axial Au atoms (Figure 4.7) increased by 0.03 Å, while the central-to-equatorial bond C-E decreased by 0.07 Å relative to the octahedral structure. This results in a slight cylindrical distortion of the cluster. As the electronic configuration in D_{4h} exhibits a singly occupied b_{2g} HOMO, no first-order Jahn-Teller distortion is possible by further symmetry reduction. Thus, the same structure as for D_{4h} is obtained in D_{2h} symmetry. In case of a symmetry reduction from O_h to D_{3d}, even smaller effects on the structure than for D_{4h} were obtained. Both pertinent bond lengths C-A and C-E changed by less than 0.01 Å, thus the cluster preserves its overall spherical shape. In all cases, angles changed by less than one degree.

IPs and EAs changed at most 0.1 eV when the symmetry constraint was reduced (Table 4.8). Whereas identical in all other properties, the D_{4h} and D_{2h} structures showed a small difference in the IP. In the case of D_{4h} symmetry, ionization occurs from the fully occupied e_g set, whereas in D_{2h} symmetry a singly occupied b_{2g} spin orbital is emptied. Thus, the final states of the cation differ in these two symmetries.

In Table 4.9, pertinent geometric parameters related to the coordination of SR ligands to Au_{13} are collected for R = H, Me and increasing ligand coverage from 4 to 8. Also axial and equatorial types of ligand orientation, i.e. roughly parallel and perpendicular to the main axis, are distinguished. For D_{2h} symmetry and top coordination, only one type of ligand orientation (axial) has been listed because it is equivalent to equatorial orientation, the latter being "axial" with respect to the horizontal C_2 axes.

In all cases considered, the low coordinated sites, on-top and bridge, are favored by SH and SMe ligands (Figs. 4.8 and 4.10). Comparing S-Au and next-nearest distances S-Au2 (Table 4.9), one notes that secondary contacts S-Au2 are considerably longer than the contacts S-Au involved in top or bridge coordination. The shortest S-Au2 distances are obtained for eight ligands in bridge coordination and axial orientation; they amount to 3.06 Å for SH and 2.98 Å for SMe and are about 0.6 Å longer than S-Au bonds. For this coordination weak steric repulsion among the ligands arranged around the top (100) facet of the cluster leads to the largest displacement of S centers in the direction to a threefold site. Still, the ligands are far from a threefold coordination, as seen in Figures 4.8 and 4.10.

This rationalization is corroborated by comparing the same cluster species, but with equatorial ligand orientation where steric crowding around the top (100) facet is avoided. This latter situation results in a shift of the ligands towards the bridge site, increasing the S-Au2 distance by about 0.1 Å.

Simplified bonding arguments also result in a preference for low coordinated sites. The neutral species $Au_{13}(SR)_n$ can be partitioned into a neutral metal cluster and a set of sulfanyl radicals. The sulfur center of the ligands carries a singly occupied p orbital as well as a 3p lone pair, besides the low lying 3s orbital and the third p orbital involved in bonding to H or Me. On-top binding involves only the free valence, while bridge coordination also benefits from a dative bond via the S 3p lone pair. No further orbitals are available for bonding without strong rehybridization. A Mulliken analysis of the orbitals reveals that the situation is more involved. The low lying 3s orbital of S also participates in the bonding to H or Me in the ligand and the preference of low coordinated sites may be due to the different orientations of S 3p lone pairs. Also for gold-phosphin thiolate complexes, two- and three-fold coordination of sulfur is most common,[220] which corresponds to top and bridge coordination at the cluster surface, respectively.

The binding energies compiled in Table 4.9 clearly imply a preference for bridge sites. While top coordinated ligands are bound by 175 to 220 kJ/mol, bridge coordination of ligands entails a stabilization by 210 to 260 kJ/mol. For clusters with the same number of ligands, bridge coordination is calculated to be favored by 20 to 40 kJ/mol per ligand, irrespective of the ligand orientation. SMe ligands are calculated to be bound less strongly than SH ligands by 20 to 30 kJ/mol (Table 4.9). Surprisingly, ligand coverage in the range

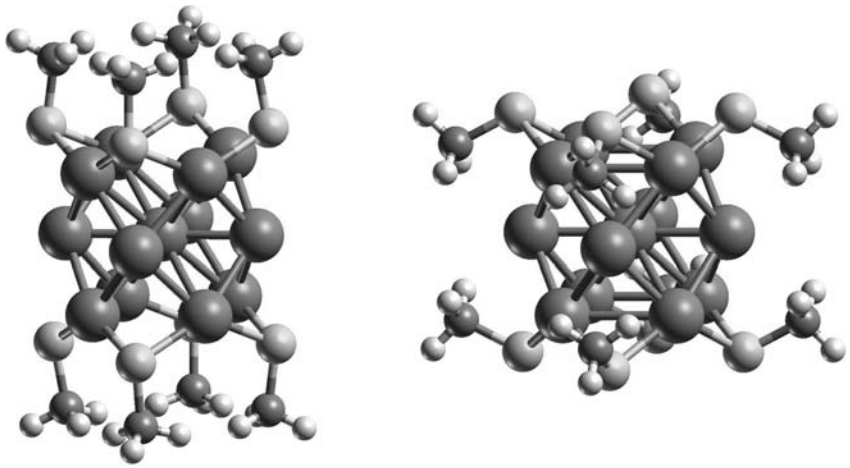

Figure 4.10 Au_{13} clusters with SMe ligands in bridge positions and axial (a) as well as equatorial (b) orientation.

considered does not affect the binding energy per ligand in a major fashion. For both types of ligands examined, the strongest bonds are calculated if only four ligands are attached in bridge coordination. Increasing the number of ligands to six and eight decreases the binding energy per ligand by less than 20 kJ/mol, i.e. by about 10% only. In case of bridging SH ligands, no difference is seen between six and eight ligands; eight SMe ligands are even slightly stronger bound than six.

Similar but even weaker trends were obtained for singly coordinated ligands. Four ligands are stronger bound than six or eight, but no notable difference is found between clusters with six and eight ligands. This result can be rationalized by appealing to bonding competition at the metal centers forming the bonding sites. For four ligands in on-top coordination, the neighboring Au centers of the site do not carry ligands, whereas two of the neighboring Au atoms are ligated when six or eight ligands are present. For four bridge-bonded ligands, each Au atoms is involved only in a single bridge site, whereas for

Table 4.9 Ligand-related characteristics of $Au_{13}(SR)_n$, R = H, Me: nearest (S-Au) and next nearest (S-Au2) bond lengths between S and Au in Å, bonding angles in degree, and binding energies BE per ligand in kJ/mol. The structures are labeled by symmetry, coordination site (b = bridge, t = top), and ligand orientation (ax = axial, eq = equatorial).

Structure		n	S-Au		S-Au2		S-R		Au-S-R		BE	
			H	Me	H	Me	H	Me	H	Me	H	Me
D_{2h}	b ax	4	2.396	2.373	3.529	3.182	1.366	1.815	96.1	102.1	256	232
	b eq		2.394	2.366	3.567	3.480	1.366	1.815	98.1	107.4	258	238
	t ax		2.270	2.266	4.352	4.338	1.364	1.812	95.8	105.1	220	199
D_{3d}	b ax	6	2.404	2.396	3.290	3.245	1.370	1.836	97.7	105.5	244	218
	b eq		2.417	2.394	3.509	3.607	1.370	1.812	96.9	112.3	242	220
	t ax		2.278	2.275	3.766	3.772	1.365	1.811	94.8	104.3	205	184
	t eq		2.264	2.260	4.510	3.833	1.365	1.817	95.3	113.1	209	174
D_{4h}	b ax	8	2.416	2.406	3.058	2.979	1.369	1.830	97.7	108.6	244	215
	b eq		2.434	2.425	3.163	3.197	1.366	1.825	97.7	107.0	242	211
	t ax		2.266	2.267	4.123	4.152	1.365	1.812	94.5	103.1	215	194
	t eq		2.263	2.261	4.106	4.171	1.365	1.812	96.6	106.2	216	191

Table 4.10 Cluster-core related characteristics of $Au_{13}(SR)_n$, R = H, Me: average Au-Au coordination numbers c and distances <d> as well as selected Au-Au bond lengths and angles. Structures are labeled by symmetry, coordination site (b = bridge, t = top), and ligand orientation (ax = axial, eq = equatorial). Bond lengths in Å, angles in degree. For the atom labels C, A, and E, see Fig. 4.7.

Structure		n	c		<d>		C-A		C-E		A-C-A	
			H	Me	H	Me	H	Me	H	Me	H	Me
D_{2h}	b ax	4	5.54	5.54	2.766	2.771	2.797	2.811	2.723	2.657	58.5	56.4
	b eq		5.54	5.54	2.766	2.768	2.793	2.778	2.724	2.735	58.7	58.0
	t ax		5.54	5.54	2.742	2.742	2.710	2.715	2.671	2.766	60.1	60.1
D_{3d}	b ax	6	5.54	5.54	2.827	2.830	2.938	2.944	2.710	2.709	63.0	62.6
	b eq		4.62	4.62	2.816	2.826	2.895	2.909	2.735	2.739	65.0	65.6
	t ax		5.54	5.54	2.738	2.738	2.752	2.748	2.725	2.728	59.7	59.8
	t eq		5.54	5.54	2.759	2.735	2.808	2.728	2.702	2.742	63.1	60.4
D_{4h}	b ax		4.31	4.31	2.845	2.843	2.935	2.930	2.646	2.649	65.1	64.4
	b eq	8	4.31	5.54	2.837	2.824	2.930	2.915	2.629	2.623	64.5	63.2
	t ax		5.54	5.54	2.744	2.744	2.749	2.755	2.731	2.721	61.0	60.9
	t eq		5.54	5.54	2.743	2.744	2.758	2.756	2.717	2.720	60.8	61.1

six and eight ligands, each of these Au atoms is involved in two bridge sites. The binding energy per ligand of the two ligand orientations inspected deviates at most by 10 kJ/mol (Table 4.9). Thus, steric interactions are not of strong importance for the small ligands considered in this study. In similar model calculations on $Cu_{13}(SEt)_8$, using a hybrid force field and density functional approach (QM/MM), which will be presented in the next section. it was found that steric interactions among the ethyltsulfanyl ligands become noticeable.[120]

Top and bridge coordinated sulfanyl ligands also result in clearly different structural characteristics. Parameters with regard to the ligand coordination are compiled in Table 4.9, while pertinent data for the Au_{13} cluster core are collected in Table 4.10. The S-Au bond length varies between 2.26 and 2.29 Å for top sites, whereas 2.37 to 2.43 Å are obtained for bridge coordinated ligands. Thus, the bonds at top sites are ~0.1 Å shorter

than the two bonds to the Au centers that form a bridge site. The two distance ranges are hardly different for the two types of ligands considered: 2.26–2.29 Å for top and 2.39–2.43 Å for bridging SH; 2.26–2.29 Å for top and 2.37–2.43 for bridging SMe. A more detailed inspection of the results uncovers only weak differences. With regard to coverage, no clear trend of bond lengths is identified for top coordination. For SH as well as SMe at bridge positions, the Au-S bond lengths increase slightly with coverage, in line with the decrease of the binding energy (see above). On going from four to six ligands, the Au-S bonds elongate by 0.01 to 0.03 Å for both types of ligands, independent of orientation; yet again the same elongation is calculated when the coverage increases further to eight ligands (Table 4.9). This finding is in line with the concept of bonding competition; this argument also nicely explains why no such trend is found in case of on-top coordination where bond competition is absent. Comparing SH and SMe ligands, the latter show a trend to shorter S-Au bonds by as much as 0.02 Å, although for SMe a tendency to lower binding energies is calculated (see above). This finding can be traced back to the strength of the intra-ligand bond, which is weaker in S-Me than in S-H.

In all cases, bond angles Au-S-R are larger than the corresponding angles H-S-R in the free thiols, 92º for HSH and 98º for HSMe. For SH, this increase amounts to 3–6º, but it may be up to 15º for SMe. The intra-ligand bond length S-H of SH is always calculated somewhat longer than in HSH, where it is 1.359 Å. This bond length hardly varies, at most by 0.006 Å. A larger variation is obtained for the S-C bond in SMe, which also is always longer than the value of 1.811 Å in HSMe. Here, an almost regular trend of longer bonds was found, up to 1.84 Å, for the stronger bound bridge coordination whereas in top coordination 1.82 Å is not exceeded.

Because the average binding energy per Au atom in Au_{13}, 194 kJ/mol (Table 4.8), is comparable to the weakest ligand binding energies, one expects that ligand association to the cluster significantly affects the geometry of the cluster core. Nevertheless, inspection of average Au-Au distances of thiolate covered clusters (Table 4.10) shows only a moderate elongation by 0.01–0.05 Å in most cases. Stronger ligand effects occur for six and eight bridging ligands where the average Au-Au distance is enlarged by about 0.1 Å to 2.83 Å. Ligand coordination to a bridge site always entails a stronger effect on average Au-Au distance of the cluster than top coordination, in line with the higher binding energy.

On the other hand, the small difference between binding energies for top and bridge coordination (Table 4.10) is probably not the primary reason for the stronger effect of bridging coordination on the structure of the metal core: once again, bond competition seems to be more important. Also the angles between the surface and central atoms stay close to the ideal value of 60° of a cuboctahedron. As an example, the angles A-C-A are

listed in Table 4.10. They vary at most by 5°, but for the majority of species this angle deviates less then 3° from the reference value. In agreement with the stronger interaction of bridged ligands, larger deviations from 60° are obtained for bridging than for top coordination (Table 4.10). In most cases, opening of the A-C-A angle by some degrees is accompanied by an oblate distortion of the quasi-spherical cluster shape; only in the case of four bridging ligands, the angle A-C-A decreases slightly (prolate distortion).

Close inspection of different metal-metal bonds reveals that individual distances vary considerably although the cluster core on average expands only moderately (Table 4.10). For the C-E bonds, values between 2.62 and 3.15 Å were calculated, and the C-A bond scattered from 2.70 to 2.94 Å. Compared to the Au-Au bond length of the bare cluster (2.73 Å) and the experimental bulk inter-atomic distance of gold of 2.88 Å,[221,] some of the Au-Au distances in the thiolate-ligated compounds are rather long. In Table 4.10 the (average) gold-gold coordination numbers c is listed as indicator for the presence of especially long Au-Au bonds; to determine the coordination number, 3.1 Å was used as somewhat arbitrary upper value for "bonding" interactions. As discussed for the average Au-Au distance, species with six and eight bridging ligands show a decrease in coordination below the value of 5.5 for Au_{13}. Summarizing the geometric results for regular structures, one notes that the metal core reacts in a rather flexible way to ligand coordination, but essentially preserves its overall structure and the inter-metal coordination. With this flexible response on ligand coverage one is able to rationalize a possible existence of stable disordered structures.[204]

Rather small thiolate-stabilized gold clusters have been synthesized.[222,223] Yet, there is no experimental information regarding ligand binding energies and structural parameters of such thiolate-covered gold clusters. For a few clusters (Au_{28}, Au_{38}), disordered structures, with the sulfur atoms of the alkylsulfanyl ligands incorporated in the strongly distorted surface layer of the gold cluster, have been computationally determined to be more stable than ordered structures.[204,207,224] Unfortunately, no definite information about binding energies and coordination sites has been published for these species; inspecting sketches of these structures,[224] one notes that different sites are occupied. Taking into account the rather small energy variation between top and bridge coordination calculated in this work, it seems plausible that different coordination modes occur on the facets of a highly disordered cluster surface.

Table 4.11 Comparison of computational results of SR coordination in thiolate-ligated gold clusters $Au_m(SR)_n$. S-Au and S-C bond lengths in Å, binding energy BE per ligand in kJ/mol.

Method	R	m	n	Site[a]	S-Au	S-R	BE	Ref.[b]
AE-SR VWN/BP	H	13	4	b	2.39	1.37	258	pw
	H	13	6	b	2.40	1.37	244	pw
	H	13	8	b	2.42	1.37	244	pw
	CH_3	13	4	b	2.37	1.82	238	pw
	CH_3	13	6	b	2.40	1.84	217	pw
	CH_3	13	8	b	2.41	1.83	215	pw
ECP VWN/BP	CH_3	38	24	b	2.52	1.87	134	16
ECP PBE	CH_3	38	2	b	2.46	-	209	191
ECP B3LYP	CH_3	13	1	h	2.55	1.84	-	190

[a] Sites: bridge – b, threefold hollow – h. [b] References, pw = present work.

The computational study most similar to the present model investigation also used a DF-LDA approach, but a rather different computational technology based on pseudopotentials (explicitly accounting only for 11 valence electrons of Au) and a plane-wave representation of the Kohn-Sham orbitals.[16] With this methodology, the structure of $Au_{38}(SMe)_{24}$ was optimized without symmetry constraints. In agreement with the findings here, a structure was obtained where methylsulfanyls were coordinated at bridge sites of the (111) facets of the truncated cuboctahedral cluster core. The Au-S bond lengths of 2.52 Å are longer than those calculated here for $Au_{13}(SMe)_8$, ~2.4 Å; also, the Au-S-C angles of 126° exceeded those obtained in this work, ~110° (Table 4.9). Because the ligand coverage of the Au clusters was similar in both studies [0.75 ligands per surface Au atom in $Au_{38}(SMe)_{24}$ and 0.67 for $Au_{13}(SMe)_8$], one can most likely rule out steric differences as source of these discrepancies, but calculated binding energies provide a hint. The GGA value for the binding energy per gold atom in Au_{38} was calculated slightly larger, 203 kJ/mol,[16] than the GGA value of the present study (194 kJ/mol, Table 4.8). Note also that the binding energy per metal atom is known to increase with cluster size size.[9,10] On the other hand, the GGA ligand binding energy in $Au_{38}(SMe)_{24}$ of 134 kJ/mol[16] is considerably smaller than the present values (Table 4.11) and also results of other computational studies[191] (see below). Thus, in the study of Ref. 16, bond competition at metal atoms of the cluster surface is different due to a severe underestimation of Au-S bonds compared to Au-Au bonds; this systematic difference seems to rationalize the observed structural discrepancies.

In a DF-GGA study of $Au_{38}(SMe)_2$,[191] also employing pseudopotentials, the thiolate ligands have been found to prefer bridge sites between two (111) facets. There, considerably shorter Au-S bonds of 2.46 Å and a ligand binding energy of 209 kJ/mol have been determined. The bond strength of the thiolates seems again underestimated, especially if one takes into account the low coverage. The Au-S bonds were calculated longer than in the case of $Au_{13}(SMe)_4$ (Table 4.11); this may be due to fact that a GGA exchange-correlation functional has been used for the geometry optimization.[10,96,97]

Another computational study, applying the hybrid exchange-correlation functional B3LYP together with a small-core pseudopotential for Au, examined the coordination of a single SMe ligand to the cluster Au_{13}.[190] At variance with the present work and results of other calculations discussed above, a threefold hollow site was determined as most stable; unfortunately, the value of the binding energy was not reported. The rather strong elongations of Au-Au bond lengths (up to 3.62 Å or 0.7 Å compared to Au_{13}![190]) in that work seem questionable when contrasted with the smaller ligand effect on Au-Au distances determined in the present calculations for higher ligand coverages. Similar results were obtained for a phenylsulfanyl ligand SPh.[190]

For very small gold particles with a few atoms only, a preference for low coordination of thiolate bonding has been proposed on the basis of pseudopotential DF LDA[198] and hybrid functional calculations,[199] but this result was questioned in a more extensive GGA DF pseudopotential plane wave calculation.[200]

Also Au(111) surfaces with adsorbed alkylsulfanyl overlayers have been examined computationally.[191,212,214] A comparison with the results obtained here seems worthwhile, but has to take into account two major differences with these surface model studies which aimed at self-assembled monolayers of thiolates on gold substrates. The structure of dense thiolate overlayers is not only determined by the ligand-substrate interaction, but also by ligand-ligand interaction, especially for sulfanyls with larger substituents. For the Au clusters studied here and in other computational investigations, ligand coverage as well as ligand size (SMe) prevents any sizeable ligand-ligand interaction. This is different when sulfanyls with longer alkyl chains are simulated,[120,192] which will be clearly visible in the next chapter.' Secondly, the atoms of a Au(111) surface are coordinated by nine other metal atoms. This coordination of the substrate atoms is much larger than that (5–6) of atoms forming surface facets of small Au clusters (Table 4.10). Thus, one anticipates that sulfanyls interact weaker with an ideal Au(111) surface. DF GGA pseudopotential calculations yielded 178 kJ/mol for a boundary corrected cluster model and 163 kJ/mol in a periodic slab model with the favorite site close to a bridge.[214] These values are in agreement with an older estimate of 167 kJ/mol per adsorbate.[225] In agreement with a

weaker bond, also Au-S distances of 2.56 Å (cluster) and 2.50 Å (slab model)[214] have been calculated longer than in the present work (Table 4.9).

Experiments[209,210] on self-assembled monolayers favored on-top adsorption of thiolate ligands and hence re-opened the discussion of adsorption sites of alkylsulfanyls on gold surfaces. This latest turn of the case underlines the complexity of thiolate-gold adsorption systems and points toward the necessity of employing sophisticated substrate models for surfaces as well as for clusters that allow a flexible structural response to thiolate adsorption.

To provide insight into the way how alkylsulfanyl ligands affect the electronic structure of the model cluster Au_{13}, the density of states for $Au_{13}(SR)_8$, R = H, Me is discussed with ligands at the most stable bridge positions (axial orientation). Figure 4.11 hows various densities of states (DOS) which are based on valence orbital spectra of Kohn-Sham energies subjected to a Gaussian level broadening with half width of 0.25 eV. The Fermi energy is determined by integrating the resulting DOS up to the total number of electrons of each cluster compound and is in very close proximity to the highest occupied molecular orbital. Furthermore, partial densities of states, based on Au(sp), Au(d), and ligand contributions, have been derived from on a Mulliken population analysis of individual spin orbitals.

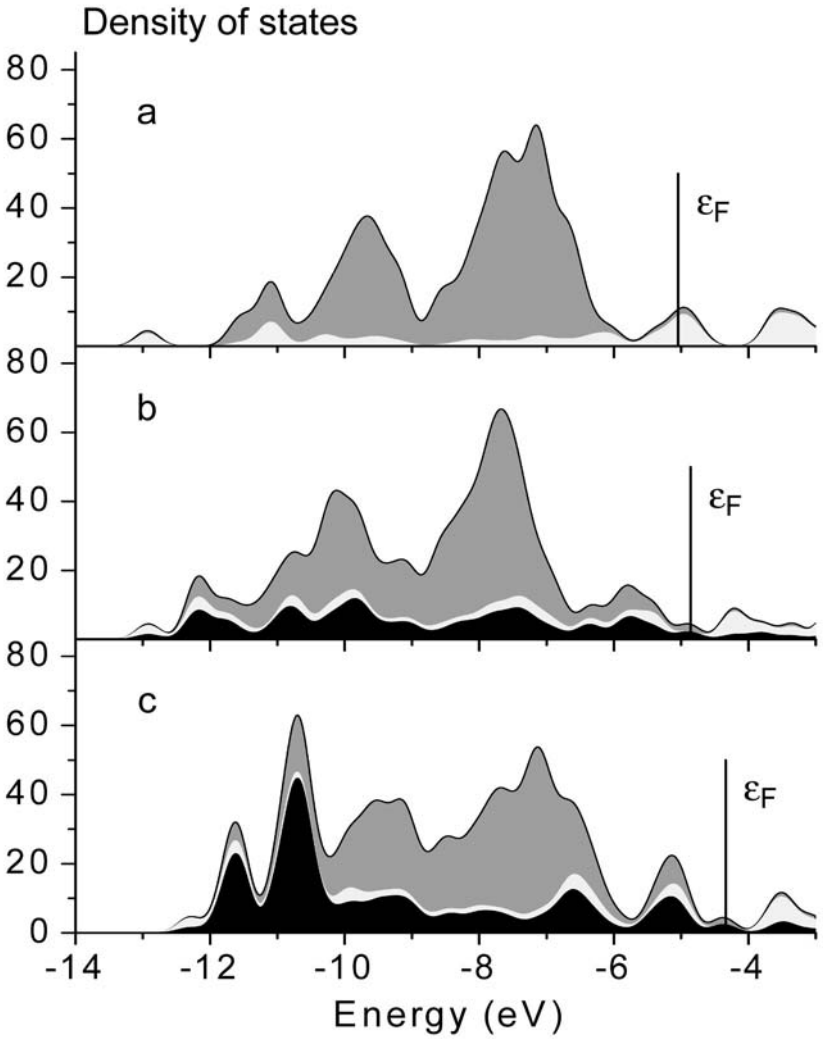

Figure 4.11 Density of states (DOS) of an Au_{13} cluster in D_{4h} symmetry. Bare cluster (a), and clusters covered with eight SH (b) and SMe (c) ligands in bridge coordination and axial orientation. Local DOS contributions from a Mulliken analysis. Ligands – dark, Au sp – white, Au d – grey shading. The Fermi level is indicated by a vertical line.

The cluster Au_{13} exhibits a 5d band (Fig. 4.11a) that is nearly 6 eV wide and features three major peaks. As the density of states was generated from scalar relativistic results (spin-orbit interaction is neglected), the energies have to be interpreted as averages over the $4f_{5/2}$ and $4f_{7/2}$ components.[10] Therefore no direct comparison with the experimentally observed spectra[226,227] affected by spin-orbit interaction is possible. The valence 6sp DOS is very broad; it contributes to the total DOS in an appreciable fashion only near the Fermi energy, at ~ -5 eV and above. Attachment of sulfanyl ligands induces DOS contributions mainly between -6 and -12 eV as well as a smaller peak below the Fermi energy. Methylsulfanyl ligands give rise to strong peaks at -11.5 eV and -10.5 eV which mainly represent C-H bonding orbitals (Fig. 4.11c). As a result of ligand coordination, the Au 5d

band broadens slightly, but the most important effect results near the Fermi energy. The DOS in that energy range is reduced and consists of small Au 5d and some ligand contributions, but a notable Au 6sp component is restricted to the unoccupied levels. Moreover, the Fermi level is shifted upward by about 0.2 eV due to SH (Fig. 4.11b) and 0.7 eV due to SMe (Fig. 4.11c) coordination. These changes may be interpreted as propensity to reducing (or even quenching) the metal character of the core of the small Au_{13} cluster. The trends discussed are, not unexpectedly, less pronounced for smaller numbers of ligands. For on-top coordination of eight ligands, the Au(sp) partial DOS is also considerably reduced, but a larger total DOS with mainly ligand and Au(d) contribution is obtained close to the Fermi level.

Electronic structure related parameters of all species considered are collected in Table 4.12 In line with the upward shift of the Fermi energy, the ionization potentials (IP)

Table 4.12 Electronic structure of $Au_{13}(SR)_n$ clusters for R = H, Me, from LDA calculations: Mulliken charges q per ligand and of the cluster core Au_{13} in e, ionization potential IP, electron affinity EA, and energy ε_{HOMO} of the HOMO, in eV. Structures are labeled by symmetry, coordination site (b = bridge, t = top), and ligand orientation (ax = axial, eq = equatorial).

Structure		n	q(SR)		q(Au_{13})		IP		EA		ε_{HOMO}	
			H	Me	H	Me	H	Me	H	Me	H	Me
D_{2h}	b ax	4	-0.17	-0.09	0.70	0.36	6.94	6.21	3.60	3.23	-5.29	-4.88
	b eq		-0.15	-0.08	0.61	0.30	6.04	6.29	3.46	3.32	-5.15	-4.92
	t ax		-0.21	-0.15	0.86	0.61	6.88	6.50	3.77	3.51	-5.37	-5.06
D_{3d}	b ax	6	-0.19	-0.13	1.17	0.80	6.19	5.56	3.06	2.59	-4.63	-4.08
	b eq		-0.15	-0.11	0.91	0.69	6.60	6.13	3.45	3.14	-5.03	-4.64
	t ax		-0.18	-0.14	1.10	0.82	7.18	6.57	4.07	3.68	-5.70	-5.16
	t eq		-0.19	-0.11	1.13	0.66	7.11	6.65	3.99	3.81	-5.60	-5.24
D_{4h}	b ax	8	-0.22	-0.18	1.75	1.41	6.46	5.85	3.31	2.89	-4.93	-4.41
	b eq		-0.16	-0.10	1.25	0.82	6.47	5.81	3.33	2.87	-4.95	-4.38
	t ax		-0.18	-0.15	1.43	1.19	7.06	6.43	4.22	3.75	-5.65	-5.09
	t eq		-0.18	-0.15	1.47	1.16	7.06	6.48	4.22	3.80	-5.64	-5.13
Au_{13} O_h			0		0		7.17		3.77		-5.47	

of all ligand covered clusters are calculated smaller (Table 4.12). Compared to the bare octahedral cluster Au_{13}, the IP is reduced by up to 0.7 eV for top coordinated thiolates and by up to 1.6 eV for ligands at bridge positions. The IPs show hardly any trend with variation of the ligand coverage. In almost all cases, SMe ligands reduce the IP more than the SH model ligands. This result may be rationalized with the stronger donor capability of a methyl group (compared to H) which results in an overall upward shift of the DOS (see above). EA values scatter around the value calculated for the free cluster Au_{13}, 3.77 eV. While on top coordination of ligands yields preferentially higher EAs, bridge coordinated ligands tend to lower the EA. EA values scatter over a smaller range than IP values; maximum deviations are 0.5 eV for top coordinated ligands and -1.2 eV for bridge coordinated ligands. As for the IP, EA values for SMe ligands are always smaller than those for the corresponding clusters with SH ligands. The present IP and EA values calculated for $Au_{13}(SR)_n$ are in very good agreement with results for $Au_{38}(SMe)_{24}$.[16] For that larger cluster, an IP of 5.31 eV and an EA of 3.41 had been calculated at the LDA level. The trends discussed for IP and EA naturally correspond to the variation of the orbital energy ε_{HOMO} (Table 4.12). For the most stable configurations with ligands in bridge positions, the HOMO is raised to about -4.1 eV from -5.5 eV for the bare cluster Au_{13} (Table 4.12). This upward shift of the HOMO energy is smaller for ligands at on-top positions (up to -5.1); for six and eight SH ligands at on-top positions, the HOMO is even slightly stabilized, by up to -0.2 eV. Due to the donating capability of the methyl substituents, SMe ligands always induce a stronger upward shift of the HOMO than the SH model ligands.

The charge distribution in the ligated Au_{13} cluster has been monitored by means of a Mullikan population analysis. Charges of ligands and of the metal core of the cluster are collected in Table 4.12. As thiolate ligands (as a whole) are withdrawing electron charge density, the effective number of electrons on the gold cluster decreases with increasing number of ligands. For the largest coverage examined, about 1–1.5 e are transferred to the ligand shell. On the other hand, the charge per ligand stays rather constant at -0.1 to -0.2 e, independent of coverage, at variance with the simple expectation that the charge per ligand decreases with increasing number of ligands. However, the tendency of the HOMO to shift to higher energies with increasing ligand decoration balances the effect of increasing charge withdrawal from the metal core, by facilitating transfer of electron density to the ligand. This leads to a more or less constant amount of charge drawn per ligand. The amount of charge separation estimated for $Au_{13}(SR)_n$ is in line with the findings in a previous calculation on $Au_{38}(SMe)_{24}$, where a charge transfer of ~ 2 e in total or about 0.08 e per ligand was estimated.[16] In a calculation on $Au_{13}SMe$,[190] the charge of the single

thiolate ligand was determined at -0.11 e. Apparently, the amount of charge take-up by SMe ligands is fairly independent of the coverage and of the computational method used for these various results. As for other properties discussed above, the stronger electron donating capability of methyl substituents compared to H is also apparent in the population analysis. Thus, irrespective of the coordination site, the negative charge per ligand is slightly lower for ethylsulfanyl than for SH model ligands, resulting in a smaller overall charge separation between metal core and ligand shell by ~0.25 e.

For reasons of completeness the aspect of irregular cluster structures shall be mentioned briefly although these results have been represented earlier.[102] In some of the calculations with D_{3d} symmetry constraints, structures with considerably elongated Au-Au distances were obtained where ligands were attached at bridge positions of the six-ring in the central metal layer of Au_{13}.[102] Examples of such "irregular" structures are shown in Figure 4.12. These structures were obtained for SH as well as for SMe as ligand. A common feature of this type of structures is a long C-E distance. The metal cores of these structures may be described as antiprisms, where the six edges on the side are decorated by further Au atoms. The coordination of the central Au atom of the cluster is no longer bulk-like and the average Au coordination is lower than in "regular" structures. Thus, compared to the compact Au_{13} core of the regular structures, these more open structures may better be considered as complex compounds than as ligated metal clusters.[102] These irregular structures are slightly (< 4 kJ/mol) more stable than regular ones for SH as ligand.

4.3.4 Summary and conclusions

All-electron scalar relativistic density functional calculations have been performed to study the effect of SH and SMe ligands on the model cluster Au_{13}, while various symmetry constraints were imposed on the cluster. Different ligand coordinations have been

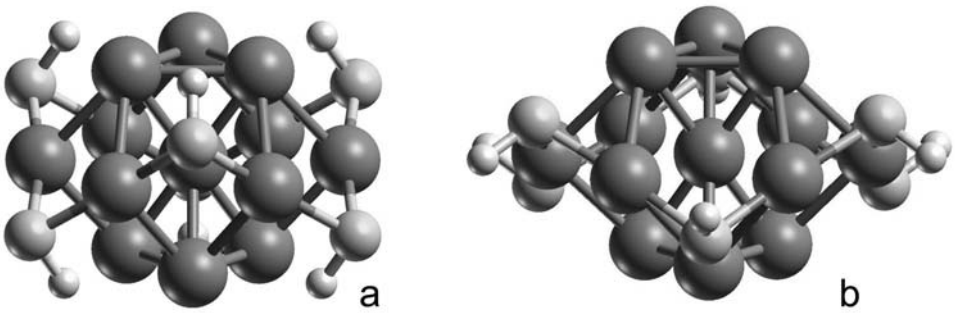

Figure 4.12. Complex-like (irregular) structures of $Au_{13}(SH)_6$ with bridging SH in axial (b3 ax – a) and equatorial (b3 eq – b) orientation.

inspected for four, six, and eight ligands, where the largest coverage is comparable to estimates for experimentally studied larger gold thiolate clusters. In this way, for the first time a detailed comparison of structural as well as electronic features of gold thiolate clusters was carried out with a rather accurate method, thus providing information on how the properties of such species vary with ligand coverage and coordination mode.

For all cases inspected, twofold coordination of thiolate ligands has been preferred. No structures were found with ligands at sites with higher metal coordination. However, the energetic difference between top (175–200 kJ/mol for SMe) and bridging coordination (210–240 kJ/mol for SMe) as well as the flexibility of the gold cluster core does not allow one to exclude definitely three- or fourfold sites, especially when sufanyls with larger substituents are considered where ligand-ligand interaction comes into play.

In most cases considered, the internal coordination as well as the structure of the Au_{13} core is stable under ligand coordination. On the other hand, more open structures have been obtained for six ligands in D_{3d} symmetry, where some of the Au-Au bonds are considerably weakened and elongated beyond the nearest-neighbor distance of bulk gold. These results as well as the rather strong variation of the Au-Au distances illustrate the flexible nature of the Au cluster structure. Because the binding energy per Au atom in Au_{13} (194 kJ/mol) is weaker than the gold-ligand interaction, stable disordered structures of gold thiolate clusters are plausible.[207]

With increasing number of ligands, only moderate effects have been obtained for structures with bridging coordination, e.g., a slight reduction of the ligand binding energy (by less than 20 kJ/mol), an elongation of the average Au-Au distance (by 0.05 Å), as well as a tendency to smaller IP and EA values. No clear trends resulted for top-coordinated ligands. Due to the weak electron donating character of the methyl group, SMe ligands were found to bind weaker than the simple model ligand SH. Also the amount of charge drawn per ligand from the metal core of the cluster is slightly lower for SMe. While the charge of the Au_{13} cluster core increases with increasing number of ligands, the charge per ligand shows no definite trend. The charge separation between metal core and ligand shell is small, less than 1.5 *e* for the largest coverage of methylsulfanyls. Especially for bridging ligands, IP and EA values are considerably reduced due to ligand coordination.

Because the differences between clusters with SH and SMe ligands are rather uniform, SH may well serve as a reliable model ligand in computational studies of larger species, provided the interpretation of results takes into account the differences discussed here. Also one should keep in mind that results for situations with notable ligand-ligand interactions have to be taken with due caution as long as common exchange-correlation

functionals are used.

Although the model clusters of this study were subjected to symmetry constraints, the resulting structural variations admit the conclusion that gold thiolate clusters are rather flexible species, even at small size. Thus, more elaborate studies probably will reveal an even wider range of ligand coordination geometries and cluster structures.

4.4 $Cu_{13}(SCH_2CH_3)_8$: Comparison of DF and IMOMM calculations

4.4.1 Background

Extending previous work on small model complexes,[59] a recently developed implementation of the IMOMM approach was applied to the ligand-stabilized copper cluster $Cu_{13}(SCH_2CH_3)_8$.[228] In fact, that study continued the work on $Au_{13}(SR)_n$ described in the preceding chapter and a diploma thesis.[102] When the cluster $Cu_{13}(SCH_2CH_3)_8$ had originally been studied,[228] difficulties were encountered during the interpretation of the results, in particular due to a lack of clear trends.[228] In the course of this thesis these earlier results have been replaced by calculations obtained with improved computational parameters. As will be discussed in this section, careful analysis of these results allowed to determine a set of minima for various structural isomers which eventually lead to a consistent interpretation.

To assess the capability of the IMOMM approach for the treatment of ligand stabilized clusters, its results are compared to those of the corresponding all-electron treatment. For this purpose, the copper thiolate cluster $Cu_{13}(SCH_2CH_3)_8$ was chosen as a simple, yet realistic example. In this way, the implementation will be validated and the performance of the IMOMM approach for a new class of systems examined. The choice of the model compound was inspired by gold thiolate clusters which recently attracted considerable interest as versatile building blocks of nanostructured materials and as realizations of quantum dots. [3,229] Although most of the experimental work on transition metal thiolate clusters is devoted to gold species (see Section 4.3), the corresponding copper compounds have also been synthesized.[230,231] The special interest in thiolate-stablized metal clusters is due to their rather simple synthesis, yielding stable products that are easy to handle, as well as to the versatile chemistry of the thiolate ligands which allows tailoring of the cluster surface for various purposes.[15,46]

This chapter is organized as follows. First specific features of the IMOMM implementation of the parallel DF program PARAGAUSS will be discussed:[56,57] subsequently computational details are given. In the following the model cluster $Cu_{13}(SCH_2CH_3)_8$ is presented and its properties are discussed on the basis of results from density functional calculations. Subsequently these results are compared to those of IMOMM calculations which combine DF and force-field methods.

4.4.2 The IMOMM implementation of ParaGauss

The QM/MM approach used in the present work is an adaptation of the IMOMM method[110] which, besides standard IMOMM calculations, also allows one to treat ligated metal clusters.[59] The implementation of IMOMM in PARAGAUSS, as used for the present work (cf. Section 3.4), relies on the newly developed MM module MOLMECH[232] of PARAGAUSS[56,57] and the geometry-optimizing module OPTIMIZER.[52] The latest IMOMM implementation of PARAGAUSS simplifies QM/MM calculations compared to a previous version[59] which invoked an external MM program. QM/MM calculations carried out with MOLMECH benefit from the efficient symmetry treatment of PARAGAUSS.[233] The capability for QM/MM calculations is implemented in PARAGAUSS as an interface module which exchanges data between QM and MM modules on the one hand and the OPTIMIZER module on the other. Relevant tasks are the preparation and distribution of data derived from a master input, the gathering of QM and MM contributions to energy gradients, and finally the calculation of the total QM/MM energy of the entire system *XY* where *X* refers to the QM part and *Y* to its MM "environment".[59]

The module MOLMECH was designed to perform energy minimizations of molecules as well as of systems with two- and three-dimensional periodic boundary conditions. Electrostatic interactions of isolated molecules are treated either by direct summation over atomic charges, or by bond centered dipoles as realized in the MM3 force field.[234] Electrostatic and van der Waals interactions of isolated systems are evaluated without cutoffs. Long-range electrostatic interactions in periodic systems, e.g. in two- or three-dimensional arrays of ligated metal clusters, are calculated by Ewald techniques.[235,236] As this treatment of electrostatics is the computationally most demanding part of a FF calculation, it has been been implemented as a parallel algorithm.

4.4.3 Computational details

The binding energy E_b per thionyl ligand SCH_2CH_3 of $Cu_{13}(SCH_2CH_3)_8$ is defined as appropriate fraction of the difference of total energies:

$$E_b = E_{tot}[SCH_2CH_3] + \{E_{tot}[Cu_{13}] - E_{tot}[Cu_{13}(SCH_2CH_3)_8]\}/8 \qquad (5)$$

The energy of the ethylthionyl ligand was determined in the conformation it featured in the cluster. For instance, the energy of SCH_2CH_3 in eclipsed configuration was taken as reference for a copper cluster with eclipsed ligands (see below).

For four isomers (buis, buie, tuis, tuie, buos; see below for the terminology) the basis set superposition error (BSSE) was probed. The results were compared for the ligand shell $(SCH_2CH_3)_8$ (with 8 unpaired electrons) obtained without and with accounting for the Cu_{13} basis set. Correspondingly, results for Cu_{13} were compared without and with accounting for the basis set of the ligand shell. The total energy of Cu_{13} was lowered by up to 46 kJ/mol due to the ligand basis set and the ligand shell gained up to 19 kJ/mol due to the Cu_{13} basis set. As our discussion later on is based on relative values of E_{tot}, namely differences to the energy for the configuration buos (see below), the BSSE of these relative energies was estimated to at most 18 kJ/mol (E_b will be affected by at most 2 kJ/mol), on the basis of differences between the BSSE corrected results for the isomers just mentioned and the BSSE corrected result for isomer buos.

In the MM part of the QM/MM calculations the parameters of the MM3 force field were employed.[234] For the metal-metal interactions, only the van der Waals interaction was parameterized because all other interactions cancel in the IMOMM scheme as they are short ranged.[59] For the organic components, like the alkyl chains, MM3 FF parameters[234] describing stretching, bending and torsion potentials were adopted.

As expected, the QM/MM approach is computationally advantageous; for a given geometry, the time required for the electronic structure calculation (including the forces on the atoms) was reduced by about a factor of two compared to a QM calculation both using one 2.2 MHz Opteron CPU. Since this is done with only one methyl group described exclusively by the force field, larger speed ups for bulkier ligands can be expected.

4.4.4 The model cluster $Cu_{13}(SCH_2CH_3)_8$

To examine the performance of the IMOMM approach for metal cluster compounds, the copper thiolate cluster $Cu_{13}(SCH_2CH_3)_8$ in D_{4h} symmetry was selected as a realistic, but also computationally feasible model system. Ethylthionyl ligands are the shortest alkane thionyls for which steric interactions in the ligand shell are to be expected. In the last chapter on $Au_{13}(SCH_3)_n$ (cf. Section 4.3 and Ref. 237), it was found that steric interactions are essentially absent between the smaller methylthionyl ligands. For the Cu_{13} metal core, a cuboctahedral reference structure was adopted, comprising a central atom surrounded by a shell of 12 “surface” atoms. It is the smallest cluster that features a bulk-like coordinated atom at its center. The cuboctahedral shape of Cu_{13} was preferred over the icosahedral one because it allows one to model easily different ligand coordinations. Also, the bare cluster Cu_{13} in I_h symmetry is 46 kJ/mol less stable than Cu_{13} as cuboctahedron; this result was not

unexpected as the coinage metal cluster Au_{13} shows a similar preference.[237] For a larger cluster, e. g. Au_{55}, the icosahedral shape exhibits similar stability (cf. next chapter). During geometry optimization, D_{4h} symmetry constraints were imposed to restrict the structure of the ligand shell such that one is able to compare various ligand arrangements, optimized both at the DF and the QM/MM levels of theory. Overall, the cluster model chosen comprises all interactions present in larger transition metal thiolate clusters, yet it is simple enough to allow a full density functional treatment at the all-electron level for comparison.

Fig. 4.13 introduces the designations of the various symmetry inequivalent Cu centers of the cluster. In D_{4h} symmetry, four surface atoms Cu_{eq} form a square in the horizontal (equatorial) symmetry plane, which extends perpendicular to the C_4 main axis. Four metal atoms each form squares of (100) surface facets above and below that horizontal mirror plane; these centers Cu_{ax} are referred to as "axial". Finally, the central atom of the cluster is labeled as Cu_{ce}.

As reference, the bare metal core Cu_{13} was optimized both in O_h and D_{4h} symmetry. In O_h symmetry, all Cu-Cu bonds are equivalent and the LDA optimized bond length is 2.400 Å. The BP86 binding energy is 2636 kJ/mol in total or 203 kJ/mol per atom. Because the HOMO in O_h symmetry is only partially filled (t_{2g}^5), a Jahn-Teller distortion is expected, concomitant with a symmetry lowering. With D_{4h} symmetry constraints two different isomers could be located. A "round" isomer which is bound with 2640 kJ/mol and exhibits bonds that deviate at most 0.04 Å from those of the O_h reference. The other D_{4h} isomer features an overall oblate distortion where the equatorial atoms move outward

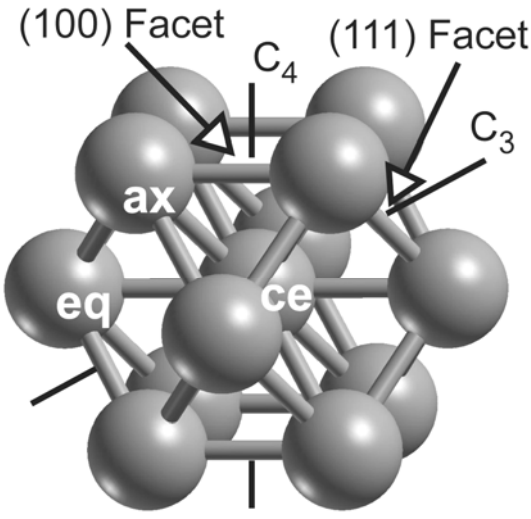

Figure 4.13. Cuboctahedral cluster Cu_{13} with labels of surface facets, pertinent C_n symmetry axes, and designators of the various atoms (ce = central, eq = equatorial, and ax

(Cu_{ce}-Cu_{eq} = 2.842 Å) and the axial atoms move inward (Cu_{ce}-Cu_{ax} = 2.296 Å). With a BP86 atomization energy of 2602 kJ/mol this oblate structure is slightly less favorable than the O_h reference. This the result differs from that of a previous work as improved basis sets have been used in the present calculation.[228]

Two starting configurations were adopted for the optimization of the ligated cluster $Cu_{13}(SCH_2CH_3)_{8.}$ In the first case, ligands were singly coordinated to the axial Cu atoms (Fig 4.14) – "on-top" in the terminology of surface science. Alternatively, the ligands were attached to pairs of axial Cu atoms in two-fold (bridge) coordination (Figs. 4.15). Threefold coordination on the eight (111) facets of Cu_{13} was not separately considered because, in D_{4h} symmetry, ligands can move from bridging to (ideal) threefold positions. For the two starting configurations of D_{4h} symmetry, the S-C-C backbones of the ethylthionyl ligands lie in vertical mirror planes, limiting the number of possible conformations and thus facilitating a direct comparison of QM/MM and full QM results.

To distinguish different conformations of the ligands, a labeling scheme is employed that reflects the orientation of the ligands attached to the top facets of the cluster (Figs. 4.14, 4.15).[102] First, the coordination of the ligands is classified as top (t) or bridging (b), according to the *starting* configuration; this designation is independent of where the ligands end up after optimization. For a ligand anchored on the metal cluster above the equatorial plane, the angle Cu_{ax}-S-C (< 180°) can be chosen to open upward (u) or downward (d) with respect to the C_4 main symmetry axis. In addition, the S-C-C moiety can be oriented toward (inward = i) or away from (outward = o) the C_4 axis. The last conformational degree of freedom in D_{4h} symmetry is the orientation of the terminal methyl group. It can be staggered (s) or eclipsed (e) with regard to the SCH_2 moiety. For example, the concatenated symbol "buos" designates a cluster isomer with bridging ligands

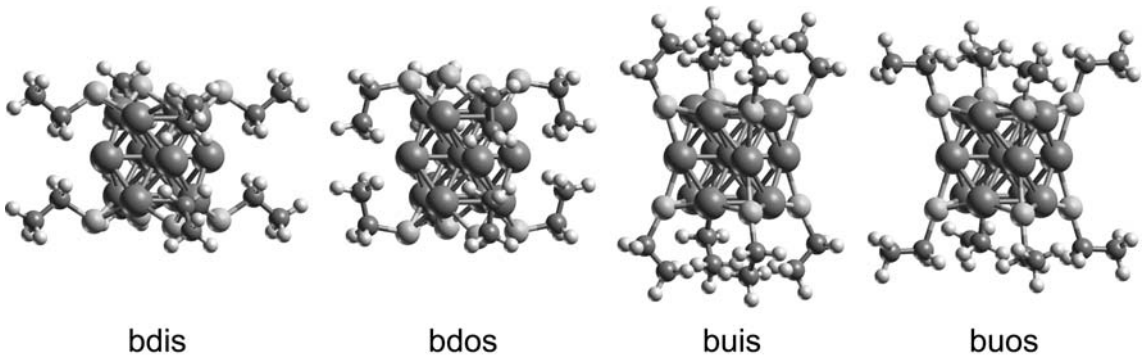

Figure 4.15. Four isomers of $Cu_{13}(SCH_2CH_3)_8$ with bridge coordination of the SCH_2CH_3 ligands and staggered orientation of the methyl group: ligands oriented downward–inward (bdis), downward–outward (bdos), upward–inward (buis), and upward–outward (buos).

(b), upward orientation (u) of the angle Cu-S-C, outward (o) opening of the angle S-C-C, and staggered conformation (s) of the methyl group. In summary, 8 different conformers result for a given *initial* coordination mode (t or b), yielding a total of 16 conformers to be inspected.

According to experience with smaller compounds,[59] the C-C ligand bond has been chosen as the boundary between QM and MM regions. Thus, in the hybrid approach, the QM model was reduced to $Cu_{13}(SCH_3)_8$ and the terminal methyl groups of the ligands have been treated at the MM level. The dangling C-C bonds were saturated by capping H atoms, using a constant ratio of the bond lengths (cf. Section 3.4) with the scaling factor set to 0.709.[59] The boundary chosen between QM and MM partitions also accounts for the fact that charge transfer between these two regions is not included in the IMOMM model applied.

4.4.5 QM calculations on the cluster $Cu_{13}(SCH_2CH_3)_8$

To set the stage for the evaluation of the QM/MM results on metal clusters, first QM reference calculations were carried out at the all-electron LDA level, optimizing structures for all 16 isomers. As visual inspection of optimized cluster geometries reveals (Figs. 4.14, 4.15), ethylthionyl ligands are large enough so that steric effects play a role in the structure of the ligand shell of eight ligands assembled on the Cu_{13} cluster. Methyl end groups of top coordinated ligands remain further away from each other above the (100) facets because the ligands do not approach the cluster surface as closely as bridging ligands do. For the latter conformations, this crowding effect is strongest for bdo isomers where the methyl end groups come close to each other near the horizontal symmetry plane (with shortest H-

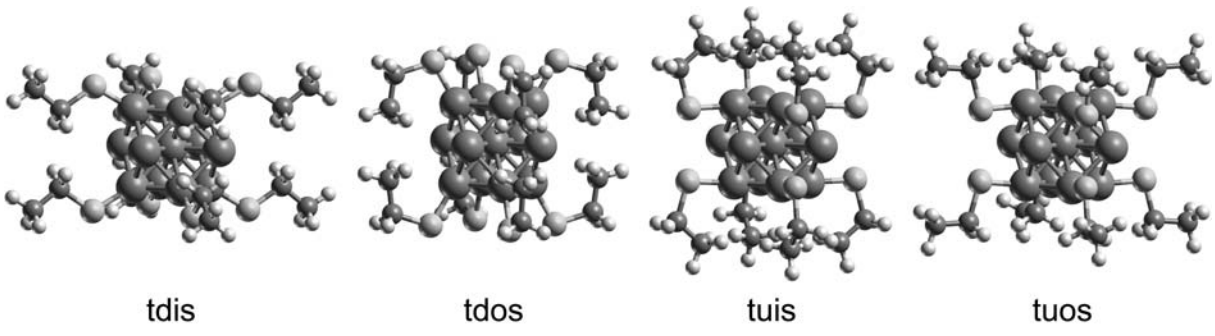

Figure 4.14. Four isomers of $Cu_{13}(SCH_2CH_3)_8$ with top coordination of the SCH_2CH_3 ligands and staggered orientation of the methyl group: ligands oriented downward–inward (tdis), downward–outward (tdos), upward–inward (tuis), and upward–outward (tuos).

H contacts at 1.81 Å); there, methyl groups also get in lose contact with Cu_{eq} atoms (with Cu-H = 1.97 Å). As top coordinated ligands are more distant from to the cluster surface, these contacts are weakened (shortest H-H at 2.18 Å and Cu-H at 2.43 Å) in tdo isomers (Fig. 2).

For a detailed discussion of these observations, pertinent structure parameters are collected in Table 4.13. First "top", then "bridge" isomers will be addressed.

The cluster-ligand bond length Cu_{ax}-S of top coordinated ligands varies only slightly, between 2.10 and 2.13 Å, where the longer bonds are obtained for tdo isomers. Next-nearest copper-sulfur distances Cu_{eq}-S exceed 3.7 Å for top ligands oriented downward, but they decrease to 3.1–3.2 Å for upward orientation because ligands are shifted toward the equatorial plane (Fig. 4.14). Ligand orientation also significantly affects the overall shape of the cluster as shown by the various Cu-Cu nearest-neighbor distances. The Cu_{ce}-Cu_{eq} distance decreases along the series tui > tuo > tdi > tdo from ~2.48 Å to 2.35 Å (Table 4.13). Concomitantly, the Cu_{ce}-Cu_{ax} distance elongates, from ~2.38 Å to ~2.45 Å. Thus, the shape of the metal cluster core changes from oblate to prolate. Clusters with "upward" oriented ligands exhibit longer distances from the center to the equatorial Cu atoms than in the corresponding conformation with the ligands oriented "downward". For instance, in td conformers, the Cu_{ce}-Cu_{eq} bonds are ~0.1 Å longer than for the corresponding tu isomers (cf. tdi vs. tui). Correspondingly, the Cu_{ce}-Cu_{ax} distance is ~0.05 Å longer in td isomers than in the corresponding tu conformers. The orientation of the methyl group, staggered or eclipsed, affects bond distances in a minor way, typically by 0.01 Å or less, but in some cases these bonds can differ by up to ~0.02 Å between two corresponding isomers. Bond lengths within the ligands vary in similarly narrow ranges: 1.82–1.84 Å for S-C1, 1.50–1.53 Å for C1-C2. Bond angles for Cu_{ax}-S-C1 are ~100° for tu, ~105° for tdo, ~116° for tdi isomers.

Table 4.13 Characteristic bond lengths (in Å) of 16 isomers of $Cu_{13}(SCH_2CH_3)_8$ optimized with D_{4h} symmetry constraints.[a]

Isomer	Cu_{ce}-Cu_{eq}	Cu_{ce}-Cu_{ax}	Cu_{eq}-S	Cu_{ax}-S	S-C_1	C_1-C_2	Cu_{ax}-S-C_1
buis	2.339	2.662	2.298	2.193	1.853	1.500	118.4
buie	2.357	2.628	2.321	2.188	1.860	1.514	117.7
buos	2.345	2.604	2.365	2.201	1.860	1.503	115.4
buoe	2.356	2.614	2.326	2.196	1.863	1.516	119.4
bdis	2.283	2.573	2.837	2.236	1.847	1.510	109.5
bdie	2.286	2.572	2.835	2.234	1.850	1.523	109.8
bdos	2.299	2.603	3.281	2.254	1.815	1.493	113.6
bdoe	2.268	2.615	3.212	2.249	1.822	1.512	118.0
tuis	2.471	2.383	3.136	2.119	1.826	1.502	102.8
tuie	2.485	2.366	3.203	2.118	1.834	1.527	97.7
tuos	2.451	2.394	3.088	2.105	1.838	1.509	101.0
tuoe	2.449	2.400	3.077	2.103	1.835	1.525	104.8
tdis	2.402	2.409	3.708	2.101	1.823	1.510	116.3
tdie	2.403	2.408	3.707	2.101	1.824	1.522	116.6
tdos	2.345	2.459	4.113	2.134	1.817	1.501	104.0
tdoe	2.351	2.446	4.092	2.127	1.819	1.520	108.4
bdos[b]	2.859	2.500	2.173	2.244	1.850	1.503	138.6
bdoe[b]	2.868	2.500	2.168	2.239	1.859	1.512	138.7
tuis	2.471	2.383	3.136	2.119	1.826	1.502	102.8
tuie[b]	2.481	2.371	3.158	2.112	1.826	1.526	101.7

[a] For the designation of the various atoms, see Figs. 1 and 2; for the designation of the isomers, see text.

[b] New isomers found with the help of IMOMM results

The equilibrium geometries of clusters, with initially bridge coordinated ligands, show rather different trends. Inspection of Fig. 4.15 as well as comparison of the distances Cu_{ax}-S and Cu_{eq}-S reveals that true two-fold coordination is obtained only for the four types of isomers with downward oriented ligands (bd). For these isomers, the Cu_{ax}-S bond length is 2.23–2.25 Å, while the Cu_{eq}-S distance remains considerably longer, ~2.8 Å for bdi isomers and ~3.2 Å for bdo structures (Table 4.13). Bridge-hollow coordination is found for the four types of bu isomers. There the S atom lies still closer to the axial copper atoms, with Cu_{ax}-S bonds of 2.19–2.20 Å, but the Cu_{eq}-S contacts are only 0.11–0.17 Å longer, giving rise to some additional bonding interaction in these bridge-hollow coordination modes. In agreement with steric considerations, S atoms shift furthest to the

threefold coordination site for bui rotamers (Fig. 4.15). The ligands try to avoid the steric stress above the (100) facet by moving the S atom closer to the Cu_{eq} centers. Cu_{ax}-S bonds of bridging ligands are systematically longer than those of top coordinated ligands by ~0.1 Å, as found for $Au_{13}(SMe)_n$ clusters (Section 4.3).[237] Comparison of Cu_{ce}-Cu_{eq} and Cu_{ce}-Cu_{ax} bonds of a given isomer shows that all these structures are prolate, with the Cu_{ce}-Cu_{ax} bonds longer by 0.26–0.35 Å; however, in contrast to the clusters with top coordinated ligands, there is no clear trend. Cu_{ce}-Cu_{eq} distances are 2.34–2.36 Å for bu isomers (with upward oriented bridging ligands) and 2.27–2.30 Å for bd isomers (with downward oriented ligands). The orientation of the methyl group affects Cu-Cu bonds in a similarly minor fashion as in the top coordinated clusters, with two exceptions: the two pairs buis–buie and bdos–bdoe feature changes of the Cu_{ce}-Cu_{eq} and Cu_{ce}-Cu_{ax} bonds, up to 0.03 Å, in opposite directions. The bond lengths within the ligands also vary within similar margins as for cluster isomers with top coordination: 1.82–1.86 Å for S-C_1, 1.49–1.52 Å for C_1-C_2. Cu_{ax}-S-C_1 angles are 114–120° for bu as well as bdo isomers, and 110° for bdi isomers.

Comparing clusters of the same ligand orientation, one finds Cu_{ce}-Cu_{eq} bonds for top coordination longer than for bridge coordination and Cu_{ce}-Cu_{ax} bonds shorter. Cu_{ce}-Cu_{eq} bonds can differ by 0.08–0.13 Å, Cu_{ce}-Cu_{ax} bonds by 0.14–0.28 Å (Table 1).

In Table 2 various energetic parameters of the 16 isomers are compared. The total energy is referenced to that of the most stable isomer, buos. In general, isomers with bridging ligands are 350–500 kJ/mol more stable than isomers with top coordinated ligands of the same orientation. While the total energies of isomers with bridging ligands span an interval of ~360 kJ/mol, the energies of isomers with top coordinated ligands scatter over an interval of ~280 kJ/mol. The most stable isomer with top coordinated ligands, tuos, is 70 kJ/mol less stable than the least stable isomer with bridge coordinated ligands, bdoe, and more than 400 kJ/mol less stable than the most stable isomer buos. These energy differences result from variations of the ligand binding energies E_b which are 44–63 kJ/mol for a given ligand orientation (Table 4.14). In a previous thesis no clear energetic differences between top and bridge coordinated ligands could be identified.[228]

Among the "top" conformers, tdo isomers exhibit the smallest ligand binding energies, ~185 kJ/mol, followed by tdi isomers with ~200 kJ/mol; tu isomers have the largest ligand binding energies, ~205 kJ/mol. The binding energy of bridge coordinated ligands varies typically between 230 and 264 kJ/mol and shows the same ordering as for top coordinated ligands. bdo isomers have the lowest binding energy, 230 kJ/mol, followed by bdi isomers with 245 kJ/mol and bu isomers with ~260 kJ/mol. Because E_b values are referenced to corresponding rotamer structures, staggered and eclipsed, they show more clearly than E_{tot} values the direct ligand-cluster interaction including steric effects. This

Table 4.14 Total energies E_{tot} relative to that of the isomer buos and binding energies E_b per ligand for the various isomers of $Cu_{13}(SCH_2CH_3)_8$ as well as corresponding energy differences ΔE_{tot}, and ΔE_b between staggered (s) and eclipsed (e) conformers of a given ligand coordination mode.[a]

Isomer	E_{tot}	ΔE_{tot}	E_b	ΔE_b
buis	6.9	-105.7	263.2	2.4
buie	112.6		260.8	
buos	0.0	-97.3	264.0	1.3
buoe	97.3		262.7	
bdis	125.8	-105.8	248.3	2.4
bdie	231.6		245.9	
bdos	270.7	-89.0	230.2	0.3
bdoe	359.7		229.9	
tuis	444.3	-169.0	208.5	10.3
tuie	613.3		198.2	
tuos	430.2	-105.7	210.3	2.4
tuoe	535.9		207.9	
tdis	513.3	-108.0	199.9	2.7
tdie	621.3		197.2	
tdos	632.1	-79.3	185.0	-0.9
tdoe	711.4		186.0	
bdos [b]	9.3	-98.3	262.9	1.4
bdoe [b]	107.5		261.5	
tuis	444.3	-130.8	208.5	5.5
tuie [b]	575.1		203.0	

[a] Energies in kJ/mol.

[b] New isomers found with the help of IMOMM results

conclusion is supported by the very small differences ΔE_b between corresponding values of staggered and eclipsed structures (Table 4.14).

As expected, the eclipsed form of the ethyl end group leads to a higher total energy. For isolated ethylthionyl ligands SCH_2CH_3, the energy difference between staggered and eclipsed conformations was calculated at 10.8 kJ/mol. The corresponding rotational barrier of ethylthiol $HSCH_2CH_3$ was calculated slightly higher, at 12.6 kJ/mol. For a cluster with 8 ligands, these values extrapolate to ~86 kJ/mol and 101 kJ/mol, respectively. Accordingly, the energies of most pairs of rotamers between staggered (s) and eclipsed (e) conformations differ by 98–105 kJ/mol (see ΔE_{tot}, Table 2). For the bdo and tdo isomers, this energy difference ΔE_{tot} is ~11 kJ/mol and 21 k/mol, respectively, smaller (by absolute value) than the average value of 100 kJ/mol; however, these energy variations translate into binding energy changes of less than 4 kJ/mol per ligand (see ΔE_b, Table 4.14). Only the tui rotamers are separated notably further in energy as the eclipsed rotamer is 169 kJ/mol less stable than the corresponding staggered structure. This increase of the energy difference is due to specific ligand-ligand interactions which are enforced by the constraints of the ligand conformation (Fig. 4.14). Indeed, in the tuie conformation, the energy of the ligand shell $(SCH_2CH_3)_8$ (in a configuration with 8 unpaired spins) is 57 kJ/mol *destabilized* relative to the energy of eight isolated ligands in eclipsed conformation. Yet, a single ethylthionyl in the optimized conformation of the tuie isomer is only 0.4 kJ/mol less stable than as free ligand. In contrast, the ligand shell $(SCH_2CH_3)_8$ is *stabilized* by 21 kJ/mol relative to the energy of eight isolated ligands in staggered conformation. Thus, the unusual high destabilization of the eclipsed tui rotamer derives from an unfavorable inter-ligand interaction.

As expected, a doublet ground state was determined for all but two isomers of the cluster $Cu_{13}(SCH_2CH_3)_8$, reflecting the odd number of electrons of the system. The tdo pair of isomers was found to be more stable in the quartet state. For structures with bridging ligands, the gap between highest occupied and lowest unoccupied spin orbitals is 0.5–0.9 eV, whereas it is considerably smaller, 0.05–0.2 eV, for isomers with terminal ligand coordination, rationalizing to some extent the exceptional quartet state of two t-type structures.

Finally, additional cluster isomers of td type shall be mentioned here with an overall oblate shape (not listed in the tables) which were found, when the flat bare Cu_{13} was used as underlying cluster core. Because these cluster conformations represent states of higher energy compared to their prolate congeners (E_{tot} 15.5 kJ/mol higher for tdie and tdoe, 23.0 kJ/mol for tdis, and 31.0 kJ/mol for tdos), they will not be further discussed.

4.4.6 IMOMM calculations on the cluster $Cu_{13}(SCH_2CH_3)_8$

To assess applicability and accuracy of the IMOMM QM/MM approach for metal cluster compounds, now IMOMM results will be compared to those obtained previously in all-electron QM calculations. At first, the very same initial structures were used for the QM/MM geometry optimizations as previously for the pure QM optimizations – to locate, as far as possible, the same local minima. The discussion will begin with the results of these optimizations. For some isomers this strategy failed to identify analogous local minima and the search had to be expanded as will be detailed later on.

To characterize the consequences of the different computational methods, the largest structural deviations will be discussed first. The geometric parameters of IMOMM optimized cluster compounds are displayed in Table 4.15, together with the deviations from the corresponding QM results. Inspection of the bond distances and their deviations reveals that the largest differences between QM and QM/MM results occur for the bdo isomers; these structures will be discussed separately below. For the remaining structures, the average absolute deviations are 0.013 Å (0.033 Å) for Cu_{ce}-Cu_{eq}, 0.010 Å (0.024 Å) for Cu_{ce}-Cu_{ax}, 0.030 Å (0.055 Å) for Cu_{eq}-S, 0.006 Å (0.018 Å) for Cu_{ax}-S, and 6.0° (18.9°) for Cu_{ax}-S-C_1; maximum absolute deviations are given in parentheses. From these values one concludes that the IMOMM method works rather well for such ligated metal cluster compounds. Distances Cu_{ax}-S are particularly well reproduced. In contrast, discrepancies in the angles Cu_{ax}-S-C_1 indicate a propensity for easy deformation in this structural characteristic. As these angles are not stabilized by any additional direct bond, they react strongly on (small) changes in the environment and, therefore, can be used as sensitive indicators for (other) very small structural discrepancies. According to this criterion, the isomers bdo, tui, and tdo deserve special attention (Table 4.15) as the discrepancies in the angles range from 10–25°. Also the bui isomers, with differences in the Cu_{ax}-S-C_1 angle of 4–6°, can be mentioned in this context.

The bdo isomers show the largest structural differences between IMOMM and full QM calculations and shall be discussed first. In the QM/MM structures, the Cu_{eq}-S distances are significantly elongated, more than 1 Å, compared to the corresponding QM structures (Table 4.15). This strong discrepancy reflects the displacement of the ligands from bridge sites in the QM optimized structure to three-fold hollow positions in the QM/MM case (Fig. 4.16). Also, the structures of the Cu_{13} core differ noticeably between the two types of calculations. In the IMOMM calculations, the Cu_{ce}-Cu_{eq} distances are ~0.5 Å longer and the axial bonds Cu_{ce}-Cu_{ax} 0.1 Å shorter.

Thus, the shape of the cluster core as determined by the QM/MM calculations is quite similar to that of the oblate bare cluster Cu_{13}. Recall that the latter isomer of the bare cluster is only ~12.5 kJ/mol less stable than the prolate isomer. These very substantial differences for the bdo isomers between the results of the two computational methods, which obviously do not present the same minimum at the potential energy surface, can be traced to the corresponding ligand arrangements. In the all-electron case, the ligands of the bdo rotamers wrap around the cluster surface (Fig. 4.16), resulting in rather short contacts (< 2.5 Å) between the methyl groups of the ligands and the Cu_{eq} centers. In the bdoe conformer, the corresponding Cu_{eq}-H contacts are just 1.97 Å, but this distance is 2.31 Å in the bdos isomer. One expects this nonbonding interaction to be clearly repulsive. Indeed,

Table 4.15 Characteristic geometric parameters of the Cu_{13} cluster core and the cluster-ligand interface of 16 conformers of $Cu_{13}(SCH_2CH_3)_8$ from QM/MM calculations and deviations δ(QM/MM-QM) from the corresponding QM results.[a]

Isomer	Cu_{ce}-Cu_{eq}	δ	Cu_{ce}-Cu_{ax}	δ	Cu_{eq}-S	δ	Cu_{ax}-S	δ	Cu_{ax}-S-C_1	δ
buis	2.368	0.029	2.644	-0.018	2.287	-0.011	2.187	-0.006	124.1	5.6
buie	2.370	0.013	2.631	0.003	2.314	-0.006	2.188	0.000	121.9	4.2
buos	2.357	0.012	2.619	0.015	2.322	-0.043	2.193	-0.008	118.4	3.1
buoe	2.358	0.003	2.620	0.006	2.320	-0.006	2.192	-0.004	118.4	-1.0
bdis	2.276	-0.007	2.578	0.005	2.874	0.036	2.234	-0.002	107.2	-2.3
bdie	2.276	-0.009	2.579	0.006	2.882	0.047	2.234	-0.001	107.0	-2.9
bdos	2.807	0.508	2.509	-0.095	2.177	-1.104	2.240	-0.014	138.8	25.2
bdoe	2.811	0.543	2.507	-0.108	2.177	-1.035	2.235	-0.014	138.3	20.2
tuis	2.485	0.014	2.368	-0.015	3.163	0.027	2.111	-0.007	113.1	10.2
tuie	2.483	-0.002	2.369	0.003	3.169	-0.034	2.109	-0.008	116.7	18.9
tuos	2.482	0.030	2.376	-0.018	3.132	0.044	2.112	0.006	102.9	1.9
tuoe	2.482	0.033	2.376	-0.024	3.132	0.055	2.111	0.008	103.0	-1.9
tdis	2.394	-0.007	2.414	0.005	3.733	0.025	2.103	0.003	113.0	-3.3
tdie	2.395	-0.008	2.414	0.005	3.735	0.027	2.103	0.002	112.9	-3.8
tdos	2.349	0.005	2.442	-0.017	4.072	-0.041	2.116	-0.018	116.1	12.1
tdoe	2.339	-0.011	2.445	-0.001	4.069	-0.023	2.115	-0.013	121.8	13.3
bdos[b]	2.807	-0.053	2.509	0.009	2.177	0.005	2.240	-0.004	138.8	0.2
bdoe[b]	2.811	-0.057	2.507	0.007	2.177	0.008	2.235	-0.004	138.3	-0.4
tuis	2.485	0.014	2.368	-0.015	3.163	0.027	2.111	-0.007	113.1	10.2
tuie[b]	2.483	0.002	2.369	-0.002	3.169	0.011	2.109	-0.003	116.7	14.9

[a] Bond lengths and their differences in Å, angles and their differences in degree.

[b] Differences to new DF isomers found with the help of IMOMM results

the QM/MM structure (Fig. 4.16) seems to imply a strong repulsion as the Cu_{eq}-H contacts elongate substantially, to 3.29 Å in the bdoe conformer and to 3.57 Å in the bdos conformer.

These significant differences between the results for the bdo structures can be attributed to the different representation of nonbonding interactions by the DF and FF methods. The currently popular exchange-correlation approximations of LDA and GGA type are unable to account for dispersion interaction[238] although some success has recently been claimed with specially parameterized functionals as well as a TDDFT approach.[239–243] For the LDA functional applied here, this methodological deficiency becomes manifest in too short nonbonding contacts[244] which may be rationalized by an artificial attraction due to density overlap;[245] this artifact is also observed for GGA functionals.[245] In addition, a common feature of all mathematically local density functionals is the lack of dispersion interaction.[238,245] On the other hand, force fields explicitly account for van der Waals interaction via their parameterization. Thus, for short nonbonding contacts, one can expect proper repulsion and consequently more reliable results from a FF (or a QM/MM) approach than from a standard DFT-based method. Furthermore, if nonbonding contacts are present, the risk of locating different minima in QM/MM and DF optimizations is increased due to artificial stabilization of non-bonding contacts in LDA or GGA calculations.[245]

As a check of this hypothesis, the difference ΔE_{MM} of the force field energy contributions was evaluated at QM and QM/MM optimized geometries for the isomers bdo, buo, tui, and tdo:

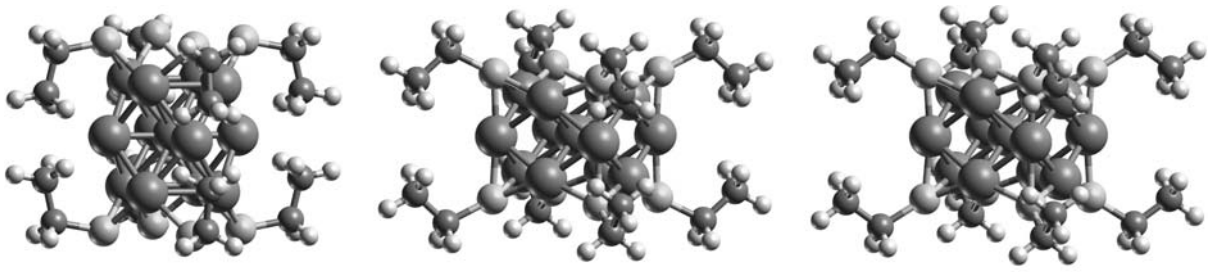

Figure 4.16. Geometries of the bdos isomer with bridge coordinated ligands in "downward" orientation with outward pointing methyl tail groups. Structures of geometry optimizations from full DF (QM1) and QM/MM calculations which have been started from the same initial structure as well as DF (QM2) result obtained when starting from the QM/MM geometry.

$$\Delta E_{MM} = \left[E_{MM}(XY) - E_{MM}(X) \right]_{\text{QM geometry}} - \left[E_{MM}(XY) - E_{MM}(X) \right]_{\text{QM/MM geometry}} \quad (5)$$

The isomers with largest deviations between QM and QM/MM and one pair with small structure differences as counterexamples (buo) were chosen. More than 95% of ΔE_{MM} derives from van der Waals interaction. Just as expected, ΔE_{MM} values for the bdo isomers are unusually large, more than 1674 kJ/mol (!). Also, ΔE_{MM} of isomer tuie is quite large, 1381 kJ/mol. The analogous values for other conformers are notably smaller, 456 kJ/mol for tdoe, 218 kJ/mol for tdos and 251 kJ/mol for tuis. As expected, ΔE_{MM} values are very small, 4.6 and 27.6 kJ/mol, for the buo counterexamples.

According to these findings, QM and QM/MM results for other isomers with short inter-ligand H-H or Cu-H contacts should also differ. Indeed, bui, tui, and tdo conformers (in addition to the bdo structures) exhibit such relatively short inter-ligand contacts. Cu-H contacts of the tdo isomers from the all-electron QM calculations (with Cu_{ax}: tdos – 2.77 Å, tdoe – 2.43 Å) are quite a bit longer than in the bdo isomers (2.31 Å, 1.97 Å; see above). Consequently, differences between QM and QM/MM results for bond lengths were considerably smaller for tdo than for bdo isomers although Cu_{ax}-S-C bond angles increased notably in the tdo isomers, by 12–13° (Table 4.15). In the same spirit, relatively short H-H contacts of about 2.3 Å and 2.5 Å for the tuis and tuie isomers, respectively, did not prevent good agreement among bond distances obtained from QM and QM/MM calculations, but were reflected in larger values of Cu_{ax}-S-C angles from QM/MM calculations, 10° (tuis) and 19° (tuie). For bui isomers, the structural trends seem comparable to those of the tui isomers, but the change in the Cu_{ax}-S-C angles are much smaller (Cu-H 3.11, 3.16 Å and H-H 2.42, 1.91 Å for buie and buis, respectively) (Table 4.15). Because bridge coordinated ligands are closer to the "surface" of the cluster core, they have to bend less to form H-H contacts comparable to those of tui structures. For the tuie isomer even a very short Cu_{ax}-H contact of 2.085 Å was obtained in full QM calculation.

The structures with close Cu-H and H-H contacts are the very same structures that were previously singled out with the help of the criterion of the Cu_{ax}-S-C_1 angles. Whereas the Cu_{ax}-S-C_1 angles from QM/MM and full QM calculations differ noticeably in the bui, tdo, and tui conformers, bond distances deviate at most by 0.04 Å. Apparently the ligands are just differently oriented, but the individual structures both of the ligands and the cluster core remain largely unchanged. Indeed, the shape of the clusters stays oblate for "bridge"

Table 4.16 Relative total energies E_{tot}, binding energies E_b per ligand from QM/MM calculations on 16 conformers of $Cu_{13}(SCH_2CH_3)_8$ as well as corresponding energy differences ΔE_{tot}, ΔE_b between staggered (s) and eclipsed (e) conformers of a given ligand coordination mode. Also shown are the differences δE_{tot}, δE_b from the corresponding QM energies.[a]

Isomer	E_{tot}	ΔE_{tot}	δE_{tot}	E_b	ΔE_b	δE_b
buis	-29.0	-129.3	35.9	279.1	-1.0	-15.9
buie	100.3		12.3	280.1		-19.3
buos	0.0	-142.8	0.0	275.5	0.6	-11.4
buoe	142.8		-45.5	274.8		-12.1
bdis	137.0	-145.2	-11.2	258.4	0.9	-10.0
bdie	282.2		-50.5	257.4		-11.5
bdos	-12.7	-166.0	283.4	277.1	3.5	-46.9
bdoe	153.3		206.4	273.5		-43.6
tuis	419.3	-191.5	24.9	223.1	6.7	-14.5
tuie	610.9		2.4	216.3		-18.1
tuos	421.5	-145.4	8.7	222.8	1.0	-12.5
tuoe	566.9		-31.0	221.8		-13.9
tdis	528.2	-144.8	-14.9	209.5	0.9	-9.6
tdie	672.9		-51.6	208.6		-11.3
tdos	534.8	-180.0	97.4	208.6	5.3	-23.6
tdoe	714.8		-3.3	203.3		-17.4
bdos[b]	-12.7	-166.0	22.0	277.1	3.5	-14.2
bdoe[b]	153.3		-45.8	273.5		-12.1
tuis	419.3	-191.5	24.9	223.1	6.7	-14.5
tuie[b]	610.9		-35.8	216.3		-13.3

[a] Energies in kJ/mol.

[b] Differences to new DF isomers found with the help of IMOMM results

coordination and prolate for "top" coordination. Also, the IMOMM approach yields the same two- or threefold coordination as the full QM calculations.

The differences between the results from QM and QM/MM approaches are reflected by the energetics as well (Table 4.16). Also for the IMOMM calculations the buos structure was used as energy reference. Bridge coordinated clusters have IMOMM energies that are up to 282 kJ/mol higher than the reference, spanning an interval of 310 kJ/mol, compared to 360 kJ/mol at the full QM level. The relative total energies of top-coordinated clusters fall into the range from 420 to 715 kJ/mol, compared to 430 to 711 kJ/mol at the full QM level. The energy separation of clusters with bridge and top coordinated ligand shells is somewhat more pronounced at the QM/MM (138 kJ/mol) than at the full QM level (67 kJ/mol).

The buos structure features a low energy also at the IMOMM level, but the buis and bdos structures are even lower in energy, although only slighty. At the QM/MM level the buis structure is 36 kJ/mol stabilized compared to the full QM calculation (δE_{tot}, Table 4.16). In fact, the total energies from both types of calculations correlate reasonably well (Fig. 4.17), with differences δE_{tot} typically ranging from -50 to 38 kJ/mol, with three rather notable exceptions: the structures bdos (283 kJ/mol), bdoe (206 kJ/mol), tdos (97 kJ/mol), and tuie (36 kJ/mol). Below, these structures will be discussed in more detail.

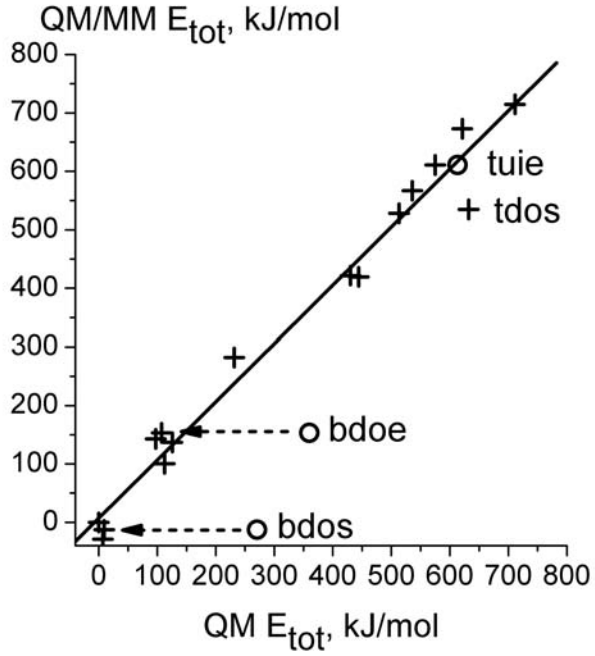

Figure 4.17. Correlation of E_{tot}, QM vs. QM/MM values (in kJ/mol). Crosses denote results of corresponding minima, circles refer to deviating minima obtained when invoking the same starting condition in the optimization. For details see text.

As in the full QM calculations, isomers with staggered methyl substituents are always more stable than those with eclipsed orientation of the methyl groups. The differences ΔE_{tot} from IMOMM calculations, ranging from 129 to 192 kJ/mol, are notably larger than in the full QM calculations. IMOMM values typically are close to 145 kJ/mol, ~ 40 kJ/mol larger than typical QM values (Table 4.16). This difference is traced back to corresponding differences for the isolated thionyl ligands. In the QM/MM approach the rotational barrier of the ethyl end group is calculated at 16.7 kJ/mol, whereas a full DF treatment yields a value of 10.8 kJ/mol. Test calculations on ethane yielded rotational barriers of 12.1 kJ/mol for QM/MM and 10.8 kJ/mol for QM, in good agreement with experiment (12.1 kJ/mol[246]).

The ligand binding energies E_b from full QM calculations are very well reproduced with the IMOMM approach. Ligand binding energies of bridge coordinated structures from IMOMM calculations, 258–280 kJ/mol, are again notably larger than for top coordinated structures, 203–223 kJ/mol. These E_b values show the same independence of the orientation of the methyl substituents (staggered vs. eclipsed) when referenced to the appropriate rotamer structure; the largest difference ΔE_b is 6.7 kJ/mol. Inspection of Table 4.16 reveals that the ligand binding energies E_b from IMOMM calculations are consistently larger than those from full QM calculations, by 9.6 to 23.4 kJ/mol if one leaves aside the bdo isomers with δE_b values of -46.9 and -43.6 kJ/mol, respectively. These differences are mainly due to approximating ethylthionyl ligands by their methylthionyl congeners in the QM subsystem of the IMOMM calculations.[59] Slight variations among the (regular) ligand binding energies, e.g. from δE_b = -11.4 kJ/mol for buos to δE_b = -15.9 kJ/mol for buis, stabilizes the latter structure and cause it to become the ground state of the QM/MM calculations.

No major differences in the electronic structure were observed between QM and QM/MM results, although the QM system in the IMOMM approach is reduced to $Cu_{13}(SCH_3)_8$. As in the QM calculations, doublet ground states were obtained for all isomers except for the pair tdo, for which again quartet states were determined. Gaps between highest occupied and lowest unoccupied spin orbitals amounted to 0.6–0.85 eV for structures with bridge coordinated ligands and to 0.05–0.1 eV for structures with terminally coordinated ligands, again in good agreement with the QM results. Thus, truncation of the ligand at the first CC bond preserves also essential features of the electronic structure of the cluster in the QM/MM calculation.

After this examination of the QM/MM results and their deviations from a full DF treatment, an adequate overall similarity between the energetics at the two levels of theory

shall be noted. The bdo isomers with their artificially close Cu-H contacts at the all-electron DF level have already been identified as special cases when their structures were analyzed. Above, it was concluded that IMOMM structures can be considered as more realistic than the pure QM structures which are significantly higher in energy for bdo isomers (by 206–283 kJ/mol, Table 4.16). Given these large energy differences, it seems worth studying whether the more realistic energetics at the QM/MM level in fact produces a local minimum that corresponds to the one located previously at the all-electron QM level.

To probe this conjecture, all-electron QM structure optimizations were started from *all* geometries optimized at the IMMOM level. Indeed, for three of the 16 isomers new minima were found with lower full QM total energies than obtained previously. It is not too surprising that the two special structures bdos and bdoe were among them; the new QM structures turned out to be substantially more stable (by 261 and 252 kJ/mol, respectively) than the previous QM structures. The third case was the isomer tuie, also discussed before as case with unusually close non-bonding contacts (see above); its new QM structure is by 38.2 kJ/mol more stable. As expected, ΔE_{MM} values characterizing the van der Waals repulsion decreased substantially for the new QM structures (bdos: 46.0 kJ/mol, bdoe: 167.4 kJ/mol, tuie: 740.6 kJ/mol). The corresponding structure and energy data for the bdo and tui isomers are displayed in the lower sections of Tables 4.13 to 4.16. Note that there is only one QM structure for the tuis isomer; the corresponding data are shown to allow a full comparison of all table entries.

The new bdo structures are now the only bridge coordinated systems for which an oblate cluster core was found (Fig. 4.16, QM2). Their ligands are threefold bound, as in the bu isomers. The S-C bond lengths of the new structures now fit better with values for other clusters with bridging ligands. The new full QM structures of the bdo isomers agree well with the corresponding QM/MM structures, with the largest differences (0.053–0.057 Å) occurring for the Cu_{ce}-Cu_{ax} distances (Table 4.15). The new QM structure of the tuie isomer is structurally quite similar to the old one, also yielding a relatively large difference of 14.9° to the QM/MM result of the sensitive angle Cu_{ax}-S-C_1 (Table 4.15). Now the average absolute (and maximum) deviations between QM and QM/MM results of *all* isomers are 0.018 Å (0.057 Å) for Cu_{ce}-Cu_{eq}, 0.010 Å (0.024 Å) for Cu_{ce}-Cu_{ax}, 0.026 Å (0.055 Å) for Cu_{eq}-S, 0.006 Å (0.018 Å) for Cu_{ax}-S, and 5.1° (14.9°) for Cu_{ax}-S-C_1.

The three new isomers, bdos, bdoe, tuie, also fit very well the energetic characteristics from the corresponding full DF calculations. The energy difference ΔE_{tot} between the staggered and eclipsed tui conformers is now reduced to -130.8 kJ/mol from

previously -169.0 kJ/mol (Table 4.14). Most noticeable is the agreement of the new QM energies for the bdo isomers with the corresponding QM/MM values; the δE_{tot} values (bdos: 22.0 kJ/mol, bdoe: -45.8 kJ/mol) now fall in the normal range (see above and Table 4.16). With these new total energies, the correlation between QM an QM/MM improves drastically; the regression coefficient r^2 for the values of E_{tot} increases from 0.87 for the original data to now 0.98 (Fig. 4.17). A similar improvement is observed for the differences δE_b between QM and QM/MM ligand binding energies. The deviation, previously ~45 kJ/mol, decreased to less than 15 kJ/mol (bdos: -14.2 kJ/mol, bdoe: -12.1 kJ/mol; Table 4.16).

From this reoptimization of QM structures, it is concluded that the overestimation of nonbonding interactions in the DF approach may lead to local minima that are different from those obtained with the IMOMM approach because the DF energetics favors structures involving artificially close contacts. Of course, on a potential energy surface in a high-dimensional space, it is quite difficult with a standard optimization procedure to avoid localizing a metastable local minimum instead of the true ground state. Yet, it is encouraging that, in the example discussed above, the more realistic treatment of van der Waals interactions in the QM/MM approach resulted in the identification of low-lying minima.

4.4.7 Conclusions

This QM/MM study on a ligand-protected d metal cluster was considerably improved and extended compared to a previous work, using a density-functional based IMOMM approach.[228] As a model compound the copper thiolate cluster $Cu_{13}(SCH_2CH_3)_8$ was chosen, imposing D_{4h} symmetry constraints to enable the evaluation of ligand arrangements with bridge-hollow and top coordination at the Cu_{13} cluster core. Various orientations of the ligands relative to the surface of the metal particle were considered as well as staggered and eclipsed forms of the ethyl end group of the ligands, yielding a test set of 16 conformers. Structures have been optimized with an LDA functional, energies were evaluated in single-point fashion using a GGA functional. To assess performance and accuracy of the IMOMM approach, all 16 isomers of $Cu_{13}(SCH_2CH_3)_8$ were optimized both at the all-electron DF and the QM/MM levels, using one starting geometry for each isomer.

With some exceptions, it was found that the QM/MM approach reproduces the

results of the full QM calculations in satisfactory fashion, both for structure and energy data. The structures of a pair of staggered and eclipsed rotamers (bdoe/bdos) showed close Cu-H or H-H contacts in the (original)[228] QM structures which were not reproduced in the corresponding QM/MM calculations. In that case, QM and QM/MM results for structure and energetics differed substantially. Less severe differences were found for other isomers exhibiting short nonbonding contacts (buis/buie, tuis/tuie, tdos/tdoe). In the *full* DF calculations with standard exchange-correlation functionals, such close nonbonding contacts lead to artificial attractive interactions which are absent in QM/MM calculations when van der Waals interactions are handled at the MM level. Reoptimization of all QM structures starting from QM/MM optimized geometries yielded new QM structures for those three isomers that previously had exhibited the strongest deviations from QM/MM results. The isomers of bdo obtained with the new full QM calculations exhibit ~0.8 Å longer Cu-H distances (bdoe 2.76 Å, bdos 3.24 Å). Nevertheless, the H-H contacts increased by only 0.2 Å for bdoe compared to the old isomer. Fig. 4.16 (QM2) reveals that even the ligands approach each other more closely in the new full DF structures than in those obtained with the QM/MM treatment. Thus, one obtains overall good agreement between QM and QM/MM calculations. The shortcomings regarding nonbonding interactions displayed by the DF approach, based on a standard exchange-correlation functional, in general lead to small deviations of structural and energetic results. For certain cases with largest structural discrepancies, the optimization actually had resulted in two different local minima.

Based on this study, it is concluded that the IMOMM approach is capable of treating metal cluster compounds comprising extended ligand shells. However, one has to be aware of potential deviations from a full quantum mechanical treatment when short non-bonding contacts occur, especially across the boundary of the QM and MM parts of the model. This issue is particularly crucial if the QM treatment is based on LDA or GGA density functional calculations. Such exchange-correlation functionals are known to fail for nonbonding (dispersion) interactions. Thus, in contrast to other systems, one may expect that a QM/MM approach, employing a suitably parameterized force field, will yield more reliable results for systems involving many van der Waals contacts in the ligand shell or across the boundary of the QM and MM regions.

4.5 The cluster compound $Au_{55}[P(C_6H_5)_3]_{12}Cl_6$

Quickly after its synthesis, the cluster compound $Au_{55}[P(C_6H_5)_3]_{12}Cl_6$ received a considerable amount of interest because it was assigned to be monodisperse and relatively stable even under standard conditions.[19] Monodispersity is an extremely important feature for the purposes of nanosciences as this entails precise (size dependent) properties of the material, at variance with cluster samples that feature a non negligible size distribution.[3] Size specific synthesis of cluster compounds would make also size dependent effects readily available to experimentalists without using special cluster sources. Experimental efforts were made with a variety of methods to characterize the $Au_{55}[P(C_6H_5)_3]_{12}Cl_6$ and to gain insight into its electronic structure.[247] As this Au_{55} cluster compound does not yield crystals suitable for x-ray crystallographic investigations, information on its structure is restricted to results obtained by other indirect approaches. Yet, no unequivocal answer to open questions regarding structure and dispersity could be given; therefore, the controversy about $Au_{55}[P(C_6H_5)_3]_{12}Cl_6$ is still alive,[248] even 25 years after the first report on its synthesis.[19] For $Au_{55}[P(C_6H_5)_3]_{12}Cl_6$ also ordered nanostructures in one, two, and three dimensions have successfully been generated,[34] which opens prospects of building materials with new properties. In this thesis the first accurate quantum chemical calculations on a model for $Au_{55}[P(C_6H_5)_3]_{12}Cl_6$ are presented and discussed, as well as compared to the body of experimental knowledge.

4.5.1 Experimental results

The synthesis of $Au_{55}[P(C_6H_5)_3]_{12}Cl_6$ by the group of Schmid[19] was a remarkable success, because for the first time a high surplus of metal atoms with respect to ligands seemed to have been achieved in a monotypical ligand-protected transition metal cluster species.[19] Before, only well defined gold clusters of the type $Au_{11}L_7X_3$ and $[Au_{13}(LL)_6]^{4+}$ (L = phosphane, LL = diphosphane, X = halogen) had been synthesized, which contain only slightly more gold atoms than ligands.[249-251] Whereas these small clusters Au_{11} and Au_{13} were generated by reduction of gold-phosphanes with $NaBH_4$, the Au_{55} cluster was synthesized by reducing $(C_6H_5)_3PAuCl$ with B_2H_6 in benzene at 50 °C. This cluster compound is stable enough to be purified by reprecipitation in CH_2Cl_2, but decomposes slowly in solution.[19] This decomposition can be prevented by adding $P(C_6H_5)_3$ to the solution, which gave rise to the hypothesis that the decomposition takes place by dissociating phosphanes and coagulation to form metallic gold.[19] An elemental analysis

was resolved with the sum formula $C_{36}H_{30}Au_{9.2}ClP_2$. Molecular weight analysis delivered the following weight percentages:[19]

$C_{36}H_{30}Au_{9.2}ClP_2$:	C 18.28	H 1.28	Au 76.33	Cl 1.50	P 2.62
Experimental:[19]	C 17.66	H 1.28	Au 76.10	Cl 1.70	P 2.60

Apparently, the proposed sum formula is reasonable well confirmed, although deviations of 0.6 and 0.2 are to be noted for carbon and chlorine. A different cluster like $[Au_5(LL)_4]^{2+}$, confirmed by x-ray crystallography, shows a smaller deviation of 2 % in the mass weight for carbon which may rationalize the previously found deviation as it is also the parameter with the largest deviation.[251] Further evidence to back up the sum formula of $C_{36}H_{30}Au_{9.2}ClP_2$ is provided by the following two reactions, which have been followed quantitatively:[19]

$$Au_{9.2}[P(C_6H_5)_3]_2Cl + X \rightarrow (C_6H_5)_3PAuCl + (C_6H_5)_3PAuX + 7.2\ Au; \qquad X = Br, I$$

$$Au_{9.2}[P(C_6H_5)_3]_2Cl \rightarrow 8.2\ Au + [(C_6H_5)_3P]_2AuCl$$

Thus, the ratio of elements contained in the cluster compound is definite, but it has to be determined how many of these basic formula units form the cluster compound. To clarify this open question, the molecular mass has been measured by two different methods. Assuming a spherical compound and applying Stoke's law, analysis of the sedimentation speed in a sedimentation experiment resulted in a mol mass of 15760 g/mol.[19] An osmometric measurement of the mol mass yielded a value of 13000 g/mol.[19] Several years later a different group recorded by ^{252}Cf plasma desorption mass spectroscopy a sample prepared by Schmid's group and received a distribution of mol masses with a maximum at 16600 m/z.[252] One formula weight of $Au_{9.2}[P(C_6H_5)_3]_2Cl$ amounts to a mol mass of 2372.1 g/mol. Thus, by osmometry 5.5 times the formula weight is found, while the ^{252}Cf plasma desorption mass spectroscopy yields 7.0 times and the sedimentation analysis 6.6 times this value. All together, the measurements of mol masses can be interpreted in such a way that the cluster compound contains about 6 or 7 formula units. Based only on the data from the ^{252}Cf plasma desorption mass spectra a cluster with the formula $Au_{67}[P(C_6H_5)_3]_{14}Cl_8$ (molecular mass of 17152.5 g/mol) has been suggested,[252] which is inconsistent with the formula derived by Schmid and higher in mass than the maximum of the mass spectrum.[252] Following this latter suggestion an element analysis of the Au_{67} compound is calculated here and compared to the data in the literature.[19] The following weight percentages result:

$Au_{67}[P(C_6H_5)_3]_{14}Cl_8$:	C 17.65	H 1.23	Au 76.94	Cl 1.65	P 2.53
Experimental:[19]	C 17.66	H 1.28	Au 76.10	Cl 1.70	P 2.60

As this comparison shows, the data measured fit the sum formula proposed by Schmid with about the same quality.[19] For the Au_{67} compound, carbon and chlorine weight

percentages match better; on the other hand hydrogen, phosphorus and gold show stronger deviations than for an Au_{55} derived species. All together the average absolute deviation in percent of mass weight percent is 2 % for an Au_{67} cluster, compared to 3 % for an Au_{55} structure model. A further uncertainty with respect to the identity and stability of $Au_{55}[P(C_6H_5)_3]_{12}Cl_6$ is that the mol mass distributions vary with time, depend on the storage temperature, and on the group which prepared the sample.[252,253] On the other hand, it was also stated that the conditions of the plasma desorption mass spectroscopy experiment could change the nuclearity and shape of the gold clusters in the sample.[254] Thus the identity of the cluster compound and its narrow size distribution still remain somewhat controversial.[248,252,254- 259]

In the original work by Schmid a closest packing structure of cuboctahedral shape was assumed as a precondition for a structure proposal.[19] The proposal of a cuboctrahedral shape was suggested by analogy to the example of the smaller cluster $[Au_{13}(LL)_6]^{4+}$,[19] although in the publication cited by Schmid the Au_{13} cluster core is reported to be of icosahedral shape.[251] Assuming a cuboctahedron, one infers that 6 $Au_{9.2}[P(C_6H_5)_3]_2Cl$ units form the compound, simply by comparison to the possible sizes of ideal cuboctahedra, which contain 13, 55, 147, or 309 atoms.[8] Based on these assumptions, the cluster $Au_{55}[P(C_6H_5)_3]_{12}Cl_6$ was introduced. Cuboctahedra feature 12 corners and 6 facets, it is straightforward to suggest chlorine to be located at the centers of the facets and phosphine ligands at the corner atoms.[19] The alternative compound $Au_{67}[P(C_6H_5)_3]_{14}Cl_8$, as suggested by a different group, has a structural motif of vertex sharing Au_{13} icosahedra with phosphines attached to elevated gold corners and chlorines on outside bridge sites.[252,260] A Mößbauer spectrum reported in original publication[19] provided further evidence for the cuboctahedral structure of the Au_{55} cluster. According to the cuboctahedral cluster model four different types of gold atoms should be found: 13 inner ones (12-fold coordination) (A), 24 peripheral not coordinated to ligands (B), 12 peripheral atoms coordinated to $P(C_6H_5)_3$ (C), and 6 peripheral gold atoms coordinated to chlorine (D).[19] For the fitting procedure relative intensities of B, C, and D were assumed to obey the ratio 4:2:1.[19] The peak with lowest isomeric shifts (I.S.), which is close to the value for bulk gold, was assigned to category A atoms. Gold atoms B were assigned to I.S. 1.13 mm/s, where no data for comparison are available.[19] An I.S. of 0.88 mm/s was assigned to C, because in previous studies of Au-$P(C_6H_5)_3$ 1.5 mm/s were found in $[Au_{11}[P(C_6H_5)_3]_8Cl_2]^+$.[261] For chlorine coordinated Au atoms an I.S. of -0.09 mm/s was determined, compared to 0.6 mm/s for Au_{11}-Cl in $[Au_{11}[P(C_6H_5)_3]_8Cl_2]^+$.[261] It is difficult to interpret this Mößbauer spectrum in any other direction, as the fitting procedure was adapted to fit the four types of gold atoms, and for other structural suggestions one would have to reinterpret the original

data. The cuboctahedral model has been similarly controversially discussed as the size uniformity and the nuclearity before.[252-256,262]

For $Au_{55}[P(C_6H_5)_3]_{12}Cl_6$ calorimetric measurements have been performed to investigate the overall stability and the Au-Au bond strength.[263] A destructive reaction can be triggered thermally and happens as a "strong sharp exothermic decomposition"[263] which was interpreted as additional sign for having investigated a single well defined compound.[263] Based on the decomposition in solution the following reaction was suggested:

$$Au_{55}[P(C_6H_5)_3]_{12}Cl_6\ (s) \rightarrow 6\ (PC_6H_5)_3AuCl\ (s) + 49\ Au\ (s)$$

A decomposition enthalpy of 1590 kJ/mol was measured at 156 °C.[263] With the number of ligand bonds being equal before and after the decomposition, the strength of Au-Au bonds in the cluster can be estimated by relating the change in the number of Au-Au bonds to the reaction enthalpy.[263] The cluster comprises 216 nearest-neighbor metal-metal bonds, while for 49 bulk gold atoms 294 bonds are counted.[263] From the atomization energy of bulk gold a binding energy of 16442 kJ/(mol Au_{55}) has been calculated which translates into an energy of 76.1 kJ/mol per Au-Au bond.[263]

Even though nuclearity and structure of the Au_{55} core could not yet convincingly be proven, experimentalists tried to determine geometrical parameters for gold atoms in the cluster core and for the ligands binding to them. Several EXAFS experiments were carried out.[259,262,264] Results from these experiments are collected in Table 4.17. Different publications quote inconsistent gold inter metal distances of 2.75–2.80 Å, with 2.785±0.003 Å being the result with the smallest error range.[259] All these values are noticeably shorter than the bulk Au-Au distance of 2.88 Å.[9] Coordination numbers scatter similarly for different studies, 7.8,[264] 7.6,[262] and 6.5,[259] but are consistent; their uncertainties range from 0.4 to 1. For an ideal cuboctahedron of 55 gold atoms, the average coordination number is 7.85. The results for the Au-Cl bond lengths in Table 4.17 contradict each other with 2.31 and 2.50 Å, but the explanation is straightforward: The signals for the Au-Cl and Au-P bonds have been interpreted differently.[262,264] Benfield et al. justify their assignment by a measurement on $Au_{11}L_7I_3$ where they find a Au-P distance of 2.27 Å, and by the larger scattering of gold-chlorine bonds in other cluster and coordination compounds of gold.[262] The Au-Cl bond length was determined at 2.31 Å with a coordination number of 0.2±2,[264] or 2.50 with a coordination number of 2.3±1.[262] Correspondingly, the gold–phosphorus bond length is 2.30 Å with a coordination number of 0.66±0.3,[262,259] which is in agreement with the Au-Cl bond lengths of Reference 264. One investigation was able to resolve more than a single shell of Au-Au distances:[262] second and third shells were found at 3.93 Å and 4.88 Å with coordination numbers of

Table 4.17 Nearest neighbor distances d (Å) and coordination numbers N of $Au_{55}[P(C_6H_5)_3]_{12}Cl_6$ from EXAFS experiments.

Reference	d(Au-Au)	N	d(Au-Cl)	N	d(Au-P)	N
264	2.80 ± 0.01	7.8 ± 1	2.31 ± 0.01	0.2 ± 2	−	−
262	2.75 ± 0.01	7.6 ± 1	2.50 ± 0.01	2.3 ± 1	2.30 ± 0.02	0.66 ± 0.3
	3.93 ± 0.04	5.0 ± 8				
	4.88 ± 0.01	0.6 ± 0.5				
259	2.785 ± 0.003	6.5 ± 0.4	−	−	2.30 ± 0.02	

5.0±8 and 0.60±0.5, respectively.[262] An ideal icosahedral cluster shows a bimodal distribution of gold bond lengths with 5 % difference between shorter radial and longer tangential bonds. For the cluster $Au_{11}L_7I_3$ these two different bond lengths have been resolved in EXAFS spectra, but not for $Au_{55}[P(C_6H_5)_3]_{12}Cl_6$.[262] This is in contrast to the structure proposed in Reference 252 with vertex sharing icosahedra. An Au-Cl stretching frequency was determined to be 280 cm^{-1} in $Au_{55}[P(C_6H_5)_3]_{12}Cl_6$, while the reactant of the synthesis, $(C_6H_5)_3PAuCl$, exhibits this mode at 330 cm^{-1}.[19]

Also the electronic structure of the cluster compound $Au_{55}[P(C_6H_5)_3]_{12}Cl_6$ was subject to intense experimental research.[18,265- 274] Several UV-VIS and XPS spectra have been recorded for either the region close to the Fermi level or selected core levels (Au 4f orbitals).[265,266,269] A very interesting result is summarized in Table 4.18 where Au 4 $f_{7/2}$ orbital energies are assigned to various types of gold atoms of the cluster.[266] The ligand coordination shows a strong effect on these core levels; see later on the comparison with computational results.

Table 4.18 Au $4f_{7/2}$ core level binding energies of $Au_{55}[P(C_6H_5)_3]_{12}Cl_6$ (in eV) according to Ref. 266.

Type	Au $4f_{7/2}$
core	84.4
bare surface	84.0
P-bonded	85.3
Cl-bonded	86.3
bulk gold	84.0
gold surface	83.6

A destructive effect of x-ray irradiation was observed, when the time dependent changes of core level spectra were inspected: The $Au_{55}[P(C_6H_5)_3]_{12}Cl_6$ cluster compound looses chlorine atoms upon irradiation.[265] After 30 hours of exposure no chlorine signals were detectable anymore (cf. Figure 4.18).[265] Thus, one may be able to investigate this gold cluster compound without the chlorine ligand. Especially in the vicinity of the Fermi level the removal of chlorine increases the intensity of UPS spectra from close to zero by a factor of 6 similar to the intensity measured for a gold film.[265] This was interpreted as an insulator-to-metal transition due to the removal of the chlorine ligands.[265] As $Au_{55}[P(C_6H_5)_3]_{12}Cl_6$ has an uneven electron count, it should be ESR active. Nevertheless, several attempts to get reproducible ESR spectra at low temperature remained unsuccessful.[247,275] A signal could be recorded at room temperature with a g-value of 2.00 and line width of 0.15 mT, but it disappeared on evacuating the sample tube for low temperature studies.[247] A different study found a g factor of 1.9204 and a line width of 67 mT at 4.4 K.[276] For $Au_{55}[P(C_6H_5)_3]_{12}Cl_6$ a conductivity of the order of 10^{-5} $\Omega^{-1}cm^{-1}$ was found, which is considerably higher than the value of 10^{-11} Ω^{-1} cm^{-1} determined for $Ni_{38}Pt_6(CO)_{48}H_2(PPN_4)$.[268]

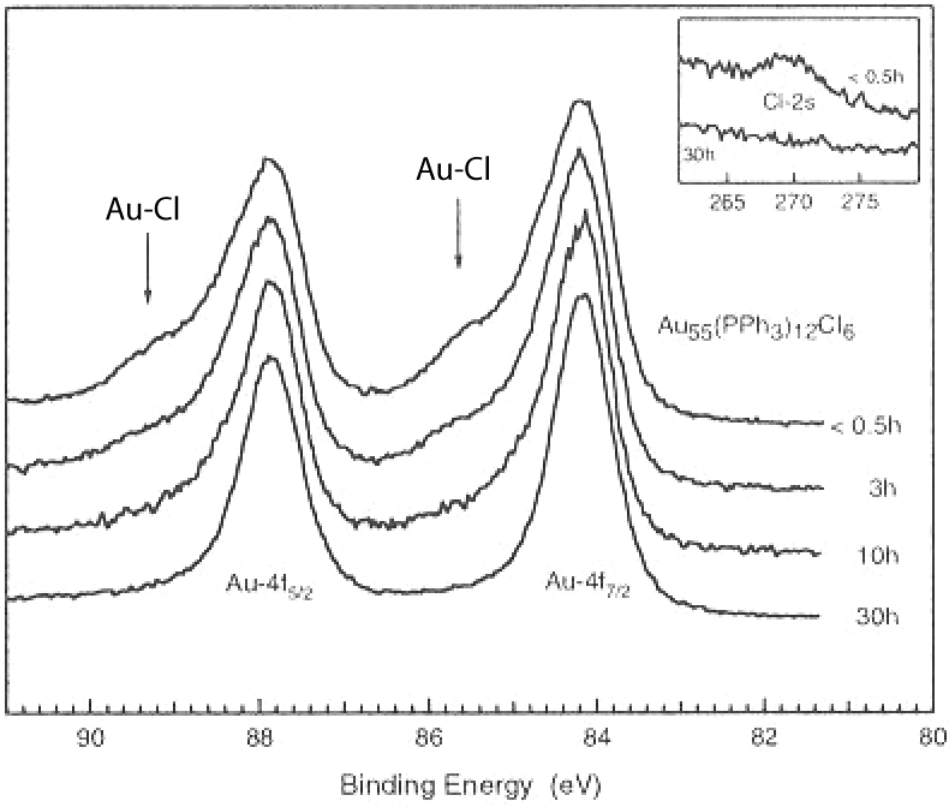

Figure 4.18 Au 4f core level spectra for $Au_{55}[P(C_6H_5)_3]_{12}Cl_6$ in dependence of x-ray exposure time. The inset shows the Cl 2s binding energy region, indicating removal of chlorine after 30 hours. Figure adapted from Ref. 265.

Despite extensive experimental effort as discussed above, open questions are evident, like a confirmation of structure and nuclearity as well as of metal-metal and the metal-ligand bonding. A quantum chemical treatment of $Au_{55}[P(C_6H_5)_3]_{12}Cl_6$ can help to contribute to the interpretation of experimental findings and to gain more insight into these open questions.

4.5.2 Density functional calculations

In this theoretical investigation, the cluster $Au_{55}[P(C_6H_5)_3]_{12}Cl_6$ was investigated with the help of simplified model compounds. A nuclearity of 55 gold atoms was assumed, as well as a cuboctahedral shape of the metal cluster as proposed by several experiments.[19,262] First, a bare Au_{55} cluster model was investigated in different symmetries and geometries as reference. Second, chlorine coordination at various sites of on a Au_{55} cluster was investigated. The evaluation of model ligands replacing $P(C_6H_5)_3$ is discussed and effects of this approximation are described in the next part of the investigation. Later, model phosphine ligands were coordinated to Au_{55} to test the effects of only these ligands. Taken together, all this leads to the final model $Au_{55}[PH_3]_{12}Cl_6$. The results for this model are discussed and finally they are compared to experimental information presented above. In this work different coordination modes of chlorine are classified by μ_1 for terminal, μ_2 for bridge and μ_3 for hollow coordination. The second label is the standard notation for the symmetry of the molecule investigated. Several isomers of one type of chlorine coordination in one symmetry are discriminated by labels "α" and "β". For example, $Au_{55}(PH_3)_{12}(\mu_3\text{-}Cl)_6$ S_6 α denotes one isomer of an Au_{55} model cluster with chlorine at hollow sites, calculated in S_6 symmetry.

4.5.3 Methodological details

Besides the computational details summarized in Section 3.2 the following comments are specific to the computational investigation of $Au_{55}[P(C_6H_5)_3]_{12}Cl_6$. In all calculations, the elements of the density matrix were converged to at least 10^{-8} au in the SCF procedure. Geometries were considered to be converged when the maximum component of the energy gradient and the optimization step had dropped below 10^{-5} au.

Ligand binding energies have been calculated according to

$$E_b = E_{tot}[Au_{55}] + E_{tot}[X] - E_{tot}[Au_{55}X]$$

where X represents the ligand studied. The total energy of the Au_{55} cluster isomer in the corresponding symmetry was taken as a reference. When different ligands are bound to Au_{55} and the binding energy of a specific ligand is given, it has been evaluated according to

$$E_b(X) = E_{tot}[Au_{55}Y] + E_{tot}[X] - E_{tot}[Au_{55}XY]$$

4.5.3.1 Bare Au_{55}

First, calculations on the bare cluster Au_{55} will be presented as reference for changes due to the effects of ligation. Different symmetry constraints have been imposed. Besides O_h symmetry of the cuboctahedron and its sub group D_{2d} (not shown in Table 4.19, as results were identical to those in O_h symmetry) also as an alternative structure the icosahedron was inspected. A distorted icosahedral structure was obtained when symmetry constraints according to S_6 were imposing to a cuboctahedral cluster. The icosahedral distortion is possible because I_h and S_6 share the S_6 axes.[277] For a cuboctahedral Au_{55} cluster an average inter-metal distance of 2.774 Å was calculated, while the icosahedral model yielded 2.800 Å. A distorted icosahedral structure in S_6 yielded a slightly longer average Au-Au distance, 2.803 Å. The ideal icosahedral cluster model is the only one in this comparison with a quartet electronic state, while others form a doublet. In the case of I_h a Jahn-Teller distortion is expected because the degenerate HOMO ($66\ g_g^1$) is only singly occupied. Therefore, it does not come as surprise that the I_h structure has also the largest HOMO-LUMO gap of 0.9 eV while the cuboctahedron has a gap of 0.22 eV and the gap of a distorted icosahedral species is 0.14 eV. The ionization potential is 6.31 eV for cuboctahedral shapes, 6.13 and 6.18 eV for icosahedral shape and its distorted congener, respectively. A similar trend was obtained for the electron affinities with 4.1 eV for a cuboctahedral shape and 3.9 eV for icosahedral forms. The binding energy per Au-Au bond varies by about 10 % for different shapes, from 64 to 59 kJ/mol, for the simple reason that the total number of bonds varies with shape. Indeed the binding energy per atom for all three shapes is 251 kJ/mol.

Table 4.19 Au_{55} clusters in O_h, S_6, and I_h symmetry. Average bond length <Au-Au>, ground state spin multiplicity M, HOMO-LUMO Gap, ionization potential IP, electron affinity EA, and relative total energies E_{rel} referenced to the most stable structure S_6 and binding energies per Au-Au bond E_{bond} as well as their count n are given. Distances in Å, energies in eV and binding energies in kJ/mol.

Symmetry	<Au-Au>	M	Gap	IP	EA	E_{rel}	E_{bond}	n
O_h	2.774	2	0.22	6.31	4.09	6.6	64	216
I_h	2.800	4	0.90	6.13	3.88	20.8	59	234
S_6	2.803	2	0.14	6.18	3.93	0.0	59	234

The comparison of total energies illustrates that these structures are rather close in energy. Therefore, they can easily transform into each other given the influence of a ligand environment. In a previous study with a larger basis set the icosahedral structure was calculated 265 kJ/mol more stable than the cuboctahedral shape, which translates to a difference per atom of less than 5 kJ/mol.[10] Because in the present study larger systems and systems of low symmetry were treated, it was mandataory to use a smaller basis set and the uncertainty of the shape has to be clarified later on. Early studies, using a density functional method[10] and a tight binding approach,[278] predicted for bare Au_{55} that an icosahedral shape is 265 kJ/mol and 26 kJ/mol, respectively, preferred over a cuboctahedral shape. In a recent density functional study[279] the icosahedral shape was determined 106 kJ/mol more stable. For averaged inter and intra shell distances, a bimodal

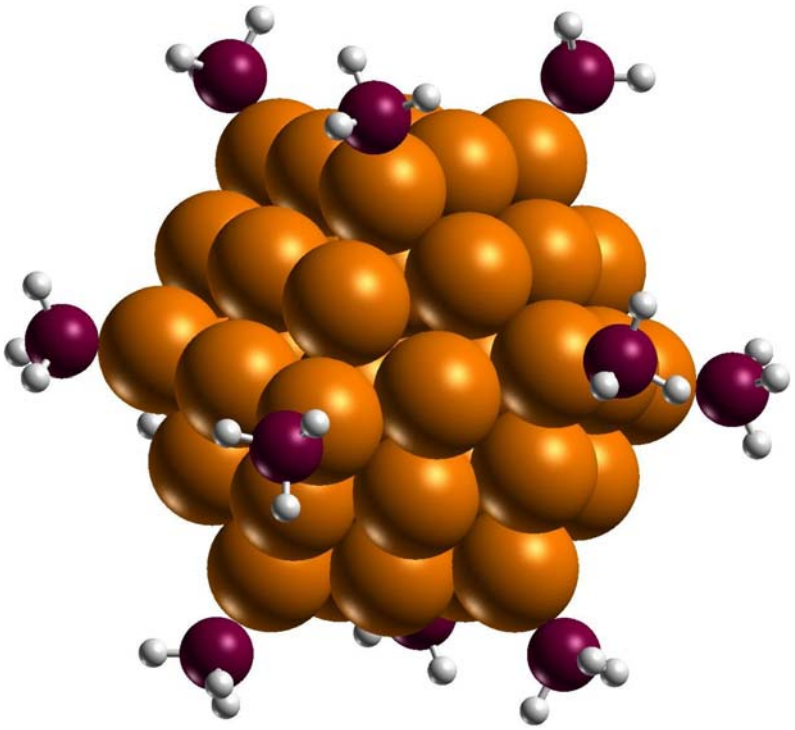

Figure 4.19 Cluster $Au_{55}(PH_3)_{12}$ in D_{2d} symmetry.

distribution is found for the distorted icosahedral structure, with inter shell bonds of 2.72 Å and intra shell bonds of 2.83 Å. This difference may be identified in an EXAFS analysis, provided the accuracy is good enough; this would allow a distinction between octahedral and icosahedral shapes of the Au_{55} metal core.

4.5.3.2 Phosphine ligand models

To simplify the calculations, the triphenylphosphine groups $P(C_6H_5)_3$ of $Au_{55}[P(C_6H_5)_3]_{12}Cl_6$ were modeled as simple phophanes, PH_3, and the effect of this replacement was tested on the molecule $P(C_6H_5)_3AuCl$. Another study investigated the effects of simplification of the phosphine ligand on the slightly different molecule (CH_3AuPR_3) and found that the effect on bond lengths is less than 0.03 Å and energetics can be accurate to 1% if the Au-CH_3 bond is inspected, which is not directly involved in the replacement.[280] Table 4.20 shows that crystal structure and EXAFS measurements for $ClAuP(C_6H_5)_3$ match with at most 1 % deviation in direct bond lengths.[281] When PH_3 is used as model ligand the Au-P distance of $ClAuP(C_6H_5)_3$ is reproduced with 1 % deviation as well. The Au-Cl bond length on the other hand is calculated 2 % too short compared to the XRD result for $ClAuP(C_6H_5)_3$, while the EXAFS results reproduce exactly the value of the x-ray diffraction experiment. As this calculated Au-Cl is too short compared to experimental findings, it is not surprising that the corresponding stretching frequency, 386 cm^{-1}, is too high compared with experiment, 330 cm^{-1}.[19] For this bond the electron donating effect of the $P(C_6H_5)_3$ group may play a role. To test this hypothesis, the ligand was modeled by $P(CH_3)_3$. Then the Au-P bond matches even better the value of the crystal structure of $ClAuP(C_6H_5)_3$, with a deviation of only 0.012 Å,[282] whereas the Au-Cl bond is elongated slightly (0.014 Å) and thus somewhat closer to the experimental value (1.5 % deviation). The Au-Cl vibrational frequency, 350 cm^{-1}, agrees better with experiment (20 cm^{-1} deviation). This is a quite reasonable accuracy taking into account the approximate representation of the phosphine moiety. Results of similar accuracy have been determined in a previous study.[280] When the results for $ClAuP(CH_3)_3$ are compared with experimental data for this molecule, a deviation in the Au-P distance of 0.01 Å is found as well.[283] The fact that the Au-Cl bond length is 0.07 Å longer in the crystal structure than in the calculation may be due to a special aspect of the crystal structure, which orients the molecules in a loose Au-Au chain; this may result in elongated bond distances and may also rationalize the low vibrational Au-Cl mode of 312 cm^{-1}.[284] This argument makes the good agreement for the Au-P distance look somewhat coincidental, unless it would not be affected by the chain formation and is rather independent of changes in the molecule,

Table 4.20 Results of $ClAuP(C_6H_5)_3$ from x-ray diffraction of crystal structures, EXAFS experiments, IR spectroscopy, and calculations with different model ligands. Distances d in Å and vibrational frequencies ν in cm^{-1}.

	$ClAuP(C_6H_5)_3$ EXAFS[a]	$ClAuP(C_6H_5)_3$ XRD[b]	$ClAuP(CH_3)_3$ XRD[c]	$ClAuP(CH_3)_3$ Calc	$ClAuPH_3$ Calc
d(Au-P)	2.214	2.235	2.233	2.223	2.212
d(Au-Cl)	2.277	2.279	2.310	2.245	2.231
d(Au-C)	3.7	3.4		3.406	–
ν(Au-Cl)	330[d]	–	312[e]	350	386

[a] Ref. 281 [b] Ref. 282 [c] Ref. 283 [d] Ref. 19 [e] Ref. 284

which might be plausible as the Au-P bond remains constant even for the replacement of $(C_6H_5)_3P$ to $(CH_3)_3P$ (Table 4.20). PH_3 was chosen as a first approximation to study phosphine effects on Au_{55}, but one should keep in mind that the length and the strength of the Au-Cl bond may be slightly underestimated.

4.5.3.3 Model phosphine ligands PH_3 on Au_{55}

The effects of the model ligand PH_3 were investigated on a cuboctahedral Au_{55} cluster in D_{2d} symmetry, which has the very same geometry as the structure with O_h symmetry. For the 12 ligands terminal coordination at the corners of facets was considered following the structure model of Schmid for $Au_{55}[P(C_6H_5)_3]_{12}Cl_6$.[19] In general, the effects of PH_3 on the cluster are small. The Au-P bond length amounts to 2.31 Å which is 0.1 Å longer than calculated for $ClAuPH_3$ (Tab. 4.20), in line with the higher coordination of Au. The average Au-Au bond length is increased by 0.01 Å to 2.78 Å. The gold atoms bound to the phosphane ligand relax their distances to their Au neighbors by 0.02 Å. Based on a Mulliken analysis a small charge transfer of about 0.3 e from the ligand shell to the Au_{55} cluster is estimated. The binding energy per PH_3 on Au_{55} amounts to 71 kJ/mol and is rather weak compared to the atomization energy per Au atom, 251 kJ/mol, of the bare cluster, but stronger than the average Au-Au bond of ~ 64 kJ/mol. The ligated cluster is computed as doublet. The 12 PH_3 ligands have a strong effect on ionization potential and electron affinity. IP and EA values are reduced by 1.7 and 1.5 eV, respectively compared to the Au_{55} cluster in S_6 symmetry. On the basis of previous results,[280] one would assume that the binding energy would be stronger for $P(C_6H_5)_3$. However, steric effects may play a role in the $Au_{55}[P(C_6H_5)_3]_{12}Cl_6$ cluster and destabilize the binding of the latter ligand. When the two effects discussed are taken together one would estimate that PH_3 should be a good indicator for the phosphine ligand bond strength.

4.5.3.2 Chlorine coordination on Au_{55}

The coordination of chlorine was examined separately before investigating the full model cluster compound. To do that, the energy profile along various binding sites of chlorine was scanned. Table 4.21 shows the coordination modes that were inspected in D_{3d} symmetry and the corresponding scan parameter α. This scanning angle α was defined as the angle between the main symmetry C_3 axis and a line between central atom and chlorine. In this way one- to three-fold coordination could be investigated as illustrated in Figure 4.20. Au-Cl distances vary strongly with coordination modes from 2.31 Å for the strongest bound top coordination between the two adjacent facets to 2.56 Å for a hollow coordination on the (111) facet (cf. Fig. 4.20). Apparently, the gold-chlorine bond length is a sensitive probe for the coordination site; it increases by 0.1 Å per coordinated gold atom. Among these models, the average Au-Au bond lengths vary by only 0.03 Å and also increases with increasing Cl coordination, at variance with the trend of binding energy (see above). Thus, chlorine ligands affect the overall cluster geometry slightly on average, but for single bonds, like a Cl-bridged Au-Au bond, changes can be up to 0.4 Å. The Cl binding energies clearly show that the on-top chlorine position proposed for the $Au_{55}[P(C_6H_5)_3]_{12}Cl_6$ is the least stable one.[19] One gains 40 kJ/mol per atom if the chlorine ligands slide to the nearest bridge position. There is even no barrier for this shift of a top coordinated chlorine atom to a bridge position on the very same (100) facet. A second top position at edges between the two facet types was also tested and found to be slightly more stable by 6 kJ/mol compared to the central (100) top site. The hollow position is the second most stable coordination site with a 12 kJ/mol weaker binding energy per chlorine. Inline with this result for the edge top coordination, the Au-Cl bond is 0.04 Å shorter and Au-Au distances to the nearest neighbor are longer, while the average Au–Au distance remains unchanged.

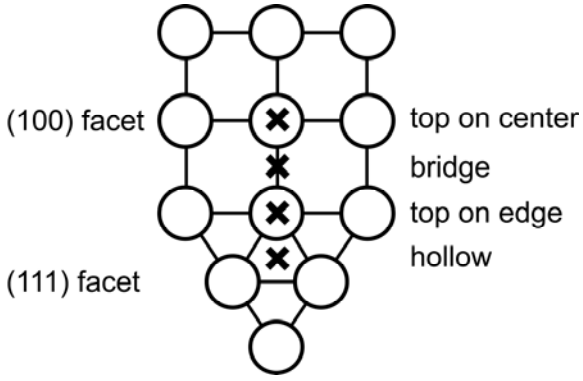

Figure 4.20 Schematic sketch of different investigated chlorine positions on facets of the cuboctahedral Au_{55} cluster.

Table 4.21 Calculated properties of $Au_{55}Cl_6$ in D_{3d} symmetry, scanning chlorine positions (α is the angle between the main symmetry axis and a line from the central Au atom and to the chlorine), bond lengths, average distances <X-Y>, binding energies BE per chlorine atom, Cl-Au vibrational frequencies ν evaluated in a D_{3d} symmetry restricted normal mode analysis and total charge $q(Cl_6)$ of the Cl ligand shell for different binding sites of chlorine. Au1 and Au2 denote different gold atoms in the vicinity of chlorine. For hollow coordination, there are two Au2-Cl bonds. For coordinations see Figure 4.20. Angles in degree, distances in Å, binding energies in kJ/mol, and vibrational frequencies in cm^{-1}.

α	Coordination	facet	Au1-Cl	Au2-Cl	<Au-Au>	BE	ν	$q(Cl_6)$
54.5	top on center	(100)	2.343	3.763	2.783	204	305/*66i*	-1.6
60.0		(100)	2.347	3.161	2.786	213		-1.4
66.0		(100)	2.394	2.575	2.792	241		-1.0
68.7	bridge	(100)	2.459	2.456	2.795	246	261/181	-0.9
90.0	top on edge	(100)/(111)	2.307	4.517	2.783	210	330/58	-1.5
111.4	hollow	(111)	2.555	2.566	2.811	234	234/131	-0.5

The Au-Cl frequencies given in Table 4.21 can be taken as rough estimates only because the frequency has been evaluated in D_{3d} symmetry, i.e. the normal mode analysis was restricted to degrees of freedom that conform with this symmetry. Overall, it can be seen from Table 4.21 is that the Au-Cl frequency of $Au_{55}Cl_6$ varies over a range of nearly 100 cm^{-1} with the chlorine coordination, and thus is just as variable as the Au-Cl bond length. This indicates that different coordination modes of chlorine should be discernible experimentally. Also the charge withdrawn from the Au_{55} cluster by the chlorine ligand shell shows a nice trend towards lower charge separation for higher coordinated chlorine

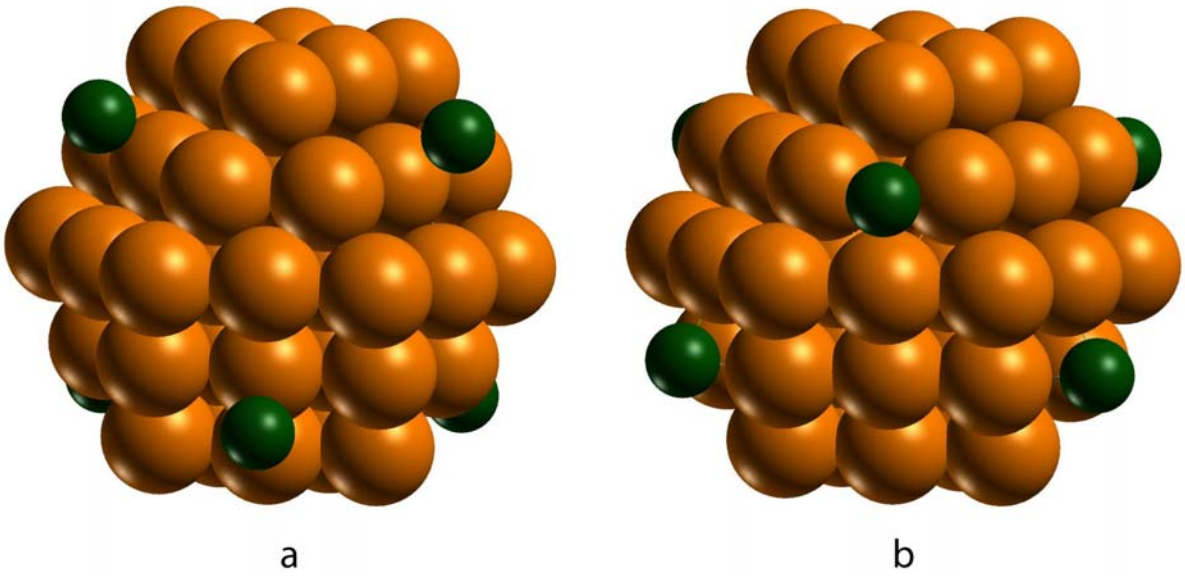

Figure 4.21 Cluster $Au_{55}Cl_6$ with chlorine coordinated a) on top on (100) and b) in bridge-hollow sites on (111) facets of Au_{55} in O_h and D_{3d} symmetry, respectively.

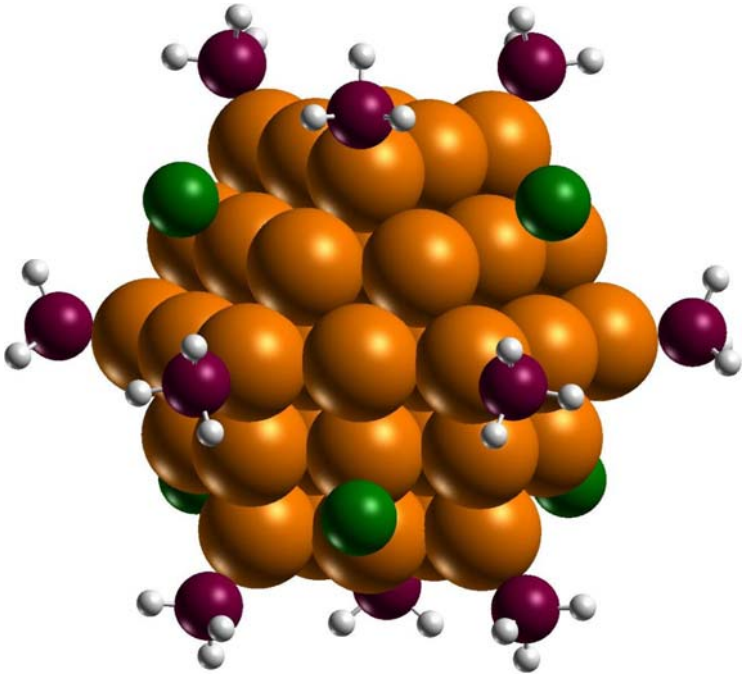

Figure 4.22 Optimized cluster model $Au_{55}(PH_3)_{12}(\mu_1\text{-}Cl)_6$ D_{2d}.

atoms. For top coordinated ligands, a total of -1.5 e is found on the ligands, while for bridge coordination -0.9 e, and for hollow coordination -0.5 e are transferred to the shell of chlorine ligands. One has to keep in mind that this trend could be an artifact of the Mulliken analysis, because more basis functions of gold atoms are brought close to the chlorine atoms with increasing coordination.

In summary, for $Au_{55}Cl_6$ bridge coordination of chlorine is most favorable and 20 kJ/mol per chlorine more stable than hollow coordination and 40 kJ/mol per chlorine more stable than terminal coordination proposed previously.[19] The same trends have been found for chlorine atoms on an Au(100) surface, where bridge sites were calculated as most stable, ~20 kJ/mol per chlorine more stable than terminal coordination.[285] On the (100) surface, the second most stable site is the four-fold hollow site, 9 kJ/mol per Cl less stable than the bridge site.[285] Combining all these preparatory studies, the next section will present results for several chlorine coordination sites on Au_{55} clusters with model phosphane ligands PH_3.

4.5.3.3 $Au_{55}[PH_3]_{12}Cl_6$

Because of the size of this problem not all possible sites of chlorine at the cluster $Au_{55}(PH_3)_{12}$ could be studied. In the focus of this study were the top site on the center of the (100) facet, which was suggested in the literature,[19] the bridge site on a (100) facet as well as a hollow site on a (111) facet, which turned out in preparatory studies of $Au_{55}Cl_6$ to

be quite stable. A D_{2d} symmetry model of Au_{55} was used to investigate the structure as proposed by Schmid, where the chlorine atoms are located at the center of a (100) facet (Figure 4.21a).[19] To model bridge sites on (100) facets or threefold-hollow sites on (111) facets (Figure 4.21b), a structure in S_6 symmetry had to be used. Theoretically all possible coordination sites of chlorine could be computed in S_6 symmetry, which is the minimum restriction to ensure all sites of the 6 chlorine atoms to be equivalent. Even this restriction is somewhat artificial because in general one can imagine the chlorine atoms to move independently of each other. Nevertheless it seems to provide an adequate approximation where one is able to cover all types of coordination sites. Four-fold sites on the (100) facets were not studied because they should be affected rather strongly by steric hindrance with the triphenylphosphine ligands. For similar reasons, also top sites on edges were not discussed further. In all cases, the phosphine model PH_3 was bound terminally to the 12 corner Au atoms. In all structures studied, chlorine was more than 3.2 Å away from the closest hydrogen of the PH_3 group; thus, artifacts due to an overestimation of dispersion interactions due to the LDA approximation as in the previous chapter (p. 105) are unlikely.

The discussion will start with terminal coordinated structures as discussed in the literature,[19] continue with bridge coordinated species and finally present results for hollow sites which will turn out to be most favorable on this model cluster. Figure 4.22 shows the optimized cluster in D_{2d} symmetry, where it is clearly visible that the cluster core is preserved in a cuboctahedral shape. Also the surface, where the ligands are attached is not strongly relaxing. Table 4.22 lists characteristic properties, calculated for the model cluster compound $Au_{55}(PH_3)_{12}Cl_6$. For top coordination, two different isomers with different multiplicity were located: a doublet (isomer α) and a quartet (isomer β). Both isomers have rather similar structures.

First the cluster $Au_{55}(PH_3)_{12}(\mu_1\text{-}Cl)_6$ D_{2d} α with a doublet multiplicity shall be examined. For top coordinated chlorine, two slightly different bond distances, 2.381 Å and 2.400 Å, were calculated There are also two inequivalent sets of Au-P bond lengths, 2.297 Å and 2.303 Å, but their values are very similar, so that just the average Au-P bond length is given in the Table 4.22. Compared to the cluster model $Au_{55}Cl_6$, the Au-Cl bonds are elongated by 0.04 Å and 0.06 Å. With 2.782 Å the average gold-gold distance of $Au_{55}(PH_3)_{12}Cl_6$ is the same as in $Au_{55}Cl_6$, but one notices a small change of 0.01 Å with respect to Au_{55}. If one assumes the phosphane-gold bond strength to remain as in $Au_{55}(PH_3)_{12}$, one derives a binding energy of 226 kJ/mol per chlorine atom. The very close lying quartet state $Au_{55}(PH_3)_{12}(\mu_1\text{-}Cl)_6$ D_{2d} β was found to be 2 kJ/mol more stable than the doublet state; it features essentially the same structural properties except for the Au2-Cl distance, 2.388 Å, which is 0.012 Å shorter than the value of the doublet state. This lowers

the difference between the two sets of Au-Cl distances from 0.02 Å for the doublet structure to 0.01 Å in the quartet structure. If one takes the overall accuracy of the computational method used into account, one has to consider both states, separated by a few kJ/mol only, as essentially degenerate. Note that the total energy of this model is $-2.7 \cdot 10^9$ kJ/mol.

In the cluster model $Au_{55}(PH_3)_{12}(\mu_2\text{-}Cl)_6$ S_6, where the chlorine ligands are coordinated at bridge sites of the (100) facets, Au-Cl bond lengths of 2.49 and 2.51 Å result, which are ~0.05 Å longer than at the analogous sites of $Au_{55}Cl_6$. Deviating from the small $Au_{55}Cl_6$ model $Au_{55}(PH_3)_{12}(\mu_2\text{-}Cl)_6$ S_6 features a by 0.01 Å asymmetric bridge coordination of Cl with the bond to the gold atom between the two PH_3 coordinated gold atoms being slightly shorter. The close proximity of chlorine ligands affects the Au-P bonds; they are ~0.02 Å longer than for terminal coordination of chlorine. An influence between the two ligands by non-bonded interactions seems still unlikely, since the chlorine atom is more than 3.2 Å apart from hydrogen, and 5.4 Å apart from phosphorus. The Cl-H distance is 0.25 Å larger than the sum of the van-der-Waals radii of chlorine and hydrogen and the Cl-P distance is by 1.85 Å larger than the sum of van-der-Waals radii.[162] The average Au-Au distance of the model is elongated by 0.2 Å compared to top coordinated Cl and with 2.80 Å equals the result of bridge coordination in $Au_{55}Cl_6$. In contrast to $Au_{55}Cl_6$ bridge coordination turned out to be only of average stability; the energy is 100 kJ/mol higher than that of the most favorable isomer (Table 4.22). This translates into a binding energy per chlorine of 234 kJ/mol.

Table 4.22 Calculated results for various isomers of the model cluster $Au_{55}(PH_3)_{12}Cl_6$: multiplicity M, gold-ligand bond lengths, average distance <Au-Au>, energy difference E_{rel} to the most stable model cluster, and binding energies BE per chlorine atom. Au1, Au2, and Au3 denote different neighbors of the chlorine ligands. Coordination modes are abbreviated with T for on-top, B for bridge, and H for hollow. Distances in Å, energies in kJ/mol.

Isomer	M	Au1-Cl	Au2-Cl	Au3-Cl	Au-P	<Au-Au>	E_{rel}	BE
$Au_{55}(PH_3)_{12}(\mu_1\text{-}Cl)_6$ D_{2d} α[a]	2	2.381/ 2.400	–	–	2.301	2.782	153	226
$Au_{55}(PH_3)_{12}(\mu_1\text{-}Cl)_6$ D_{2d} β[a]	4	2.379/ 2.388	–	–	2.300	2.783	151	226
$Au_{55}(PH_3)_{12}(\mu_2\text{-}Cl)_6$ S_6[a]	2	2.491	2.510	–	2.317	2.799	100	234
$Au_{55}(PH_3)_{12}(\mu_3\text{-}Cl)_6$ S_6 α[a]	2	2.582	2.603	2.622	2.304	2.828	79	238
$Au_{55}(PH_3)_{12}(\mu_3\text{-}Cl)_6$ S_6 β[b]	2	2.512	2.636	2.680	2.315	2.801	0	251
exp	–	2.50			2.30	2.75		

[a] cuboctahedral [b] icosahedral

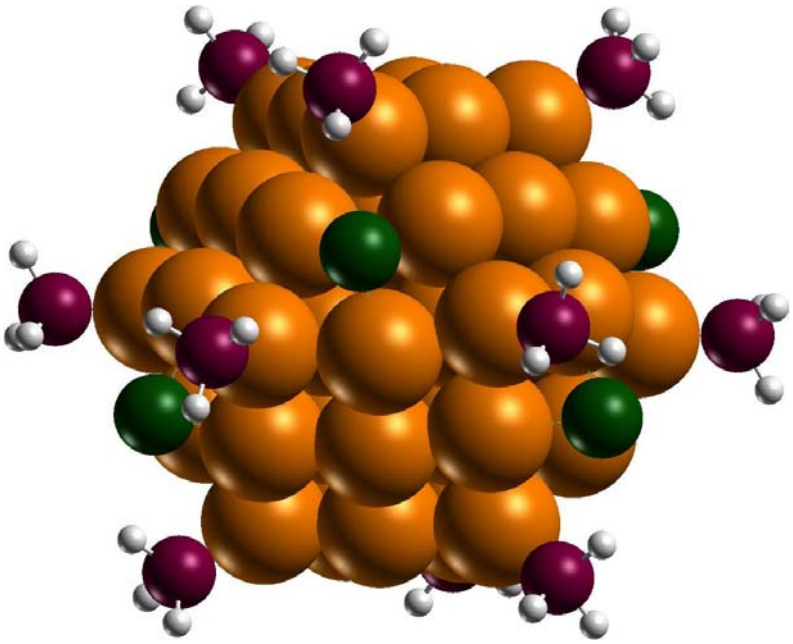

Figure 4.23 Optimized cluster model in $Au_{55}(PH_3)_{12}(\mu_3\text{-}Cl)_6$ S_6 α.

Central hollow coordination of chlorine on the (111) facet of a cuboctahedral shaped cluster was investigated in the model $Au_{55}(PH_3)_{12}(\mu_3\text{-}Cl)_6$ S_6 α. Rather strong changes of all parameters resulted compared to the isomer with top coordination. The Au-Cl bonds lengthen to 2.582, 2.603, and 2.622 Å, which are even longer than those determined for $Au_{55}Cl_6$ with chlorine in analogous hollow sites. The Au-P bonds, on the other hand, remain at 2.304 Å, only 0.01 Å shorter than in $Au_{55}(PH_3)_{12}$. The average metal-metal distance increases by 0.02 to 2.828 Å compared to the bare cluster in S_6 symmetry. The isomer $Au_{55}(PH_3)_{12}(\mu_3\text{-}Cl)_6$ S_6 α was calculated to be the second most stable structure with a binding energy per chlorine of 238 kJ/mol. Overall, this isomer is 79 kJ/mol less stable than the most stable structure $Au_{55}(PH_3)_{12}(\mu_3\text{-}Cl)_6$ S_6 β, to be discussed in the following. Figure 4.23 shows several distortions of gold atoms due to the hollow coordination of chlorine on the (111) facet. Partly they derive from the quasi-unsymmetrical placement, because only 6 of the 8 (111) facets are covered by chlorine atoms and therefore only 6/8 of all (111) facets increase their size due to coordination of chlorine.

Finally, in the isomer $Au_{55}(PH_3)_{12}(\mu_3\text{-}Cl)_6$ S_6 β (Figure 4.24), the cluster assumes a quasi-icosahedral shape. This is the most stable isomer identified in this study (Table 4.22), with a chlorine binding energy of 251 kJ/mol. With this quasi-icosahedral distortion, no clear hollow coordination of chlorine can be located anymore. Instead, a distorted hollow coordination with two longer Au-Cl contacts was determined. Correspondingly, different bond distances of 2.512, 2.636, and 2.680 Å were obtained. The Au-P bond length was calculated at 2.315 Å, similar to that of $Au_{55}(PH_3)_{12}$. The average Au-Au distance shifted to 2.801 Å, which falls between the values of top and hollow coordination of clusters with cuboctahedral shape.

Only the Au-Cl bond lengths of isomer $Au_{55}(PH_3)_{12}(\mu_2\text{-}Cl)_6$ S_6 with bridge coordinated chlorine ligands compare well with the experimental result of 2.50 Å.[262] For isomers with chlorine in μ_3 (hollow) coordination, the short Au-Cl distance of 2.51 Å matches the experimental value, but it remains unclear whether the other, significantly longer Au-Cl bonds (> 2.6 Å) should not also have been detected in experiment. On top coordination of Cl with a computed Au-Cl bond lengths of ~2.38 Å is at variance with EXAFS results. The experimentally found Au-P distance of 2.30 Å is well reproduced for all investigated geometries, which cover the range of 2.30–2.32 Å and fall within the error margin of the experimental result. The computed average Au-Au distances, 2.78–2.83 Å, are compatible with the larger experimentally determined values: 2.80,[264] 2.75,[262] and 2.785.[259]

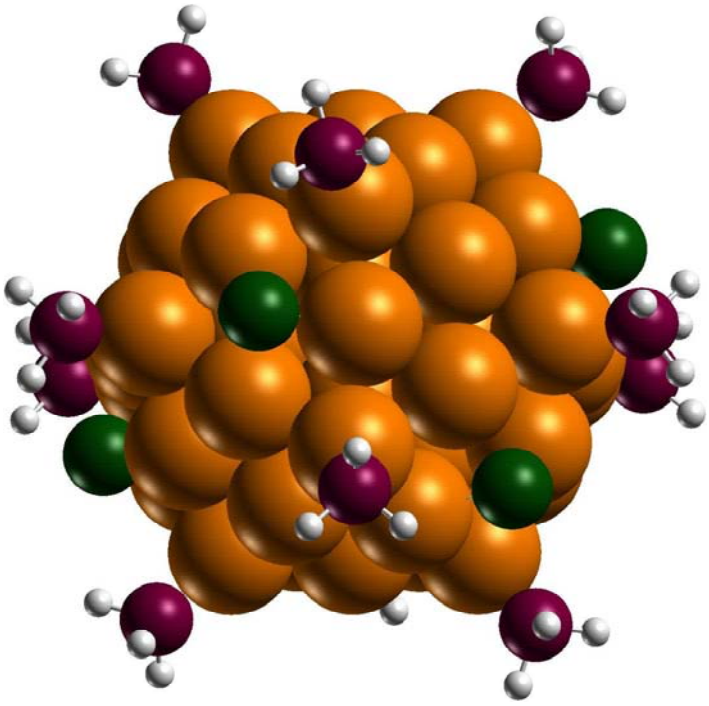

Figure 4.24 The most stable structure optimized: cluster model $Au_{55}(PH_3)_{12}(\mu_3\text{-}Cl)_6$ S_6 β.

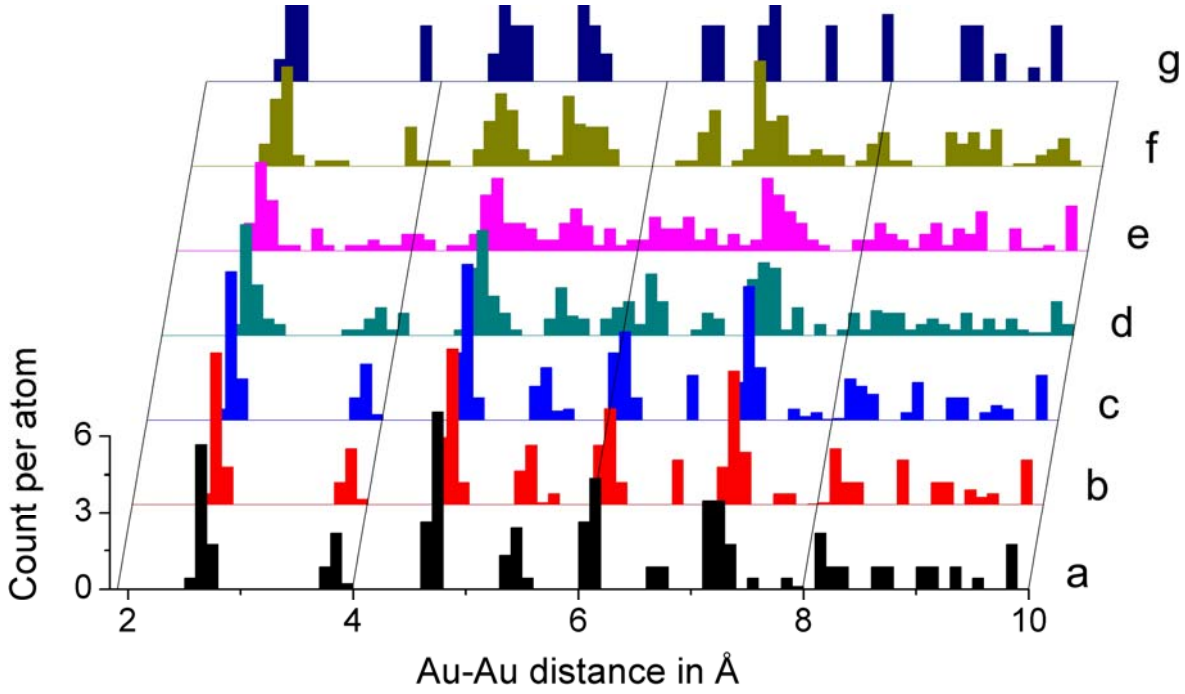

Figure 4.25 Radial distribution functions of Au atoms as histograms (bin width 0.1 Å) of various $Au_{55}(PH_3)_{12}Cl_6$ cluster models compared to bare Au_{55} clusters in O_h and I_h symmetry. **a** Au_{55} O_h; **b** $Au_{55}(PH_3)_{12}(\mu_1\text{-}Cl)_6$ D_{2d} α; **c** $Au_{55}(PH_3)_{12}(\mu_1\text{-}Cl)_6$ D_{2d} β; **d** $Au_{55}(PH_3)_{12}(\mu_2\text{-}Cl)_6$ S_6; **e** $Au_{55}(PH_3)_{12}(\mu_3\text{-}Cl)_6$ S_6 α; **f** $Au_{55}(PH_3)_{12}(\mu_3\text{-}Cl)_6$ S_6 β; **g** Au_{55} I_h; Count per atom: see text.

Also the second shell of Au-Au distances have been reported experimentally.[262] Figure 4.25 displays the results of an analysis of the distributions of Au-Au distances per gold atom in all model clusters studied in this work. The number of Au-Au distances per Au atom is evaluated by counting all distances in the cluster as histogram (bin width 0.1 Å) and multiplying it by 2 (the number of gold atoms participating in this bond) and dividing it by 55 to have a single Au atom as reference. The number of Au-Au distances per atom occurring in the cluster models is then plotted versus the radial distance. It is apparent that the first three cluster models, Au_{55}, $Au_{55}(PH_3)_{12}Cl_6$ μ_1 α and β with cuboctahedral cluster core, show essentially the same features. This indicates that the two D_{2d} structures remain quite similar to an ideal cuboctrahedron. In addition, the overall similarity between the two isomers of D_{2d} symmetry with different spin can easily be seen. For the quasi-cubocahedral cluster model in S_6 symmetry, $Au_{55}(PH_3)_{12}(\mu_3\text{-}Cl)_6$ S_6 α, one notices a strong broadening of the main features in the radial distribution function, reflecting the degree of distortion of the cluster structure.

The icosahedral isomer in S_6 symmetry $Au_{55}(PH_3)_{12}(\mu_3\text{-}Cl)_6$ S_6 β, on the other hand, shows again clear peaks shifted with respect to the cuboctahedral features as expected. When chlorine is coordinated to the bridge site in S_6 symmetry, a pattern corresponding to a cuboctahedral shape is found, with some broadening of peaks. Nevertheless, all

investigated structures reproduce the experimentally found first shell reasonably well with values between 2.7 and 2.8 Å; at the resolution of the histogram (0.1 Å), inter- and intra-shell distances of the icosahedral structure coincide. All structures except $Au_{55}(PH_3)_{12}(\mu_3\text{-}Cl)_6$ S_6 α show a second pronounced shell at 3.9 Å, in agreement with the experimentally found second shell at 3.93 Å.[262] Near 4.7–4.8 Å, a third peak shows up in all geometries, matching the experimental value of 4.88 Å for a third shell.[262] Leaving aside the $Au_{55}(PH_3)_{12}(\mu_3\text{-}Cl)_6$ S_6 α structure, overall good agreement for the Au-Au distances was found for all other structures. The deviations of 5% between inter- and intrashell distances in the icosahedral structure resulted only in some broadening of peaks, but not in a completely different pattern, which would have been well distinguishable by experiment. On the other hand, the peak at 6 Å distance for cuboctahedral shapes is completely absent in the radial distribution function of icosahedral structures and thus its absence might be a good indicator for that shape. Note that the patterns of the radial distribution functions of cuboctahedral and isohedral clusters essentially agree for the first three shells. However, they differ notably in the position of the fourth shell which peaks near 6 Å for all cuboctahedral structures, but only at about 6.5 Å for icosahedral clusters.

After inspection of the geometry and the stability of the various cluster isomers, now electronic properties will be discussed. Table 4.23 shows a slight variation in the HOMO-LUMO gap for different shapes and chlorine bonding sites. The largest gap, 0.37 eV, is calculated for top coordination in a doublet state, while the quartet state of the same species results in the lowest gap among the systems studied, 0.02 eV. Hollow coordination of chlorine results in a gap of ~0.2 eV. Ionization potentials and electron affinities are ~0.1 eV larger for top coordinated species than for Cl at other sites. In general, the ligands affect IP and EA strongly with a trend of lowering the IP by >1.3 eV and EA by >1.0 eV compared to the bare cluster; this has been already noted for the model $Au_{55}(PH_3)_{12}$. Both IP and EA show a weak trend to lower values with increasing stability of the cluster compound. The Mulliken charges vary as expected from simple coordination chemistry. The chlorine atoms are withdrawing charge from the metal particle, while the PH_3 ligands are donating. When the charges are compared to those of $Au_{55}Cl_6$ (Table 4.21), it appears that the charge on the Au_{55} cluster core is not changed due to coordination by phosphanes, which leads to the conclusion that the extra electrons brought to the cluster by PH_3 are transferred to the chlorine ligand shell. Indeed, compared to $Au_{55}Cl_6$, the charge on the chlorine atoms is approximately increased by the charge donated by PH_3 ligands.

Table 4.23 $Au_{55}(PH_3)_{12}Cl_6$: cluster shapes S, chlorine coordination C, multiplicities M, HOMO-LUMO Gap, ionization potentials IP, electron affinities EA, Mulliken charges q. Energies in are given in eV, charges in e.

Isomer	Gap	IP	EA	$q(Cl_6)$	$q((PH_3)_{12})$	$q(Au_{55})$
$Au_{55}(PH_3)_{12}(\mu_1\text{-}Cl)_6$ D_{2d} α[a]	0.37	4.83	2.91	-2.3	0.8	1.5
$Au_{55}(PH_3)_{12}(\mu_1\text{-}Cl)_6$ D_{2d} β[a]	0.02	4.86	2.87	-2.3	0.8	1.4
$Au_{55}(PH_3)_{12}(\mu_2\text{-}Cl)_6$ S_6[a]	0.12	4.69	2.75	-1.7	0.5	1.3
$Au_{55}(PH_3)_{12}(\mu_3\text{-}Cl)_6$ S_6 α[a]	0.25	4.74	2.79	-1.3	0.7	0.5
$Au_{55}(PH_3)_{12}(\mu_3\text{-}Cl)_6$ S_6 β[b]	0.17	4.60	2.60	-1.2	0.5	0.7
Au_{55}	0.14	6.18	3.93			

[a] cuboctahedral [b] icosahedral

Relative energies of core levels provide another interesting aspect of the electronic structure, because they reflect the chemical environment of the various atoms.[286] Core level energies are influenced by charge, coordination and chemical environment.[41] In general, coordination leads to weaker bound orbitals, higher d-population increases the orbital binding energy, positive charges lead to a stabilization, and negative charges to a destabilization.[41,287]

As detailed in the above review of experimental results, several studies have addressed the XPS spectrum of the cluster compound $Au_{55}[P(C_6H_5)_3]_{12}Cl_6$. Especially interesting are the results of one study, which resolved various peaks in this spectrum and assigned them to different types of gold atoms.[266] For the following discussion, calculated Kohn-Sham energies of core orbitals, in particular their relative values, may be taken to approximate trends of experimental XPS spectra. As detailed in Section 4.3, the present calculations, carried out with a scalar relativistic method, lack information on the effect of spin orbit interaction. For the cluster models and electronic states investigated, trends were derived from the orbital energies. First this discussion starts with the bare Au_{55} cluster, then the effect of both types of ligands is discussed separately, before turning to model clusters $Au_{55}(PH_3)_{12}Cl_6$.

In the following, the binding energy of Kohn-Sham levels shall be associated with the negative of the orbital energies, to facilitate the discussion. Actually, Kohn-Sham orbital energies represent only initial state effects and the resulting binding energy values underestimate the corresponding ionization potentials due to the fact that in the local density approximation used here these energies incorporate part of the self-energy which is only incompletely cancelled in all common local density approximations.[288] As a result, Kohn-Sham orbitals lie to high in energies; this artifact can amount to several eV for core levels. On the other hand, the present scalar relativistic calculations lack the effect of spin-orbit interaction. The effect of spin-orbit interaction is estimated to reduce the binding

energy of the Au $4f_{7/2}$ level by about 1.8 eV,[265] compared to the spin-orbit averaged energy of the present scalar relativistic levels.

The 4f orbital energies of the bare cluster Au_{55} differ between the atoms in the cluster core Au_{13} (core in Table 4.24), at 84.2 eV, and the 42 Au atoms in the surface of the cluster (denoted as surface, P-coordinated, and Cl-coordinated in Table 4.24), at ~83.4 eV. When the bare Au_{55} is coordinated by six chlorine atoms in terminal positions, the Au 4f levels of all centers undergo a nearly constant shift of ~0.4 eV to higher binding energies; the shifts of the Au atoms directly coordinated by Cl are slightly larger, 0.5 eV. On the other hand, chlorine atoms coordinated at hollow sites exert a smaller effect on the 4f orbital energies; they shift at most 0.2 eV to higher binding energies. When 12 PH_3 ligands are attached to Au_{55}, the Au 4f orbital energies of the gold atoms at the coordination sites shift to lower binding energy, by 0.9 eV, while the 4f binding energies of the other gold centers are reduced by ~1.7 eV.

For the fully ligated clusters first the two species with top coordinated chlorine shall be examined together because corresponding energies differ at most by 0.1 eV from each other. and later the two isomers with three-fold coordinated Cl will be discussed together; analogous core levels have identical energies. For the 4f binding energies of core and P-coordinated gold atoms of the clusters with top coordinated chlorine, the effect of the ligands discussed before are approximately additive. Thus, core level binding energies are increased by 0.5 eV due to chlorine coordination and reduced by 1.7 eV or 0.9 eV as a result of phosphane coordination. For other types of gold atoms the shifts induced by the ligands vary by 0.1 eV only compared to the effects of a single ligand group. When chlorine is coordinated to a hollow site, the by chlorine induced core level shifts scatter for different gold atoms. This shift amounts to 0 eV for core, 0.4 eV for surface, and ~0.15 eV for ligand coordinated gold atoms, similar to what was found when hollow coordinated chlorine is the only type of ligands of the cluster. On the other hand, phosphane ligands decrease core level binding energies for the $Au_{55}(PH_3)_{12}(\mu_3\text{-}Cl)_6\ S_6$ cluster, by 2.2 eV for core, 1.7 eV for surface, 1.1 eV for P-coordinated, and 1.6 eV for Cl-coordinated gold atoms. The isomer $Au_{55}(PH_3)_{12}(\mu_3\text{-}Cl)_6\ S_6$ with bridge coordinated chlorine shows essentially the same core levels (deviations at most 0.1 eV) which are found for hollow coordinated chlorine. All together it is noteworthy that for most coordinated Au atoms the effects which the different ligands excert is simply additive and the effects are not influenced by the presence of other ligands.

Now the effects of different coordination environment differences on the Au 4f orbital energies shall be explored. For this purpose, shifts of Au 4f core levels will be used

which have been calculated as differences to Au 4f core level energies of atoms in the Au_{13} core of the corresponding Au_{55} moiety (Table 4.24). In other words, the 4f binding energies of Au atoms in the surface of a Au_{55} moiety are reduced by the Au 4f binding energy of the corresponding cluster core Au_{13}.

The Au 4f levels of atoms in the surface of Au_{55} are ~0.8 eV destabilized compared to the levels in the cluster core Au_{13}. When 6 chlorine atoms are coordinated terminally, the shifts of the 4f levels of Cl-coordinated Au atoms are 0.1 eV smaller than in bare Au_{55}, while other Au 4f levels remain unaffected. Bridge coordination of chlorine results in a slight reduction of 4f level *shifts* of surface gold atoms. When Cl atoms are coordinated at hollow sites of $Au_{55}Cl_6$, the 4f shift of Cl-coordinated Au atoms becomes even smaller, about -0.4 eV; this is about 0.4 eV lower than in bare Au_{55}. Coordination of phosphanes strongly destabilized the 4f level of P-coordinated atoms; their shifts are reduced from -0.8 eV relative to the inner atoms to +0.1 eV. The effect of phosphane ligands is as before the dominating one: for $Au_{55}(PH_3)_{12}(\mu_1\text{-}Cl)_6$, *shifts* agree within 0.2 eV with those of $Au_{55}(PH_3)_{12}$. When chlorine atoms are coordinated at hollow sites, shifts of surface atoms

Table 4.24 Estimated averaged Au 4f core binding energies (approximated as negative Kohn-Sham energies) of different types of gold atoms of various cluster models of Au_{55}, with and without ligands. Core – average value of Au_{13} at the center of the Au_{55} moiety, surface – Au atoms in the surface of Au_{55} that are not nearest neighbors of ligands, P-coord – Au atoms where phosphane ligands are coordinated, Cl-coor – Au atoms at the adsorption site of chlorine atoms. Also shown are shifts relative to the core level binding energy of the atoms in the corresponding cluster core Au_{13}. All energies in eV.

System	Core	surface	P-coord	Cl-coord	surface[a]	P-coord[a]	Cl-coord[a]
Au_{55} O_h	84.2	83.4	83.4	83.5	-0.8	-0.8	-0.7
$Au_{55}(\mu_1\text{-}Cl)_6$	84.6	83.8	83.8	84.0	-0.8	-0.8	-0.6
$Au_{55}(\mu_3\text{-}Cl)_6$	84.0	83.6	83.5	83.6	-0.4	-0.5	-0.4
Au_{55} $(PH_3)_{12}$	82.4	81.7	82.5	81.8	-0.7	0.1	-0.6
$Au_{55}(PH_3)_{12}(\mu_1\text{-}Cl)_6$ D_{2d} α	82.9	82.0	83.0	82.5	-0.9	0.1	-0.4
$Au_{55}(PH_3)_{12}(\mu_1\text{-}Cl)_6$ D_{2d} β	82.8	82.0	83.0	82.4	-0.8	0.2	-0.4
$Au_{55}(PH_3)_{12}(\mu_2\text{-}Cl)_6$ S_6	82.6	82.0	82.7	82.1	-0.6	0.1	-0.4
$Au_{55}(PH_3)_{12}(\mu_3\text{-}Cl)_6$ S_6 α	82.4	82.1	82.7	82.0	-0.3	0.3	-0.4
$Au_{55}(PH_3)_{12}(\mu_3\text{-}Cl)_6$ S_6 β	82.4	82.1	82.7	82.0	-0.3	0.3	-0.4
exp[b]	84.4	84	85.3	86.3	-0.4	0.9	1.9

[a] Referenced to Auf 4f levels of atoms in the cluster core.

[b] Au $4f_{7/2}$ orbital energies, Ref. 266

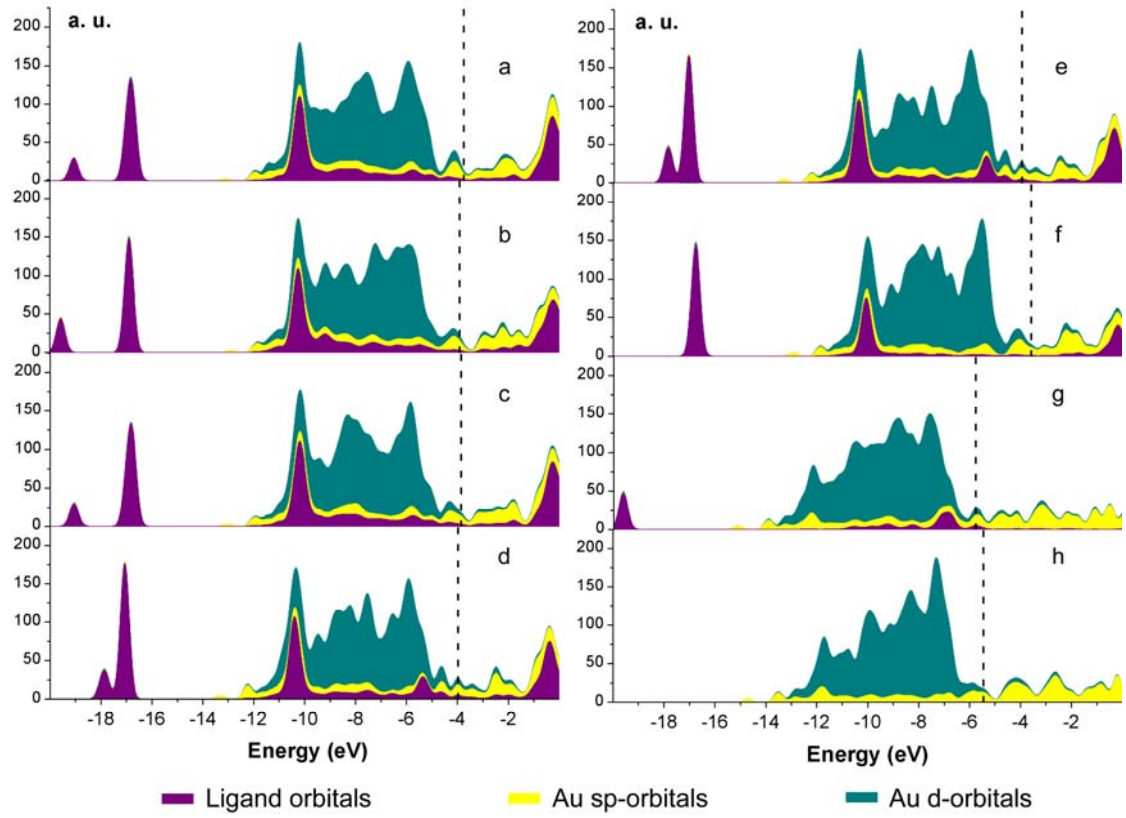

Figure 4.26 Density of states for various cluster models: **a** $Au_{55}(PH_3)_{12}(\mu_3\text{-}Cl)_6$ S_6 β **b** $Au_{55}(PH_3)_{12}(\mu_3\text{-}Cl)_6$ S_6 α **c** $Au_{55}(PH_3)_{12}(\mu_2\text{-}Cl)_6$ S_6 **d** $Au_{55}(PH_3)_{12}(\mu_1\text{-}Cl)_6$ D_{2d} β **e** $Au_{55}(PH_3)_{12}(\mu_1\text{-}Cl)_6$ D_{2d} α **f** $Au_{55}(PH_3)_{12}$ D_{2d} **g** $Au_{55}(\mu_1\text{-}Cl)_6$ O_h **h** Au_{55} O_h. Fermi level indicated as dashed line.

are strongly reduced in size, to -0.3 eV; shifts of P-coordinated centers are 0.3 eV (i.e. these levels are notably stabilized compared to the 4f levels of the corresponding core Au_{13}), and 4f levels of Cl-coordinated centers feature a shift of -0.4 eV relative to the corresponding levels of the cluster core. The latter species resemble closest the experimental finding, where surface $4f_{7/2}$ levels exhibits shifts of -0.4 eV (compared to the experimental levels assigned to the cluster core Au_{13}), P-coordinated gold atoms are characterized by a shift 0.9 eV, and Cl-coordinated gold atoms by a shift of 1.9 eV. This large experimental shift of 4f levels of Cl-coordinated gold atoms is not reproduced by any of the models used in the present work. Experimentally this core level energy is the one most investigated; from Figure 4.18 this strong shift due by to chlorine coordination is clearly visible. It is possible that this large shift is in part due to a final state effect, which is not accounted here, where only differences of Kohn-Sham energies have been discussed. For the other two types of gold atoms in the outer shell of the Au_{55} moiety, good qualitative agreement has been found between experiment and the results for the model clusters $Au_{55}(PH_3)_{12}(\mu_3\text{-}Cl)_6$ S_6.

The density of states (DOS) plots, shown in Figure 4.26 for various cluster models,

provide an overview of the valence electronic structure. In the region between -7 and -12 eV the d-band of the gold cluster is visible as the main feature, whereas at the Fermi edge the DOS consists of s-type levels. Surprisingly the effect of terminally coordinated chlorine is small and consists essentially of a slight shift of the Fermi energy to lower energy and insertion of a shoulder (Cl 3p) in the gold d-manifold. A small peak of chlorine 3s orbitals appears close to -20 eV. Phosphane ligands coordinated to the cluster result in a strong shift of the density of states. The Fermi energy as well as the d-manifold are shifted by ~2 eV to higher energy. Two PH_3 ligand peaks at -17 eV and -10 eV can be noticed. The peak at -17 eV is a mixture of P 3s and H 1s orbitals, while the feature at -10 eV describes P 3p, H 1s, as well as Au 5d orbitals.

The shift of the gold d-manifold and the Fermi energy induced by the phosphane ligand PH_3 is conserved when looking at the two fully ligated isomers $Au_{55}(PH_3)_{12}(\mu_1\text{-}Cl)_6$ D_{2d}. The model clusters with doublet and quartet states have essentially the same DOS.

Just as the Au related DOS, also the chlorine levels are affected by interaction with the phosphane ligands; the corresponding peaks are shifted to lower energies by 2 eV. This shift is homogeneous for all Cl contributions to the DOS; there is no shift relative to the Fermi level. The DOS plot of $Au_{55}(PH_3)_{12}(\mu_2\text{-}Cl)_6$ S_6 is very similar to those of the ligated clusters with terminal Cl (D_{2d} symmetry), except for the chlorine contributions. Compared to the structures with terminal chlorine coordination the chlorine 3s peak is shifted by 1 eV to -19 eV, while the Cl 3p peak is broadened into the range of the gold d-manifold. The two isomers in S_6 symmetry with distorted cuboctahedral and icosahedral metal cores and hollow coordinated chlorine feature rather similar DOS plots, even though they represent different structures. For hollow coordinated chlorine the lower energy Cl 3s feature shifts back to -20 eV; also the gold d-manifold changes slightly. Overall, the energy of the Fermi level correlates with the ionization potentials as expected (see above). The HOMO orbital of the cluster is destabilized when phosphane ligands are coordinated, while chlorine coordination has a small opposite effect. In the experiment a change in the valence band spectrum induced by the removal of chlorine was found, as mentioned above in the background part.[265] In the calculated DOS, the $Au_{55}(PH_3)_{12}$ cluster has low density of states at the Fermi level and all fully coordinated species show a similar DOS (Figure 4.26). Thus, the insulator-to-metal transition, observed upon removal of chlorine,[265] can not be associated with appropriate changes in the corresponding DOS of $Au_{55}(PH_3)_{12}Cl_6$ and $Au_{55}(PH_3)_{12}$.

4.5.4 Conclusions

Geometrical and electronic properties of several possible structures of the cluster compound $Au_{55}[P(C_6H_5)_3]_{12}Cl_6$ have been investigated by density functional calculations of the model compound $Au_{55}(PH_3)_{12}Cl_6$. A cluster with top coordinated chlorine atom, as suggested by experiment, was examined as well as structures with Cl atoms at two- and three-fold coordinated sites, while the phosphane ligands were assumed to be always terminally coordinated. Terminal Cl coordination turned out to be energetically unfavorable for all species investigated, with an Au-Cl binding energy of 226 kJ/mol. For a bridge coordinated chlorine a binding energy of 234 kJ/mol was computed. The Au-Cl binding energies was calculated larger for chlorine at threefold coordinated sites, 238 kJ/mol on a cuboctahedral cluster core and 251 kJ/mol for an icosahedral one. The Au-Cl bond lengths increased by ~0.1 Å per Au neighbor coordinated, on average with 2.4 Å for terminal, 2.5 Å for two-fold and 2.6 Å for three-fold coordinated Cl atoms. When chlorine is threefold coordinated, the metal framework underneath undergoes a transformation into an quasi-icosahedral structure, with an overall energy gain of 80 kJ/mol. Interestingly, bridge coordinated chlorine, which is most favorable on the model cluster $Au_{55}Cl_6$, turned out to be slightly less favorable than a three-fold coordination at the model cluster $Au_{55}(PH_3)_{12}Cl_6$. The model phosphane ligand, being always terminally coordinated, shows an Au-P bond length of 2.3 Å for all species. This ligand exerts a strong electronic donating effect, pushing the HOMO orbital to higher energies, hence shifting the ionization potential and electron affinity to lower values by ~1 eV.

Comparison to experiment shows that the shells of Au-Au distances determined for the gold cluster by EXAFS fit both cuboctahedral and icosahedral shapes of the model calculation. The first three shells, which are determined experimentally at 2.75 Å, 3.93 Å, and 4.88 Å, were reproduced within 0.1 Å for all structures, except for a distorted cuboctahedral cluster. Au-P distances derived from experimental data are well reproduced, while for chlorine the experimental value of 2.50 Å is in line with computed shorter Au-Cl bond distances of bridge and hollow sites of ~2.51 Å. On-top coordinated chlorine atoms have a shorter Au-Cl distance of about ~2.38 Å. Qualitatively, the trends of an XPS spectrum of the 4f-orbitals shifts of gold atoms could be reproduced with a notable exception for the gold atoms coordinated to chlorine, irrespective of coordination.

In summary this computational study indicated that chlorine is very likely higher coordinated, at variance with an earlier suggestion of a terminal coordination.[19] Calculated geometrical parameters are in good qualitative agreement with evidence from EXAFS studies.[266] As a new result the distortions of the Au_{55} cluster core also suggest a more

icosahedral than distorted cuboctahedral structure. Thus, the calculated results are in reasonable agreement with the hypothesis of an $Au_{55}[P(C_6H_5)_3]Cl_6$ cluster compound, but with Cl ligands at high coordination sites and a distorted icosahedral metal core as novel features. No indications for possible metal – insulator changes of the electronic structure due to ligand removal could be found.

To gain more information about the Au_{55} cluster compound, it would be worthwhile to calculate more realistic models with triphenylphosphine ligands. In general, the cluster compound $Au_{55}[P(C_6H_5)_3]_{12}Cl_6$ seems to warrant re-visiting also from the experimental side, because after more than 25 years basic properties like shape, atom count and reactivity are still under discussion.

5 Summary

Isolated metal clusters can be studied experimentally only under special conditions. Commonly such metal species are either stabilized on support or covered by ligands. Thus, the investigation of the interactions and geometries of ligand-cluster interfaces is an important topic in the research on nanoparticles under normal conditions. It is difficult to synthesize stable, well defined, size controlled transition metal clusters on a larger scale. Ligand protection of clusters in *statu nascendi* has been confirmed to be a successful way to generate clusters with narrow size dispersion and to stabilize them in such a way that they become stable under standard conditions. All this is a prerequisite for further studies and suitable applications. On the other hand, ligands are not "innocent": they change the properties of clusters and it is important to understand that effect. For catalytic purposes clusters are often employed because their surface/mass ratio is large. For most heterogeneous catalytic reactions the active species is not known. Thus, theoretical investigations, as performed in this thesis, are important means to support experimental results. Especially the coordination sites of the protective ligands as well as their bond strengths remained often vague from experimental studies.

In this work, ligand-cluster interaction was studied within the framework of density functional (DF) theory for a variety of ligated transition metal clusters. Such a quantum chemical approach furnishes information that is often complementary to experimental investigations. This work focused on ligand effects on small and medium sized transition metal clusters which belong to the non-scalable size regime. Therefore, clusters of a specific size have to be treated as individual systems. The types of ligands inspected range from monpatomic ligands to species like ethylthiol or a phosphane as a model of bulkier species like triphenylphosphines.

First the effects of impurity atoms H, C, and O on the cluster Pd_4 as well as of two hydrogen atoms on an Ir_4 particle were studied, focusing on preferred binding sites and

energetics. These investigations contributed to on-going activities of the work group. The important class of gold thiolate clusters was studied for the example of medium sized Au_{13}, with varying numbers of small model thiolate ligands SH and SCH_3. This work was supplemented by a study on Cu_{13} decorated by eight ethylthiolate ligands SCH_2CH_3. For this species also for the first time a QM/MM approach was applied to a ligand covered metal cluster. The accuracy of a specific QM/MM model was explored by comparison with results of full DF calculations. Finally, the even larger cluster Au_{55} ligated by phosphane and chlorine is studied. After some remarks on the computational method applied, pertinent results for these various ligated clusters will be summarized below.

Calculations on clusters of second and third row transition metals including a ligand shell are challenging because relativistic effects as well as electron correlation have to be treated accurately. All clusters in this thesis, except Cu_{13}, were calculated with an all-electron scalar relativistic DF method on the basis of the Douglas-Kroll approach as implemented in the program PARAGAUSS. For Cu_{13} cluster relativistic effects were neglected as is commonly done for first row transition metals.

For the impurity atoms H, C, and O on a Pd_4 cluster first high symmetry coordination sites were inspected to screen the phase space systematically; later on, the symmetry constraints were relaxed. For symmetric model clusters bridging coordination was found to be preferred for hydrogen and oxygen, while for carbon higher-order coordination at a fourfold site inside a square planar Pd_4 species was determined as preferred. For Pd_4H seven different local minima of low symmetry were identified. Hydrogen was found to move away from high symmetry structures like terminal or threefold coordination; it prefers intermediate positions. A particularly clear example for this observation is top coordination, where the Pd-H bond is tilted with respect to the 3-fold axis of a tetrahedron by 62°. The binding energy of the most stable structures amounts to 285 kJ/mol for Pd_4H, 643 kJ/mol for Pd_4C, and 365 kJ/mol for Pd_4O. These interaction energies are strong enough to allow dissociation of commonly available small molecules (CH_4, H_2, O_2) when interacting with an ensemble of Pd_4 clusters.

As a second example of impurity decorated clusters, Ir_4H_2 has been studied, extending previous work on Ir_4H. For bare Ir_4 a nonet ground state with a square planar geometry had been determined as the most stable isomer. Therefore, it came as no surprise that for Ir_4H_2 also high spin states (up to quintets) were determined. Thus, the cluster magnetism of this nonmagnetic metal survives even under low hydrogen coverage. As for the bare cluster and Ir_4H, square planar structures were the most stable geometries for Ir_4H_2 with terminally coordinated hydrogen. For butterfly and tetrahedral shaped cluster frameworks also bridge coordination was found for one and two hydrogen atoms, but these

geometries are at least 16 kJ/mol less stable than top coordination on square planar clusters. With 318 kJ/mol the binding energy per H atom is about the same as calculated for Ir_4H; this finding indicates that even more hydrogen atoms can be strongly bound on an Ir_4 cluster.

The important class of gold-thiolate clusters was examined for the example of Au_{13}. The structure of a thiolate ligand shell was studied systematically for the first time. Four, six, or eight model ligands SH and SCH_3 were placed at either top or bridge sites to explore the coverage dependency of properties. In the course of this work, the binding site of thiolate ligands, thus far not known experimentally, was determined in agreement with previous less accurate calculations. In a bridge position four SH ligands were found to bind strongest with 256 kJ/mol per ligand, while six or eight ligands were bound by 244 kJ/mol per ligand. Ligands in top position interact less strongly, by ~30–40 kJ/mol. For all coordination sites SCH_3 ligands were calculated to bind approximately 20 kJ/mol (per ligand) weaker than SH ligands. In a shell of four of these larger ligands, the binding energy per ligand is larger than in a shell with six or eight ligands due to missing bond competition. The thiolate-cluster bonds are 10–20 % stronger than the Au-Au inter-metal bonds and therefore rearrangements of the metal core may by induced by the ligand shell. As bridge coordination is only slightly energetically preferred, thiolate ligands are expected to be flexible, also occupying other sites of gold clusters in situations of higher coverage.

In an extension of the work on Au_{13} a Cu_{13} cluster with ethylthiolate ligands SCH_2CH_3 was modeled both with a full DF approach as well as in a combined quantum mechanical/molecular mechanics (QM/MM) approach. The resulting geometries and energetics of both schemes were compared for 16 conformers. As for Au_{13} the thiolate ligands were coordinated on either a top or a bridge site on the Cu_{13} cluster, allowing the compound as well to relax to a hollow coordination if preferred. Except for three special cases bond energies and geometries were well reproduced with an average deviation of 14 kJ/mol per ethylthiol for bond energies and 0.03 Å for bond lengths. The binding energy of single ligands, typically ~220 kJ/mol, was reproduced within 10–20 kJ/mol as a result of replacing ethyl by methyl in the QM part of the QM/MM model. For a shell of eight ethylthiolate ligands, binding energies per ligand range from 200 to 280 kJ/mol, depending on coordination site and computational method. These results are comparable to the values obtained for the Au_{13} cluster. A remarkable result was that due to different representation of non-bonding interactions the QM/MM approach lead to different stationary points for three conformers which showed quite short H-Cu contacts in the full DF treatment. This difference between both methods was rationalized by the fact that the (standard) DF

method applied is unable to represent dispersion interactions. When the geometry obtained from the QM/MM procedure was used as starting structure for new DF optimizations, lower lying minima for these structures could be located, where the by the full DF description artificially exaggerated non bonding interactions were reduced significantly.

The cluster $Au_{55}(PH_3)_{12}Cl_6$ with a cuboctahedral or icosahedral Au_{55} metal core was computed to model the experimentally studied cluster compound $Au_{55}[P(C_6H_5)_3]_{12}Cl_6$. Besides structures, binding energies, core levels and ligand variations were explored. This examination focused on the structure model based on suggestion derived from experiments. A point of special interest was the coordination of the chlorine on the cluster. The experimentally suggested top coordination was found to be unfavorable by 25 kJ/mol per chlorine atom compared to a hollow coordination. Furthermore, the calculations of this thesis showed that on the smaller model $Au_{55}Cl_6$ the Au-Cl bond length is a very good indicator of the coordination mode of the chlorine atom. No indications were found for the proposed metal-to-insulator transition upon removal of chlorine atoms from the cluster. Density of states plots of several coordination modes of chlorine did not indicate any significant changes in the gap.

Overall, this thesis demonstrated the applicability of scalar relativistic density functional methods as a versatile and accurate tool for studying small and medium sized transition metal clusters and their compounds. Especially detailed information about bonding characteristics of ligands and impurity atoms at the surface of clusters provides helpful information for gaining more insights from future experiments. Geometries and vibrational frequencies can be used to identify and characterize such species. With increasing computer capacity, even more powerful, dynamic simulations of systems like Ir_4H_2 or as big as Au_{55} will become affordable. In this way, more profound knowledge will be generated for systems with several quasi-degenerate structures as well as for delineating the fluxional nature of weakly bound ligand shells. The QM/MM method employed was shown to allow accurate modeling of steric effects and could be applied to clusters with larger ligands like the $P(C_6H_5)_3$ from $Au_{55}[P(C_6H_5)_3]_{12}Cl_6$ or thiolate ligands that are actually used when synthesizing small gold clusters.

Appendix A – Basis Sets

This appendix summarizes all atomic basis sets used in this thesis. The program PARAGAUSS employs products of primitive Gaussian functions of the form $\exp(-\alpha_i r^2)$ and real spherical harmonic functions Y_l^m for the representation of the molecular orbitals. In the following tables the exponents α_i will be listed for the atoms hydrogen, carbon, oxygen, phosphorus, sulfur, chlorine, copper, palladium and gold. The size of the basis sets and the corresponding size of the contracted basis sets are given in the notation introduced in Section 3.2, i.e. (n_0s, n_1p, n_2d, n_3f) and [N_0s, N_1p, N_2d, N_3f], respectively.

In addition, the size of the auxiliary basis sets to represent the charge density (see Section 3.2) is given by (n_0s, n_1r^2, m_1p, m_2d, m_3f). The exponents of the corresponding *s*- and r^2-type "fitting functions" are generated from the orbital basis (see Section 3.2). The exponents for higher angular momenta *p*, *d*, and *f* are added each as a geometric series with a progression of 2.5, starting with 0.1, 0.2, and 0.3 au, respectively; typically, five "polarization exponents" are used for each angular momentum. The corresponding exponents are given in the following table.

Exponents for polarization fitting functions

	p	**d**	**f**
α_1	0.10000000	0.20000000	0.30000000
α_2	0.25000000	0.50000000	0.75000000
α_3	0.62500000	1.25000000	1.87500000
α_4	1.56250000	3.12500000	4.68750000
α_5	3.90625000	7.81250000	11.71875000

Hydrogen (Z = 1): (6s, 1p) basis set

Ref.

Contraction (6s, 1p) → [4s, 1p]

Fitbasis (6s, $1r^2$, 5p)

	s	**p**
α_1	0.08989100	1.00000000
α_2	0.25805300	
α_3	0.79767000	
α_4	2.82385400	
α_5	12.40955800	
α_6	82.63637400	

Hydrogen (Z = 1): (6s, 2p) basis set used for Ir adsorption study

Ref.

Contraction (6s, 2p) → [3s, 2p]

Fitbasis (6s, $1r^2$, 5p)

	s	**p**
α_1	0.08989100	0.53450000
α_2	0.25805300	1.87080000
α_3	0.79767000	
α_4	2.82385400	
α_5	12.40955800	
α_6	82.63637400	

Carbon (Z = 6): (9s, 5p, 1d) basis set

Ref.

Contraction (9s, 5p, 1d) → [5s, 4p, 1d]

Fitbasis (9s, $5r^2$, 5p, 5d)

	s	**p**	**d**
α_1	0.15659000	0.12194000	0.60000000
α_2	0.51190000	0.38554000	
α_3	2.41804900	1.20671000	
α_4	6.17577600	4.15924000	
α_5	16.82356200	18.84180000	
α_6	50.81594200		
α_7	178.35083000		
α_8	782.20479500		
α_9	5240.63525800		

Oxygen (Z = 8): (9s, 5p, 1d) basis set

Ref.

Contraction (9s, 5p, 1d) → [5s, 4p, 1d]

Fitbasis (9s, $5r^2$, 5p, 5d)

	s	**p**	**d**
α_1	0.30068600	0.21488200	1.15000000
α_2	1.00427100	0.72316400	
α_3	4.75680300	2.30869000	
α_4	12.28746900	7.84313100	
α_5	33.90580900	34.85646300	
α_6	103.65179300		
α_7	364.72525700		
α_8	1599.70968900		
α_9	10662.28494000		

Phosphorus (Z = 15): (12s, 9p, 1d) basis set

Ref.

Contraction (12s, 9p, 1d) → [6s, 5p, 1d]

Fitbasis (12s, $9r^2$, 5p, 5d)

	s	**p**	**d**
α_1	0.12520400	0.08376000	0.34000000
α_2	0.34324900	0.22855000	
α_3	1.78316000	0.59584300	
α_4	4.71378000	1.73769000	
α_5	15.20630000	4.24361000	
α_6	36.19160000	10.66430000	
α_7	91.06980000	28.77880000	
α_8	248.52500000	90.62690000	
α_9	753.32800000	385.32200000	
α_{10}	2644.29000000		
α_{11}	11609.30000000		
α_{12}	77718.00000000		

Sulfur (Z = 16): (12s, 9p, 2d) basis set

Ref.

Contraction (12s, 9p, 2d) → [6s, 5p, 2d]

Fitbasis (12s, $9r^2$, 5p, 5d)

	s	**p**	**d**
α_1	0.15709300	0.10286700	0.18300000
α_2	0.43438900	0.29178100	0.65800000
α_3	2.14287000	0.77362800	
α_4	5.57096000	2.24291000	
α_5	18.11680000	5.50267000	
α_6	43.15790000	13.89380000	
α_7	108.66900000	37.49600000	
α_8	296.95400000	116.98100000	
α_9	901.84300000	494.27400000	
α_{10}	3168.04000000		
α_{11}	13921.80000000		
α_{12}	94181.10000000		

Chlorine (Z = 17): (12s, 9p, 1d) basis set

Ref.

Contraction (12s, 9p, 1d) → [6s, 5p, 1d]

Fitbasis (12s, $9r^2$, 5p, 5d)

	s	**p**	**d**
α_1	0.19355800	0.12498600	0.56000000
α_2	0.53839000	0.35827100	
α_3	2.52567000	0.95008300	
α_4	6.46497000	2.71409000	
α_5	20.81380000	6.60076000	
α_6	49.51430000	16.58850000	
α_7	124.49700000	44.79000000	
α_8	339.69100000	139.74500000	
α_9	1030.03000000	587.62200000	
α_{10}	3615.32000000		
α_{11}	15855.30000000		
α_{12}	105747.00000000		

Copper (Z = 29): (15s, 11p, 6d) basis set

Ref.

Contraction (15s, 11p, 6d) → [6s, 4p, 3d]

Fitbasis (15s, $5r^2$, 5p, 5d)

	s	**p**	**d**
α_1	0.04079100	0.09910000	0.14910000
α_2	0.11330300	0.26500000	0.41487500
α_3	0.33050000	0.71144500	1.47329000
α_4	0.96408000	1.90667000	4.51628000
α_5	2.57848000	4.69382000	13.54900000
α_6	9.39357000	11.74350000	48.54390000
α_7	22.29830000	27.05510000	
α_8	67.35910000	65.32390000	
α_9	158.39900000	172.19500000	
α_{10}	395.09900000	532.10600000	
α_{11}	1071.97000000	2245.29000000	
α_{12}	3239.82000000		
α_{13}	11373.40000000		
α_{14}	50072.90000000		
α_{15}	337200.00000000		

Palladium (Z = 46): (18s, 13p, 9d) basis set

Ref.

Contraction (18s, 13p, 9d) → [7s, 6p, 4d]

Fitbasis (18s, 13r^2, 5p, 5d)

	s	**p**	**d**
α_1	0.01350000	0.09040000	0.09700000
α_2	0.04006742	0.21430000	0.26602317
α_3	0.11247078	0.50827979	0.77945515
α_4	0.48448268	1.31341920	1.99012450
α_5	1.11647520	3.03040990	4.78979460
α_6	2.24996060	6.80629510	11.16811900
α_7	5.41188880	14.68536800	27.05091300
α_8	10.57934800	32.27830200	71.70931700
α_9	28.71975700	71.08694300	242.47077000
α_{10}	64.11928400	167.49952000	
α_{11}	165.14908000	439.60614000	
α_{12}	374.64803000	1369.83110000	
α_{13}	905.94369000	5841.59920000	
α_{24}	2398.15000000		
α_{15}	7155.55590000		
α_{16}	25013.15100000		
α_{17}	109352.60000000		
α_{18}	722049.07000000		

Iridium (Z = 77): (21s, 17p, 12d, 7f) basis set

Ref.

Contraction (21s, 17p, 12d, 7f) → [8s, 7p, 5d, 3f]

Fitbasis (20s, 17r^2, 5p, 5d, 5f)

	s	**p**	**d**	**f**
α_1	0.01170000	0.02938000	0.05756400	0.16792223
α_2	0.03162596	0.07345000	0.14391000	0.67168892
α_3	0.08765645	0.18363000	0.35243204	2.30256270
α_4	0.22220000	0.45907287	1.19477990	6.56925270
α_5	0.56331057	1.22877880	4.32692710	17.07857600
α_6	1.31653180	3.65823320	10.79205100	44.69936800
α_7	3.14997410	7.82101650	27.59822400	135.93927000
α_8	6.11593570	17.76073500	64.08823800	
α_9	17.85550200	35.90905400	156.27964000	
α_{10}	32.76410800	74.79119200	409.44817000	
α_{11}	87.57675400	155.61573000	1175.71830000	
α_{12}	188.64087000	331.89250000	3981.13740000	
α_{13}	561.34339000	743.01851000		
α_{24}	1326.63710000	1795.10760000		
α_{15}	3306.57580000	4823.81420000		
α_{16}	8737.89500000	15117.92600000		
α_{17}	24362.36300000	64366.38100000		
α_{18}	75213.17900000			
α_{19}	274591.48000000			
α_{20}	1199253.30000000			
α_{21}	8029090.90000000			

Gold (Z = 79): (19s, 15p, 10d, 6f) basis set

Ref.

Contraction (19s, 15p, 10d, 6f) → [9s, 8p, 5d, 2f]

Fitbasis (19s, $7r^2$, 5p, 5d, 5f)

	s	**p**	**d**	**f**
α_1	0.05600000	0.10000000	0.14000000	0.42000000
α_2	0.14000000	0.21000000	0.35000000	1.10000000
α_3	0.34000000	0.45500000	0.88000000	3.33817196
α_4	0.84000000	1.00000000	2.20000000	9.91205025
α_5	2.10000000	2.25000000	5.54659700	27.75035858
α_6	5.15347004	4.95650673	14.00382996	86.82437134
α_7	0.13352700	10.79928970	36.86191177	
α_8	26.24551010	26.13319016	90.53779602	
α_9	58.48051071	55.26807022	243.20320130	
α_{10}	113.61409760	127.80000310	816.72155760	
α_{11}	233.43910220	285.45651250		
α_{12}	621.27697750	677.79077150		
α_{13}	1429.49792500	1773.84399400		
α_{24}	3491.37988300	5459.12402300		
α_{15}	9358.39257800	23072.80078000		
α_{16}	28274.94141000			
α_{17}	99928.78906000			
α_{18}	446529.50000000			
α_{19}	3095417.00000000			

Bibliography

[1] Soler-Illia, G. J. de A. A.; Sanchez, C.; Lebeau, B.; Patarin, J. *Chem. Rev.*, **2002**, 102, 4093.

[2] Hancock, R. D.; Martell, A. E. *Chem. Rev.*, **1989**, 89, 1875.

[3] Daniel, M.-C.; Astruc, D. *Chem. Rev.*, **2004**, 104, 293.

[4] Schmid, G. Introduction in: *Clusters and Colloids-From Theory to Applications*, Schmid, G. (Hrsg.), Verlag Chemie, Weinheim, **1994**, S. 1.

[5] Cotton, F.A.; Wilkinson, G. *Advanced Inorganic Chemistry*, Wiley, New York, **1998**.

[6] Henzler, M.; Göpel, W. *Oberflächenphysik des Festkörpers*, Teubner, Stuttgart, **1991**.

[7] Arenz, M.; Landman, U.; Heiz, U. *Chemphyschem.* **2006**, 7(9), 1871.

[8] Vent, St. Diplomarbeit, Technische Universität München, **1997**.

[9] Krüger, S.; Vent, S.; Rösch, N. *Ber. Bunsenges. Phys. Chem.*, **1997**, 101, 1640.

[10] Häberlen, O. D.; Chung, S.-C.; Stener, M.; Rösch, N. *J. Chem. Phys.*, **1997**, 106, 5189.

[11] Boyen, H.-G.; Kästle, G.; Weigl, F.; Koslowski, B.; Dietrich, C.; Ziemann, P.; Spatz, J. P.; Riethmüller, S.; Hartmann, C.; Möller, M.; Schmid, G.; Garnier, M. G.; Oelhafen, P. *Science*, **2002**, 297, 1533.

[12] Woehrle, G. H.; Brown, L. O.; Hutchison, J. E. *J. Am. Chem. Soc.*, **2005**, 127(7), 2172.

[13] Brust, M.; Walker, M.; Bethell, D.; Schiffrin, D. J.; Whyman, R. J. *J. Chem. Soc., Chem. Commun.*, **1994**, 801.

[14] Schaaff, T.; Shafigullin, M.; Khoury, J.; Vezmar, I.; Whetten, R. L. *J. Phys. Chem. B*, **2001**, 105, 8785.

[15] Templeton, A. C.; Wuelfing, W. P.; Murray, R. W. *Acc. Chem. Res.*, **2000**, 33, 27.

[16] Häkkinen, H.; Barnett, R.; Landman, U. *Phys. Rev. Lett.*, **1999**, 82, 3264.

[17] Cleveland, C. L.; Landman, U.; Schaaff, T. G.; Shafigullin, M. N.; Stephens, P. W.; Whetten, R. L. *Phys. Rev. Lett.*, **1997**, 79 (10), 1873.

[18] Schmid, G. *Adv. Eng. Mater.*, **2001**, 3 (10), 737.

[19] Schmid, G.; Pfeil, R.; Boese, R.; Bandermann, F.; Meyer, S.; Calis, G. H. M.; van der Velden, J. W. A. *Chem. Ber.*, **1981**, 114, 3634.

[20] Cotton, F.A. *Q. Rev. Chem. Soc.*, **1966**, 466.

[21] Schön, G.; Simon, U. *Colloid. Polym. Sci.*, **1995**, 273, 101.

[22] Heiz, U.; Schneider, W.-D. *J. Phys. D: Appl. Phys.*, **2000**, 33, R85.;

[23] Brack, M. *Spek. d. Wiss.*, **1998**, 2, 32.

[24] Buck, U. *Phys. Blätter*, **1994**, 50 (11), 1052.

[25] Burda, C.; Chen, X.; Narayanan, R.; El-Sayed, M. A. *Chem. Rev.*, **2005**, 105, 1025.

[26] Templeton, A. C.; Hostetler, M. J.; Kraft, C. T.; Murray, R. W. *J. Am. Chem. Soc.*, **1998**, 120, 1906.

[27] Hostetler, M. J.; Templeton, A. C.; Murray, R. W. *Langmuir*, **1999**, 15, 3782.

[28] Woehrle, G. H.; Brown, L. O.; Hutchison, J. E. *J. Am. Chem. Soc.*, **2005**, 127, 2172.

[29] Hussain, I.; Wang, Z.; Cooper, A. I.; Brust, M. *Langmuir*, **2006**, 22(7), 2938.

[30] Nitzan, A.; Ratner, M. A. *Science*, **2003**, 300, 1384.

[31] Whetten, R. L.; Shafiguillin, M. N.; Khoury, J. T.; Schaaf, T. G.; Vezmar, I.; Alvarez, M. M.; Wilkinson, A. *Acc. Chem. Res.*, **1999**, 32, 397.

[32] Johnson, B. F. G. *Coor. Chem. Rev.*, **1999**, 190-192, 1269.

[33] Brust, M.; Kiely, C. *J. Coll. Surf. A*, **2002**, 202, 175.

[34] Schmid, G.; Bäumle, M.; Beyer, N. *Angew. Chem.*, **2000**, 39 (1), 181.

[35] Reuter, T.; Vidoni, O.; Torma, V.; Schmid, G.; Nan, L.; Gleiche, M.; Chi, L.; Fuchs, H. *Nano Lett.*, **2002**, 2 (7), 709.

[36] Rao, C. N. R.; Kulkarni, G. U.; Thomas, P. J.; Edwards, P. P. *Chem. Soc. Rev.*, **2000**, 29, 27.

[37] Turkevitch, J.; Stevenson, P. C.; Hillier, J. *Discuss. Faraday Soc.*, **1951**, 11, 55.

[38] Giersig, M.; Mulvaney, P. *Langmuir*, **1993**, 9, 3408.

[39] Goellner, J. F.; Guzman, J.; Gates, B. C. *J. Phys. Chem. B*, **2003**, 106, 1229.

[40] Gontard, L. C.; Dunin-Borkowski, R.; Hÿtch, M.; Ozkaya, D.; Chang, L.-Y.; Kirkland, A.; Hetherington, C. *Microscopy and Analysis*, **2006**, 104, 19.

[41] Bagus, P. S.; Brundle, C. R.; Pacchioni, G.; Parmigini, F. *Surf. Sci. Rep.*, **1993**, 19, 265.

[42] Nitsche, H. *J. All. Comp.*, **1995**, 223, 274.

[43] Ho, J.; Parks, E. K.; Zhu, L.; Riley, S. J. *Chem. Phys.*, **1995**, 201, 245.

[44] Parks, E. K.; Zhu, L.; Ho, J.; Riley, S. J. *J. Chem. Phys.*, **1994**, 100, 7206.

[45] Parks, E. K.; Zhu, L.; Ho, J.; Riley, S. J. *J. Chem. Phys.*, **1995**, 102, 7377.

[46] Hostetler, M. J.; Wingate, J. E.; Zhong, C.-J.; Harris, J. E.; Vachet, R. W.; Clark, M. R.; Londono, J. D.; Green, S. J.; Stokes, J. J.; Wignall, G. D.; Glish, G. L.; Porter, M. D.; Evans, N. D.; Murray, R. W. *Langmuir*, **1998**, 14, 17.

[47] Ceriotti, A.; Demarin, F.; Longoni, G.; Manassero, M.; Marchionna, M.; Piva, G.; Sansoni, M. *Angew. Chem. Int. Ed.*, **1985**, 24, 697.

[48] Dai, D.; Balasubramanian, K. *J. Chem. Phys.*, **1995**, 103, 648.

[49] Krüger, S.; Vent, S.; Nörtemann, F.; Staufer, M.; Rösch, N. *J. Chem. Phys.*, **2001**, 115, 2082.

[50] Alonso, J. A. *Chem. Rev.*, **2000**, 100, 637.

[51] Nava, P.; Sierka, M.; Ahlrichs, R. *Phys. Chem. Chem. Phys.*, **2003**, 5, 3372.

[52] Nörtemann, F. Dissertation, Technische Universität München, Munich, **1998**.

[53] Fischer, D.; Curioni, A.; Andreoni, W. *Langmuir*, **2003**, 19, 3567.

[54] Nasluzov, V. A.; Rivanenkov, V. V.; Gordienko, A. B.; Neyman, K. M.; Birkenheuer, U.; Rösch, N. *J. Chem. Phys.*, **2001**, 115, 8157.

[55] Molina, L. M.; Hammer, B. *J. Chem. Phys.*, **2005**, 123, 161104.

[56] Belling, T.; Grauschopf, T.; Krüger, S.; Mayer, M.; Nörtemann, F.; Staufer, M.; Zenger, C.; Rösch N. in: *High Performance Scientific and Engineering Computing*, Bungartz, H.-J.; Durst, F.; Zenger, C., Eds.; Lecture Notes in Computational Science and Engineering, Vol. 8, Springer: Heidelberg, **1999**, p. 439.

[57] Belling, T.; Grauschopf, T.; Krüger, S.; Nörtemann, F.; Staufer, M.; Mayer, M.; Nasluzov, V. A.; Birkenheuer, U.; Shor, A.; Matveev, A.V.; Hu, A.; Fuchs-Rohr, M.S. K.; Neyman, K.M.; Ganyushin, D.I.; Kerdcharoen, T.; Woiterski, A.; Gordienko, A.; Majumder, S.; Rösch, N. PARAGAUSS Version 3.0, Technische Universität München, **2004**. Previous versions of the code have also been used.

[58] Dunlap, B. I.; Rösch, N. *Adv. Quantum Chem.*, **1990**, 21, 317.

[59] Kerdcharoen, T.; Birkenheuer, U.; Krüger, S.; Woiterski, A.; Rösch, N. *Theor. Chem. Acc.*, **2003**, 109, 285.

[60] Fuchs, M. S. K.; Shor, A.; Rösch, N. *Int. J. Quant. Chem.*, **2002**, 86, 487.

[61] Nasluzov, V. A.; Ivanova, E. A.; Shor, A. M.; Vayssilov, G. N.; Birkenheuer, U.; Rösch, N. *Phys. Chem. B*, **2003**, *107*, 2228.

[62] Matveev, A. V.; Mayer, M.; Rösch, N. *Comp. Phys Commun.*, **2004**, 160, 91.

[63] Pyykkö, P. *Chem. Rev.*, **1988**, 88, 563.

[64] Desclaux, J. P.; Pyykkö, P. *Chem.Phys. Lett.*, **1976**, 39(2), 300.

[65] Koch, W.; Holthausen, M. C.: *A Chemist's Guide to Density Functional Theory*; Wiley, Weinheim, **2000**.

[66] Parr, R.G.; Yang, W. *Density Functional Theory of Atoms and Molecules*; Oxford University Press, New York, **1989**.

[67] Hohenberg, K.; Kohn, W. *Phys. Rev. B*, **1964**, 136, 864.

[68] Kohn, W.; Sham, L. J. *Phys. Rev. A*, **1965**, 140, 1133.

[69] Wolf, A.; Reiher, M.; Hess, B.A. *J. Chem. Phys.*, **2002**, 117, 9215.

[70] Douglas, M.; Kroll, N.M. *Ann. Phys.*, **1974**, *82*, 89.

[71] Buenker, R. J.; Chandra, P.; Hess, B. A. *Chem. Phys.*, **1984**, 84, 1.

[72] Knappe, P.; Rösch, N. *J. Chem. Phys.*, **1990**, 92, 1153.

[73] Häberlen, O. D.; Rösch, N. *Chem. Phys. Lett.*, **1992**, 199, 491.

[74] Rösch, N.; Krüger, S.; Mayer, M.; Nasluzov, V. A. in: *Recent Developments and Applications of Modern Density Functional Theory*, J. M. Seminario (Hrsg.), Elsevier, Amsterdam, **1996**, 497.

[75] Rösch, N.; Matveev, A. V.; Nasluzov, V. A.; Neyman, K. M.; Moskaleva, L. V.; Krüger S. in: *Relativistic Electronic Structure Theory - Applications*, P. Schwerdtfeger (Hrsg.),Theoretical and Computational Chemistry Series, Vol. 14, Elsevier, Amsterdam, **2004**, S. 656.

[76] Matveev, A.; Rösch, N. *J. Chem. Phys.*, **2003**, 118, 3997.

[77] Visscher, L.; van Lenthe, E. *Chem. Phys. Lett.*, **1999**, 306, 357.

[78] Balasubramanian, K.; Pitzer, K. S. *J. Chem. Phys.*, **1983**, 78, 321.

[79] Visscher, L.; Saue, T.; Nieuwpoort, W. C.; Faegri, K.; Gropen, O. *J. Chem. Phys.*, **1993**, 99, 6704.

[80] Matveev, A. V.; Majumder, S.; Rösch, N. *J. Chem. Phys.*, **2005**, 123, 164104.

[81] Neyman, K. M.; Ganyushin, G. I.; Matveev, A. V.; Nasluzov, V. A. *J. Phys. Chem. A*, **2002**, 106, 5022.

[82] Häberlen, O. D.; Chung, S.-C.; Rösch, N. *Int. J. Quantum. Chem., Quantum Chem. Symp.*, **1994**, 28, 595.

[83] Bussai, C.; Krüger, S.; Vayssilov, G. N.; Rösch, N. *Phys. Chem. Chem. Phys.*, **2005**, 7, 2656.

[84] Huzinaga, S.; *J. Chem. Phys.*, **1977**, 66, 4245.

[85] Wachters, A. J. H. *J. Chem. Phys.*, **1970**, 52, 1033.

[86] Hay, P. *J. Chem. Phys.*, **1977**, 66, 4377.

[87] 87a Sakai, Y.; Tatewaki, H.; Huzinaga, S. *J. Comput. Chem.*, **1981**, 2, 108 [Cl: d exponent 0.56]. 87b Van Duijneveldt, F. B. *IBM Res. Rep,*. **1971**, RJ 945. 87c Veillard, A. *Theor. Chim. Acta*, **1968**, 12, 405. 87d Huzinaga, S.; Andzelm, J.; Klobukowski, M.; Radzio-Andzelm, E.; Sakai, Y.; Tatewaki, H. *Gaussian Basis Sets for Molecular Calculations*; Elsevier, Amsterdam **1984** [O: d exponent 1.15; C: d exponent 0.60]. 87e Frisch, M. J.; Pople, J. A.; Binkley, J. S. *J. Chem. Phys*,. **1984**, 80, 3265 [H: p exponent 1.0].

[88] Neyman, K. M.; Strodel, P.; Ruzankin, S. P.; Schlensog, N.; Knözinger, H.; Rösch, N. *Catal. Lett.*, **1995**, 240, 542.

[89] Vosko, S. H.; Wilk, L.; Nusair, M. *Can. J. Phys.*, **1980**, 58, 1200.

[90] Becke, A. D. *Phys. Rev. A*, **1988**, 38, 3098.

[91] Perdew, J. P. *Phys. Rev. B*, **1986**, 33, 8822; ibid. **1986**, 34, 7406.

[92] Ziegler, T. *Chem. Rev.*, **1991**, 91, 651.

[93] Krüger, S.; Seemüller, T.; Wörndle, A.; Rösch, N. *Int J Quantum Chem.*, **2000**, 80, 576.

[94] Desmarias, N.; Jamorski, C.; Reuse, F. A.; Khanna, S, N. *Chem. Phys. Lett.*, **1998**, 294, 480.

[95] Ziegler, T. *Chem. Rev.*, **1991**, 91, 651.

[96] Görling, A.; Trickey, S. B.; Gisdakis, P.; Rösch, N. in: *Topics in Organometallic Chemistry*, Vol. 4; Brown, J.; Hoffmann, P., Eds.; Springer: Heidelberg, **1999**, p. 109-165.

[97] Nasluzov, V. A.; Rösch, N. *Chem. Phys.*, **1996**, 210, 413.

[98] Becke, A. D. *J. Chem. Phys.*, **1988**, 88, 2547.

[99] Lebedev, V. I. *Zh. Vychisl. Mat. Mat. Fiz.*, **1975**, 15, 48.

[100] Lebedev, V. I. *Zh. Vychisl. Mat. Mat. Fiz.*, **1976**, 15, 293.

[101] Lebedev, V. I. *Proc. Conf.* Novosibirsk, **1978**; Sobolev, S. L., Ed.; Nauka Sibirsk. Otdel., Novosibirsk, **1980.**

[102] Genest, A. Diplomarbeit, Technische Universität München, **2002**.

[103] Krüger, S.; Stener, M.; Rösch, N. *J. Chem. Phys.*, **2001**, 114, 5207.

[104] Huber, K. P. & Herzberg, G. *Molecular spectra and molecular structure. IV. Constants of diatomic molecules.* New York: Van Nostrand Reinhold, **1979**.

[105] Pyykkö, P. *Angew. Chem.*, **2004**, 116, 4512.

[106] Figgen, D. Rauhut, G. Dolg, M. Stoll, H. *Chem. Phys,*. **2005**, 311, 227.

[107] Thiel, W. *J. Mol. Struct. (Theochem)*, **1997**, 398-399, 1.

[108] Monard, G.; Merz Jr., K. M. *Acc. Chem. Res.*, **1999**, 32, 904.

[109] Sherwood, P.; de Vries, A. H.; Guest, M. F.; Schreckenbach, G.; Catlow, C. R. A.; French, S. A.; Sokol, A. A.; Bromley, S. T.; Thiel, W.; Turner, A. J.; Billeter, S.; Terstegen, F.; Thiel, S.; Kendrick, J.; Rogers, S. C.; Casci, J.; Watson, M.; King, F.; Karlsen, E.; Sjøvoll, M.; Fahmi, A.; Schäfer, A.; Lennartz, C. *J. Mol. Struct. (Theochem)*, **2003**, 632, 1.

[110] Maseras, F.; Morokuma, K. *J.* Comp. *Chem.*, **1995**, 16, 1170.

[111] Woo, T. K.; Pioda, G.; Röthlisberger, U.; Togni, A. *Organometallics*, **2000**, 19, 2144.

[112] Woo, T. K.; Margl, P.M.; Deng, L.; Cavallo, L.; Ziegler, T. *Catalysis Today*, **1999**, 50, 479.

[113] Lopez, N.; Pacchioni, G.; Maseras, F.; Illas, F. *Chem. Phys. Lett,*. **1998**, 294, 611.

[114] Kerdcharoen, T.; Liedl, K. R.; Rode, B. M. *Chem. Phys.*, **1996**, 211, 313.

[115] Bryce, R. A.; Vincent, M. A.; Hillier, I. H. *J. Phys. Chem. A*, **1999**, 103, 4094.

[116] Kerdcharoen, T.; Morokuma, K. *Chem. Phys. Lett,*. **2002**, 355, 257.

[117] Ryde, U. *J. Comput.-Aid. Mol. Des,*. **1996**, 10, 153.

[118] Eichinger, E.; Tavan, P.; Hutter, J.; Parrinello, M. *J. Chem. Phys.*, **1999**, 110, 10452.

[119] Eurenius, K. P.; Chateld, D. C.; Brooks, B. R. Int. J. *Quantum. Chem.*, **1996**, 60, 1189.

[120] Genest, A.; Woiterski, A.; Krüger, S.; Shor, A. M.; Rösch, N. *J. Chem. Theor. Comp.*, **2006**, 2, 47.

[121] Singh, U. C.; Kollman, P. A. *J. Comput. Chem.*, **1986**, 7, 718.

[122] Dapprich, S.; Komaromi, I.; Byun, K. S.; Morokuma, K.; Frisch, M. J. *J. Mol. Struct. (Theochem)*, **1999**, 461, 1.

[123] Karpinski, Z."*Catalysis by supported, unsupported, and electron-deficient palladium*", *Adv. Catal.*, **1990**, 37, 45.

[124] German, E. D.; Efremenko, I.; Sheintuch, M. *J. Phys. Chem. A*, **2001**, 105, 11312.

[125] Ciebien J.F.; Cohen R.E.; Duran A. *Supramol. Sci.*, **1998**, 5, 31.

[126] Bertani, V.; Cavallotti, C.; Masi, M.; Carra, S. *J. Phys. Chem. A*, **2000**, 104, 11390.

[127] Efremenko, I. *J. Mol. Catal. A*, **2001**, 173, 19.

[128] Astruc, D.; Lu, F.; Aranzaes, R. *Angew. Chem.*, **2005**, 117, 8062.

[129] Neyman, K. M.; Inntam, C.; Gordienko, A. B.; Yudanov, I. V.; Rösch, N. *J. Chem. Phys.*, **2005**, 122, 174705.

[130] Yudanov, I. V.; Sahnoun, R.; Neyman, K. M.; Rösch, N.; Hoffmann, J.; Schauermann, S.; Johánek, V.; Unterhalt, H.; Rupprechter, G.; Libuda, J.; Freund, H.-J. *J. Phys. Chem. B*, **2003**, 107, 255.

[131] Yudanov, I. V.; Sahnoun, R.; Neyman, K. M.; Rösch, N. *J. Chem. Phys.*, **2002**, 117 (21), 9887.

[132] Libuda, J.; Schauermann, S.; Laurin, M.; Schalow, T.; Freund, H.-J. *Monatsh. Chem.*, **2005**, 136, 59.

[133] Vayssilov, G. N.; Gates, B. C.; Rösch, N. *Angew. Chem. Int. Ed.*, **2003**, 42**,** 1391.

[134] Vayssilov, G. N.; Rösch, N. *Phys. Chem. Chem. Phys.*, **2005**, 7**,** 4019.

[135] Vajda, S.; Wolf, S.; Leisner, T.; Busolt, U.; Wöste, L. H.; Wales, D. *J. Chem. Phys.*, **1997**, 107**,** 3492.

[136] Goellner, J. F.; Neyman, K. M.; Mayer, M.; Nörtemann, F.; Gates, B. C.; Rösch, N. *Langmuir*., **2000**, 6, 2736.

[137] Alexeev, O.; Gates, B. C. *Top. Catal.*, **2000**, 10**,** 273.

[138] Armentrout, P. B. *Annu. Rev. Phys. Chem.*, **2001**, 52, 423.

[139] Li, F.; Yu, P.; Hartl, M.; Daemen, L. L.; Eckert, J.; Gates, B. C. *Zeitschrift Phys. Chem.*, **2006**, 220, 1553.

[140] Petkov, P.; Vayssilov, G.; Krüger, S.; Rösch, N. *Phys. Chem. Chem. Phys.*, **2006**, 8, 1282.

[141] Sebetci, A. *Chem. Phys.*, **2006**, 331 (1), 9.

[142] Gutsev, G. L.; Mochena, M. D.; Bauschlicher, C. W. Jr. *J. Phys. Chem. A*, **2004**, 108(51), 11409.

[143] Gutsev, G. L.; Bauschlicher, C. W. Jr.; Zhai, H.-J.; Wang, L.-S. *J. Chem. Phys.*, **2003**, 119, 11135.

[144] Petkov, P. S.; Vayssilov, G. N.; Krüger, S.; Rösch, N. *J. Phys. Chem. B*, **2007**, 111, 2067.

[145] Krüger, S.; Bussai, C.; Genest, A.; Rösch, N. *Phys. Chem. Chem*. Phys., **2006**, 8, 3391.

[146] Ertl, G.; Knözinger, H.; Weitkamp J. (Eds.) *Handbook of Heterogeneous Catalysis* Vol. 2, Wiley-VCH, Weinheim, **1997**.

[147] Hadjiivanov, K. I.; Vayssilov, G. N. *Adv. Catal.*, **2002**, 47**,** 307.

[148] Moc, J.; Musaev, D.G.; Morokuma, K. *J. Phys. Chem. A.*, **2000**, 104, 11606.

[149] Bertin, V.; Cruz, A.; del Angel, G.; Castro, M.; Poulain, E. *Int. J. Quant. Chem.*, **2005**, 102, 1092.

[150] Efremenko, I.; German, E. D.; Sheintuch, M. *J. Phys. Chem. A*, **2000**, 104, 8089.

[151] Besler, B. H.; Merz, K. M.; Kollman, P. A. *J.Comp.Chem.*, **1990**, 11, 431; Bayly, C. I.; Cieplak, P.; Cornell, W. D.; Kollman, P. A. *J. Phys. Chem.*, **1993**, 97, 10269.

[152] Shim, I.; Gingerich, K. A. *J. Chem. Phys.*, **1984**, 80, 5107.

[153] Lin, S. S.; Strauss, B.; Kant, A. *J. Chem. Phys.*, **1969**, 51, 2282.

[154] Valerio G.; Toulhoat H. *J. Phys. Chem.*, **1996**, 100, 10827.

[155] Fahmi, A.; van Santen, R. A. *J. Phys. Chem.*, **1996**, 100, 5676.

[156] Futschek, T.; Marsman, M.; Hafner, J. *J. Phys.: Condens. Matter.*, **2005**, 17, 5927.

[157] Xiao, C.; Krüger, S.; Belling, T.; Mayer, M.; Rösch, N. *Int. J. Quant. Chem.*, **1999**, 74, 405.

[158] Zacarias, A.G.; Castro, M.; Tour, J.M.; Seminario, J. M. *J. Phys. Chem. A.*, **1999**, 103, 7692.

[159] Ho, J.; Ervin, K. M.; Polak, M. L.; Gilles, M. K.; Lineberger, W. C. *J. Chem. Phys.*, **1991**, 95, 4845.

[160] Zhang, W.; Ge, Q.; Wang, L. *J. Chem. Phys.*, **2003**, 118(13), 5793.

[161] Pacchioni, G. Chung, S.-C. Krüger, S. Rösch, N. *Chem. Phys.*, **1994**, 184, 125.

[162] Atomic Radii: http://www.webelements.com/webelements/elements/text/H/radii.html; http://www.webelements.com/webelements/elements/text/Cl/radii.html; http://www.webelements.com/webelements/elements/text/P/radii.html;7.5.2007.

[163] When using a smaller angular grid of 171, distortions compared to the low symmetry structure occurred, which were up to 0.08 Å in Pd-Pd bond lengths and 0.02 Å in Pd-H distances. This deviation could be traced back to a rotation necessary to transform the C_{2v} symmetry structure in to a C_s symmetric one. To overcome this inaccuracy a very high angular grid of NANG = 291 has been chosen in this case. For other impurities this effect was considerably smaller than on the C_{2v} species.

[164] van Santen, R. A.; Neurock, M. *Molecular Heterogeneous Catalysis*, Wiley-VCH, Weinheim, Germany, **2006**.

[165] Ponec, V.; Bond, G. C. *Catalysis by Metals and Alloys*, Studies in Surface Science and Catalysis, vol. 95, Elsevier, Amsterdam, **1995**, ch. 11, p. 477.

[166] Brocker, F. J.; Kämpfer, K. *Chemie Ingenieur Technik*, **1975**, 47, 513.

[167] Argo, A. M.; Goellner, J. F.; Phillips, B. L.; Panjabi, G. A.; Gates, B. C. *J. Am. Chem. Soc.*, **2001**, 123, 2275.

[168] Deutsch, S. E.; Mestl, G.; Knözinger, H.; Gates, B. C. *J. Phys. Chem.* B, **1997**, 101, 1374.

[169] Xu, Z.; Gates, B. C. *J. Catal*., **1995**, 154, 335.

[170] Alexeev, O. S.; Gates, B. C. *J. Mol. Catal. A-Chem.*, **2000**, 162, 67.

[171] Alexeev, O. S.; Gates, B. C. *J. Cat.*, **1998**, 173, 196.

[172] Kawi, S.; Chang, J.-R.; Gates, B. C. *J. Phys. Chem.*, **1993**, 97, 10599.

[173] Ferrari, A. M.; Neyman, K. M.; Mayer, M.; Staufer, M.; Gates, B. C.; Rösch, N. *J. Phys. Chem. B*, **1999**, 103, 5311.

[174] Vayssilov, G. N.; Rösch, N. *J. Phys. Chem. B*, **2004**, 108, 180.

[175] Bhirud, V.; Goellner, J. F.; Argo, A. M.; Gates, B. C. *J. Phys. Chem. B*, **2004**, 108, 9752.

[176] Van't Blik, H. J. J.; van Zon, J. B. A. D.; Huizinga, T.; Vis, J. C.; Koningsberger, D. C.; Prins, R. *J. Am. Chem. Soc.*, **1985**, 107, 3139.

[177] Guzman, J.; Gates, B. C. *Dalton Trans.*, **2003**, 17, 3303.

[178] Dyson, P. J. *Coord. Chem. Rev.*, **2004**, 248, 2443.

[179] Yarovsky, I.; Goldberg, A. *Mol. Sim.*, **2005**, 31, 475.

[180] Jones, N. O.; Beltran, M. R.; Khanna, S. N.; Baruah, T.; Pederson, M. R. *Phys. Rev. B*, **2004**, 70, 165406.

[181] Ashman, C.; Khanna, S. N.; Pederson, M. R. *Chem. Phys. Lett.*, **2003**, 368, 257.

[182] Petkov, P. S.; Vayssilov, G. N.; Krüger, S.; Rösch, N. *Phys. Chem. Chem. Phys.*, **2006**, 8, 1282.

[183] Nayak, S. K.; Weber, S. E.; Jena, P.; Wildberger, K.; Zeller, R.; Dederichs, P. H.; Stepanyuk, V. S.; Hegert, W. *Phys. Rev. B*, **1997**, 56, 8849.

[184] Poulain, E.; Benitez, J.; Castillo, S.; Bertin, V. A.; Cruz, *J. Mol. Struct. THEOCHEM*, **2004**, 709, 67.

[185] Huda, M. N.; Kleinman, L. *Phys. Rev. B*, **2006**, 74, 195407.

[186] Zhang, W.; Xiao, L.; Hirata, Y.; Pawluk, T.; Lichang, W. *Chem. Phys. Lett.*, **2004**, 383, 67.

[187] Petrova, G. P.; Vayssilov, G. N.; Rösch, N. *to be published*.

[188] Zanchet, D.; Micheel, C. M.; Parak, W. J.; Gerion, D.; Williams, S. C.; Alivisatos, A. P. *J. Phys. Chem. B*, **2002**, 106, 11758.

[189] Niemeyer, C. M.; Ceyhan, B.; Hazarika, P. *Angew. Chem. Int. Ed. Engl.*, **2003**, 42, 5766.

[190] Larsson, J. A.; Nolan, M.; Greer, J. C. *J. Phys. Chem. B*, **2002**, 106, 5931.

[191] Andreoni, W.; Curioni, A.; Grönbeck, H. *Int. J. Quantum Chem.*, **2000**, 80, 598.

[192] Luedtke, W. D.; Landman, U. *J. Phys. Chem.*, **1996**, 100, 13323.

[193] Basch, H.; Ratner, M. A. *J. Chem. Phys.*, **2004**, 120, 5771.

[194] Majumder, C.; Briere, T. M.; Mizuseki, H.; Kawazoe, Y. *J. Chem. Phys.*, **2002**, 117 (6), 2819.

[195] Frenkel, A. I.; Nemzer, S.; Pister, I.; Soussan, L.; Harris, T.; Sun, Y.; Rafailovich, M. H. *J. Chem. Phys.*, **2005**, 123, 184701.

[196] Ramallo-López, J. M.; Giovanetti, L. J.; Requejo, F. G.; Isaacs, S. R.; Shon, Y. S.; Salmeron, M. *Phys. Rev. B*, **2006**, 74, 073410.

[197] Love, J. C.; Estroff, L. A.; Kriebel, J. K.; Nuzzo, R. G.; Whitesides, G. M. *Chem. Rev.*, **2005**, 105, 1103.

[198] Letardi, S.; Cleri, F. *J. Chem. Phys.*, **2004**, 120, 10062.

[199] Basch, H.; Ratner, M. A. *J. Chem. Phys.*, **2003**, 119, 11926.

[200] Basch, H.; Ratner, M. A. *J. Chem. Phys.*, **2003**, 119, 11943.

[201] Basch, H.; Ratner, M. A. *J. Chem. Phys.*, **2004**, 120, 5761.

[202] Grönbeck, H.; Häkkinen, H. *J. Phys. Chem. B*, **2007**, 111, 3325.

[203] Krüger, D.; Fuchs, H.; Rousseau, R.; Parrinello, M. *J. Chem. Phys.*, **2001**, 115, 4776.

[204] Garzón, I. L.; Michaelian, K.; Beltrán, M. R.; Posada-Amarillas, A.; Ordejón, P.; Artacho, E.; Sánchez-Portal, D.; Soler, J. M. *Phys. Rev. Lett.*, **1998**, 81,1600.

[205] Oviedo, J.; Palmer, R. E. *J. Chem. Phys.*, **2002**, 117, 9548.

[206] Wang, J.; Wang, G.; Zhao, J. *Phys. Rev. B*, **2002**, 66, 035418.

[207] Garzón, I. L.; Rovira, C.; Michaelian, K.; Beltrán, M. R.; Ordejón, P.; Junquera, J.; Sánchez-Portal, D.; Artacho, E.; Soler, J. M. *Phys. Rev. Lett.*, **2000**, 85, 5250.

[208] Ullman, A. *Chem. Rev.*, **1996**, 96, 1533.

[209] Kondoh, H.; Iwasaki, M.; Shimada, T.; Amemiya, K.; Yokoyama, T.; Ohta, T. *Phys. Rev. Lett.*, **2003**, 90, 066102.

[210] Roper, M. G.; Skegg, M. P.; Fisher, C. J.; Lee, J. J.; Dhanak, V. R.; Woodruff, D. P.; Jones, R. G. *Chem. Phys. Lett.*, **2004**, 389, 87.

[211] Kato, H. S.; Noh, J.; Hara, M.; Kawai, M. *J. Phys. Chem. B*, **2002**, 106, 9655.

[212] Schreiber, F. *J. Phys. Cond. Mat.*, **2004**, 16, R881 and references therein.

[213] Grönbeck, H.; Curioni, A.; Andreoni, W. *J. Am. Chem. Soc.*, **2000**, 122, 3839.

[214] Akinaga, Y.; Nakajima, T.; Hirao, K. *J. Chem. Phys.*, **2001**, 114, 8555.

[215] Morikawa, Y.; Hayashi, T.; Liew, C. C.; Nozoye, H. *Surf. Sci.*, **2002**, 507-510, 46.

[216] Häkkinen, H.; Walter, M.; Gronbeck, H. *J. Phys. Chem. B.*, **2006**, 110(20), 9927.

[217] Marks, L. D. *Rep. Prog. Phys.*, **1994**, 57, 603.

[218] Schmid, G. in G. Schmid (ed): Clusters and Colloids, p. 178, VCH, Weinheim, **1994**.

[219] Schmid, G. *Inorg. Synth.*, **1990**, 27, 214.

[220] Krüger, S.; Stener, M.; Mayer. M.; Nörtemann, F.; Rösch, N. *J. Mol. Struct. (Theochem)*, **2000**, 527, 63.

[221] R. C. Weast (ed), CRC Handbook of Chemistry and Physics, 64 ed., CRC Press Boca Raton, **1983**.

[222] Schaaff, T. G.; Knight, G.; Shafigullin, M. N.; Borkman, R. F.; Whetten, R. L. *J. Phys. Chem. B*, **1998**, 102, 10643.

[223] Donkers, R. L.; Lee, D.; Murray, R. W. *Langmiur*, **2004**, 20, 1945.

[224] Garzón, I. L.; Artacho, E.; Beltrán, M. R.; García, A.; Junquera, J.; Michaelian, K.; Ordejón, P.; Rovira, C.; Sánchez-Portal, D.; Soler, J. M. *Nanotechnology*, **2001**, 12, 126.

[225] Dubois, L. H.; Nuzzo, R. G. *Ann. Phys. Chem.*, **1992**, 43, 437.

[226] DiCenzo, S. B.; Berry, S. D.; Hartford, E. H. Jr. *Phys. Rev. B*, **1988**, 38 (12), 8465.

[227] Büttner, M.; Kröger, H.; Gerhards, I.; Mathys, D.; Oelhafen, P. *Thin Solid. Films*, **2006**, 495, 180.

[228] Woiterski, A.. Dissertation, Technische Universität München: Munich, **2003**.

[229] Andres, R. P.; Bielefeld, J. D.; Henderson, J. I.; Janes, D. B.; Kolagunta, V. R.; Kubiak, C. P.; Mahoney, W. J.; Osifchin, R. G. *Science*, **1996**, 273, 1690.

[230] Chen, S.; Sommers, J. M. *J. Phys. Chem. B*, **2001**, 105, 8816.

[231] Ang, T. P.; Wee, T. S. A.; Chin, W. S. *J. Phys. Chem. B*, **2004**, 108, 11001.

[232] Shor, A.; Rösch, N., unpublished.

[233] Matveev, A. V.; Mayer, M. M.; Rösch, N. *Comp. Phys. Comm.*, **2004**, 160, 91.

[234] Allinger, N. L.; Yuh. Y. H.; Lii, J.-H. *J. Am. Chem. Soc.*, **1989**, 111, 8551.

[235] Hayes, D. M.; Barber, M.; Clark, J. H. R. *J. Chem. Soc. Faraday Trans. II*, **1977**, 73, 1485.

[236] Perram, J. W.; Petersen, H. G.; De Leeuw, S. V. *Molec. Phys.*, **1988**, 65, 875.

[237] Genest, A.; Krüger, S; Gordienko, A. B.; Rösch, N. *Z. Naturforsch.*, **2004**, 59b, 1585.

[238] Holthausen, M. C.; Koch, W. *A Chemist's Guide to Density Functional Theory*; Wiley-VCH: Weinheim, **2000**.

[239] Osinga, V. P.; van Gisbergen, S. J. A.; Snijders, J.G.; Baerends, E. J. *J. Chem. Phys.*, **1997**, 106, 5091.

[240] Wu, Q.; Yang, W. *J. Chem. Phys.*, **2002**, 116, 515.

[241] Langreth, D. C.; Dion, M.; Rydberg, H.; Schröder, E.; Hyldgaard, P.; Lundqvist, B. I. *Int. J. Quantum. Chem.*, **2005**, 101 (5), 599.

[242] W. A. Goddard, III, private communication.

[243] Furche, F.; van Voorhis, T. *J. Chem. Phys.*, **2005**, 122, 164106.

[244] Pérez-Jordá, J. M.; Becke, A. D. *Chem. Phys. Lett.*, **1995**, 233, 134.

[245] van Mourik, T.; Gdanitz, R. J. *J. Chem. Phys.*, **2002**, 116, 9620.

[246] Wilson, E. B. *Advan. Chem. Phys.*, **1959**, 2, 367.

[247] Thiel, R. C.; Benfield, R. E.; Zanoni, R.; Smit, H. H. A.; Dirken, M. W. *Structure and Bonding*, **1993**, 81, 1.

[248] Balasubramanian, R.; Guo, R.; Mills, A. J.; Murray, R. W. *J. Am. Chem. Soc.*, **2005**, 127 (22), 8126.

[249] Cariati, F.; Naldini, L. *Inorg. Chim. Acta.*, **1971**, 5, 172.

[250] Bellon, P. L.; Manassero, M.; Sansoni, M. *J. Chem. Soc., Dalton Trans.*, **1972**, 1481.

[251] Van der Velden, J. W. A.; Vollenbroek, F. A.; Bour, J. J.; Beurskens, P. T.; Smits, J. M. M.; Bosman, W. P. *Rec. Trav. Chim. Pay-Bas*, **1981**, 100, 148.

[252] Fackler, J. P.; McNeal, C. J.; Winpenny, R. E. P.; Pignolet, L. H. *J. Am. Chem. Soc.*, **1989**, 111, 6434.

[253] McNeal, C. J.; Winpenny, R. E. P.;Hughes, J. M.; Macfarlane, R. D.; Pignolet, L. H.; Nelson, L. T. J.; Gardner,T. G.; Irgens, L. H.; Vigh, G.; Fackler, J. P., Jr. *Inorg. Chem.*, **1993**, 32, 5582.

[254] Schmid, G. *Chem. Rev.*, **1992**, 92, 1709.

[255] Vogel, W.; Rosner, B.; Tesche, B. *J. Phys. Chem.*, **1993**, 97, 11611.

[256] Rapoport, D. H.; Vogel, W.; Cölfen, H.; Schlögl, R. *J. Phys. Chem. B*, **1997**, 101 (21), 4175.

[257] Feld, H.; Leute, A.; Rading, D.; Benninghoven, A. *J. Am. Chem. Soc.*, **1990**, 112, 8166.

[258] Feld, H.; Leute, A.; Rading, D.; Benninghoven, A. *Z. Phys. D*, **1990**, 17, 73.

[259] Benfield, R. E.; Grandjean, D.; Kröll, M.; Pugin, R.; Sawitowski, T.; Schmid, G. *J. Phys. Chem. B*, **2001**, 105, 1961.

[260] Coordination sites were taken from the corresponding figure from Ref. [252].

[261] Vollenbroek, F. A.; Bour, J. J.; Trooster, J. M.; Van der Velden, J. W. A. *J. Chem. Soc., Chem. Commun.*, **1978**, 1345.

[262] Cluskey, P. D.; Newport, R. J.; Benfield, R. E.; Gurman, S. J.; Schmid, G. *Supplement to Z. Phys. D*, **1993**, 26, S 8.

[263] Benfield, R. E.; Creighton, J. A.; Eadon, D. G.; Schmid, G. *Z. Phys. D*, **1989**, 12, 533.

[264] Marcus, M. A.; Andrews, M. P.; Zegenhagen, J.; Bommannavar, A. S.; Montano, P. *Phys. Rev. B*, **1990**, 42 (6), 3312.

[265] Boyen, H.-G.; Kästle, G.; Weigl, F.; Ziemann, P.; Schmid, G.; Garnier, M. G.; Oelhafen, P. *Phys. Rev. Lett.*, **2001**, 87 (27), 276401.

[266] Thiel, R. C.; Benfield, R. E.; Zanoni, R.; Smit, H. H. A.; Dirken, M. W. *Z. Phys. D*, **1993**, 26, 162.

[267] Fauth, K.; Kreibig, U.; Schmid, G. *Z. Phys. D*, **1989**, 12, 515.

[268] Brom, H. B.; Van Staveren, M. P. J.; De Jongh, L. J. *Z. Phys. D*, **1991**, 20, 281.

[269] Joyes, P. *Z. Phys. D*, **1995**, 32, 337.

[270] Brom, H. B.; Baak, J.; De Jongh, L. J.; Mulder, F. M.; Thiel, R. C.; Schmid, G. *Supplement to Z. Phys. D*, **1993**, 26, S 27.

[271] Zhang, H.; Hartmann, U.; Schmid, G. *Appl. Phys. Lett.*, **2004**, 84 (9), 1543.

[272] Zhang, H.; Mautes, D.; Hartmann, U. N. *J. Phys.*, **2003**, 5, 30.1.

[273] Schmid, G.; Corain, B. *Eur. J. Inorg. Chem.*, **2003**, 3081.
[274] Zhang, H., Schmid, G.; Hartmann, U. *Nano Lett.*, **2003**, 3 (3), 305.
[275] Benfield, R. E. *J. Orgmet. Chem.*, **1989**, 372, 163.
[276] Goll, G.; Löhneysen, H. v.; Kreibig, U.; Schmid, G. *Z. Phys. D*, **1991**, 20, 329.
[277] Bishop, S. M. *Group Theory and Chemistry*, New York, Dover Publications, **1973**.
[278] D'Agostine, G.; Pinto, A.; Mobilio, S. *Phys. Rev. B*, **1993**, 48 (19), 14447.
[279] Barnard, A. S.; Curtiss, L. A. *Chem. Phys. Chem.*, **2006**, 7, 1544.
[280] Häberlen, O. D.; Rösch, N. *J. Phys. Chem.*, **1993**, 97, 4970.
[281] Benfield, R. E.; Filipponi, A.; Bowron, D. T.; Newport, R. J. Gurman, S. J. *J. Phys: Condens. Matter*, **1994**, 6, 8429.
[282] Baenziger, N. C.; Bennett, W. E.; Soborofe, D. M. *Acta Cryst.*, **1976**, B32, 962.
[283] Angermaier, K.; Zeller E.; Schmidbaur H. *J. Organomet. Chem.*,**1994**, 472 (1-2), 371.
[284] Angermair, K.; Bowmaker, G. A.; de Silva, E. N.; Healy, P. C.; Jones, B. E.; Schmidbaur, H. *J. Chem. Soc., Dalton Trans.*, **1996**, 3121.
[285] Kremleva, A.; Rösch, N. *unpublished results*.
[286] Egelhoff, W. F. *Surf. Sci. Rep.*, **1987**, 6, 253.
[287] Benesh, G.A.; King, D. A. *Chem. Phys. Lett.*, **1992**, 191, 315.
[288] Koch, W.; Holthausen, M. C.: *A Chemist's Guide to Density Functional Theory*; Wiley, Weinheim, **2000**, p. 85-87.